

CIGMAT/UH 2004-1

~~States (TX)~~

UH 3940 - Phase 1

**Continuous Flight Auger Pile Bridge
Foundation**

**Implementation Phase I: Texas Gulf
Coast Region**

Project No. 5-3940 (Phase I)

Final Report

Texas State Department of Transportation

by

M. W. O'Neill Ph.D., P.E.

M. G. Kim Ph.D.

and

C. Vipulanandan Ph.D., P.E.



**Center for Innovative Grouting Materials and Technology
(CIGMAT)**

Department of Civil and Environmental Engineering

University of Houston

Houston, Texas 77204-4003

Report No. CIGMAT/UH 2004-1

January 2004

**Continuous Flight Auger Pile Bridge Foundation
Implementation Phase I: Texas Gulf Coast Region**

Project No. 5-3940 (Phase I)

Final Report

Texas State Department of Transportation

by

M. W. O'Neill Ph.D., P.E.

M. G. Kim Ph.D.

and

C. Vipulanandan Ph.D., P.E.



Center for Innovative Grouting Materials and Technology (CIGMAT)

Department of Civil and Environmental Engineering

University of Houston

Houston, Texas 77204-4003

Report No. CIGMAT/UH 2004-1

January 2004

1
2
3
4
5
6
7
8
9
10
11
12
13
14
15
16
17
18
19
20
21
22
23
24
25
26
27
28
29
30
31
32
33
34
35
36
37
38
39
40
41
42
43
44
45
46
47
48
49
50
51
52
53
54
55
56
57
58
59
60
61
62
63
64
65
66
67
68
69
70
71
72
73
74
75
76
77
78
79
80
81
82
83
84
85
86
87
88
89
90
91
92
93
94
95
96
97
98
99
100

ENGINEERING DISCLAIMER

The contents of this report, reflect the views of the authors, who are responsible for the facts and the accuracy of the data presented herein. The contents do not necessarily reflect the official views or policies of the Texas Department of Transportation. This report does not constitute a standard or a regulation.

There was no invention or discovery conceived or first actually reduced to practice in the course of or under this contract, including any art, method, process, machine, manufacture, design or composition of matter, or any new and useful improvement thereof, or any variety of plant which is or may be patentable under the patent laws of the United States of America or any foreign country.

PREFACE

In the previous two projects (5-3921 and 5-3940) on continuous flight auger (CFA) piles, better known as augered, cast in-place (ACIP) piles, the axial and lateral capacity of piles were verified in the Gulf-Coast region by full-scale load tests. The test results showed that ACIP have the potential for use in bridge foundations. Also a construction specification was developed for ACIP piles. In this implementation project, a new bridge was designed and constructed entirely with 64 ACIP piles by Texas Department of Transportation (TxDOT) at the intersection of Krenek Road and highway U.S. 90 in Crosby, Texas.

This study was undertaken to verify whether ACIP piles could be used as an alternative to driven piles with acceptable in-service performance for bridge foundations in the Pleistocene soils of the Texas Gulf Coast region. In the top 65 ft of soil profile, the site had mainly clay with two thin layers of sand and the groundwater table was 5 ft below ground surface. ACIP piles were designed using the drilled shaft design procedure established by TxDOT. Before installing production piles the design capacity of the instrumented 18 in. (0.46 m) diameter ACIP pile was verified by performing a full-scale load test on site and was compared it to a driven prestressed concrete (PC) pile on an adjacent bridge (at Runneburg site) in nearly similar geotechnical conditions.

Total of 32 battered and 32 vertical ACIP piles were used to support the bridge structure. The grouting ratio (grout volume pumped/ theoretical volume of borehole) and grout line pressure at the ground level were monitored during the construction of every ACIP pile. Total of 12 ACIP production piles (plumb central bent and battered abutment piles) were instrumented with calibrated vibrating wire sister bars to measure strains to determine the long-term load transfer characteristics of the piles. All the aspects of bridge construction were monitored for the purpose of quality control, fill settlement, and footing and abutment settlements. The performance of the bridge has been monitored for 6 months under service loads.

This report summarizes the design and construction of ACIP piles, performance of the bridge system and findings of this study in 13 Chapters.

ABSTRACT

Continuous flight auger (CFA) piles better known as Augered, Cast In-Place (ACIP) piles have been widely used in the United States for several decades because of relatively rapid installation and minimum environmental impact during installation with comparable cost to other foundation systems. However, their use in transportation projects has been limited to small secondary structures such as sound barrier walls and overhead signs that exert relatively very small bearing loads.

In this implementation project, a new bridge was designed and constructed entirely with 64 ACIP piles by Texas Department of Transportation (TxDOT) at the intersection of Krenek Road and highway U.S. 90 in Crosby, Texas. This study was undertaken to verify whether ACIP piles could be used as an alternative to driven piles with acceptable in-service performance for bridge foundations in the Pleistocene soils of the Texas Gulf Coast region. In the top 65 ft of soil profile, the site had mainly clay with two thin layers of sand and groundwater table 5 ft below ground surface. ACIP piles were designed using the drilled shaft design procedure established by TxDOT. The grouting ratio (grout volume pumped/ theoretical volume of borehole) and grout line pressure at the ground level were monitored during the construction of every ACIP pile. Before installing production piles the design capacity of the instrumented 18 in. (0.46 m) diameter ACIP pile was verified by performing a full-scale load test on site and was compared it to a driven prestressed concrete (PC) pile on an adjacent bridge (at Runneburg site) in nearly similar geotechnical condition. The failure load for the ACIP pile, which was designed for an axial capacity of 90 tons with a factor of safety of 2, was 215 tons. Greater load transfer was measured along the ACIP pile shaft as compared to the designed value. The axial capacity of the 16 in. square driven pile was 165 tons.

The length of the ACIP piles varied from 57 to 62 ft and each pile was installed within 15 minutes. Total of 12 ACIP production piles (plumb central bent and battered abutment piles) were instrumented with calibrated vibrating wire sister bars to measure strains to determine the long-term load transfer characteristics of the piles. Residual axial tensile strains developed in the ACIP piles. The central bent footings and abutments were instrumented with contact pressure cells to determine the load sharing between piles and pile cap. Initially there was load sharing but with time

all the loads were transferred to the ACIP piles. All the aspects of bridge construction were monitored for the purpose of quality control, fill settlement, and footing and abutment settlements. The performance of the bridge has been monitored for 6 months under service loads.

Measured settlements in various components of the bridge were less than 0.12 in (3 mm). Most of the load transfer was along the shaft of the ACIP piles and no tip resistance was measured for pile tipped in sand. Based on the ultimate load capacity, ACIP pile was cost-effective compared to a driven prestressed concrete pile. Finite element analysis was performed to investigate the group action within the central bent piles in a pile group.

SUMMARY

The full-scale load tests performed on previous two projects (5-3921 and 5-3940) on continuous flight auger (CFA) piles, better known as augered, cast in-place (ACIP) piles, showed that ACIP have the potential for use in bridge foundations. Also a construction specification was developed for ACIP piles during the previous study. ACIP piles have been widely used in the United States for several decades because of relatively rapid installation and minimum environmental impact during installation with comparable cost to other deep foundation systems. However, their use in transportation projects has been limited to small secondary structures such as sound barrier walls and overhead signs that exert relatively very small bearing loads.

After reviewing number of potential sites, a site was selected at Crosby, Texas for this implementation project, where a new bridge was designed and constructed entirely with 64 ACIP piles by Texas Department of Transportation (TxDOT) at the intersection of Krenek Road and highway U.S. 90. The objective of this study was to verify whether ACIP piles could be used as an alternative to driven piles with acceptable in-service performance for bridge foundations in the Pleistocene soils of the Texas Gulf Coast region. In the selected site the upper 65 ft of soil had mainly clay with two thin layers of sand and the groundwater table was 5 ft below the ground surface. ACIP piles were designed using the drilled shaft design procedure established by TxDOT. The grouting ratio (grout volume pumped/ theoretical volume of borehole) and grout line pressure at the ground level were monitored during the construction of every ACIP pile. Before installing production piles the design capacity of the instrumented 18 in. (0.46 m) diameter ACIP pile was verified by performing a full-scale load test on site and was compared it to a driven prestressed concrete (PC) pile on an adjacent bridge (at Runneburg site) in nearly similar geotechnical condition. The failure load for the ACIP pile, which was designed for an axial capacity of 90 tons with a factor of safety of 2, was 215 tons. Greater load transfer was measured along the ACIP pile shaft as compared to the designed value. The ratio of average unit side resistance to average undrained shear strength (α factor) for the ACIP pile was considerably higher than that was used in the design of the ACIP pile. The axial capacity of the 16 in. square driven pile driven to a depth of 46 ft was 165 tons.

The length of the ACIP piles varied from 57 to 62 ft and each pile was installed within 15 minutes as compared to 45 minutes for installing battered driven piles. The increased time for the driven battered piles was due to the pre-boring required. In this study, total of 12 ACIP production piles (plumb central bent and battered abutment piles) were instrumented with calibrated vibrating wire sister bars to measure strains to determine the long-term load transfer characteristics of the piles. Residual tensile axial strains were measured in non-battered ACIP piles most likely because of expansion of the clay soils. While, residual strains in the abutment piles (battered) were generally compressive, presumably because the settlement of the fill materials. The central bent footings and abutments were instrumented with contact pressure cells to determine the load sharing between piles and pile cap. Initially there was load sharing but with time all the loads were transferred to the ACIP piles. All the aspects of bridge construction were monitored for the purpose of quality control, fill settlement, and footing and abutment settlements. The performance of the bridge has been monitored for 6 months under service loads.

Measured settlements in various components (abutments and footings) of the bridge were less than 0.12 in (3 mm). Most of the load transfer was along the shaft of the ACIP piles and no tip resistance was measured for pile tipped in sand. At the service loading condition, the average load carried by the footing supported by the 4 ACIP piles was about 7 to 8 % of the total load. At the service loading condition, the average load carried by the abutment was almost zero indicating that the loads have been taken completely by the abutment piles. The in-battered pile carried much higher compressive loads than the out-battered pile possibly due to the lateral load on the abutment wall provided by the fill movement. Based on the ultimate load capacity, ACIP pile was cost-effective compared to a driven prestressed concrete pile. Finite element analysis was performed to investigate the group action within the central bent piles in a pile group.

IMPLEMENTATION STATEMENT

This is an implementation project to demonstrate the potential of using continuous flight auger (CFA) pile/augered-cast in place (ACIP) pile as an alternative to driven piles in the bridge foundation system. Based on settlement measurements, the bridge with 64 ACIP piles in Crosby, Texas has performed very well.

The Report will be a guidance document to TxDOT engineers on the design and construction of ACIP piles for bridge foundation systems. The results are applicable to the soil conditions in the Gulf-Coast region.

In Memory of Michael W. O’Neill (1940 – 2003), a Co-Author of the Report

The authors would like to express our sincere gratitude to one of co-authors of this report, Professor Michael W. O’Neill (1940 – 2003) who had served as a project supervisor in this TxDOT implementation project. We would like to dedicate this report to the memory of Dr. O’Neill. His leadership, passion and dedication to this TxDOT implementation project will be greatly missed.

TABLE OF CONTENTS

	Page
LIST OF FIGURES.....	xvii
LIST OF TABLES.....	xxiv
CHAPTER 1 INTRODUCTION.....	1
1.1 Problem Statement.....	1
1.2 Research Objectives and Tasks.....	5
1.3 Organization.....	8
CHAPTER 2 LITERATURE REVIEW.....	11
2.1 General.....	11
2.2 ACIP Pile Types.....	13
2.2.1 Non-Displacement Type Pile (Continuous Flight Auger Pile).....	13
2.2.2 Displacement Type Pile.....	14
2.3 Design Methods for ACIP Piles.....	16
2.3.1 API Method (RP2A-LRFD, 1993).....	19
2.3.2 Coyle and Castello Method (1981).....	22
2.3.3 FHWA Method (O'Neill and Reese, 1999).....	26
2.3.4 German Standard (Rizkallah, 1988).....	28
2.3.5 TxDOT Method for Drilled Shafts (Houston District, 1972).....	30
2.3.6 Wright and Reese Method (1979).....	34
2.3.7 Decourt (SPT-T) Method (1993).....	35
2.3.8 LPC method (Bustamante and Giancesli, 1981).....	36
2.3.9 Neely Method (1991).....	38
2.3.10 Viggiani Method (1993).....	40
2.3.11 Discussion of Design Methods.....	41
2.4 Construction Issues.....	43

2.4.1	Drilling with “Underpowered” Rigs.....	44
2.4.2	Inappropriate Installation Procedures.....	45
2.4.3	Penetration of a Hard Refusal Layer.....	46
2.4.4	Lateral Stress Relaxation.....	46
2.4.5	Installation in Non-Saturated Soil.....	46
2.5	Quality Control.....	47
2.5.1	Grout Ratio.....	47
2.5.2	Grout Pressure.....	49
2.5.3	Non-Destructive Testing (NDT).....	50
2.6	Performance of ACIP Piles as Bridge Foundations.....	54
2.6.1	Bridge over the Rivers Garigliano and Ausente, Italy (Mandolini et al., 1992; Russo and Viggiani, 1995).....	54
2.6.2	Neuville-sur-Oise Bridge, Belgium (Van Impe and De Clercq, 1995).....	56
2.6.3	Drilled Shaft Foundation at I-45 and I-610 Interchange in Houston, Texas (Wooley and Reese, 1974).....	57
 CHAPTER 3 SITE INFORMATION.....		59
3.1	Site Description.....	59
3.2	Site Conditions.....	59
3.2.1	Krenek Road Bridge Site.....	59
3.2.2	Runneburg Road Bridge Site.....	61
3.3	Soil Sampling and Testing.....	65
 CHAPTER 4 DESIGN OF FOUNDATIONS FOR KRENEK ROAD BRIDGE.....		68
4.1	General.....	68
4.2	Pile Design of Krenek Road Bridge.....	68
4.2.1	Soil Properties by Zone.....	70
4.2.2	Side Resistance.....	75

4.2.3	Toe Resistance.....	77
4.2.4	Examples of Pile Capacity Calculations.....	79
4.3	Commentary on Local ACIP Pile Design.....	82
 CHAPTER 5 CONSTRUCTION.....		84
5.1	General Information.....	84
5.2	Construction Sequence for Krenek Road Bridge.....	85
5.2.1	Fill (Embankment).....	87
5.2.2	Test and Reaction Piles.....	87
5.2.3	Abutment Piles.....	89
5.2.4	Central Bent Piles.....	93
5.2.5	Footings (Pile Caps) and Abutments.....	94
5.2.6	Columns, Bentcaps, Girders, and Deck.....	97
5.2.7	Live Load Simulation.....	99
5.3	Bid Evaluation and Cost Effectiveness of ACIP Piles Versus Driven Piles	101
5.4	Settlement Data.....	103
5.4.1	Fill Settlement.....	103
5.4.2	Footing and Abutment Settlements.....	104
5.5	Summary.....	106
 CHAPTER 6 INSTRUMENTATION.....		107
6.1	General.....	107
6.2	Vibrating Wire Sister Bars.....	107
6.3	Vibrating Wire Contact Pressure Cells.....	114
6.4	Data Acquisition Methods (Readout Devices) and Preliminary Reduction...	117
 CHAPTER 7 GROUT PROPERTIES AND PILE STIFFNESS.....		120
7.1	General.....	120
7.2	Mix Design.....	120
7.3	Flow Cone Test (ASTM C939).....	121
7.4	Grout Strength and Modulus Tests.....	123

10.2.4	Simulated Live Load.....	178
10.2.5	Contact Pressure Cells.....	179
10.2.6	Settlements.....	179
10.3	Residual Loads in Central Bent Piles.....	180
10.4	Load Distribution of Central Bent Group Piles.....	184
10.4.1	Load-Depth Curves.....	184
10.4.2	Load Distribution.....	193
10.5	Load Sharing Between ACIP Group Piles and Pile Cap.....	194
10.6	Calculated Load vs. Settlement vs. Time for Each Central Bent Pile Group	196
10.7	Summary.....	200

**CHAPTER 11 LONG TERM BEHAVIOR AND PERFORMANCE
OF ABUTMENT PILES.....**

11.1	General.....	201
11.2	Residual Loads of Abutment Piles.....	203
11.3	Load Distribution and Settlement of Abutment Piles.....	204
11.4	Load Sharing Between ACIP Group Piles and Abutment.....	216
11.5	Summary.....	217

CHAPTER 12 FINITE ELEMENT ANALYSIS.....

12.1	General.....	219
12.2	Description of FB-PIER.....	220
12.3	Input Data.....	222
12.4	Prediction of Load-Settlement Behavior for ACIP Test Pile.....	225
12.5	Group Action.....	226
12.6	Summary.....	226

CHAPTER 13 CONCLUSIONS AND RECOMMENDATIONS....

13.1	Conclusions.....	228
13.2	Recommendations.....	231

REFERENCES.....233

APPENDICES.....245

A Boring Logs at Krenek Road Bridge Site..... 245

B Stress-Strain Curves for Grout Samples (Test and Production Piles).....249

C Grout Ratios for Test and 64 Production Piles..... 258

D Examples of Load Calculations..... 267

E Abutment Settlement vs. Time.....271

F Fill Compaction Data.....273

G 3D View of FB-Pier Modeling Components for Pile Group Analysis..... 276

LIST OF FIGURES

Figure	Page
1.1. Typical ACIP Pile Rig Set-Up (Courtesy of DFI).....	2
2.1. Load-Settlement Behavior of Three Types of Piles (O’Neill, 1994).....	12
2.2. Coyle and Castello’s Pile Capacity Versus Friction Angle and Embedment: (a) Maximum Unit Skin Friction Versus Embedment (b) Maximum Unit End Bearing Versus Embedment (Coyle and Castello, 1981).....	23
2.3. Correlation between Angle of Internal Friction, ϕ , and Standard Penetration Test N Value (After Peck et al., 1974).....	25
2.4. α factor Versus Undrained Shear Strength of Clay, per Tomlinson (Coyle and Castello, 1981).....	26
2.5. Maximum Skin Friction Versus Cone Tip Resistance: (a) Cohesive Soil (b) Cohesionless Soil (Bustamante and Gianceselli, 1981).....	37
2.6. Skin Friction Factor Versus Pile Length (Neely, 1991).....	39
3.1. Map of Krenek and Runneburg Road Bridge Sites.....	60
3.2. Soil Profile for Krenek Road Bridge Site (KR-1).....	62
3.3. Krenek Road Bridge Layout (Adapted from TxDOT).....	63
3.4. Soil Profile for Runneburg Road Bridge Site	64
3.5. CPT Records at Krenek Road Site.....	67
4.1. South and North Zones for Pile Design.....	70
4.2. Idealized Soil Profile for South Zone (KR-1).....	73
4.3. Idealized Soil Profile for North Zone (KR-2)	74
5.1. Schematic Elevation of the Krenek Road Bridge.....	86

5.2.	Layout for the Test Pile and Reaction Piles at Krenek Road Site.....	88
5.3.	Positioning the Drilling Rig for Installing Abutment Piles.....	89
5.4.	Abutment Pile Cages Attached PVC Pipes.....	91
5.5.	Installing a Battered Abutment Pile.....	92
5.6.	Inserting the Cage into the Hole Filled with Grout.....	93
5.7.	Drilling Rig Setup for Installing Central Bent Piles.....	94
5.8.	Installation of Central Bent Pile.....	95
5.9.	Placing of Concrete for Central Bent Footing.....	96
5.10.	Completed Abutment (Cap and Wall) at Krenek Road Bridge Site.....	97
5.11.	Completed Columns at Krenek Road Bridge Site.....	98
5.12.	Placing Girders at Krenek Road Bridge Site.....	98
5.13.	Placement of Deck Panels at Krenek Road Bridge Site.....	99
5.14.	Live Load Simulation with Six Trucks at Krenek Road Bridge Site.....	100
5.15.	Completed Krenek Road Bridge.....	100
5.16.	Fill Settlement vs. Time.....	105
5.17.	Placement of Settlement Pin on the Corner of the Square Cap.....	106
6.1.	Instrumentation Plan.....	108
6.2.	Sketch of Typical Vibrating Wire Sister Bar.....	109
6.3.	Vibrating Wire Sister Bars Attached to Cage with Plastic Ties.....	110
6.4.	Instrumentation Details for Test Pile.....	111
6.5.	Instrumentation Details for Central Bent Piles: (a) Type I (b) Type II (c) Type III.....	112
6.6.	Instrumentation Details for Abutment Piles: (a) Type I (b) Type II.....	113
6.7.	Vibrating Wire Contact Pressure Cell.....	115
6.8.	Placement of Contact Pressure Cell at the Bottom of Footing A.....	116

7.1.	ISM vs. Curing Time.....	130
8.1.	Load Test Arrangement.....	135
8.2.	Load-Settlement Curve for ACIP Test Pile.....	136
8.3.	Load vs. Depth Curves for Test Pile (Zeroing at the Start of Test).....	137
8.4.	Load vs. Depth Curves for Test Pile (Assuming Initial Zero Readings Correspond to Unstressed Pile).....	138
8.5.	Residual Load, True Resistance, Measured Resistance for Test Pile.....	141
8.6.	f-w Curves at 2.4 m.....	144
8.7.	f-w Curves at 10.6 m.....	144
8.8.	f-w Curves at 15.1 m.....	145
8.9.	Soil Profile for Runneburg Road Bridge Site.....	147
8.10.	Load-Settlement Curve for PC Driven Test Pile at Runneburg Site.....	148
8.11.	Undrained Shear Strength vs. Depth for Krenek Road Bridge.....	150
8.12.	Undrained Shear Strength vs. Depth for Runneburg Road Bridge.....	151
9.1.	PIR-A Monitoring in the Cab of the Drilling Rig.....	156
9.2.	Magnetic Flowmeter Attached in ACIP Pile Drilling Rig.....	156
9.3.	Rotational Potentiometer in PIR System to Measure Auger Depth.....	157
9.4.	ACIP Pile Drilling Rig with PIR System.....	157
9.5.	Grout Ratios for Test and Reaction Piles.....	159
9.6.	Maximum (Systolic) and Minimum (Diastolic) Grout Pressures for Test Pile.....	160
9.7.	Grout Ratio vs. Auger Elevation for Central Bent Piles Under Footing A...	161
9.8.	Grout Ratio vs. Auger Elevation for Central Bent Piles Under Footing B...	162
9.9.	Grout Ratio vs. Auger Elevation for Abutment Piles Under Group A.....	163
9.10.	Grout Ratio vs. Auger Elevation for Abutment Piles Under Group B.....	164

9.11.	Pulse-Echo Test for Krenek Road Test Pile.....	167
9.12.	Low Strain Integrity Testing (Pulse-Echo) Results on ACIP Test Pile (3 Separate Hammer Blows).....	168
10.1.	Residual Load Distribution for Central Bent Piles Under Footing A.....	181
10.2.	Residual Load Distribution for Central Bent Piles Under Footing B.....	182
10.3.	Average Residual Load Distribution for All Central Bent Piles.....	183
10.4.	Applied Load on Each Central Bent Pile vs. Time.....	185
10.5.	Load vs. Depth Curve for Piles Under Footing A After Placement of Deck	186
10.6.	Load vs. Depth Curve for Piles Under Footing A During Live Load Simulation.....	187
10.7.	Load vs. Depth Curve for Piles Under Footing A Under Initial Service Load.....	187
10.8.	Load vs. Depth Curve for Piles Under Footing A Six Months After Going into Service.....	188
10.9.	Load vs. Depth Curves for Piles Under Footing During Initial Service Load and Six Months After Going into Service.....	188
10.10.	Load vs. Depth Curve for Piles Under Footing B After Placement of Deck	189
10.11.	Load vs. Depth Curve for Piles Under Footing B During Live Load Simulation.....	190
10.12.	Load vs. Depth Curve for Piles Under Footing B Under Initial Service Load.....	190
10.13.	Load vs. Depth Curve for Piles Under Footing B Six Months After Going into Service.....	191
10.14.	Load vs. Depth Curves for Piles Under Footing B During Initial Service Load and Six Months After Going into Service.....	191

10.15. Measured Settlements (mm) Within Central Bent Piles Under Footings A and B During Initial Service Load.....	197
10.16. Measured Settlements Within Central Bent Piles Under Footings A and B 6 Months After Going into Service.....	198
10.17. Measured Settlements (mm) Within Central Bent Piles Under Footings A and B During Live Load Simulation.....	198
10.18. Comparison of Measured Settlements for Single Test Pile and Group Pile (Central Bent Piles) at Working Load Conditions.....	199
11.1. Elevation View of Abutment Piles.....	202
11.2. Residual Load Distribution for Abutment Piles.....	205
11.3. Load vs. Depth Curve for In-Battered Abutment Piles After Placement of Deck.....	207
11.4. Load vs. Depth Curve for In-Battered Abutment Piles During Live Load Simulation.....	208
11.5. Load vs. Depth Curve for In-Battered Abutment Piles Under Initial Service Load.....	208
11.6. Load vs. Depth Curve for In-Battered Piles Six Months After Going into Service.....	209
11.7. Comparison of Load vs. Depth Curves for In-Battered Abutment Piles.....	209
11.8. Applied Load (Estimated) on Each Abutment Pile vs. Time.....	210
11.9. Load vs. Depth Curve for Out-Battered Abutment Piles After Placement of Deck.....	211
11.10. Load vs. Depth Curve for Out-Battered Abutment Piles During Live Load Simulation.....	212

11.11. Load vs. Depth Curve for Out-Battered Abutment Piles Under Initial Service	
Load.....	212
11.12. Load vs. Depth Curve for Out-Battered Piles Six Months After Going into	
Service.....	213
11.13. Comparison of Load vs. Depth Curves for Out-Battered Abutment Piles....	213
11.14. Comparison of Average In-Battered and Out-Battered Pile Load Distribution	
Curves During Live Load Simulation	214
11.15. Cartoon for Different Loads Acting on Abutment Piles.....	215
12.1. Test Pile and Pile Group Layout and Input Parameters.....	223
12.2. Comparison Between Predicted and Measured Load Settlement Curves for	
ACIP Test Pile.....	225
12.3. Load-Settlement Curves Using Various t-Multipliers (Axial Pile Group	
Efficiency).....	227
A.1. Boring Log 2 (KR-2) at Krenek Road Site.....	246
A.2. Boring Log 3 (KR-3) at Krenek Road Site.....	247
A.3. Boring Log 4 (KR-4) at Krenek Road Site.....	248
B.1. Stress-Strain Curve for Test Pile Sample 1 (TP-1).....	250
B.2. Stress-Strain Curve for Test Pile Sample 2 (TP-2).....	250
B.3. Stress-Strain Curve for Test Pile Sample 3 (TP-3).....	251
B.4. Stress-Strain Curve for Test Pile Sample 4 (TP-4).....	251
B.5. Stress-Strain Curve for Test Pile Sample 5 (TP-5).....	252
B.6. Stress-Strain Curve for Production Pile Sample 1 (B-23).....	252
B.7. Stress-Strain Curve for Production Pile Sample 2 (B-24).....	253
B.8. Stress-Strain Curve for Production Pile Sample 3 (B-25).....	253
B.9. Stress-Strain Curve for Production Pile Sample 4 (B-26).....	254

B.10.	Stress-Strain Curve for Production Pile Sample 5 (B-31).....	254
B.11.	Stress-Strain Curve for Production Pile Sample 6 (B-32).....	255
B.12.	Stress-Strain Curve for Production Pile Sample 7 (B-34).....	255
B.13.	Stress-Strain Curve for Production Pile Sample 8 (A-15).....	256
B.14.	Stress-Strain Curve for Production Pile Sample 9 (A-16).....	256
B.15.	Stress-Strain Curve for Production Pile Sample 10 (A-17).....	257
B.16.	Stress-Strain Curve for Production Pile Sample 11 (A-18).....	257
E.1.	Abutment Settlement vs. Time.....	272
F.1.	Fill Compaction Curve.....	274
G.1.	3D View of FBPIer Modeling Components for Pile Group Analysis.....	277

LIST OF TABLES

Table	Page
2.1. Design Parameters for Cohesionless Siliceous Soil (API, 1993).....	21
3.1. UU Test Results for Krenek Road Bridge Site.....	65
3.2. UU Test Results for Runneburg Road Bridge Site.....	66
4.1. Idealized Soil Properties for South Zone (KR-1).....	72
4.2. Idealized Soil Properties for North Zone (KR-2).....	72
5.1. Construction Sequence and Timeline.....	85
7.1. Grout Mix Design.....	121
7.2. Flow Cone Test Results for Instrumented Piles, and Test and Reaction Piles.....	122
7.3. Ratio of Initial Secant Modulus (ISM) and Compressive Strength of Grout for Test Pile at Load Test Day (18 Days After Test Pile Installation).....	125
7.4. Summary of Compressive Strength of Grout, Initial Secant Modulus (ISM) of Grout, and ISM of Pile at Various Times after Casting Test Pile.....	125
7.5. Ratio of Initial Secant Modulus (ISM) and Compressive Strength of Grout for Production Piles at Age 28 Days (11 samples).....	126
7.6. Summary of Compressive Strength of Grout, Initial Secant Modulus (ISM) of Grout, and ISM of Pile at Various Days for Production Piles.....	127
7.7. Summary of Splitting Tension Test Results for Test Pile.....	128
7.8. Summary of Splitting Tension Test Results for Production Piles.....	128
8.1. Pile Information.....	149

8.2.	α Factors for ACIP and Driven Prestressed Concrete (PC) Piles from Static Load Tests.....	153
10.1.	Head Load in Piles in Central Bent Footing A.....	193
10.2.	Head Load in Piles in Central Bent Footing B.....	194
10.3.	Load Sharing Between Pile Group A and Cap A for Various Loading Events.....	195
10.4.	Load Sharing Between Pile Group B and Cap B for Various Loading Events.....	196
11.1.	Calculated Pile Load and Settlements at Various Loading Events.....	206
11.2.	Load Sharing Between Abutment Pile Group A and Cap at Various Loading Events.....	216
11.3.	Load Sharing Between Abutment Pile Group B and Cap at Various Loading Events.....	217
12.1.	Input Properties for FBPIer.....	224
C.1.	Grout Ratios for Test and Central Bent Piles Under Footings A and B.....	259
C.2.	Grout Ratios for Central Bent Piles Under Footings C and D.....	260
C.3.	Grout Ratios for Central Bent Piles Under Footings E and F.....	261
C.4.	Grout Ratios for Central Bent Piles Under Footings G and H.....	262
C.5.	Grout Ratios for Abutment Piles (Groups A, B, C, and D).....	263
C.6.	Grout Ratios for Abutment Piles (Groups E, F, G, and H).....	264
C.7.	Grout Ratios for Abutment Piles (Groups I, J, K, and L).....	265
C.8.	Grout Ratios for Abutment Piles (Groups M, N, O, and P).....	266
F.1.	Fill Compaction Data.....	266

CHAPTER 1

INTRODUCTION

1.1 Problem Statement

Augered, cast-in-place piles, also known as “ACIP” piles, continuous flight auger (CFA) piles, and augercastTM piles, have been used to support moderate vertical loads (design loads of up to about 1 MN) in the private sector in the United States for over 50 years (O’Neill, et. al., 1999). They have been particularly popular in both the private and public sectors in Europe for several decades because of low cost and minimum environmental impact. In Europe and other parts of the world, however, ACIP piles have been widely used in transportation structures to support large bearing loads. However, their use on public sector transportation projects in Texas and in the United States has been limited to small secondary structures such as sound walls and overhead signs that exert very small bearing loads (O’Neill et al., 1999). Under some circumstances ACIP piles can be both efficient carriers of bearing loads and more economical to install than competing foundation systems and should be considered as an alternative foundation system for transportation structures in Texas, especially in the relatively soft clay soils in the Texas coastal region (O’Neill et al., 1999).

In general, ACIP piles are installed by rotating a continuous, hollow-shaft flight auger into the ground to a specified depth. Then, a sand-cement-water grout is injected continuously through the auger shaft as the auger is being slowly withdrawn. A reinforcing steel cage can then be inserted into the grout after the auger is fully

withdrawn. A sketch of the unique drilling rig that is used to install simple ACIP piles is shown in Fig. 1.1. To facilitate both grouting and placing reinforcing steel before grout hardening, various additives are used in the grout to retard set and to increase fluidity.

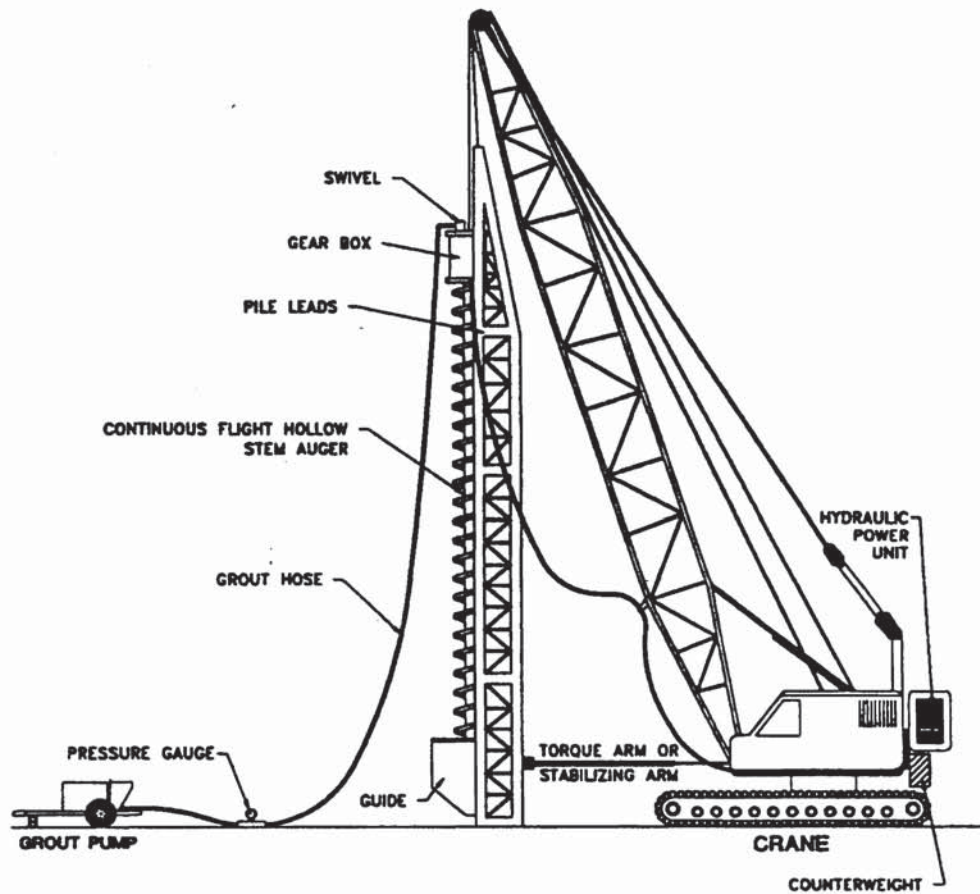


Fig. 1.1. Typical ACIP Pile Rig Set-Up (Courtesy of DFI)

ACIP piles have some advantages over other types of piles, such as driven, displacement-type piles. ACIP piles may be an economic alternative compared to other

pile types, mainly because costs are relatively low and installation is fast (O'Neill et al., 1999). Vibration and noise levels during installation are low, which can lessen the potential for damage to adjacent structures, and the potential for ground contamination is small compared to drilled shaft foundations, which usually require drilling slurry as an installation aid. ACIP piles can be installed in limited access conditions where conventional driving equipment cannot be operated and pre-manufactured piles cannot fit geometrically. Moreover, ACIP pile lengths can be easily adjusted in the field where a termination refusal criterion can be specified rather than a tip elevation criterion.

Despite those advantages, potential construction problems have been identified in the past that may adversely influence the structural integrity of ACIP piles and produce a relatively large settlement of adjacent structures (Esrig et al., 1991; O'Neill et al., 1999). The integrity of ACIP piles depends highly on construction control and the skill of the contractor's field personnel (Booth and McIntosh, 1994; O'Neill, 1998). For those reasons, the use of ACIP piles has not been widely used in transportation structures in United States, where a high standard of quality control is exercised.

Recently, improved construction management procedures have been developed by the ACIP pile industry (DFI, 1994), and automated sensing devices have been placed in service that greatly reduce the possibility of producing structural defects in ACIP piles. With this background, the Texas Department of Transportation (TxDOT) began using ACIP piles to support sound walls in the mid-1990's and sponsored two research projects at the University of Houston with a view to using ACIP piles to support bridge structures (Hassan et al., 1997; O'Neill et al., 1999). These projects have proven the importance of construction process management and automated construction monitoring procedures for

single ACIP piles in a field environment in which the geotechnical properties of the subgrade are typical of those found in the Texas Gulf Coast. Design methods and construction specifications for laterally and axially loaded piles were also developed in those studies.

In order to demonstrate that the ACIP pile foundation system is viable for an actual highway bridge, however, it is necessary to go through all of the steps in design and construction of the bridge and its foundation, and to monitor all steps, plus post-construction performance, carefully. Conditions in a highway bridge are different from the ideal test conditions utilized to date. For example, piles need to be installed in close proximity to each other, some piles (at abutments) must be installed at an angle to the vertical (“batter piles”), and piles will be subjected to long-term loading, including complex loadings produced by the settlement of fills around the battered abutment piles.

In order to implement the ACIP pile technology into its inventory of acceptable foundation systems, TxDOT designed and constructed a freeway grade separation (3-span) bridge using ACIP piles only. The project was categorized as “implementation research” and was performed to understand clearly the behavior of individual ACIP piles and groups of ACIP piles in a bridge environment using design methods for Houston-Gulf Coastal soils developed in the earlier UH studies. It was deemed equally important by TxDOT to monitor and analyze the details of construction.

1.2 Research Objectives and Tasks

The overall objective of the study is to determine whether ACIP piles can be implemented (designed and constructed with acceptable in-service performance) for bridge foundations in the Pleistocene soils of the Texas Gulf Coast. The bridge in question was selected by TxDOT based on construction schedule and appropriateness of soil conditions. It was located on highway U.S. 90 at Krenek Road, Crosby, Texas in the East Harris County Area (Residency) of the Houston District of TxDOT.

The specific objectives are the following:

- (1) Design ACIP piles based on the geotechnical conditions on the selected site and verify the capacity of the pile by full-scale load test;
- (2) Construct ACIP piles with recommended quality control procedures outlined in the specifications;
- (3) Compare the performance of ACIP pile to a driven prestressed concrete pile installed in the similar geotechnical conditions;
- (4) Evaluate the difference in the load transfer behavior between the ACIP pile and driven pile. Measure the development of residual strains in ACIP piles;
- (5) Evaluate the effects of group action on the load distribution and settlement behavior of the ACIP piles with reference to
 - a. the variability of load distribution in piles in the central bent pile groups from pile to pile;

- b. the settlement of each pile within a group for a given value of load per pile relative to that for a single test pile, which can be evaluated in a separate loading test;
- (6) Evaluate the load sharing mechanism between ACIP piles in a group and the pile cap [or footing];
- (7) Evaluate the effects of settlement of an abutment fill on the battered abutment piles;
- (8) Evaluate overall performance of the ACIP piles as foundations for a bridge at working load condition;
- (9) Identify construction problems during the process of installing ACIP piles.

The objectives were achieved in several Tasks as follows:

- Task 1: Investigate the subsurface conditions at the bridge site (also take samples for laboratory tests from borings).
- Task 2: Design the ACIP piles (number, depths, layout, diameters, reinforcement, grout properties, and batters) for axial and lateral loading.
- Task 3: Design the driven pile foundation system for an adjacent bridge (on U.S. 90 at Runneberg Road), which is nearly identical to the ACIP pile site.
- Task 4: Adapt the construction specifications for the ACIP piles that was developed from previous TxDOT projects (5-3921 and 5-3940) with minimal changes.
- Task 5: Evaluate the bids for the ACIP piles to determine the cost-effectiveness of the ACIP pile system over the driven pile system.

- Task 6: Load test an instrumented ACIP pile before installing production piles to monitor the single ACIP pile behavior and to check the pile capacity. Repeat this process with a conventional driven pile on the adjacent bridge.
- Task 7: Instrument representative ACIP piles, central bent footings and abutment with vibrating wire sister bars (strain gauges) and contact pressure cells for long-term observations of load transfer and load sharing between piles and pile cap.
- Task 8: Document the construction process for every pile, including the use of automated monitoring systems to measure grout pressures and incremental grout takes along the length of the pile and the preparation of reinforcing cages and the insertion of those cages into the columns of fluid grout, especially for long cages placed on a batter in the abutments.
- Task 9: Recover cube and/or cylinder samples of grout and determine the grout strength and modulus as a function of time (to allow the use of strain measurements to be used to compute load distribution along the piles).
- Task 10: Monitor the settlements of the abutments and central bent footings during each major construction step such as pouring abutments, pouring footings (pile caps) and columns, pouring bent caps, placing girders, placing deck and at selected times while the bridge is in service. Simultaneously, monitor the loads in representative piles and the load transfer to the soil. In particular, observe whether load is shed from side resistance to toe resistance (which can result in time-dependent settlement), especially in the case of abutment piles drilled through embankments, which may settle with time, including drag

loads on the piles and possibly inducing lateral loads on the piles through both settlement and lateral spreading of the embankment.

Task 11: Analyze the observed behavior of the groups of plumb central bent piles using state-of-the-art models, such as FB-PIER. Compare the results of the analysis with observations to ascertain how the observed behavior can best be modeled in the future by researchers and practitioners.

Task 12: Document Tasks 1 – 11 in this report.

1.3 Organization

This introduction is followed in Chapter 2 by a literature review describing the ACIP pile types, various axial design methods of driven piles, drilled shafts and ACIP piles which might be adopted or adapted for ACIP piles, construction issues, quality control and performance of bridge foundations.

Description and conditions of bridge sites are briefly discussed in Chapter 3.

The design of foundations of Krenek Road bridge is presented in Chapter 4. Texas Department of Transportation method for drilled shaft (Texas Highway Department - Houston District, 1972) was adopted for ACIP pile design. Design procedures and examples are presented.

Construction sequence and details for Krenek Road bridge are provided in Chapter 5. This chapter also provides the bid evaluation of ACIP system to evaluate cost-effectiveness over driven pile system for adjacent bridge at Runneburg Road and settlement data for embankment fill, footings and abutment monitored over an extended period of time.

The information on instrumentation is provided in Chapter 6. Representative ACIP piles including the test pile, central bent footings and abutment were instrumented with vibrating wire sister bars (strain gauges) and contact pressure cells for observations of load transfer and load sharing between piles and pile cap. Instrumentation plan and details are provided in this chapter.

Grout properties and pile stiffness are presented in Chapter 7. Grout tests including flow cone test, splitting tension test, grout strength and modulus tests, and procedure for converting strain to load are described.

Results of full-scale load tests for ACIP and prestressed driven piles are in Chapter 8.. Comparative behavior of the two piles is discussed. The development of residual stresses in ACIP piles and the effects of residual stresses on load-transfer behavior are also described.

The construction quality control procedures and construction issues identified during the bridge construction are discussed in Chapter 9.

In Chapter 10, the long-term behavior and performance of plumb central bent piles in a group monitored up to 6 months after bridge went into service are discussed. Load distribution of the piles, and load sharing within the piles, and between the piles and pile cap (footing) are described.

Long-term behavior and performance of battered abutment piles monitored up to 6 months after bridge went into service are summarized in Chapter 11. Load distribution of the piles and load sharing between the piles and abutment pile cap are provided. The effects of fill settlement on abutment piles are also described.

In Chapter 12, the FB-PIER program was used to analyze the tested ACIP pile and the group action in the central bent piles (4 central bent piles).

In Chapter 13, conclusions and recommendations for future research are summarized.

CHAPTER 2

LITERATURE REVIEW

2.1 General

Augered, cast-in-place (ACIP) piles are widely used for building construction in the United States and around the world. ACIP piles can be distinguished geotechnically from drilled shafts and driven piles by the magnitude of effective stress changes they produce in the surrounding soil during the construction (O'Neill, 1994). The drilled shaft is commonly installed as follows. An auger is repeatedly inserted into the ground and withdrawn with cuttings, forming an unsupported borehole or a borehole supported by drilling slurry. After placing reinforcing steel in the borehole, concrete is poured into the excavated borehole. Therefore, no attempt is generally made to maintain the stresses that existed in the ground before construction (O'Neill, 1994). With a driven pile, the soil is displaced and the ground stresses are generally increased. With an ACIP pile, ground stresses are maintained near the value that existed before construction by using a continuous flight auger, which is never withdrawn until the cementitious material (fluid portland cement grout) is placed by pumping the grout beneath the withdrawing auger under pressure through the hollow stem of the auger. Therefore, considering the principle of effective stress, the load-settlement behavior of the ACIP pile should fall in between that of a drilled shaft and a driven pile (O'Neill, 1994). Hypothetical differences in behavior among drilled shafts, driven piles, and ACIP piles are shown in Fig. 2.1.

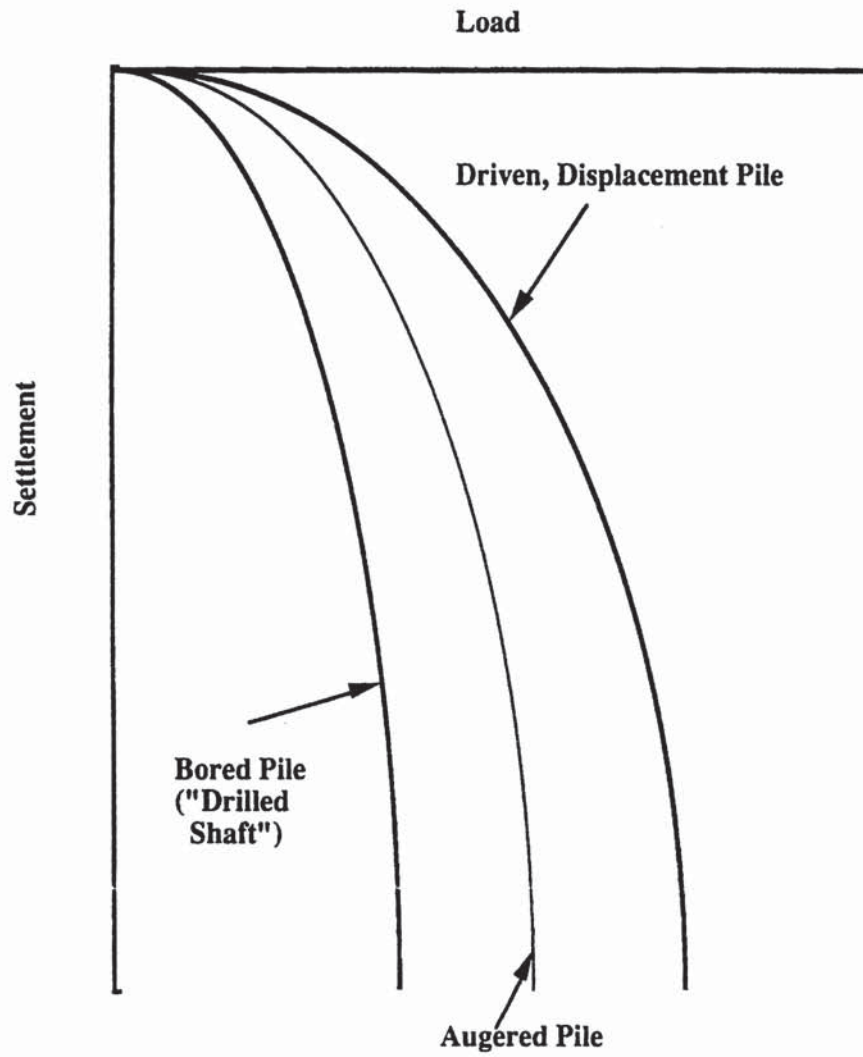


Fig. 2.1. Load-Settlement Behavior of Three Types of Piles (O'Neill, 1994)

2.2 ACIP Pile Types

There are various types of ACIP piling systems in current practice. ACIP piles used in the United States can be broadly divided into two types: the non-displacement type (the subject of this dissertation) and the displacement type.

2.2.1 Non-Displacement Type Pile (Continuous Flight Auger Pile)

Continuous Flight Auger (CFA) piles are constructed by using a continuous, hollow-stem flight auger that is drilled into the ground to a target depth. Grout is then injected continuously through the auger stem as the auger is being withdrawn. The auger is rotated continuously as the excavation is being made. In United States' practice the rate of penetration of the auger is relatively slow compared to the rate of rotation, which may result in soil, particularly clean, waterbearing cohesionless soil, being "mined" from the zone around the auger and conducted up the auger to the ground surface. This effect can both remove soil, possibly undermining adjacent piles or footings, and reduce effective stresses in the soil, possibly reducing the capacity of the pile being installed and those piles or footings already installed near the pile in question. This issue is a concern to bridge foundation designers.

CFA piles, however, are installed rapidly, and are potentially less expensive than driven piles or drilled shafts. For those reasons, TxDOT is interested in qualifying CFA piles for bridge foundations for those bridge sites at which mining of soil is a minor concern. CFA piles (a subset of ACIP piles) will be the subject of this study.

2.2.2 Displacement Type Pile

This type of pile has been widely used in Europe and has relatively recently been introduced by several construction companies in the United States. This pile uses a drilling system, as described briefly below, that tends to increase effective stresses and sometimes density of the supporting soil. It can provide a higher capacity in some loose to medium dense sands (Lacy, 1998), and more importantly, reduces the effects of mining and distressing of the soil, which can potentially occur with CFA piles. However, since rigs with higher torque and crowd are required to install displacement type ACIP piles than are required to install non-displacement piles, they tend not to be very popular in U.S. practice currently because they often lose economic advantage over competing foundation systems, including non-displacement CFA piles. This is especially true in bridge foundation construction, where frequent moves of the drilling rig are necessary due to the geometric layout of piles, such that the light rigs typical of the non-displacement ACIP pile are far more economical than the heavy rigs required to install displacement piles.

Screw Pile

A screw pile is a type of displacement-type ACIP pile that is especially popular in Europe. The screw pile can be installed by the following process. A borehole is formed by rotating a single-turn auger at the base of a large-diameter drilling axle into the ground without removing the soil. Instead, the soil is compressed back into the sides of the borehole, especially if the soil possesses some cohesion, forming a screw tap (O'Neill, 1994). When the screw pile borehole is drilled in granular soils, some soil deforms

inward, but extraction (mining) is prevented because there are no auger flights above the base of the axle. Once the target depth is reached, the reinforcing cage is inserted through the hollow axle of the auger before any concrete or grout is placed. The auger is then screwed out as the concrete/grout is placed. Various types of screw piles have been developed under the following trade names:

- (1) 'basic' cast-in-situ Atlas pile,
- (2) 'new generation' cast-in-situ or with permanent casing Franki-Atlas pile,
- (3) cast-in-situ Omega (Ω) pile, and
- (4) the most recent cast-in-situ screw pile, the Spire pile (Bustamante et al., 1998).

Bustamante and Gianceselli (1993; 1998) and O'Neill (1994) have articulated further details of each type of screw pile.

Augered (Drilled) Displacement Pile

The use of drilled (screwed) displacement piles is a relatively new concept in the United States, and the technology that led to the processes currently being used emerged in the 1960's as the Atlas and Fundex systems that have been used in Europe since the late 1980's (Nesmith, 2002). There are significant differences in tooling among the systems now being used. A common feature, however, is a displacing element that provides for forcing the horizontal movement of the soil that is penetrated. In those geomaterials that densify in response to displacement, and concrete or grout is cast against the soil, shaft and toe resistances can be higher than developed with a non-displacement (CFA) pile system (Nesmith, 2002). Rather than screwing an auger with a

large central axle into the soil, as in the case of the screw pile, the augered displacement pile removes the soil from near the bottom of the auger in the manner of a CFA pile. However, instead of the soil's being transported up the flights of the auger to the surface (which allows more soil to enter the auger flights continuously near the bit), it is blocked from such movement by a packer within the flights of the auger, which ultimately forces the excavated soil to be thrust out into the ambient soil formation, thus minimizing mining and increasing effective stresses in the surrounding soil mass.

Since the more economical CFA piles are used in this project, the research focuses on them rather than on screw or displacement-type auger piles.

2.3 Design Methods for ACIP Piles

For most grade separation structures in the TxDOT system with non-curving lanes lateral loads on foundations are small [no more than 17.8 kips (2 tons) to 44.5 kips (5 tons)]. Where lateral loads on bridge components such as abutment walls are routinely computed, these lateral loads are carried by placing the piles supporting the walls at an angle to the vertical (on a "batter") and carrying the horizontal load axially through the pile into the soil. Therefore, pile foundations are designed exclusively to carry axial loads, recognizing that most piles have a nominal lateral load capacity of 17.8 to 44.5 kips without verification. The piles are therefore not designed for lateral load (Major water crossings, where ship or barge impact and wave loading occur, are an exception). As with all piles, all of the following design methods assume ACIP piles resist applied load through side resistance (skin friction) and toe resistance (end bearing). The total ultimate load is evaluated using the equation

$$Q_t = Q_s + Q_p , \quad (2.1)$$

where

Q_t = ultimate capacity of the pile,

Q_s = capacity in side resistance, and

Q_p = capacity in toe resistance or end bearing.

The general equation for side resistance can be written as

$$Q_s = \pi D \int_{z=0}^{z=L} f_s(z) dz , \quad (2.2)$$

or as

$$Q_s = f_{sa} \pi DL , \quad (2.3)$$

where

D = nominal pile diameter (= diameter of the auger),

z = depth,

L = penetration of the pile,

$f_s(z)$ = unit side resistance at depth z , and

f_{sa} = average unit side resistance over the length L of the pile.

The area of the side of the pile (A_s), $A_s = \pi DL$.

The general equation for toe (tip, base) resistance can be written as

$$Q_p = q_p A_p \quad , \quad (2.4)$$

where

q_p = the ultimate unit toe resistance (end bearing), and

A_p = the end bearing area of the pile.

The critical parameters are f_s and q_p , which depend upon the soil's mineralogy and stress history, effective stress state, pore water pressure conditions and, the factor most relevant to this dissertation, the effects of the method of construction.

ACIP piles are used frequently in the private sector in the Texas Coastal area, mostly in industrial plants and commercial development projects. Geotechnical engineers use various design methods to predict the resistance of such piles. The methods vary; some consider ACIP piles as driven piles, while others view them as drilled shafts. Lately, a number of design methods specific to ACIP piles have been proposed by Neely (1991) and Viggiani (1993) and others.

The following are design methods that can potentially be used to predict the ultimate compressive capacity of ACIP piles. These methods are described in detail.

2.3.1 API Method (RP2A-LRFD, 1993)

The API general equation for evaluating the ultimate bearing capacity of piles, Q_u , including belled piles, is applied using Equations (2.1), (2.2), and (2.4). Although the API method was developed to calculate the capacity of driven steel pipe piles, it is of interest to compare this method with other potential ACIP pile design methods, where the ACIP pile is viewed as analogous to a plugged, driven pipe pile.

Cohesive Soils

For piles in cohesive soils, the unit resistance, $f_s(z)$, at any point along the pile is calculated by

$$f_s(z) = \alpha s_u(z) , \quad (2.5)$$

where

α = dimensionless correction factor, and

$s_u(z)$ = undrained shear strength at depth z (center of a layer).

The α -factor is computed by

$$\alpha = 0.5 \psi^{-0.5} \quad \psi \leq 1.0 , \text{ and} \quad (2.6)$$

$$\alpha = 0.5 \psi^{-0.25} \quad \psi > 1.0 , \text{ and} \quad (2.7)$$

with the constraint that $\alpha \leq 1.0$,

where

$\psi = s_u(z) / \sigma'_0(z)$ for the depth of interest, and

$\sigma'_0(z)$ = vertical effective soil pressure at depth z (center of a layer) below the soil surface

For underconsolidated clays, the value α can usually be taken as 1.0.

In cohesive soils, the unit toe resistance, q_p , is computed by

$$q_p = 9s_u, \quad (2.8)$$

where

s_u = the undrained shear strength at the toe.

For piles considered to be plugged (as in the case of ACIP piles), the end bearing pressure can be assumed to act over the entire cross section of the pile.

Cohesionless Soils

For pipe piles in cohesionless soils, the unit side resistance at depth z is

$$f_s(z) = K\sigma'_0(z) \tan \delta, \quad (2.9)$$

where

K = dimensional coefficient of lateral earth pressure (ratio of horizontal to vertical normal effective stress), and

δ = friction angle between the soil and pile wall at depth z.

For open-ended pipe piles driven unplugged, it is usually appropriate to assume K as 0.8 for both tension and compression loading. Values of K for full displacement piles (plugged or closed-ended) may be assumed to be 1.0, which can be used for ACIP piles. Table 2.1 is used for the selection of δ if other data are not available. The value of $f_s(z)$ does not indefinitely increase linearly with the overburden pressure. In such cases, $f_s(z)$ is limited to the values given in Table 2.1.

Table 2.1. Design Parameters for Cohesionless Siliceous Soil* (API, 1993)

Density	Soil Description	Soil-Pile Friction Angle (δ), degrees	Limiting Skin Friction Values, kPa (kips/ft ²)	N_q	Limiting Unit End Bearing Values, MPa (kips/ft ²)
Very loose Loose Medium	Sand Sand-Silt** Silt	15	47.8 (1.0)	8	1.9 (40)
Loose Medium Dense	Sand Sand-Silt** Silt	20	67.0 (1.4)	12	2.9 (60)
Medium Dense	Sand Sand-Silt**	25	81.3 (1.7)	20	4.8 (100)
Dense Very Dense	Sand Sand-Silt**	30	95.7 (2.0)	40	9.6 (200)
Dense Very Dense	Gravel Sand	35	114.8 (2.4)	50	12.0 (250)

* The parameters listed in this table are intended as guideline only. Where detailed information such as in situ cone tests, strength tests on high quality samples, model tests, or pile driving performance is available, other values may be justified.

**Sand-Silt includes those soils with significant fractions of both sand and silt. Strength values generally increase with increasing sand fractions and decrease with increasing silt fractions.

For piles in cohesionless soils, the unit end bearing, q_p is compared by

$$q_p = \sigma_{0t}' N_q , \quad (2.10)$$

where

σ_{0t}' = vertical effective overburden pressure at the pile toe, and

N_q = dimensionless bearing capacity factor (Table 2.1).

Limiting values of σ_{0t}' are also given in Table 2.1.

2.3.2 Coyle and Castello Method (1981)

Coyle and Castello (1981) estimate the side resistance of piles driven in sand from Fig. 2.2 using the angle of internal friction of the sand, ϕ , and the ratio of the pile's embedded depth, L , to its width, D . Coyle and Castello (1981) recommend that the angle of internal friction, ϕ , be obtained from Fig. 2.3, the correlation given by Peck et al. (1974) for the number of blows N (from the SPT) vs. ϕ . In the case of silty sands below the water table, Coyle and Castello recommend that N -values from the SPT in excess of 15 be corrected to a value termed N' with the following expression and than N' be used in place of N in Fig. 2.3.

$$N' = 15 + 0.5 (N - 15). \quad (2.11)$$

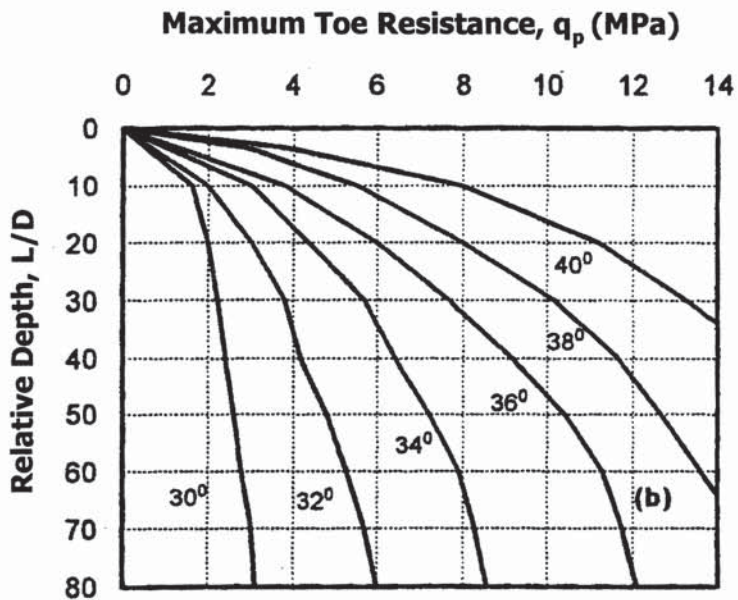
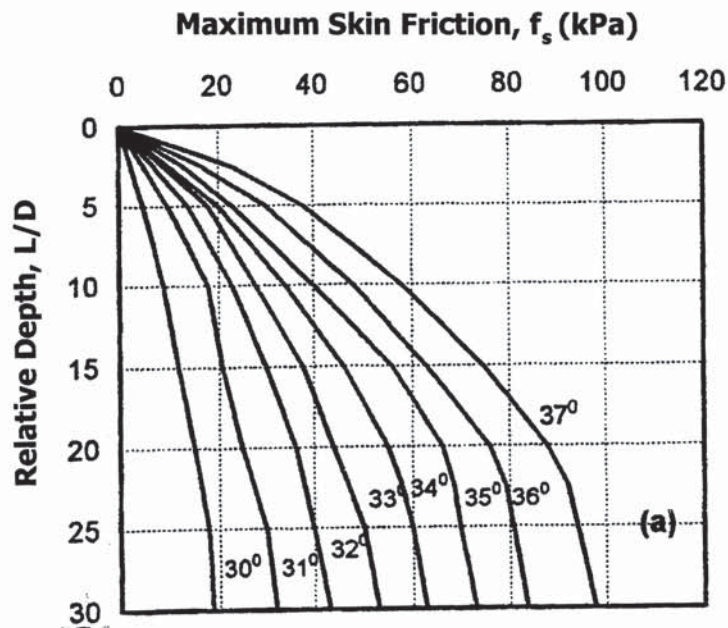


Fig. 2.2. Coyle and Castello's Pile Capacity Versus Friction Angle and Embedment: (a) Maximum Unit Skin Friction Versus Embedment (b) Maximum Unit End Bearing Versus Embedment (Coyle and Castello, 1981)

Copying Error

Go to the



next page (# 24)

From Fig. 2.2 (a) the average unit skin friction along the pile can be obtained from ϕ and L/D . The unit end bearing q_p , at the pile toe is estimated from Fig. 2.2 (b) as a function of L/D and ϕ of the soil at the toe, where the maximum toe resistance should not exceed 9.58 MPa (100 tsf) for driven piles founded in sand.

In the case of clays Coyle and Castello (1981) recommended the use of Tomlinson's method (1957) where the average unit side resistance, f_{sa} , is given by

$$f_{sa} = \alpha s_{ua} , \quad (2.12)$$

The α -factor, which varies between 0.2 to 1.0, is given in Fig. 2.4 as a function of the average undrained shear strength, s_{ua} , of the clay layer along the pile.

The end bearing capacity, q_p , is given by

$$q_p = 9 s_u , \quad (2.13)$$

where

s_u = the undrained shear strength of the clay layer at the toe.

Note that the limiting unit end bearing values in both the API and Coyle and Castello methods in cohesionless soils are associated with driven piles, in which the soil below the pile toe is compacted and highly stressed after driving. It is likely that the true limiting values for ACIP piles are much smaller.

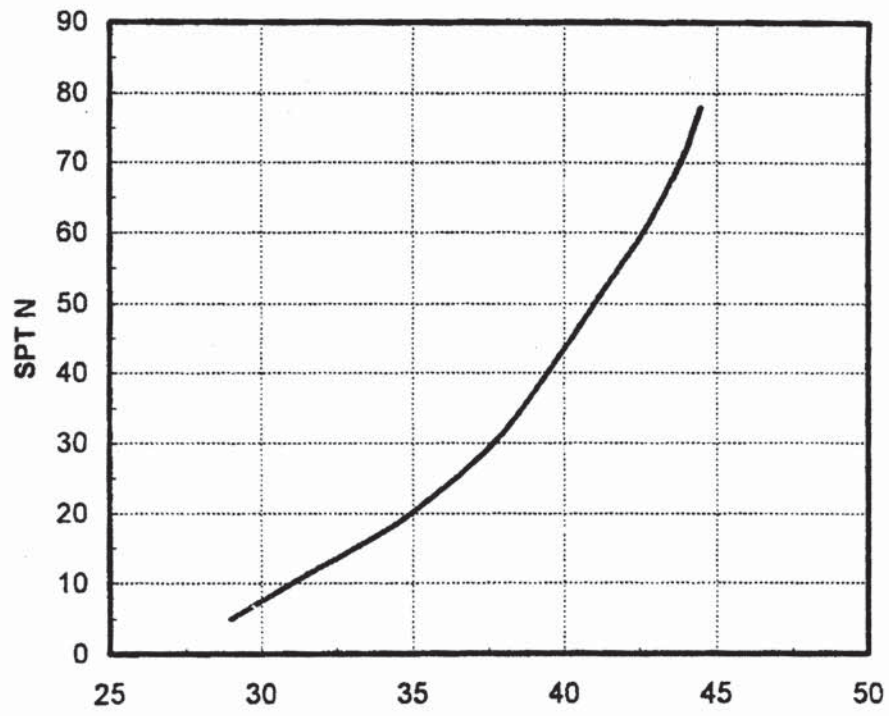


Fig. 2.3. Correlation between Angle of Internal Friction, ϕ , and Standard Penetration Test N Value (After Peck et al., 1974)

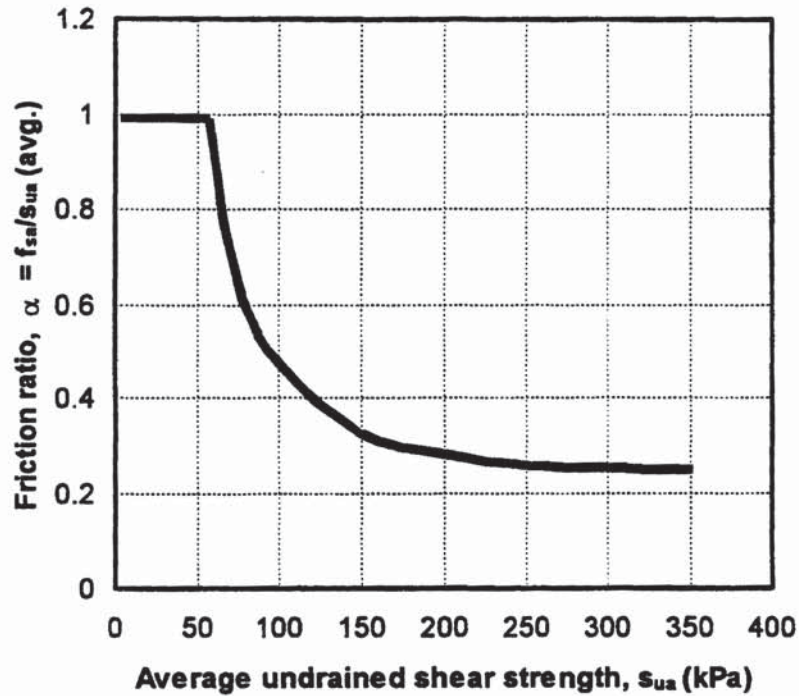


Fig. 2.4. α Factor Versus Undrained Shear Strength of Clay, per Tomlinson (Coyle and Castello, 1981)

2.3.3 FHWA Method (O'Neill and Reese, 1999)

O'Neill and Reese (1999) developed a design procedure for drilled shafts using an extensive database of drilled shaft loading tests in both cohesive and cohesionless soils.

Cohesive Soil

At a given depth z along the pile (midpoint of a soil layer), the unit side resistance (f_{max}) for a pile in the layer of cohesive soil is given by

$$f_{\max} = 0.55s_{uz} , \quad (2.14)$$

where

s_{uz} = undrained shear strength of the soil at depth z .

The unit end bearing resistance for piles in cohesive soils is determined as

$$q_{\max} = N_c s_u , \quad (2.15)$$

where

N_c = a bearing capacity factor taken as 9, and

s_u = the undrained shear strength of the soil in the vicinity of the pile's toe.

Cohesionless Soil

At a given depth z along the pile (midpoint of a soil layer), the unit side resistance for a pile in the layer of granular soil is given by

$$f_{\max z} = K_z \sigma'_{vz} \tan \delta_z = \beta_z \sigma'_{vz} , \quad (2.16)$$

where

K_z = coefficient of lateral pressure at depth z ,

σ'_{vz} = vertical effective stress in the geomaterial at depth z ,

- z = depth below the ground surface,
 δ_z = friction angle between concrete and soil at depth z , and
 $\beta_z = K_z \tan \delta_z$.

In cohesionless soils,

$$\beta_z = 1.5 - 0.245 [z (m)]^{0.5} \text{ for } SPT N_{60} (\text{uncorrected}) \geq 15B / 0.3m (B\text{-ft}) , \quad (2.17)$$

or

$$\beta_z = [N_{60}/15] \{1.5 - 0.245 [z (m)]^{0.5}\} \text{ for } SPT N_{60} (\text{uncorrected}) < 15B/0.3 m (B/ft) . \quad (2.18)$$

The unit toe resistance, q_{max} , is based on the N_{SPT} value from the in-situ SPT at the toe of the pile, according to the following equations:

$$q_{max} (kPa) = 57.5 N_{SPT} \leq 2.9 MPa , \quad (2.19a)$$

$$q_{max} (tsf) = 0.6 N_{SPT} \leq 30 tsf . \quad (2.19b)$$

The above equations (2.19a) and (2.19b) are only applicable to cohesionless soil $[N_{SPT} \leq 50B / 0.3 m (B/ft)]$.

2.3.4 German Standard (Rizkallah, 1988)

According to Rizkallah (1988), the German standard for estimating capacity of ACIP piles does not distinguish between bored piles and ACIP piles. DIN 4014 (1987) specifies computations based on the tip resistance, q_c in the cone penetration test, as follows:

Cohesionless Soil

$$f_{max} = 0.008 q_c , \quad (2.20)$$

$$q_{0.05} (MPa) = 0.12 q_c + 0.1 (q_c \leq 25 MPa) , \quad (2.21)$$

where

f_{max} = the maximum unit side shearing resistance on the pile, which has the nominal diameter of the auger, and

$q_{0.05}$ = the unit end-bearing corresponding to a movement of 5 percent of the pile diameter.

Note that the ultimate axial capacity of the pile is equal to the net unit base capacity $q_{0.05}$ times the base area, plus the unit shaft capacity f_{max} times the shaft area.

Cohesive Soil

$$f_{max} (MPa) = 0.02 + 0.2 c_u \quad (0.025 \leq c_u \leq 0.2 MPa) , \quad (2.22)$$

$$q_{0.05} = 6 c_u \quad (0.025 \leq c_u \leq 0.2 \text{ MPa}) , \quad (2.23)$$

where the undrained shear strength c_u is given by the following Equation (2.24).

$$c_u = \frac{q_c - \sigma_{vz}}{16 - 22} , \quad (2.24)$$

where

σ_{vz} = the total vertical stress at the elevation of the bottom of the pile.

Presumably, c_u could also be determined conservatively from unconfined compression tests, with $c_u = 0.5 q_u$ where q_u = unconfined compression strength. This method is typical of other methods used currently in Europe.

Rizkallah compared the results of axial loading tests from a large database and concluded that the above formulae were accurate for prediction of capacity of "nondisplacement" ACIP piles and were conservative for predicting capacity of "displacement type" screw piles.

2.3.5 TxDOT Method for Drilled Shafts (Houston District, 1972)

Cohesive Soils

- **Side Resistance**

The TxDOT-Houston District design method for drilled shafts was used as a candidate design method. The side resistance is based on the undrained shear strength of the soils penetrated and the perimeter and the length of the drilled shaft. The length of the drilled shaft is therefore selected to be a function of its diameter, the design load and the shear strength of the various soil strata penetrated. The undrained shear strength is determined by laboratory unconfined and/or undrained triaxial compression tests.

The TxDOT-Houston District method for drilled shafts implies an ultimate unit side resistance at depth z (center of a layer), $f_s(z)$, according to

$$f_s(z) = 0.7 s_u(z), s_u \leq 120 \text{ kPa (1.25 tsf)} , \quad (2.25)$$

$s_u(z)$ is half of the compression strength of the soil at depth z (representing a layer of thickness Δz). TxDOT-Houston District ordinarily uses an allowable stress design approach and applies a factor of safety of 2.0 to obtain an allowable unit side resistance value from this equation. Therefore,

$$Q_s(\text{allowable}) = \frac{1}{2} \pi D \sum f_s(z) \Delta z , \quad (2.26)$$

where the summation is carried out over all clay layers (i) in the soil profile and

$Q_s(\text{allowable})$ = allowable side resistance in the clay layers,

$f_s(z)$ = ultimate unit side resistance at depth z (representing clay layer i), and

Δz = thickness of clay layer i.

When the surface soil layer is clay, $f_s(z)$ is taken as zero to a depth of 1.5 m (5 ft), mainly in consideration of the fact that clay soils shrink away from the heads of the piles if they are unprotected from the atmosphere.

- **Toe Resistance**

The TxDOT-Houston District design method uses the blow count from a TxDOT dynamic cone penetrometer (N_{TxDOT}) and a net allowable end bearing resistance of $N_{\text{TxDOT}}/16.5$ (tsf) in stiff clay and sand-clay mixtures and uses a presumptive upper limit for allowable toe resistance in such clay soils [q_p (allowable)] of 0.19 MPa (2.0 tsf) when the pile diameter is less than 0.61 m (24 in). The equations for the allowable toe resistance that were used were

$$q_p (\text{allowable}) = 0.19 \text{ MPa (2 tsf)} , \text{ or} \quad (2.27a)$$

$$Q_p (\text{allowable}) = q_p (\text{allowable}) A_p . \quad (2.27b)$$

Assuming that the allowable value of unit end bearing is based on a factor of safety of 2, which is the usual practice in the Houston District,

$$Q_p (\text{ultimate}) = 2 Q_p (\text{allowable}) . \quad (2.28)$$

Cohesionless Soils

Generally, the TxDOT design method is based upon visual soil classification and the TxDOT dynamic cone penetrometer test. If the TxDOT penetrometer test gives N_{TxDOT} values less than 45 blows per 0.3 m (1 ft) without increase in the number of blows for the last 0.15 m (6 in.), the sand is reasonably dense, and the higher the value of N_{TxDOT} the better the material is in end bearing.

- **Side Resistance**

The value for the allowable unit side resistance, $f_s(z)$ (allowable), for each sand layer in the profile is determined for the average value of N_{TxDOT} for the layer using Equation (2.29).

$$f_s(z) \text{ (allowable) (tsf)} = 0.7[N_{TxDOT}/80], N_{TxDOT}/80 \leq 1.25 \text{ (120 kPa)} . \quad (2.29)$$

The ultimate side resistance $f_s(z)$ is then given by

$$f_s(z) = 2 f_s(z) \text{ (allowable)} . \quad (2.30)$$

Q_s (allowable) for all sand layers in the profile is then computed using Equation (2.26) with the $f_s(z)$ values from Equation (2.30).

- **Toe Resistance**

The allowable unit toe resistance of the piles with toes in sand is computed from Equation (2.31). As with toes in clay, a 0.19 MPa (2.0 tsf) limit is applied.

$$q_p \text{ (allowable) (tsf)} = N_{TxDOT} / 11 \leq 2.0 \text{ (0.19 MPa)} \quad (2.31)$$

Assuming that the allowable value of unit end bearing is based on a factor of safety of 2, which is the usual practice in the Houston District, Q_p (ultimate) for sand layer can be calculated using Equations (2.27b) and (2.28).

2.3.6 Wright and Reese Method (1979)

Wright and Reese (1979) presented a design method for predicting the ultimate capacity of drilled shafts in sand, which can presumably be applied to ACIP piles. The average unit side resistance is given by

$$f_{sa} = P_0' K_s \tan \phi \leq 0.15 \text{ MPa (1.6 tsf)} , \quad (2.32)$$

where

P_0' = average vertical effective stress along the pile (or the effective stress at the center of the pile),

K_s = lateral earth pressure coefficient (taken by Wright and Reese as 1.1), and

ϕ = an angle of internal friction of the sand (using a weighted average angle of internal friction of each layer in a layered sand profile).

The ultimate unit toe resistance for the pile is given by

$$q_p \text{ (tsf)} = 2/3 N \leq 40 \text{ tsf} , \text{ or} \quad (2.33)$$

$$q_p \text{ (MPa)} = 0.064 N \leq 3.8 \text{ MPa} , \quad (2.34)$$

where N is the value from the standard penetration test (SPT) in blows/0.3 m (blows/ft) near the toe of the pile.

2.3.7 Decourt (SPT-T) Method (1993)

Decourt (1993) proposed a method for estimating the capacity of ACIP piles in residual silts from the maximum torque measured when twisting a standard split-spoon sampler after having been driven into the bottom of the sample borehole as per a normal standard penetration test (SPT), to remove the influence of the dynamic driving conditions in the normal SPT. Correlations with loading tests indicate that

$$f_{max} = f_{max} \text{ (SPT-T test)} , \quad (2.35)$$

$$q_b = 0.5K' N_{eq} , \quad (2.36)$$

where

K' = a soil factor [0.10 MPa for clays, 0.12 MPa for clayey silts, 0.14 MPa for sandy silts, and 0.20 MPa for sands (at the base of the pile)] and

N_{eq} = the average equivalent N value from the SPT-T (blows/0.3 m) test near the base of the pile, which can be taken as a dimensionless correlation factor. According to

Decourt, in residual silts, $N_{eq} = T/1.2$, where T is the torque (in kgf-m, units reported in Decourt's original publication) measured by twisting the SPT split-spoon sampler. For large bored piles and barrettes, Decourt suggests that the corresponding values from Equations (2.35) and (2.36) be halved [for unit shaft resistance, Equation (2.35)] and doubled [for base capacity, Equation (2.36)].

2.3.8 LPC Method (Bustamante and Gianeslli, 1981)

Bustamante and Gianeslli (1981) developed a design procedure for both driven and bored piles in cohesive and cohesionless soils. The procedure uses the results from the in situ cone-point resistance, q_c to calculate the side resistance and toe resistance capacities.

For ACIP piles Fig. 2.5 (a) is used to evaluate the unit side resistance for piles in cohesive layers, while Fig. 2.5 (b) is used to evaluate the unit side resistance for piles in cohesionless layers. The value of $f_s(z)$ is determined by interpolation between the two limiting curves in Fig. 2.5 (a) and Fig. 2.5 (b) based on the average q_c along the pile. The total ultimate side resistance capacity in layered soils can be calculated as

$$Q_s = \sum \Delta Q_{st} = \sum A_{si} f_{si} \quad , \quad (2.37)$$

where

ΔQ_{st} = side resistance for each layer i of the pile,

A_{si} = $\pi D \Delta L_i$, and

ΔL_i = length of the pile in layer i .

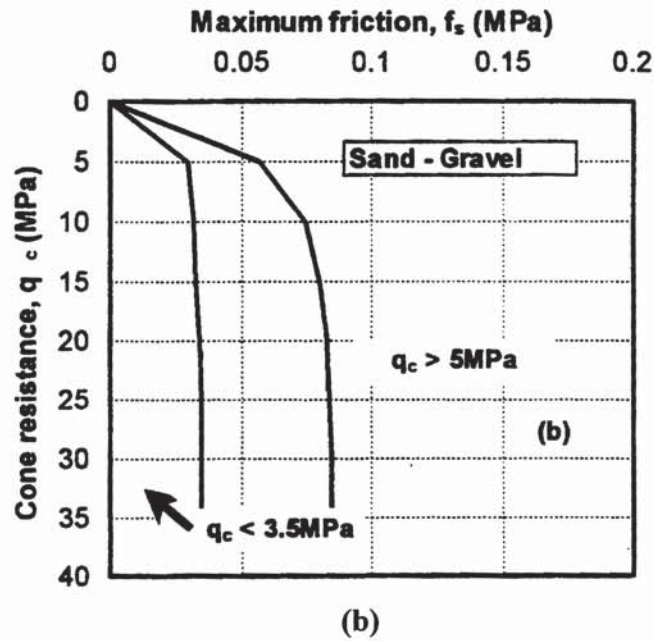
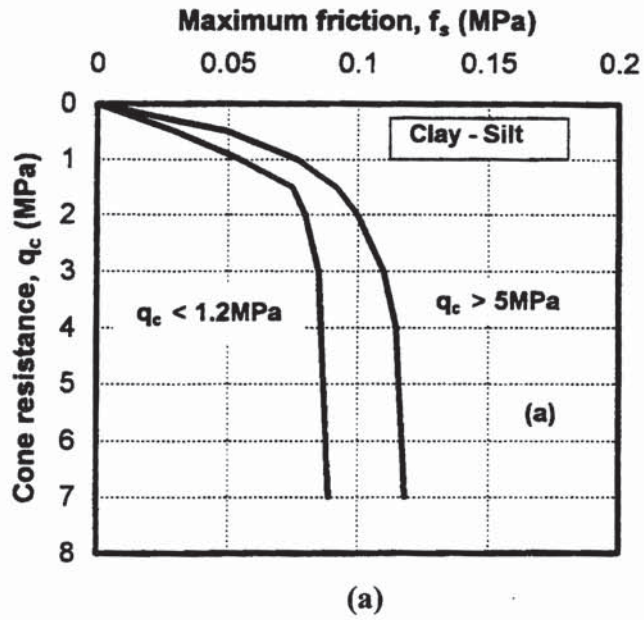


Fig. 2.5. Maximum Skin Friction Versus Cone Tip Resistance: (a) Cohesive Soil (b) Cohesionless Soil (Bustamante and Gianceselli, 1981)

The ultimate unit toe resistance, q_p , of a CFA pile by the LPC approach is given by the following expressions.

For cohesionless soils,

$$q_p = 0.15 q_c , \quad (2.38)$$

For cohesive soils,

$$q_p = 0.375 q_c . \quad (2.39)$$

2.3.9 Neely Method (1991)

Neely (1991) summarized the results from a database of 66 CFA pile tests in sand and established that the average unit side resistance can be computed by

$$f_{sa} = \beta P_0' \leq 0.135 \text{ MPa (1.4 tsf)} , \quad (2.40)$$

where

$$\beta = K_s \tan \delta ,$$

K_s = coefficient of lateral earth pressure (not necessarily equal to 1.1), and

δ = angle of friction at the pile-soil interface.

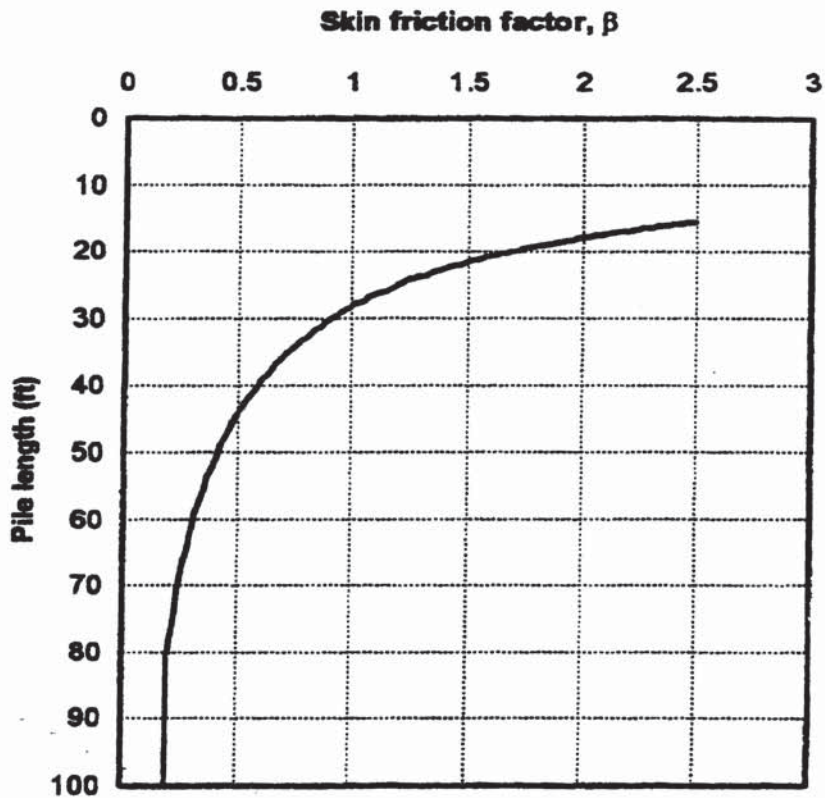


Fig. 2.6. Skin Friction Factor Versus Pile Length (Neely, 1991)

β was found to be dependent on the length of the pile, as shown in Fig 2.6. It is evident from Fig. 2.6 that the β factor decreases with increasing pile length and approaches a minimum constant value of 0.2 for pile lengths in excess of about 24 m (80 ft). Neely (1991) suggested limiting the maximum value of the average side resistance in Equation (2.40) to 0.135 MPa (1.4 tsf), which corresponds to the maximum value evaluated from the pile load tests considered in his study.

Using data from both compression and tension testing, Neely (1991) estimated the ultimate unit toe resistance from

$$q_p \text{ (tsf)} = 1.9 N \leq 7.2 \text{ MPa (75 tsf)} , \quad (2.41)$$

where

N = the number of SPT blows per 0.3 m (blows/ft) near the toe of the pile.

The unit toe resistance is limited to 7.2 MPa (75 tsf).

2.3.10 Viggiani Method (1993)

Viggiani suggests simple correlations for ACIP piles in cohesionless soils, based on pile-loading tests and corresponding cone penetration tests in the Naples, Italy, area, where the soils are volcanic in nature (mostly pyroclastics):

$$f_{max} = \alpha q_c , \quad (2.42)$$

$$q_b = q_{c \text{ avg } (+4d, -4d)} , \quad (2.43)$$

where

q_b = net ultimate unit-bearing capacity of the pile base,

$q_{c \text{ avg } (+4d, -4d)}$ = average CPT tip reading between 4 pile diameters above the base and 4 diameters below the base, and α = a correlation factor given by Equation (2.44).

$$\alpha = [6.6 + 0.32 q_c \text{ (MPa)}] / [300 + 60 q_c \text{ (MPa)}] \quad . \quad (2.44)$$

2.3.11 Discussion of Design Methods

Different design methods available in practice were reviewed by some researchers to adopt and/or adapt methods for ACIP piles based on analysis of load test database in local soils. O'Neill et al. (1999) concluded that the LPC method was the most accurate method among those examined for single ACIP piles entirely in clay profiles after comparison of seven different design methods with load tests in a database of ACIP pile load tests at sites along the Gulf Coast. The TxDOT (Houston District) method for drilled shafts, the second most accurate method, was recommend for use by TxDOT for ACIP piles in clay soil profiles because the LPC method requires the use of a static cone penetrometer to characterize the soil for design, which is not an exploration tool that is utilized by TxDOT. The method proposed by Reese and O'Neill (FHWA method, 1988) for drilled shafts was the most accurate for ACIP piles in sand profiles, and the method was reasonably accurate for ACIP piles in mixed soil profiles. The FHWA method, was therefore, recommended for use in sands and mixed soil profiles. The TxDOT-Houston District method was found to be less accurate but acceptable for ACIP piles in mixed soil profiles.

McVay et al. (1994) also evaluated the performance of 21 single ACIP piles constructed and load tested in Florida (primarily in sand) and used five different design methods to predict the pile capacities to compare with measured pile bearing capacities. After the comparison, they concluded that the FHWA method and the Wright and Reese method (1979) are the most accurate methods to predict the ultimate pile capacities.

Zelada and Stephenson (2000) studied 43 compression load tests, including five fully instrumented and ten pullout tests of ACIP piles in sand. Eight different design methods being used in practice were chosen to predict the ultimate pile capacities. After comparing predicted capacities by 8 different methods and measured capacities from the load tests, they concluded that the FHWA method (1988) for drilled shafts gave the best correlation for the computation of the ultimate side friction resistance, and that Coyle and Castello (1981) (for driven piles) and Neely (1991) (for ACIP piles) gave the best correlations for the computation of the ultimate end bearing capacity for ACIP piles. They suggested new unit capacity correlations by applying a coefficient of 0.8 to Reese and O'Neill's β factor equation and lowering Neely's end bearing capacity correlation from $q_b = 1.9 N$ to $1.7 N$, where N is the number of blows per 0.3 m penetration for a Standard Penetration Test, to estimate ACIP pile capacity as shown below.

$$q_b = 1.7 N \leq 75 \text{ tsf} , \text{ or} \tag{2.45a}$$

$$q_b = 0.163 N \leq 7.2 \text{ MPa} . \tag{2.45b}$$

All of the design methods considered here are generally mean value methods, except for the FHWA method for sand, which is a near-lower-bound method. This means that the true capacity is as likely to be lower than the computed capacity as it is to be higher than the computed capacity. Selection of appropriate factors of safety in an allowable stress design (ASD) format, or resistance factors in a load and resistance design (LRFD) format, therefore requires knowledge of the coefficient of variation of the ratio

of measured to computed capacity from a given design method and the selection of a target reliability index. O'Neill et al. (1999) concluded from their data base that a factor of safety of 2.4 is needed to assure a reliability index of 3 for ACIP piles in mixed sand-clay profiles, typical of the Houston area, using the FHWA design method for drilled shafts for bridge foundations with dead to live load ratios exceeding 1.25. A reliability index of 3 corresponds to a probability of failure of 0.0013, which is acceptable in a pile foundation where redundancy exists (i. e., where the piles are installed in groups) and where quality assurance procedures will be employed that will rule out blunders in construction.

2.4 Construction Issues

Potential construction problems have been identified in the past that may produce relatively large settlement of adjacent structures and adversely influence the integrity of piles due to disturbance of the surrounding soil in the process of ACIP pile installation and improper placement of grout. Cutter and Warder (1998) and Esrig et al. (1991; 1994) have discussed the disturbance to the soil during the installation of ACIP piles. The extent and significance of this disturbance depend on the soil and ground water conditions, the method of pile installation and the sensitivity of the surroundings. Construction problems have occurred mostly when the ACIP piles are installed in granular soils below the ground water level. Kenny and Andrawes (1997) presented a paper on soil mining by allowing the auger to be rotated without vertical penetration during ACIP pile installation in sand. They indicated that the risk is considered to be greatest when ACIP piling is installed in loose cohesionless soils. Thorburn et al. (1993)

stated that ACIP piling in sandy soils resulted in the subsidence of adjacent structures. Van Impe (1988), Van Weele (1988), and Cutter and Warder (1998) clearly indicated that installation of ACIP piles through loose to medium dense sandy soils below the ground water level can lead to significant over-excavation, subsidence of the ground surface, and settlement of adjacent structures. Evidence of this effect in the soils at a specific construction site will be investigated in this study.

The primary causes of significant over-excavation, subsidence of the ground surface, and settlement of adjacent structures during ACIP pile installation are discussed by the investigators cited above. The majority of construction problems seem to be associated with one or more of the following:

2.4.1 Drilling with “Underpowered” Rigs

“Underpowered” rigs whose torque is too low can lead to partial filling of the auger from the soil excavated by the bit at the tip of the auger and allow the partially filled auger flights to accept loosened soil from the sidewalls and transport such soils up along the auger to the surface, leaving room for more soil to fill the auger and be transported upward. This effect results in decompression and removal of the soil surrounding the pile and consequent loss in pile capacity (“mining”). According to Cutter and Warder (1998) decompression and consequent loss in pile capacity can be minimized [but by no means eliminated] by specifying a drilling rig with a minimum torque of 27 kN-m (20,000 ft-lbs) with a torque converter that allows for the use of the highest torque at a slow rotational speed. The rig with this minimum torque is the most common rig used presently by current U.S. contractors in ACIP piling.

Hassan et al. (1997) provided a simple formula that describes whether the torque is adequate to prevent mining of soil by relating the rate of penetration to rate of rotation for an auger of a given design. The rate of vertical penetration V needed to avoid the potential for mining of clean, waterbearing sand is related to the rotational velocity of the auger through Equation (2.46).

$$V \geq N p (1 - d_o^2 / d^2) , \quad (2.46)$$

where N is the rate of rotation of the auger (rpm); p is the pitch of the auger (pitch length per turn), d_o is the outside diameter of the stem of the auger, and d is the outside diameter of the auger from tip to tip of the auger flights.

O'Neill et al. (1999) measured average auger penetration rates, V_m , of approximately 2.5 m / min. and auger rotation rates, N , of about 50 rpm in a variety of Houston area soils with a rig having a torque capability of 51.5 kN-m and standard CFA pile augers ($d_o = 99$ mm, $d = 457$ mm, $p = 260$ mm). $V_m / V = 0.20$ on the average, indicating that even rigs with torques higher than 27 kN-m can potentially produce mining in clean, waterbearing sands.

2.4.2 Inappropriate Installation Procedures

One of the most common procedures leading to decompression of the soil, the subsidence of the ground surface, and/or the movement of adjacent structures is extracting the auger before pumping the grout to the bottom of the borehole with adequate pressure and/or failure to retain adequate grout head in the borehole while the

auger is being withdrawn. A related problem is withdrawal of the auger at a rate that exceeds the rate of rise in head of the grout in the borehole at any time during the installation process. This effect can produce piles that have deep necks or are completely separated along their lengths. These types of problems can be minimized by continuously monitoring the incremental volume of the supplied grout and grout pressure (O'Neill et al., 1999).

2.4.3 Penetration of a Hard Refusal Layer

As the bit at the bottom of the auger penetrates rock or hard material like glacial till, the rate of penetration slows, resulting in overrotation (O'Neill et al., 1999). This can lead to the same problems as when “underpowered” rigs are used.

2.4.4 Lateral Stress Relaxation

The risk of soil decompression and overexcavation is significantly increased when ACIP piles are installed where the soil is in a state of high lateral stress. This problem can occur if the ACIP piles are installed in the soil at the toe of a slope, in front of an earth retaining structure, or adjacent to high capacity bulb piles such as Franki piles, which produce high lateral stress in the soil (O'Neill et al., 1999).

2.4.5 Installation in Non-Saturated Soil

O'Neill et al. (1999) noted that cages for ACIP piles were difficult to thrust into fluid grout at a site where the soil to the full depth of the pile consisted of moist (but unsaturated) sand. This observation suggested that the unsaturated soil temporarily had a

higher water demand (suction potential) than the fluid grout and rapidly removed water from the fluid grout, causing the viscosity of the grout to increase more rapidly than if the pile had been installed in saturated soil. The limiting depth to which reinforcing cages could be thrust under such circumstances was about 9 m (30 ft). This observation suggests that designers should use ACIP piles in such soils only when structural considerations do not require full reinforcing cages that penetrate deeper than about 9 m (30 ft).

2.5 Quality Control

It is widely recognized that the integrity of an ACIP pile is highly dependent on the skill and experience of the contractor (Booth and McIntosh, 1994; O'Neill, 1998). Quality control during ACIP pile installation is crucial to the success of an ACIP pile project. As a minimum, the grout supply ratios and grout pressures along the piles should be monitored to assure the quality of the piles during the grouting phase of installation.

2.5.1 Grout Ratio

Gout supply ratio, or simply “grout ratio” (total grout volume pumped divided by theoretical volume of the borehole) is often used as a means of confirming the pile integrity. Booth and McIntosh (1994) concluded that a grout ratio of 1.3 or less for stiff and hard cohesive soils or dense sands and 1.7 or more for porous limestones, soft clays, gravels, or very loose sands would be generally expected. In addition, an overall grout ratio less than about 1.10 may indicate a problem and would be considered as defective piles.

Lacy (1998) suggested some performance criteria for CFA pile construction. The continuous integrity of CFA piles should be controlled by monitoring the incremental volume of grout pumped for each 1.5 m of auger withdrawal and that 1.10 to 1.15 times the neat volume of the auger hole needs to be pumped for each increment of auger withdrawal. It is more successful for pile installation if the auger is withdrawn slowly instead of removed more quickly in interrupted increments. In order to avoid significant soil compression due to the large amount of soil being raised to the ground surface on the auger flights high-torque, low-speed augers need to be used. Using these methods, the number of auger rotations used per unit of penetration equal to the auger pitch has at some sites been reduced from 20 to 2, significantly reducing the volume of soil removed from the borehole but also requiring rigs with higher torque (more expensive foundations).

McVay et al. (1994) evaluated the performance of 21 CFA piles constructed and load tested primarily in sand sites in Florida. For the pile installation, they concluded that the construction parameters that had the greatest influence on axial capacity were the rate of penetration, grout fluidity, grout pumping pressures and rates, and the rate of extraction of the auger. McVay et al. (1994) recommended that (a) the pitch of the auger be reduced to one-half of the auger's outer diameter, (b) the grout pressure be monitored and maintained as the auger is being withdrawn, and (c) the grout ratio be monitored to show that it is 1.2 to 1.5 times the neat volume of the borehole. It is observed that the recommendations that McVay et al. and Lacy et al. made are quite different concerning the grout ratios. This reflects differences in the geological environments in which the two investigators worked. O'Neill et al. (1999) also recommended that the grout ratio be

at least 1.2 for typical subsurface conditions in the Houston/Texas Gulf Coast area. O'Neill et al. (1999) suggested that the monitoring of incremental grout placement be conducted by means of flowmeters instead of manual counting of pump strokes.

2.5.2 Grout Pressure

Maintenance of insufficient lateral stress in the soil may be accompanied by inward movement of the soil and loss of ground, which can be detrimental to adjacent structures, and maintenance of concrete or grout pressures lower than the total soil pressures beneath the extracting auger may lead to necking and structurally defective piles (O'Neill, 1994). Grout pressures should be monitored in grouting phase of the pile installation in addition to monitoring incremental grout takes.

Leznicki et al. (1992) presented a case describing the installation of about 200 ACIP piles. After installation of the first 19 ACIP piles, a large settlement of the ground surface occurred due to the over-rotation during the augering operation. In order to minimize the settlement, revised technical procedures were adopted. In the new technical procedure, the systolic grout pressure was kept above 1725 kPa (250 psi). Hassan et al. (1997) recommended, from a slightly different perspective, that the diastolic grout pressure, measured at the ground surface, be at least equal to the estimated vertical total stress in the ground at the depth of the discharge orifice on the ACIP auger.

Note that the pressure in the grout at the outlet orifice at the bottom of the auger should ideally be equal to or greater than the total pressure in the ground (vertical or horizontal, whichever is greater), so that the appropriate place to measure the grout pressure is at the tip of the auger. However, no practical tool has been developed to do

this, so systolic pressure (and/or diastolic pressure) at the level of the grout pump (on the ground surface), which can be monitored with electronic pressure transducers, is used as a semi-empirical surrogate. Most current design criteria require systolic pump pressures at the ground level to be from 1035 to 1725 kPa (150 to 250 psi) and that, in addition, at least 4.5 m (15 feet) of grout head be maintained in the flights of the auger at all times. The latter criterion can be verified, in part, visually by noting the depth of the auger tip at the time grout return is seen at the surface.

2.5.3 Non destructive Testing (NDT)

The purpose of NDT in ACIP pile construction is to ensure that the completed pile is constructed without voids or necks that might have been caused by poor construction controls. As such, it is more properly called a quality assurance technique than a quality control technique. The probability of such defects being produced in an ACIP pile during placement of grout where the grouting operation has been monitored by automated measurement of incremental grout take and pressure is very small. However, ACIP piles for bridge foundations require that large reinforcing cages be thrust into the grout immediately after grouting. It is possible that insertion of the cage could produce defects, especially if such action is performed as the grout is beginning to set. Only a post-construction NDT has the capability of identifying such defects.

Two types of NDT procedures have been used for ACIP piles in recent practice.

Low-Strain Integrity Testing

Low-strain integrity testing is performed by impacting top of a pile using a hand-held hammer, which generates compressive stress waves in the pile (Rausche et al., 1994). An accelerometer is attached to the top of the pile to measure the resulting pile top motion caused by wave reflections as a function of time after impact. Pile top acceleration data are collected and integrated to obtain pile top velocity as a function of time. Early reflections of the compressive waves are an indication of a change in the pile cross-section and a possible defect. Variations of low strain integrity testing include the pulse echo method, the transient response method, and the impedance profile analysis (Roberts, 1998). The impedance profile is virtually the only way to estimate the shape of the pile after construction, provided it can be established that the Young's modulus of the pile material does not vary, which may be useful for interpretation of strain gauge data.

The main advantage of this type of testing is that it is very simple, quick and inexpensive. It is possible that many production piles can be tested in a day. The pile surface (head) must be smooth enough on which to mount the accelerometer securely. However, there are also some limitations. The main limitation of this testing is that at least 7 days need to elapse after installation in order for sufficient grout stiffness to develop to obtain data down to the pile toe. Long slender piles with penetration length to diameter ratios more than 30 may not be fully evaluated if the impact wave reflection from the pile tip is not evident. In general, this testing is best applied to piles with penetration length to diameter ratios below about 30. Piles with multiple or highly varied cross section changes and/or located in highly layered soil profiles, which affect the wave reflections, may be difficult to interpret.

Sonic Integrity Testing

Sonic Integrity Logging is another NDT method to evaluate the structural integrity of an ACIP pile. Generally, the method requires the placement of one or more access tubes during construction of the pile. Single-hole sonic logging (SSL) and crosshole sonic logging (CSL) techniques have been used. The type of sonic integrity logging is selected depends on the diameter of the pile and to a limited extent on the site soil conditions. The sonic integrity testing is ordinarily conducted after the grout has hardened; however, some researches in Asia and in the United States [Brettmann and Frank (1996) and Brettmann et al. (1996)] have suggested that accurate detection of defects in the grout can be made while the grout is still unset using a single-tube ultrasonic device, providing the contractor a second chance to remove the grout and reinstall the pile if a defect is detected.

- **Single-Hole Sonic Logging (SSL)**

A single tube (usually PVC pipe) is placed on the reinforcing cage using standard tie wire. Then, the tube is filled with water to provide additional weight. The water also acts to reduce expansion and shrinkage due to temperature effects so as to provide acoustic coupling to the grout. The tension reinforcing steel and the transmitter and receiver probes are lowered down the central PVC pipe after initial grout set and the transit time and strength of the ultrasonic pulse through the pile material between the probes is measured and recorded on a data acquisition system. A vertical profile of the signal transit time and signal strength is obtained by recording a continuous series of measurements along the full length of the pile (Roberts, 1998). Changes in the recorded

signal travel time and signal strength can readily identify the presence of non-uniformities in the pile shaft such as soil inclusions and voids (Roberts, 1998). SSL is most appropriate for ACIP piles with diameters of 0.61 m (24 in.) or less. SSL should be performed within 3 days of pile installation due to the potential for the grout to debond from the PVC access tube (Roberts, 1998).

- **Cross-Hole Sonic Logging (CSL)**

Two or more Schedule 40 steel access tubes are placed on the reinforcing cage using standard tie wire. The pipes are filled with water - the same as with SSL testing. The reinforcing cage and the water-filled access tubes are then inserted into the grout while it is still fluid. Ultrasonic transmitter and receiver probes are lowered down separate steel access tubes after initial grout set. With the probes at the same depth, the transit time and strength of the ultrasonic pulse through the pile material between adjacent access pipes is measured and recorded on a data acquisition system. Vertical profiles of the signal transit time and signal strength are obtained by recording a continuous series of measurements between each of the adjacent access tubes. Changes in the recorded signal travel time and signal strength similar to the SSL technique can readily identify the presence of non-uniformities in the pile shaft such as soil inclusions and voids. CSL is most appropriate for ACIP piles with diameters 0.61 m (24 in) and larger (Roberts, 1998). The number of recommended access pipes increases with the pile diameter. Ordinarily, in drilled shafts, one tube is used for each foot (0.3 m) of shaft diameter (O'Neill and Reese, 1999).

2.6 Performance of ACIP Piles as Bridge Foundations

Few comprehensive studies have been performed regarding long-term performance of piles as bridge foundations. No literature on the long-term performance of ACIP piles as bridge foundations, either in United States or Europe, could be found. A few papers were found on the performance of driven piles and drilled shafts used in combination with mats (i. e., piled rafts) as bridge foundations. Two such case studies are summarized as follows in order to indicate experiences with load sharing between piles and caps (rafts), which will be one issue in the project described herein. In addition, there was a literature on the long-term performance of drilled shaft as a bridge foundation. This is an example of long-term performance monitoring. However, it was not very successful because of electrical drift and lack of accuracy in the strain gauges. This case study is summarized followed by above two cases.

2.6.1 Bridge over the Rivers Garigliano and Ausente, Italy (Mandolini et al., 1992; Russo and Viggiani, 1995)

The central pier (No. 7) of a cable-stayed bridge over the rivers Garigliano and Ausente was instrumented and observed. The cable-stayed bridge is located in the outer part of the alluvial plain of the river Garigliano (Italy). The soils at the site have been deposited under a coastal marsh environment. The subsoil consists of normally consolidated or slightly overconsolidated silty and sandy clays with substantial organic content down to a depth exceeding 50 m, where a sand and gravel base is located. Pockets and lenses of sand and peat horizons are scattered within the clay deposit. The ground water table is found a few meters below the ground surface.

A rectangular group of 9 x 16 piles arranged in a square grid with a spacing of 1.2 m axis to axis was installed. Closed-end steel tubular driven piles were installed, and reinforcing cages in the upper 12 m were inserted after filling the piles with concrete. The piles, 356 mm in outer diameter, 6 mm in wall thickness, and 24 m in length, were used as foundations of the bridge. The plan dimensions of the raft (pile cap) are 10.8 m X 109.2 m. The thickness of the cap is 4.0 m at the center, decreasing to 2 m at the edges of the shortest sides.

Thirty-five piles out of 144 were instrumented with vibrating wire load cells for recording the load on the head of each pile, and the soil-raft contact pressure was recorded at 8 points with pressure cells. 24 of the 35 instrumented piles were in the same quarter of the pile group arrangement, and the other 11 were at different locations in the other three-quarters of the group.

Predicted and measured distribution of loads to piles and raft was compared. 92% of deck loads were recorded by piles over a construction period of about three years. Meanwhile, analyses by Russo (Russo and Viggiani, 1995) using an FE method described below predicted a range of pile load of 88 to 92 % of the applied deck load with upper and lower limits of Young's moduli for concrete. Russo used a comprehensive, approximate analysis method for pile-raft-pile interaction, with an FE model for the raft and coupled, interacting springs to represent the piles and supporting soil.

Total settlement of the piled raft was measured to be approximately 40 mm with an accuracy of 0.1 mm. Starting from the construction of the bridge deck, the measured settlement of the pier foundation was approximately 26 mm. The corresponding

predictions by Russo were in the range of 17 to 19 mm. No significant differential settlement was recorded.

2.6.2 Neuville-sur-Oise Bridge, Belgium (Van Impe and De Clercq, 1995)

The seven-span bridge is 337 m long. One of the central piers of the bridge not in the river, denoted "P4," was instrumented and observed. Bored piles, 1.0 m in diameter and 6.66 m in length, were used. The piled raft (cap) was rectangular with plan dimensions of 6.40 X 7.40 m and a thickness of 1.5 m. The subsoil at the site consists of loamy-sandy alluvium to a depth of about 7 m below the ground surface, below which was a layer of coarse sand. The ground water table was at the approximate elevation of the base of the raft.

A total of 36 Glötzl-type contact pressure cells were placed under the raft in order to obtain a precise contact pressure distribution. Twenty-nine vibrating wire strain gages were used to measure load in the bridge pier, in the piles and in the raft. Settlement points were also placed on the raft.

Under the full load of 11.63 MN, measurements indicated that 73 % of the applied load was carried by the piles, and 27 % was carried by the raft. The retrospective analysis summarized below predicted that about 76 % of the load would be taken by the piles and 24 % would be taken by the raft. An average settlement of the raft was recorded as 17 mm. The retrospective analysis predicted 18.4 mm. The predicted values by the retrospective analysis gave a good agreement with the measured values in load distribution between the piles and the raft as well as settlement.

The retrospective analysis of this bridge pier foundation consisted of the following. The piles were characterized as elastic cylinders in an elastic soil medium per the Randolph-Wroth model (Randolph and Wroth, 1978), with interaction factors based on the displacements in the soil mass computed at various distances radially away from the pile. This method was extended to conditions of layered soil along the shaft of the piles, nonlinear base response for each individual pile, a decay function for G/G_{\max} (where G is the soil shear modulus and G_{\max} is the soil shear modulus for very small strain) based on computed shear strain level, and an approximately modified influence radius for pile-soil-pile interaction. Raft-soil, raft-pile, and pile-raft interaction were accounted for using elasticity methods. For this case study the raft was considered rigid, so flexure of the raft did not need to be considered. The analysis method, however, is fully adaptable to rafts with finite rigidity.

2.6.3 Drilled Shaft Foundation at I-45 and I-610 Interchange in Houston, Texas (Wooley and Reese, 1974)

Drilled shaft in Bent 11, at the I-45 and I-610 interchange in Houston, Texas, where the soil profile consisting of a layer of over-consolidated clay, about 9.8 m (32 feet) deep, overlying a layer of sand, was instrumented with strain sensing devices such as Mustran cells and vibrating wire strain gauges in order to study load shedding behavior in the long-term shaft. Thirty-eight strain sensing devices were installed in the shaft. Twenty-six of these were Mustran cells and twelve were vibrating wire strain gauges for the study. It was concluded that load shedding was substantially absent at the site for the period of the test. However, it was not very successful because of electrical drift and lack

of accuracy in the strain gauges. Mustran cells generally performed satisfactorily appearing to remain stable over an extended period of time. However, vibrating wire strain gauges employed in this study did not possess sufficient reliability, sensitivity, or repeatability for the purpose of experiment. The lesson learned from this study was to use more reliable, stable, and accurate instrumentation system in monitoring long-term production piles along with the short-term test pile.

Advanced vibrating wire strain gauges and readout devices that eliminate precedent errors were available and employed to study the behavior and performance of ACIP bridge foundations in this project.

CHAPTER 3

SITE INFORMATION

3.1 Site Description

The ACIP pile foundation bridge site is located at Krenek Road on U.S. Highway 90 in Crosby, Texas, approximately 54 kilometers (35 miles) northeast of the University of Houston main campus. TxDOT has designed and constructed this new freeway bridge entirely on ACIP piles. This is the first such bridge in Texas and, to the knowledge of the author, in the United States.

The prestressed concrete driven pile foundation bridge site is located at Runneburg Road adjacent to Krenek Road along U. S. Highway 90 in Crosby, Texas. Runneburg Road bridge was structurally identical with Krenek Road bridge. Full-scale load tests were performed on both ACIP pile in Krenek Road and driven pile in Runneburg Road for comparative behavior of two different piles in nearly similar geotechnical condition. The load tests will be described in Chapter 8. The location of both Krenek and Runneburg Road bridge sites is shown in Fig. 3.1.

3.2 Site Conditions

3.2.1 Krenek Road Bridge Site

The Krenek Road bridge site consists of a mixed soil profile of generally stiff clays and medium dense sands. The site is located in the Beaumont formation, a

Pleistocene-aged deposit on the Texas Gulf Coastal plain where ACIP piles are well suited (O'Neill et al., 2002).

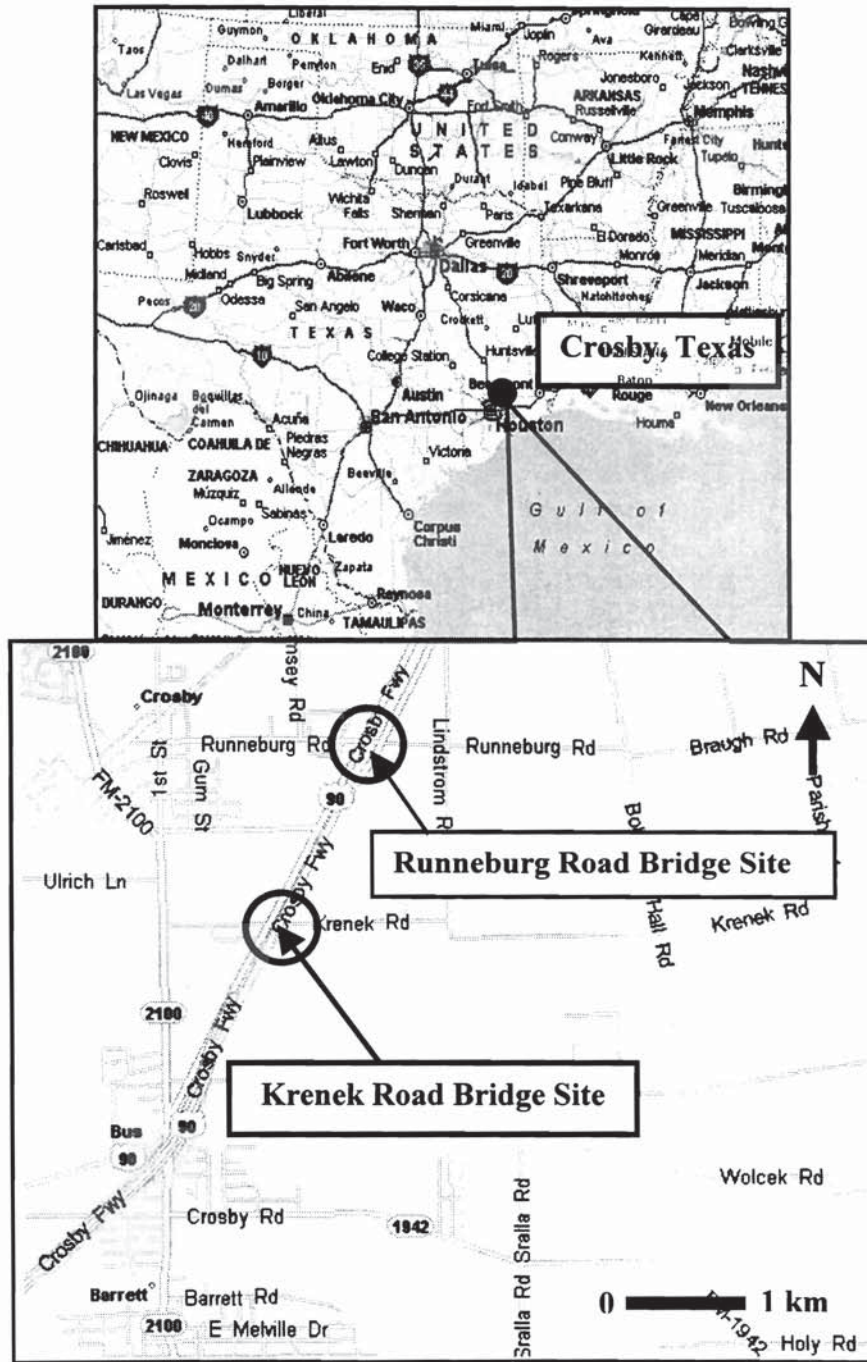


Fig. 3.1. Map of Krenek and Runneburg Road Bridge Sites

Four soil borings were carried out for design of ACIP piles and retaining walls by the TxDOT Houston District boring crew. Boring logs (KR-1 and KR-2) were used for ACIP pile design. Boring log 1 at Krenek Road (KR-1) is shown in Fig. 3.2 and was used for the project to define the soil conditions for instrumented test pile and production piles (central bent piles and abutment piles) on the south part of Krenek Road. N_{TxDOT} , N_{SPT} , undrained shear strength (s_u), unit weight (γ), plasticity index (PI), and soil classification are shown in boring log (KR-1). The other boring logs (KR-2 through KR-4) are attached in Appendix A. Fig. 3.3 shows the bridge layout that includes the boring locations.

The top layer is generally stiff and sandy clay to a depth of 2.1 m below the ground surface. Stiff clay layers were observed from 2.1 m to 12.8 m. A 1.5-m thick-layer of waterbearing, medium dense clayey sand was found from 12.8 m to 14.3 m. A layer of stiff clay was present from 14.3 m to 15.8 m. Below 15.8 m is a stratum of dense, fine and relatively clean waterbearing sand. The ground water level was about 1.5 m below the natural ground surface. The site was essentially flat, and very little net excavation or filling was needed, except for the approach fills (header banks), which were constructed of imported clay fill.

3.2.2 Runneburg Road Bridge Site

The Runneburg Road bridge site also had a soil profile of generally stiff clays with a few seams of medium dense clayey sand, which is geologically similar with Krenek site. However, stiff clay layers are predominant along the entire pile length and under the pile toe (unlike the Krenek site).

Depth m (ft)	Log	N _{TRDOT} blows/0.30 m	N _{SPT} blows/0.30 m	Avg. s _u kPa (psi)	Avg. PI	Avg. γ _t kN/m ³ (pcf)	Soil Classification		
1.5 (5)	▼	17		57.6 (8.4)	23.6	19.9 (127)	CLAY, stiff		
3 (10)		19		110.1 (16.0)	33.0	20.7 (132)			
4.6 (15)		17		87.2 (12.6)	41.0	19.4 (124)			
6.1 (20)		10							
7.6 (25)		23		108.3 (15.7)	37.1	20.2 (129)			
9.1 (30)		24							
10.7 (35)		32							
12.2 (40)		32							
13.7 (45)		40		Pile Toe at 13.2 m (43 ft) for Abutment Piles				20.7 (132)	SAND, clayey
15.2 (50)		22		84.2 (12.2)	45.9	19.1 (122)		CLAY, stiff	
16.8 (55)	100/0.11 m				SAND, very dense -clay seams				
18.3 (60)	39	Pile Toe at 18.9 m (62 ft) for Test and Central Bent Piles				SAND, slightly compact			
19.8 (65)	100/0.23 m				SAND, dense				
21.3 (70)	100/0.27 m	47							
22.9 (75)	67				SAND, compact				
24.4 (80)	35	22				CLAY, stiff			

Fig. 3.2. Soil Profile for Krenek Road Bridge Site (KR-1)

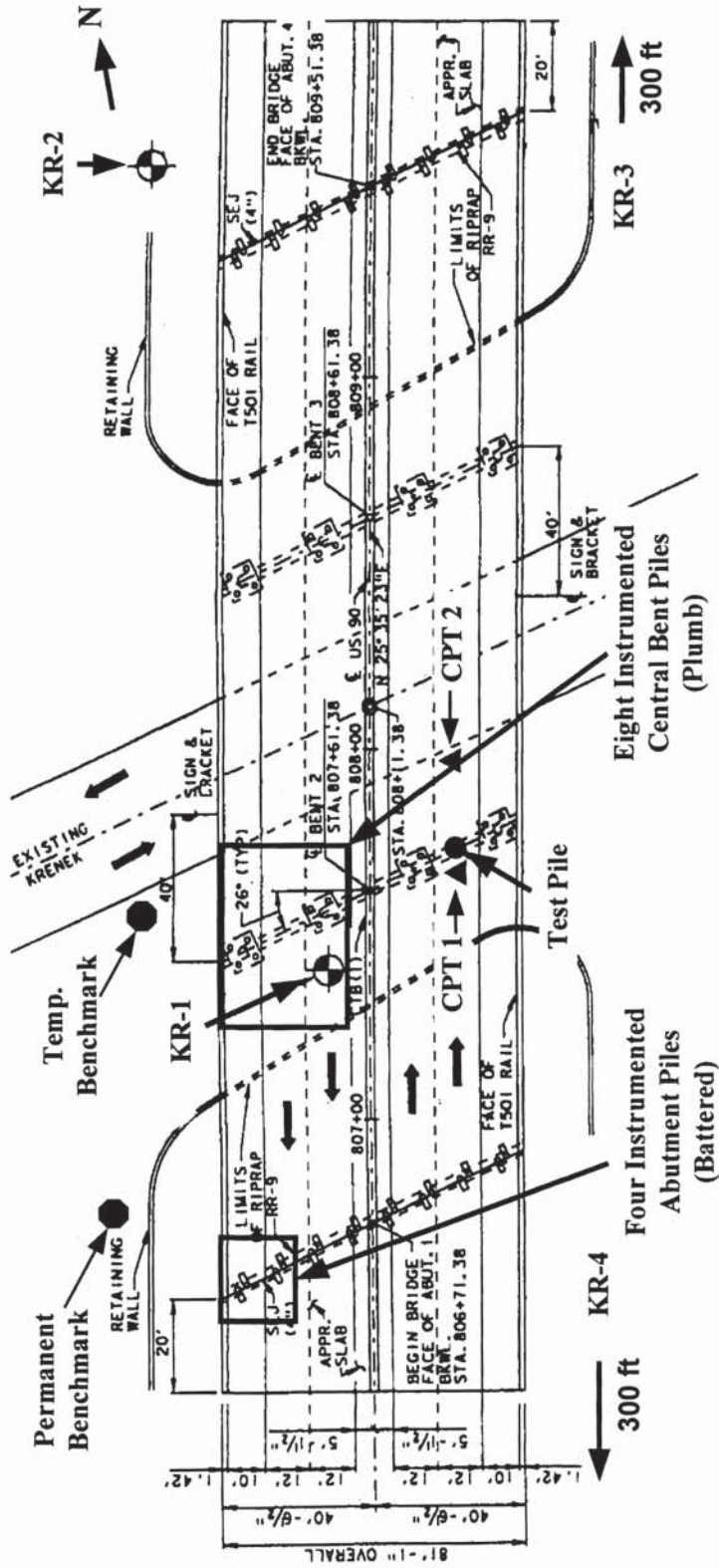


Fig. 3.3. Krenek Road Bridge Layout (Adapted from TxDOT)

The site is also located in the Beaumont formation, a Pleistocene-aged deposit on the Texas Gulf Coastal plain. The ground water level was also about 1.5 m below the natural ground surface. N_{TxDOT} , N_{SPT} , undrained shear strength (s_u), unit weight (γ), plasticity index (PI), and soil classification are shown in Fig. 3.4.

Depth m (ft)	Log	N_{TxDOT} blows/ 0.30 m	Avg. s_u kPa (psi)	Avg. γ_t kN/m ³ (pcf)	Soil Classification
1.5 (5)	▽	12	105.2 (15.3)	20.2 (128.6)	CLAY, brown, tan, stiff
3.0 (10)		12	137.0 (19.9)	20.7 (131.5)	CLAY, w/little sand, tan, stiff
4.6 (15)		13	71.1 (10.3)	20.1 (128.0)	CLAY, sandy, tan, gray, stiff
6.1 (20)		15	115.6 (16.8)	20.7 (131.8)	
7.6 (25)		15	70.7 (10.3)	21.2 (134.6)	CLAY, brown, gray, stiff
9.1 (30)		20	151.8 (22.0)	20.2 (128.3)	
10.7 (35)		38	140.8 (20.4)	21.0 (133.4)	
12.2 (40)		63	114.8 (16.6)	21.2 (135.2)	SAND, light brown, clayey @ 11.9~12.2 m
13.5 (45)		28	116.8 (16.9)	21.3 (135.4)	CLAY, gray, brown, organic, stiff
15.0 (50)		84	69.0 (10.0)	21.5 (136.9)	SAND, brown, clayey @ 14.9~15.2 m
16.5 (55)					CLAY, very stiff

**Pile Toe at
13.2 m (43 ft)**

Fig. 3.4. Soil Profile for Runneburg Road Bridge Site

3.3 Soil Sampling and Testing

Soil sampling was done using TxDOT wash boring rig. Cohesive soil samples with a diameter of 76.2 mm (3 in) were collected with a TxDOT lug sampler, which is a relatively thick-walled tube and which is equipped with small vanes on the exterior surface to allow the sampler to be used as a drill bit to advance it to the next sampling location. This reduced the number of times the drill string needs to be removed from the borehole and increased the efficiency of the sampling operation.

In-situ tests including TxDOT Cone test and SPT were performed by TxDOT Houston District boring crew during the soil sampling. Several laboratory tests were also conducted. Those include UU (Unconsolidated-Unconfined) triaxial compression, water content, unit weight, and Atterberg limit tests.

Table 3.1. UU Test Results for Krenek Road Bridge Site

Sample	Depth (m)	Confining Pressure, σ_3 (kPa)	Undrained Shear Strength, s_u (kPa)	Water content, w (%)	Unit weight, γ_t (kN/m ³)
KR-1 (1)	1.2	34.5	58.0	23	20.3
KR-1 (2)	2.7	62.1	112.3	23	20.4
KR-1 (4)	5.8	131.1	123.3	28	19.9
KR-1 (6)	8.8	200.1	132.0	26	19.9
KR-1 (8)	11.6	262.2	110.4	22	20.4
KR-2 (2)	2.7	62.1	95.2	25	20.0
KR-2 (6)	8.8	200.1	131.0	25	20.1

Table 3.2. UU Test Results for Runneburg Road Bridge Site

Sample	Depth (m)	Confining Pressure, σ_3 (kPa)	Undrained Shear Strength, s_u (kPa)	Water content, w (%)	Unit weight, γ_t (kN/m ³)
Run-1	0.6	13.8	86.9	23	20.5
Run-2	1.5	34.5	123.5	23	19.9
Run-3	2.7	62.1	135.9	24	20.4
Run-4	3.0	69.0	138.0	24	20.9
Run-5	4.6	103.5	71.1	26	20.1
Run-6	5.8	131.1	107.0	25	20.4
Run-7	6.1	138.0	124.2	25	21.0
Run-8	7.3	165.6	85.6	27	21.0
Run-9	7.6	172.5	55.9	26	21.3
Run-10	8.8	200.1	176.0	28	19.9
Run-11	9.1	207.0	127.7	28	20.4
Run-12	10.4	234.6	125.6	25	20.9
Run-13	10.7	241.5	155.9	25	21.0
Run-14	11.6	262.2	78.7	26	21.0
Run-15	11.9	269.1	153.2	26	21.3
Run-16	12.2	276.0	112.5	25	21.4
Run-17	13.1	296.7	189.1	27	21.7
Run-18	13.4	303.6	69.0	26	20.9
Run-19	13.7	310.5	92.5	25	21.2
Run-20	15.2	345.0	69.0	27	21.5

UU triaxial compression tests were performed in accordance with ASTM D 2850 to determine undrained shear strength of clay samples recovered from both Krenek Road and Runneburg Road. Samples were cylindrical and had a diameter of 76.2 mm (3 in)

and a height of 152.4 mm (6 in). The height to diameter ratio for all samples was 2. The UU test results for both sites are summarized in Tables 3.1 and 3.2, respectively. The results of the in-situ and laboratory tests were shown in Fig. 3.2 for Krenek Road and Fig. 3.4 for Runneburg Road, respectively.

After the installation of the ACIP test pile at Krenek Road site (will be described in Chapter 8), Cone Penetration Test (CPT) was performed at two locations (CPT 1 and 2), immediately adjacent [0.15 m (6 in)] to the test pile and 4.3 m (14 feet) away from the test pile toward Krenek Road, respectively. CPT records (CPT 1 and 2) are shown in Fig. 3.5.

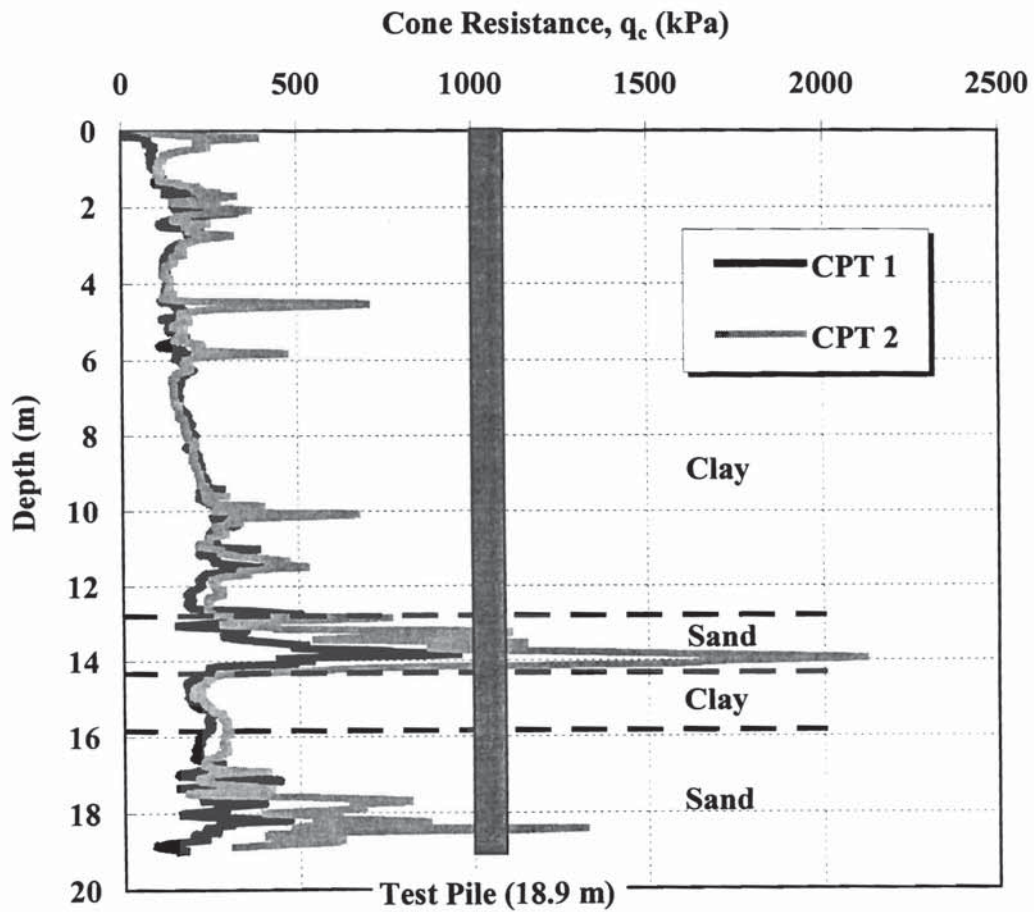


Fig. 3.5. CPT Records at Krenek Road Site

CHAPTER 4

DESIGN OF FOUNDATIONS FOR KRENEK ROAD BRIDGE

4.1 General

This chapter describes the design procedure used for ACIP piles and the estimation of pile capacities for the Krenek bridge foundations. The TxDOT method for drilled shafts (Houston District, 1972) was adopted in the design of ACIP piles since the Krenek bridge site consists primarily of clay. Previous research performed by O'Neill et al. (1999) recommended the TxDOT method for drilled shafts as the primary design method for ACIP piles in clay soil profiles and one of two candidate design methods for ACIP piles in mixed soil profiles of sand and clay. The other candidate method for ACIP piles in mixed soil profiles of sand and clay was the FHWA method for drilled shaft (Reese and O'Neill, 1988).

4.2 Pile Design of Krenek Road Bridge

Krenek Road bridge is a three-span with spans of 27.4 m (90 ft), 30.5 m (100 ft) and 27.4 m (90 ft) and 4 lanes. The structure has four supports: two abutments and two columns piers on ACIP piles. The functional classification of the bridge is rural minor arterial. Design speed for this bridge is 112 km/hour (70 mile/hour).

ACIP piles were designed for geotechnical considerations by TxDOT Houston District laboratory engineers based on design loads (dead load + live load) provided by the Houston District bridge office (structural engineering division). Axial design loads

were 0.80 MN (90 tons) and 0.49 MN (55 tons) for each central bent pile and abutment pile, respectively. The loads were based on a standard abutment and column layout for a grade separation of the type employed at Krenek Road and the decision by the UH team to use four piles per footing in the interior bents instead of the standard five piles per interior footing, in order to assure strains in the pile grout that could be sensed adequately by available instrumentation. No explicit design was made for lateral loading. For most grade separation structures in the TxDOT system with non-curving lanes lateral loads on foundations are small [no more than 17.8 kips (2 tons) to 44.5 kips (5 tons)]. Where lateral loads on bridge components such as abutment walls are routinely computed, these lateral loads are carried by placing the piles supporting the walls at an angle to the vertical (on a “batter”) and carrying the horizontal load axially through the pile into the soil. Therefore, pile foundations are designed exclusively to carry axial loads, recognizing that most piles have a nominal lateral load capacity of 17.8 to 44.5 kips without verification. The piles are therefore not designed for lateral load (Major water crossings, where ship or barge impact and wave loading occur, are an exception).

TxDOT-Houston District applies a factor of safety of 2.0 in pile design. However, for this specific project, ACIP piles were designed more conservatively by using a factor of safety slightly higher than 2.0, since this type of deep foundation was a prototype that had never been designed for a major transportation structure in Texas. In order to affect this conservatism, the designers ensured that the interior bent piles were drilled about 2 m into the sand stratum that can be seen below a depth of about 15.7 m in Fig. 3.2. Experience indicated that deep foundations terminated in sand had high side resistance, and perhaps high end bearing resistance, in the sand (although the high end

bearing resistance normally attributed to sand at depth is disregarded in design calculations for small diameter piles, even driven piles, by TxDOT). The abutment piles were installed through about seven meters of compacted clay fill. It is TxDOT's practice to assume that side resistance will not develop against piles in fill, so that side resistance in the fill was not included in the ACIP pile design calculations.

4.2.1 Soil Properties By Zone

In order to design the ACIP piles at the Krenek bridge site, the site was divided into two zones (North and South) as shown in Fig. 4.1. ACIP Piles in the South zone, where piles are instrumented and where long-term movement observations were made, were designed based on boring log KR-1. ACIP Piles in the North zone were designed based on boring log KR-2.

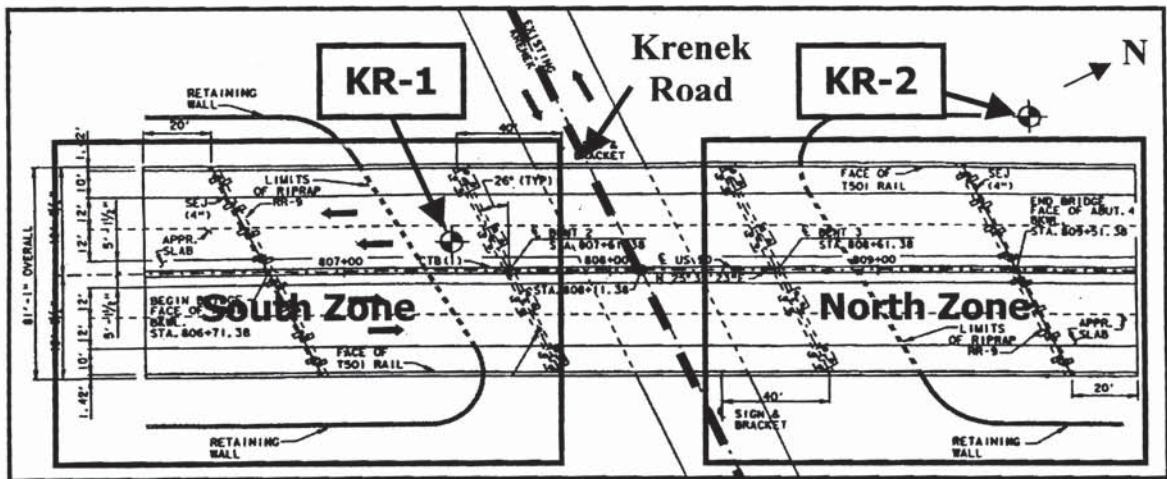


Fig. 4.1. South and North Zones for Pile Design

As described in Chapter 3, the Krenek bridge site consists of a soil profile of generally stiff clays and medium dense sands. In the South zone, the surface layer is generally stiff sandy clay to a depth of 2.1 m below the ground surface. Stiff plastic clay layers were observed from 2.1 m to 12.8 m. A 1.5-m-thick layer of waterbearing, medium dense clayey sand was found from 12.8 m to 14.3 m. A layer of stiff clay was present from 14.3 m to 15.8 m. Below 15.8 m is a stratum of dense, fine and relatively clean waterbearing sand.

In the North zone, the near-surface layer is stiff sandy clay to a depth of 4.3 m below the ground surface. Stiff plastic clay layers were observed from 4.3 m to 11.3 m. Again, stiff sandy clay was found from 11.3 m to 12.8 m. A layer of stiff clay was present from 12.8 m to 16.8 m. Below 16.8 m is a stratum of dense, fine and relatively clean waterbearing sand. The piezometric level in this sand stratum, which was also observed in the South zone, was about 1.5 m below the natural ground surface across the site. Tables 4.1 and 4.2 summarize the idealized South and North soil profiles used for the ACIP pile design for the Krenek site.

Undrained shear strength (s_u) values vs. depth from UU triaxial and unconfined compression tests were plotted for each soil profile. Idealized (interpreted) undrained shear strength profiles, along with data from the undrained shear strength tests, are shown in Figs. 4.2 and 4.3 for the South and North zones of the Krenek bridge site, respectively.

Table 4.1. Idealized Soil Properties for South Zone (KR-1)

Interval (m)		Soil	S_u avg. (kPa)	N_{TxDOT} avg. (blows/0.3 m)
0.0	2.1	Stiff Clay	57.6	17
2.1	3.7	Stiff Clay	110.1	19
3.7	6.7	Stiff Clay	87.2	14
6.7	12.8	Stiff Clay	108.4	24
12.8	14.3	Med. Clayey Sand	-	40
14.3	15.8	Stiff Clay	84.2	22
15.8	22.9	Dense Sand	-	100

Table 4.2. Idealized Soil Profiles for North Zone (KR-2)

Interval (m)		Soil	S_u avg. (kPa)	N_{TxDOT} avg. (blows/0.3 m)
0.0	4.3	Stiff Sandy Clay	69.0	17
4.3	11.3	Stiff Clay	96.6	22
11.3	12.8	Stiff Sandy Clay	96.6	64
12.8	16.8	Stiff Clay	124.2	30
16.8	25.0	Dense Sand	-	75

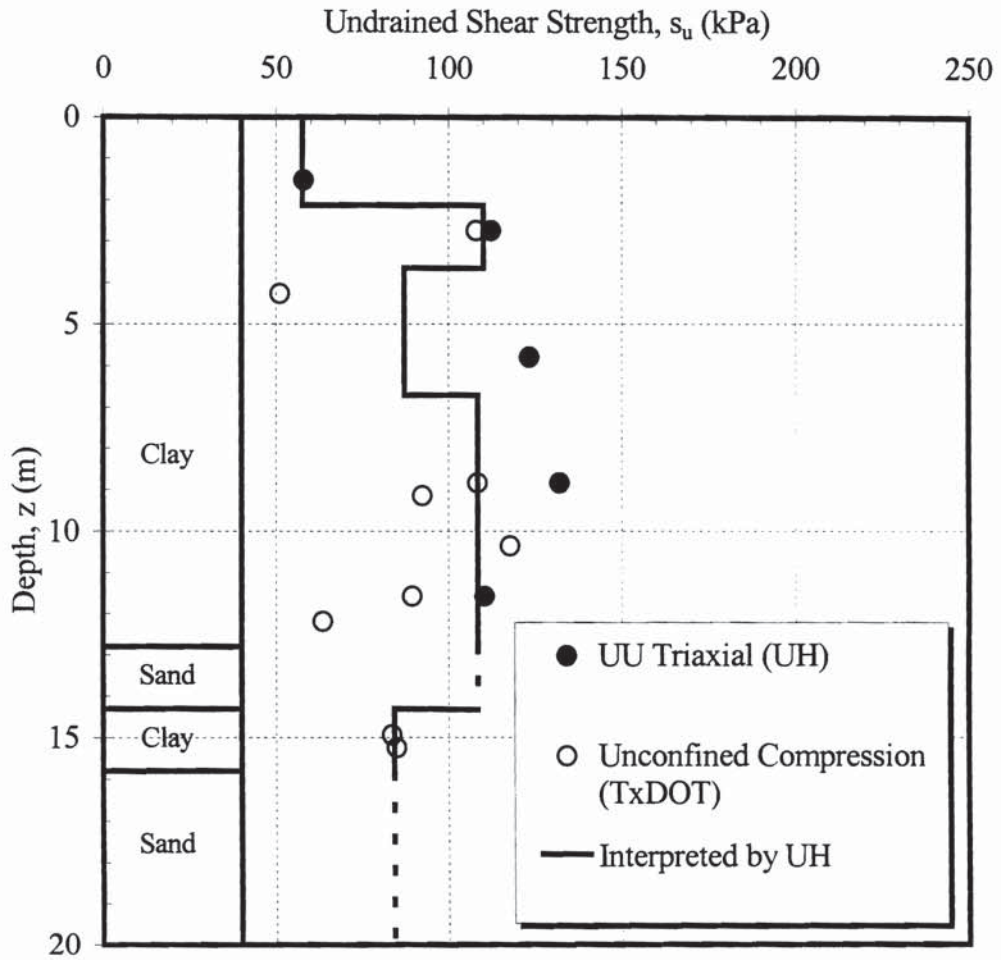


Fig. 4.2. Idealized Soil Profile for South Zone (KR-1)

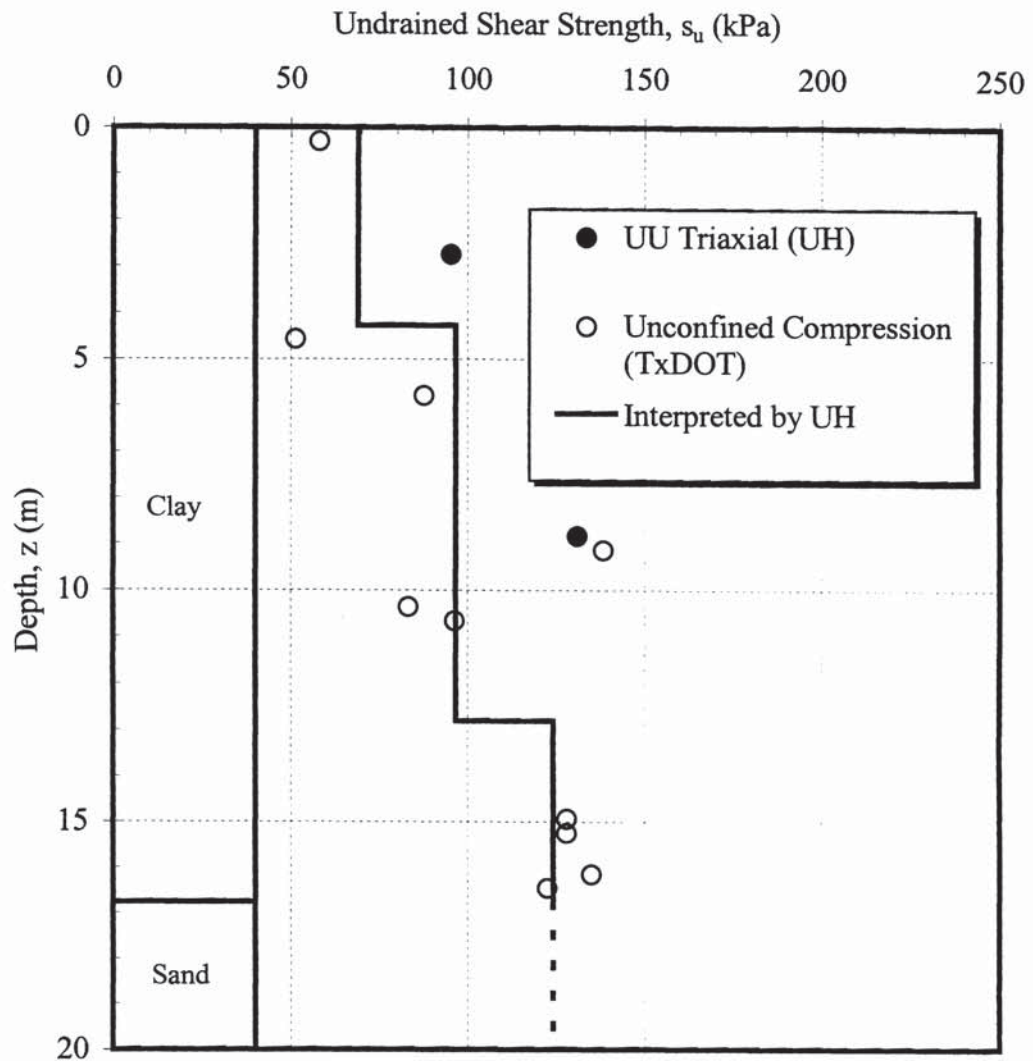


Fig. 4.3. Idealized Soil Profile for North Zone (KR-2)

4.2.2 Side Resistance

Cohesive Soil

The side resistance in cohesive layers is based on the undrained shear strength of the soils penetrated and the perimeter and the length of the pile within the layer. The pile length is therefore selected to be a function of its diameter, the design load and the shear strength of the various soil strata penetrated, considering also the resistance afforded by cohesionless soil layers and end bearing, if any. The undrained shear strength was determined by laboratory unconfined, and unconsolidated and undrained triaxial compression tests.

The TxDOT-Houston District method for drilled shafts implies an ultimate unit side resistance at depth z (center of a layer), $f_s(z)$, according to

$$f_s(z) = 0.7 s_u(z), s_u \leq 120 \text{ kPa (1.25 tsf)} , \quad (4.1)$$

$s_u(z)$ is half of the unconfined compression strength of the soil at depth z (representing a layer of thickness Δz). TxDOT-Houston District ordinarily applies a factor of safety of 2.0 to obtain an allowable unit side resistance value from this equation. Therefore,

$$Q_s(\text{allowable}) = \frac{1}{2} \pi D \sum f_s(z) \Delta z , \quad (4.2)$$

where the summation is carried out over all clay layers (i) in the soil profile and

$Q_s(\text{allowable})$ = allowable side resistance in the clay layers,

$f_s(z)$ = ultimate unit side resistance at depth z (representing clay layer i), and

Δz = thickness of clay layer i .

When the surface soil layer is clay, $f_s(z)$ is taken as zero to a depth of 1.5 m (5 ft), mainly in consideration of the fact that clay soils can shrink away from the heads of the piles if they are unprotected from the atmosphere (Reese and O'Neill, 1988). It was applied for ACIP test pile. However, this was not done for the ACIP production pile design for the Krenek Road bridge because (1) the design unit side resistance for the abutment piles was already zero, and (2) the soils surrounding the heads of the piles in the central bents would be protected from atmospheric conditions that would cause soil shrinkage by the footings.

Cohesionless Soil

The value for the allowable unit side resistance, $f_s(z)$ (allowable), for each sand layer in the profile is determined for the average value of N_{TxDOT} for the layer using Equation (4.3).

$$f_s(z)(allowable) (tsf) = 0.7 [N_{TxDOT}/80], N_{TxDOT}/80 \leq 1.25 (120 kPa) . \quad (4.3)$$

The ultimate side resistance $f_s(z)$ is then given by

$$f_s(z) = 2 f_s(z) (allowable) . \quad (4.4)$$

Q_s (allowable) for all sand layers in the profile is then computed using Equation (4.2) with the $f_s(z)$ values from Equation (4.4). Q_s (allowable) for all sand layers is then added to Q_s (allowable) for all clay layers (preceding section) to obtain the allowable side resistance for the entire pile.

4.2.3 Toe Resistance

Cohesive Soils

The TxDOT-Houston District design method uses the blow count from a TxDOT dynamic cone penetrometer (N_{TxDOT}) and a net allowable end bearing resistance of $N_{TxDOT}/16.5$ (tsf) in stiff clay and sand-clay mixtures and uses a presumptive upper limit for allowable toe resistance in such clay soils [q_p (allowable)] of 0.19 MPa (2.0 tsf) when the pile diameter is less than 0.61 m (24 in.). Since the diameter of the ACIP piles for the Krenek Road bridge was 0.457 m (18 in.), the equations used for the allowable toe resistance were

$$q_p \text{ (allowable)} = 0.19 \text{ MPa (2.0 tsf)} , \text{ or} \quad (4.5)$$

$$Q_p \text{ (allowable)} = q_p \text{ (allowable)} A_p . \quad (4.6)$$

Assuming that the allowable value of unit end bearing is based on a factor of safety of 2.0, which is the usual practice in the Houston District,

$$Q_p (\text{ultimate}) = 2 Q_p (\text{allowable}) . \quad (4.7)$$

[The limit appears to be the result of experience with small-diameter drilled shafts, in which drilling slurries and the cuttings they carry are not fully displaced from the bottom of the drilled shaft borehole and remain there after the concrete is placed (Reese and O'Neill, 1988). Because of the way ACIP piles are constructed, however, this will not happen and there appears to be no need to limit unit end bearing to such small values if the soil at the toe is cohesive.]

Cohesionless Soils

Generally, the TxDOT design method is based upon visual soil classification and the TxDOT dynamic cone penetrometer test. The higher the value of N_{TxDOT} the better the material is in end bearing.

The allowable unit toe resistance of ACIP piles with toes in sand is computed from Equation (4.8). As with toes in clay, a 0.19 MPa (2.0 tsf) limit is applied. Allowable toe resistance is then calculated using Equation (4.6).

$$q_p (\text{allowable}) (\text{tsf}) = N_{\text{TxDOT}} / 11 \leq 2 \text{ tsf} (0.19 \text{ MPa}) . \quad (4.8)$$

Because of the way ACIP piles are constructed, which causes mining problems in bearing soils, end bearing in cohesionless soils should be excluded in ACIP pile design. This will be demonstrated later in the analysis of the data from the Krenek Road bridge.

4.2.4 Examples of Pile Capacity Calculations

ACIP piles with 0.457 m (18 in) diameters were used throughout, based on cost and the need to carry nominal lateral loads on the piles. Reinforcing cages, consisting of about 1 % longitudinal steel, were used for each ACIP pile. Each pile had an axial design load of 0.80 MN (90 tons) for each central bent pile and 0.49 MN (55 tons) for each abutment pile, assuming a factor of safety of 2.0, as is customary in the Houston District TxDOT design office. The following are examples of pile capacity calculations for central bent and abutment piles.

Example 1. Central Bent Pile (South)

Design Load:	0.80 MN (90 ton)
Diameter:	0.457 m (18 in)
Pile Length:	17.4 m (57 ft)
Toe Elevation:	18.9 m (62 ft)
Soil Profile:	KR-1 (See Table 4.1)

Example 2. Abutment Pile (South)

Design Load:	0.49 MN (55 ton)
Diameter:	0.457 m (18 in)
Pile Length:	17.4 m (62 ft)
Toe Elevation:	13.2 m (43 ft)
Soil Profile:	KR-1 (See Table 4.1)

Example 1. Central Bent Pile

1. Side Resistance (Q_s)

Clay

Layer (m)		s_u	Δz	πD	A_s	f_s	Q_{s1}	Remarks
from	to	kPa	m	m	m^2	kPa	kN	
0.0	1.5	58.0	1.5	1.4	2.2	40.6	44.4	→ Excluded (Pile Cap)
1.5	2.1	58.0	0.6	1.4	0.9	40.6	17.8	
2.1	3.7	112.5	1.5	1.4	2.2	78.7	86.2	
3.7	6.7	86.9	3.0	1.4	4.4	60.9	133.2	
6.7	12.8	108.3	6.1	1.4	8.8	75.8	332.0	
14.3	15.8	84.2	1.5	1.4	2.2	58.9	64.5	

$Q_{s1} = 633.6$ kN

Sand

Layer (ft)		N_{TDR}	f_s	Δz	πD	A_s	Q_{s2}
from	to	tsf	kPa	m	m	m^2	kN
12.8	14.3	40.0	33.5	1.5	1.4	2.2	73.4
15.8	18.9	75.0	62.9	3.0	1.4	4.4	275.2

$Q_{s2} = 348.6$ kN

2. Toe Resistance (Q_p)

N_{TDR}	q_p	r	A_p	Q_p	Remarks
	tsf	m	m^2	kN	
100	9.1	876.8			
	2.0	191.6	0.2	31.5	(q_p is limited to 2.0 ts)

$Q_p = 31.5$ kN

3. Total Resistance (Q_T)

$$Q_T = Q_{s1} + Q_p = 1013.7 \text{ kN} > \text{Design Load } 800.7 \text{ kN} \quad (\text{O.K.})$$

Example 2. Abutment Pile

1. Side Resistance (Q_s)

Layer (m)		s_u	Δz	πD	A_s	f_s	Q_{s1}	Remarks
from	to	kPa	m	m	m^2	kPa	kN	
0.0	1.5	58.0	1.5	1.4	2.2	40.6	44.4	Excluded (Fill)
1.5	2.1	58.0	0.6	1.4	0.9	40.6	17.8	
2.1	3.7	112.5	1.5	1.4	2.2	78.7	86.2	
3.7	6.7	86.9	3.0	1.4	4.4	60.9	133.2	
6.7	12.8	108.3	6.1	1.4	8.8	75.8	332.0	
							$Q_{s1} =$	613.5 kN

Sand

Layer (ft)		N_{T-DOT}	f_s	Δz	πD	A_s	Q_{s2}	
from	to		tsf	m	m	m^2	kN	
12.8	13.1	40	0.4	0.3	1.4	0.4	14.7	
							$Q_{s2} =$	14.7 kN

2. Toe Resistance (Q_p)

N_{T-DOT}	q_p	r	A_p	Q_p	Remarks
	tsf	m	m^2	kN	
40	3.6	0.2	0.2	31.5	q_p is limited to 2.0 tsf
	2.0	191.6	0.2	31.5	
				$Q_p =$	31.5 kN

3. Total Resistance (Q_T)

$$Q_T = Q_s + Q_p = 659.7 \text{ kN} > \text{Design Load } 489.3 \text{ kN} \quad (\text{O.K.})$$

4.3 Commentary on Local ACIP Pile Design

It is pointed out that although the central bent piles were 17.4 m (57 ft) long, they penetrated to a depth of 18.9 m (62 ft) below finished grade because their heads were encapsulated within caps whose bases were approximately 1.5 m (5 ft) below the ground surface. Similarly, the abutment piles penetrated 13.2 m (43 ft) below natural grade because their footings were positioned within the upper portion of the fill (header banks). In order to design the piles conservatively, the piles were extended into the lower sand layer (Fig. 3.2), and the pile toe was designed to bear on sand layer below the stiff clay. The subsequent load test on an ACIP test pile and monitoring of production ACIP piles supporting the structure, described later, indicate that the ACIP piles, as designed, were too long for this soil profile. Previous experience by members of the UH team indicated that ACIP piles tend not to be effective when drilled through a thick clay layer (almost impermeable) into a highly permeable sand layer that is under hydraulic pressure, which was the geologic profile at Krenek Road. In such a geologic environment, the drilling process is like popping the cork on a bottle. Once the bit penetrates the sand, groundwater rushes up the auger, bringing some sand with it and loosening the sand stratum, which apparently significantly inhibits transfer of load from the pile into the sand. Thus, a pile penetrating into the sand may have no higher capacity than a pile terminated just above the sand.

Local consultants who design ACIP piles use various α factors for skin friction in clay in their ACIP pile design. Some use an α value of 0.55, per the FHWA method for drilled shafts (O'Neill and Reese, 1999), or 0.7 as used in the TxDOT method for drilled

shafts (TxDOT-Houston District, 1972). Others often assume an α value of as high as 1.0.

CHAPTER 5

CONSTRUCTION

5.1 General Information

Based on the soil borings and design load information the Krenek Road and Runneburg Road bridges were designed to be supported on ACIP piles and driven piles, respectively. The design for the ACIP piles is described in Chapter 4. TxDOT personnel designed the driven pile system with 0.406 m (16 in) square prestressed concrete piles following a procedure similar to that described in Chapter 4, with the major exception that the reduction factor for skin friction in clay for driven piles was taken as 1.0. It should be noted that the reduction factor of 0.7 for skin friction in clay was used for ACIP piles in the TxDOT design procedure for drilled shafts. This resulted in piles that were shorter than the ACIP piles. The general contractors were required to bid on both alternatives. The successful contractor bid \$22 per linear 0.3 m (foot) for the driven piles and \$20 per linear 0.3 m (foot) for the ACIP piles and subcontracted the installation of ACIP piles. Although the driven pile system was about 10 percent more costly per 0.3 m (foot) of pile length, the shorter pile lengths for the driven piles actually made the driven pile system cheaper as designed. As will be seen, however, using the linear 0.3 m (foot) costs given above, the ACIP piles were cheaper than driven piles on the basis of dollars per unit of load carried.

5.2 Construction Sequence for Krenek Road Bridge

Bridge construction required about one-and-one-half years. A table of chronological construction events is given in Table 5.1. Fig. 5.1 shows a schematic elevation of the Krenek Road bridge.

Table 5.1. Construction Sequence and Timeline

Date	Day	Construction
04/05/00 – 04/10/00		Soil Survey for Krenek Road Bridge Site
05/30/01	0	Fill Placement
01/25/02	240	Installation of Test and Reaction Piles (3 piles)
01/28/02	243	Installation of Reaction Piles (2 piles)
02/12/02	258	Load Test on ACIP Pile at Krenek Rd.
02/26/02	272	Battered pile Installation (South Forward, 8 piles)
02/28/02	274	Battered pile Installation (South Backward, 8 piles)
03/04/02	278	Battered pile Installation (North Forward, 8 piles)
03/05/02	279	Battered pile Installation (North Backward, 8 piles)
03/07/02	281	Central Bent pile Installation (8 piles)
03/11/02	285	Central Bent pile Installation (8 piles)
03/12/02	286	Central Bent pile Installation (6 piles)
03/13/02	287	Central Bent pile Installation (6 piles)
03/21/02	295	Installation of Driven PC Test and Reaction Piles
04/04/02	309	Footings and Abutment Cap (South)
04/05/02	310	Load Test on Driven PC Pile at Runneburg Rd.
04/10/02	315	Column (South)
04/11/02	316	Abutment Wall (South)
04/16/02	321	Column (North)
04/17/02	322	Abutment Wall (North)
04/20/02	325	Bent Caps (South)
04/22/02	327	Bent Caps (North)
04/23/02	328	Backfilling (South)
04/29/02	334	Riprapping (South) and Backfilling (North)
05/09/02	344	Riprapping (North)
06/26/02	392	Soil Survey for Runneburg Road Bridge Site
06/29/02	395	Placing Girders
07/17/02	413	Placing Decks
08/07/02	434	Pouring grout for wearing surface (Deck Completion)
09/17/02	475	Live Load Simulation
11/27/02	576	Bridge in Service

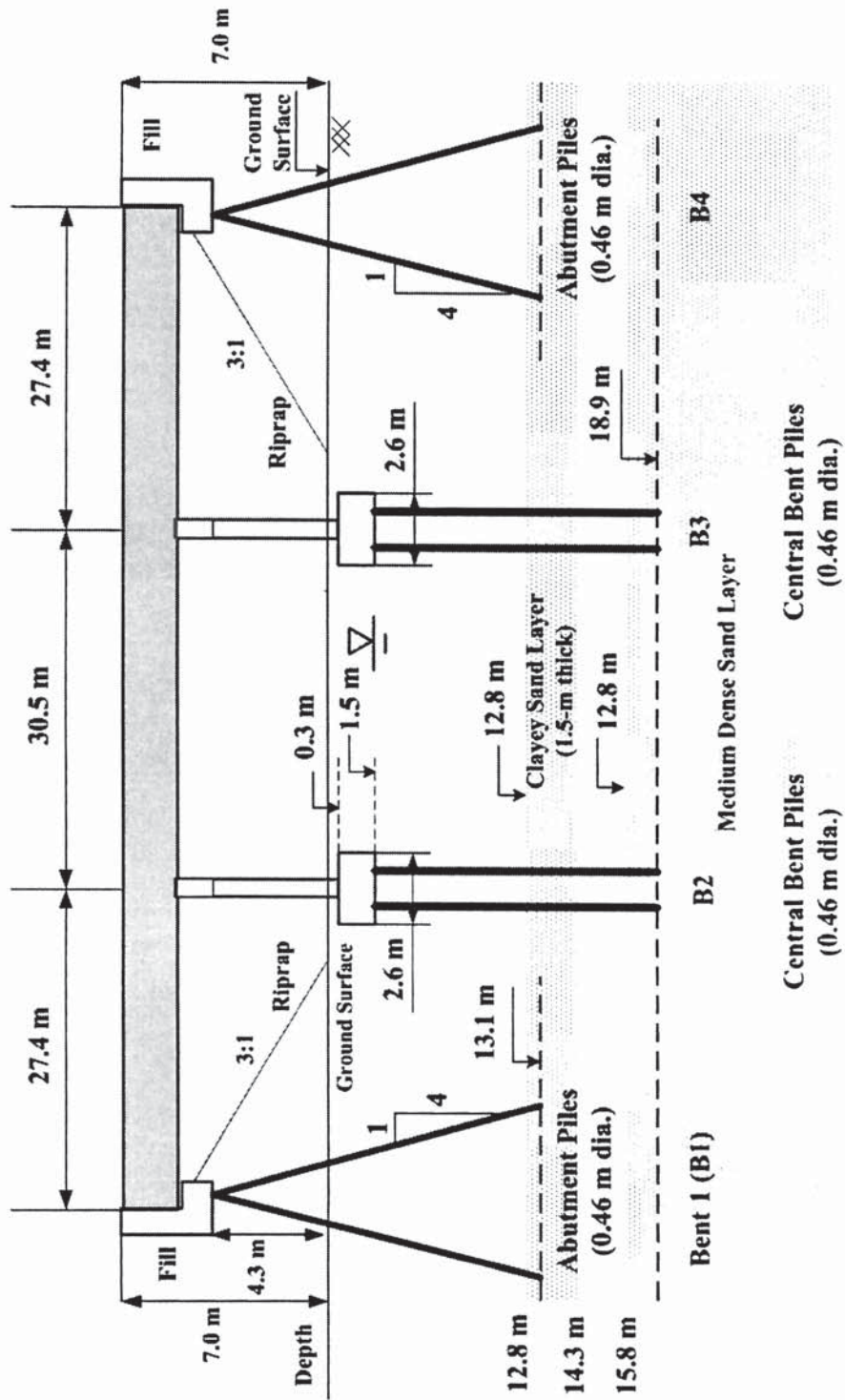


Fig. 5.1. Schematic Elevation of the Krenek Road Bridge

5.2.1 Fill (Embankment)

Construction started by placing embankments (“header banks” for the abutments) on each side of Krenek Road. Soft, organic clay soil was excavated to a depth of 0.6 m below natural grade and replaced by borrow (stiff, plastic clay) and compacted. About 7.0 m of fill soil (borrow) was then placed on the compacted subgrade to form the header banks. The final height of each embankment fill was about 7.6 m at its crest, including the compacted subgrade. Borrow soils (stiff, plastic clay) were taken from the site of the new channel of Jackson Bayou which is located about 1.8 km northwest of the Krenek Road bridge site. During the fill placement settlements of the fill were monitored continuously until the central bent piles were installed from a temporary benchmark on the south shoulder of Krenek road, in asphalt, near the center line of the bridge and about 33.5 m northwest of the South abutment by optical surveying technique (using a loop closure method). The benchmark was far enough from the header banks that they should have had no measurable effect on its vertical stability.

5.2.2 Test and Reaction Piles

Test and four reaction piles were installed before installing production piles. Four piles reaction piles for the ACIP pile load test were used as central bent production piles. Pile installation sequence for ACIP pile load test was FD/P3, FC/P2, Test Pile, FD/P4, and FC/P1 in Fig. 5.2. The ACIP test pile had a diameter (0.46 m) of a typical central bent pile and was placed between two footings as shown in Fig. 5.2. Load test was performed to geotechnical failure on the test pile 18 days after it was installed. This test

and a similar loading test on a driven pile at the nearby Runneburg Road grade separation will be discussed in a later chapter (Chapter 8).

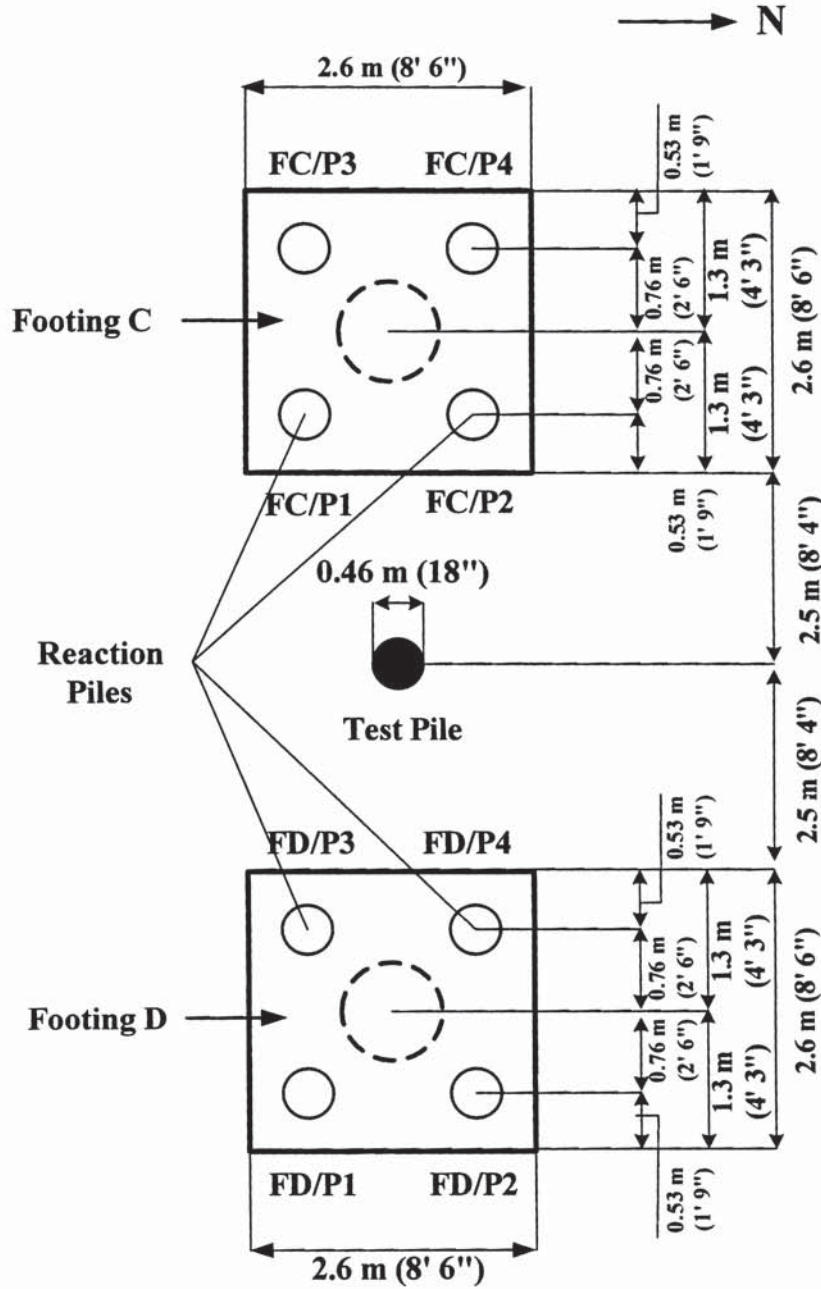


Fig. 5.2. Layout for the Test Pile and Reaction Piles at Krenek Road Site

5.2.3 Abutment Piles

This loading test verified a factor of safety of more than 2 for ACIP piles at the Krenek Road bridge site so that the abutment piles were installed, starting with the South abutment, and then proceeding to the North abutment, before the central bent piles were installed. Each abutment had 8 pile groups (each group consisted of one in-battered and one out-battered pile), with a total of 16 battered abutment piles in each header bank. Each abutment pile was battered at 4:1 (vertical: horizontal).

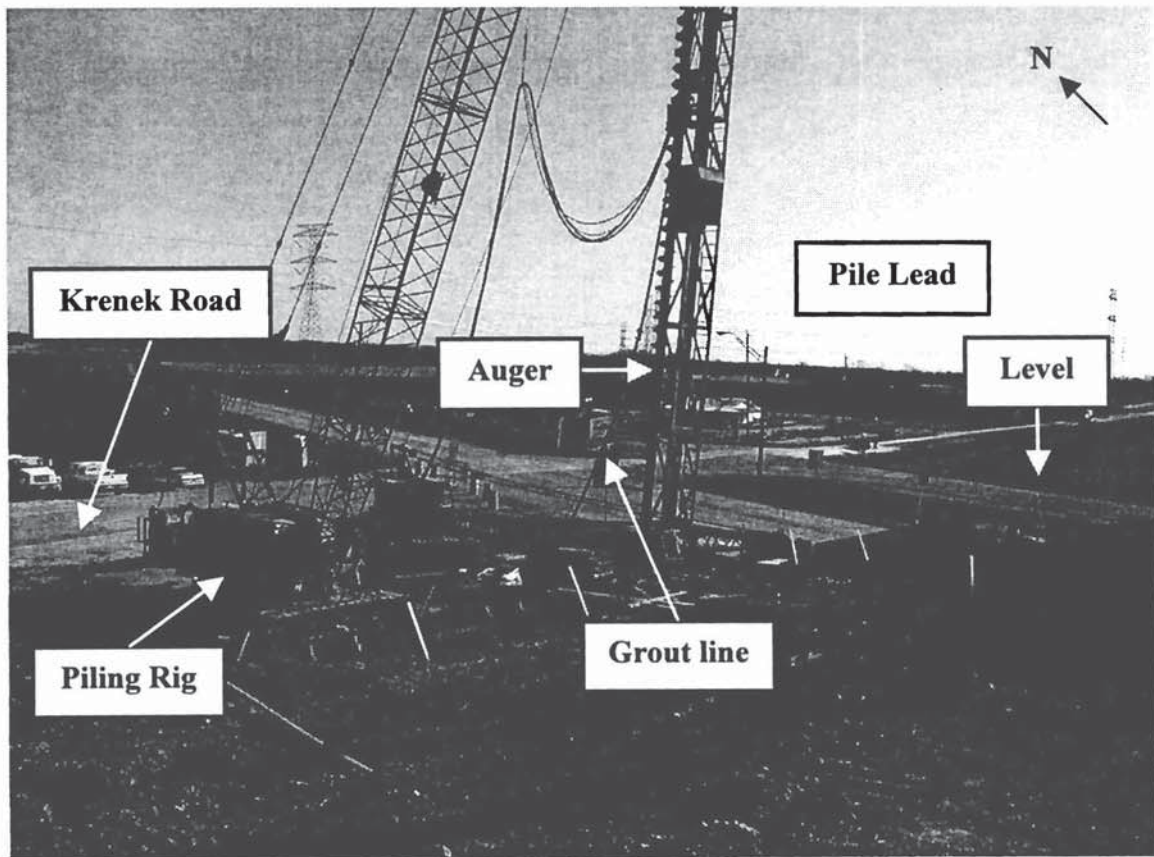


Fig. 5.3. Positioning the Drilling Rig for Installing Abutment Piles

The ACIP pile subcontractor chose to use an 890-kN (100-ton) crane (rig) with hanging leads to suspend his hydraulic motor, grout lines and auger. This is not the normal practice for ACIP piles, which are generally installed with truck-mounted drilling equipment. Such equipment has a relatively short horizontal reach, such that the rig must be positioned within 5 or 6 m of the pile location. However, the ACIP pile subcontractor decided to install all of the abutment piles with his rig positioned on the shoulders of Krenek Road, using the long reach of the crane to position the auger-motor-leads system on location rather than driving a truck-mounted rig up onto the header bank and positioning his rig there as shown in Fig. 5.3, although the latter procedure could have been followed. The drilling and grouting operation required about 15 minutes for each pile provided the grout supply was completely available. In a few cases the contractor had to wait for several minutes between the completion of drilling and the beginning of grouting because grout had not arrived from the ready-mix supplier. During this time he continued to turn the auger so that it would not “freeze up” in the borehole. This may have served to degrade the contact surface between the grout and soil. As soon as grouting was completed, the grout at the top of ACIP pile was hand-screened to remove any small lumps of soil that may have fallen into the grout. A sheet metal collar with the diameter of the pile was then placed in the grouted hole to prevent any further infiltration for soil from the surface.

Within five minutes of the completion of grouting, a full-depth cage, 19 m (62.3 ft) long, was thrust into the fluid grout. The prepared cages had been placed on top of the header banks prior to drilling. As soon as the drill rig swung away from the hole, the free line on the crane picked up a cage and set it into the grout, to aid in thrusting the full-

depth cages into the grout the contractor had attached three 50-mm-diameter open-ended PVC pipes to one side of the cage with steel tie wires as shown in Fig. 5.4. These PVC pipes acted as skids to allow the cages for the batter piles to slide easily along the inside of the borehole wall to their full lengths. The longitudinal rebar was bent inward in the bottom 0.6 m (2 ft) length of each cage (for both the battered abutment piles and the vertical interior bent piles), so that they had the appearance of “bullet noses,” in order to prevent the longitudinal bars from hanging on the side of the borehole and stopping the cage penetration process.

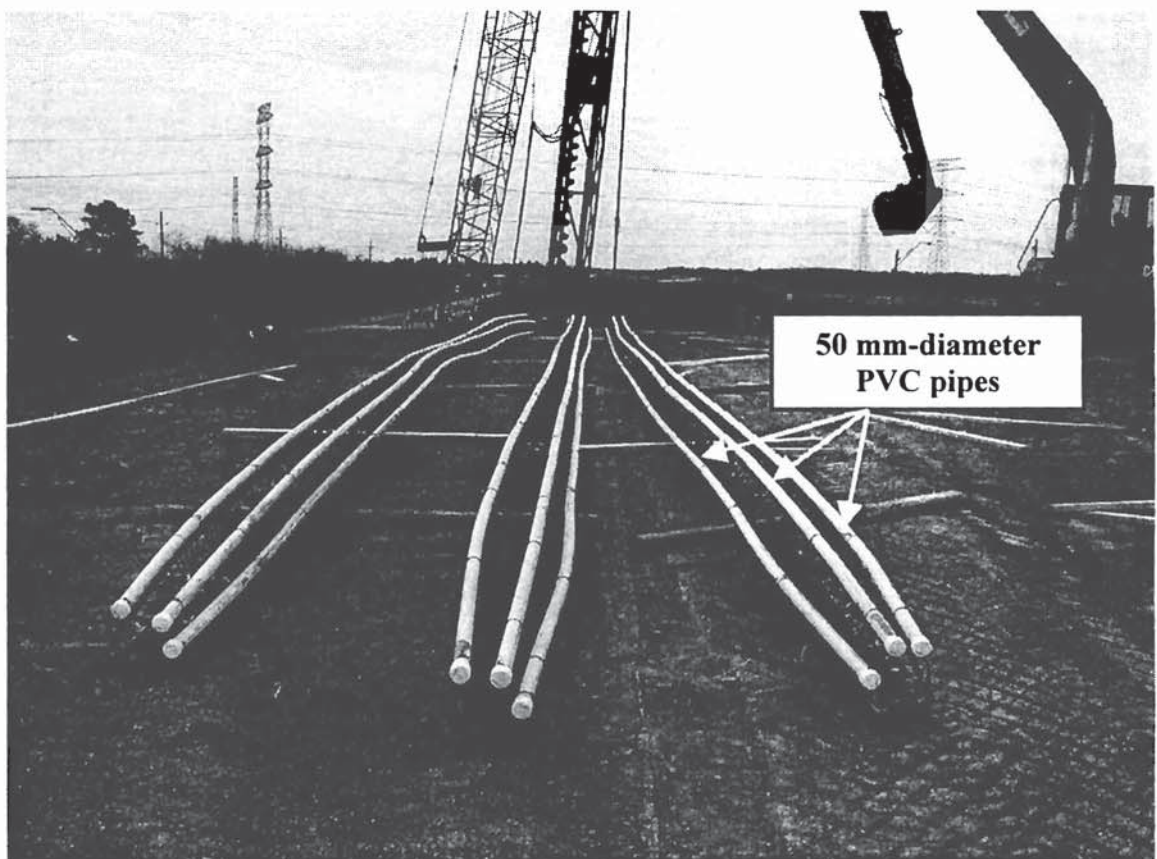


Fig. 5.4. Abutment Pile Cages Attached PVC Pipes

Eight battered (forward) piles were installed in one day. Then, the other battered piles (backward) were installed the next day. Total of 32 abutment piles were installed for 4 days. Including 4 small wing wall piles. In all, 36 piles were installed in 4 days. The average pile installation cycle time was about 45 min. Piling installation cycle time includes positioning the drilling rig, augering (drilling), grouting and inserting the cage. The installation of a battered abutment pile is shown in Fig. 5.5. Inserting the cage into the hole filled with grout is shown in Fig. 5.6.

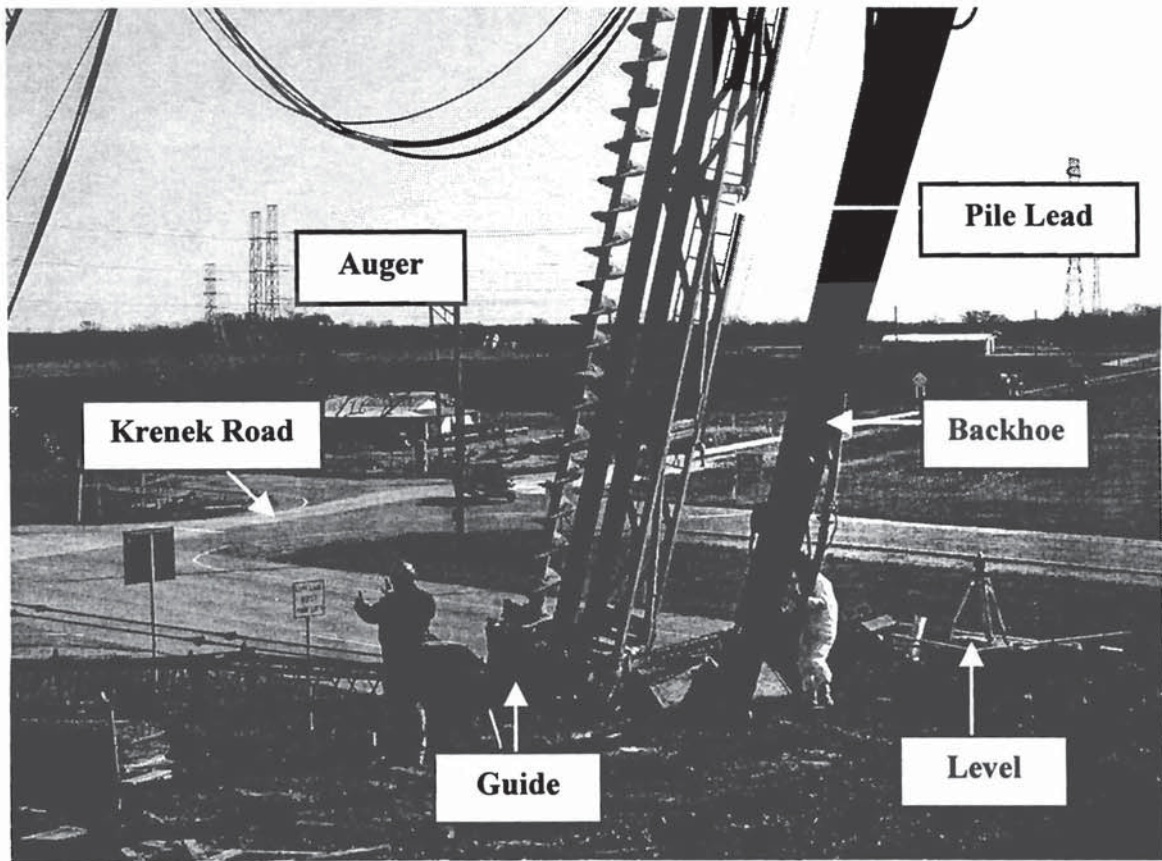


Fig. 5.5. Installing a Battered Abutment Pile

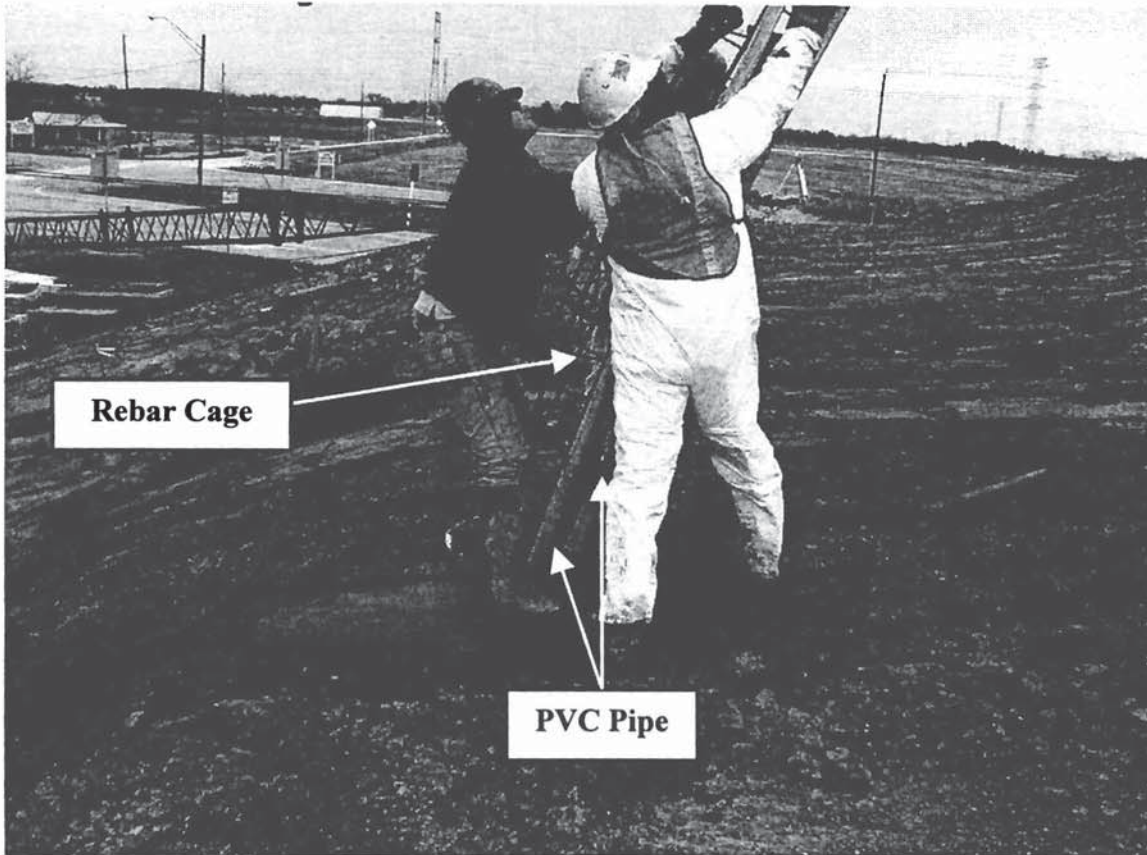


Fig. 5.6. Inserting the Cage into the Hole Filled with Grout

5.2.4 Central Bent Piles

Total of 32 central bent piles were also installed over a period of four working days. The contractor was prohibited from installing more than one pile in each footing each day, since there was a restriction in the ACIP construction specification that adjacent piles in a group within a spacing of 6 diameters of each other could not be placed within a 24 hour period. It is noted that 6 diameter spacing rule in a group was adopted from drilled shaft specification. The piling contractor elected to install one pile under each footing each day (a total of 8 piles in a day). The cycle time for the vertical

piles under the central bent footings was about 40 minutes. Therefore, the contractor could not take full advantage of the 8-hour working day. Figures 5.7 and 5.8 show the drilling rig setup and installation of the central bent piles, respectively.

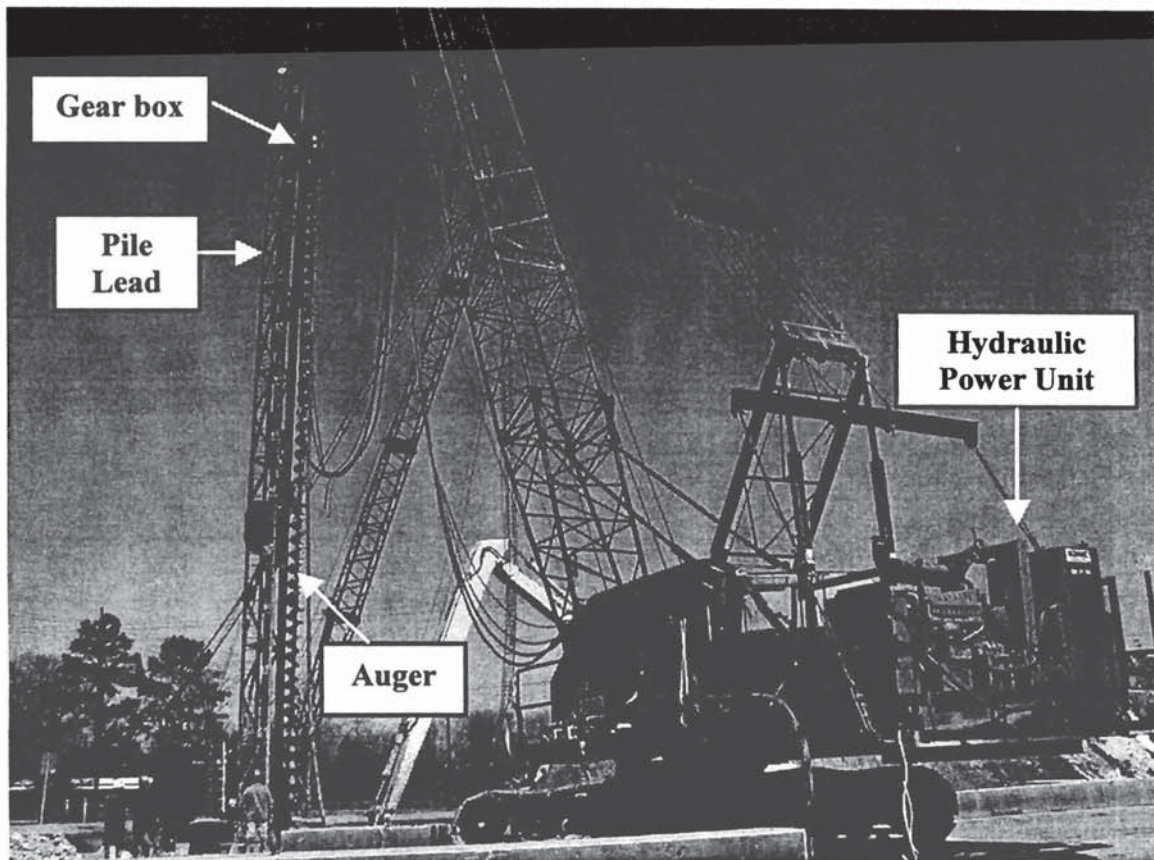


Fig. 5.7. Drilling Rig Setup for Installing Central Bent Piles

5.2.5 Footings (Pile Caps) and Abutments

Although the initial plans called for the general contractor to excavate the footing pits to a depth of about 1.5 m prior to installing the ACIP piles for the central bents, the piles were in fact installed without excavating the footing pits. Therefore, the central bent piles were installed from the existing natural ground surface to a depth of 18.9 m

[design pile length (17.4 m) + depth to be excavated later for placing footings (1.5 m)]. Later, 1.5 m of soil below the natural grade was excavated. The extra length of pile was then cut off, leaving about 0.6 m of longitudinal steel protruding for connecting the piles to the footing (cap).

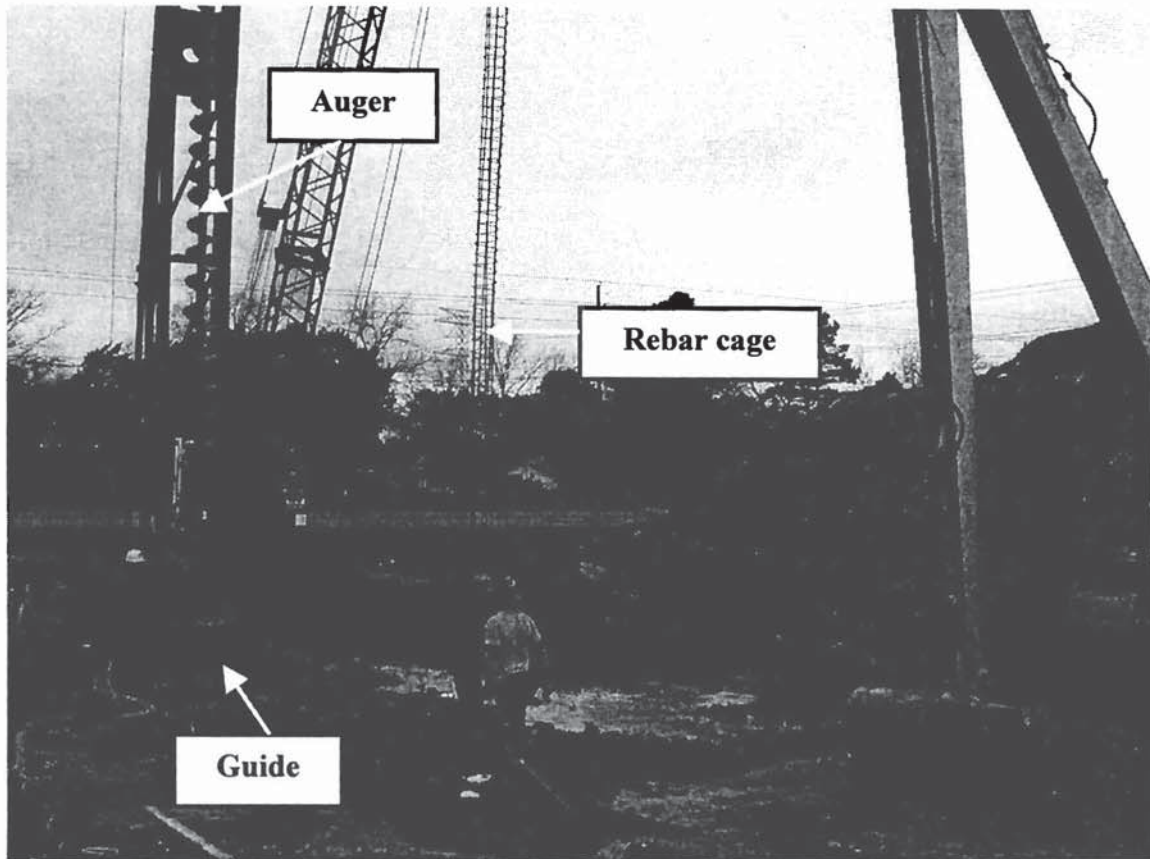


Fig. 5.8. Installation of Central Bent Pile

Once the footing excavation was completed, 0.15 m of cement stabilized sand was placed in the bottom of the excavation and around the pile heads, and then 0.15 m of lean concrete was poured to form the seal slab. Note is made of the fact that no attempt was made by the contractor to compact the subgrade soils in the footing excavation. These

subgrade soils were visibly soft when the seal slab was placed. Note is also made of the fact that subgrade compaction for piled footings is not required by TxDOT and that not compacting the footing subgrade is standard practice in the Houston area. Forms were then set on top of the seal slab, the reinforcing steel was placed in the forms, and the footings was concreted as shown in Fig. 5.9.

At the abutments 0.15 m of compacted cement-stabilized sand was placed around and between the heads of the abutment piles to provide a pad for setting forms for the abutment footing, which was continuous across the face of the abutment. After setting these forms and rebar, concrete was poured for abutment footings (abutment caps) and walls as shown in Fig. 5.10. Cement-stabilized soils were used as backfill behind the abutment walls.

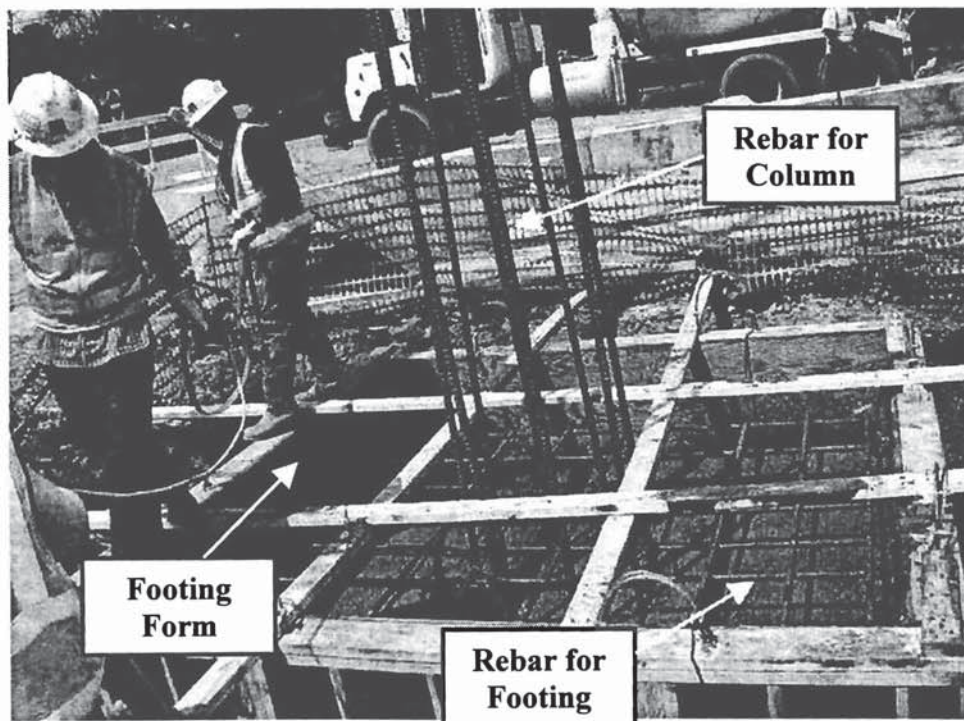


Fig. 5.9. Placing of Concrete for Central Bent Footing

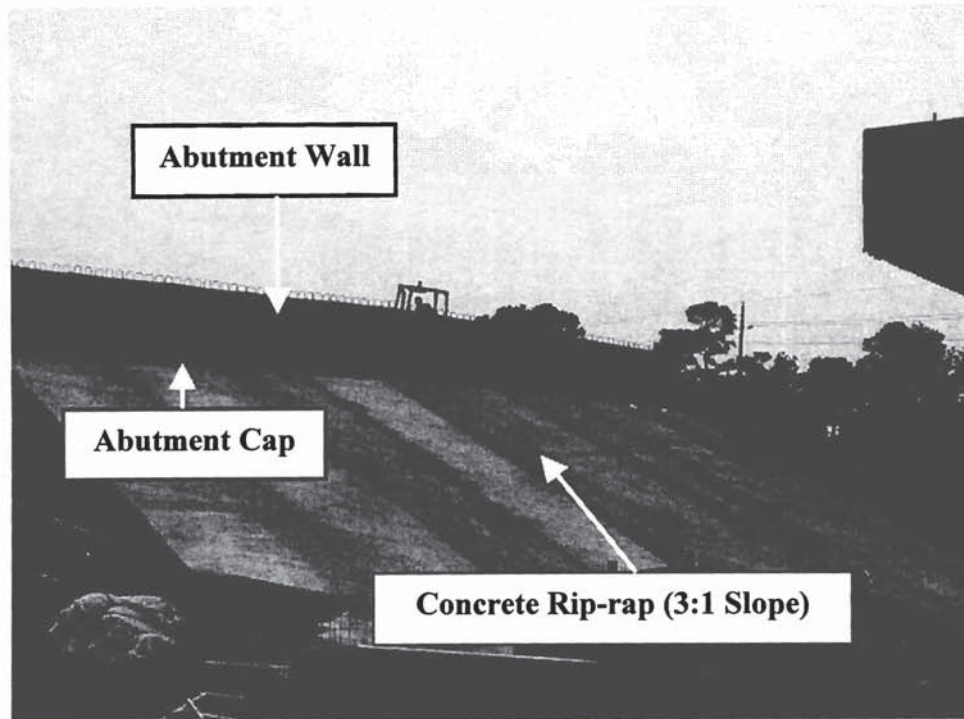


Fig. 5.10. Completed Abutment (Cap and Wall) at Krenek Road Bridge Site

5.2.6 Columns, Bentcaps, Girders, and Deck

The columns and bentcaps were placed on footings. A row of four completed columns in South side of Krenek Road is shown in Fig. 5.11. Prestressed concrete girders were then placed as shown in Fig. 5.12, followed by placement of the deck. The deck consisted of composite precast concrete slabs about 0.1 m thick spanning between the girders on top of which a cast-in-place concrete slab 0.1 m thick was poured to form the wearing surface. Fig. 5.13 shows a picture of the placement of deck panels. Bridge construction was finished by placing the approach slabs and rails. After cleaning the deck surface, painting, and placing signs, the bridge finally went into service on November 27, 2002.

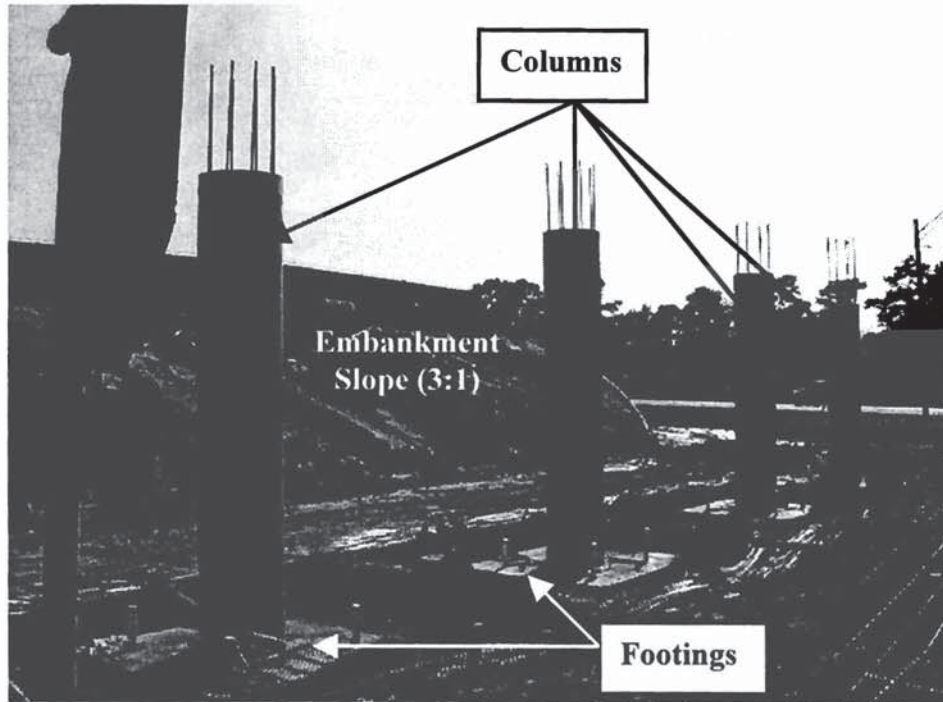


Fig. 5.11. Completed Concrete Columns at Krenek Road Bridge Site

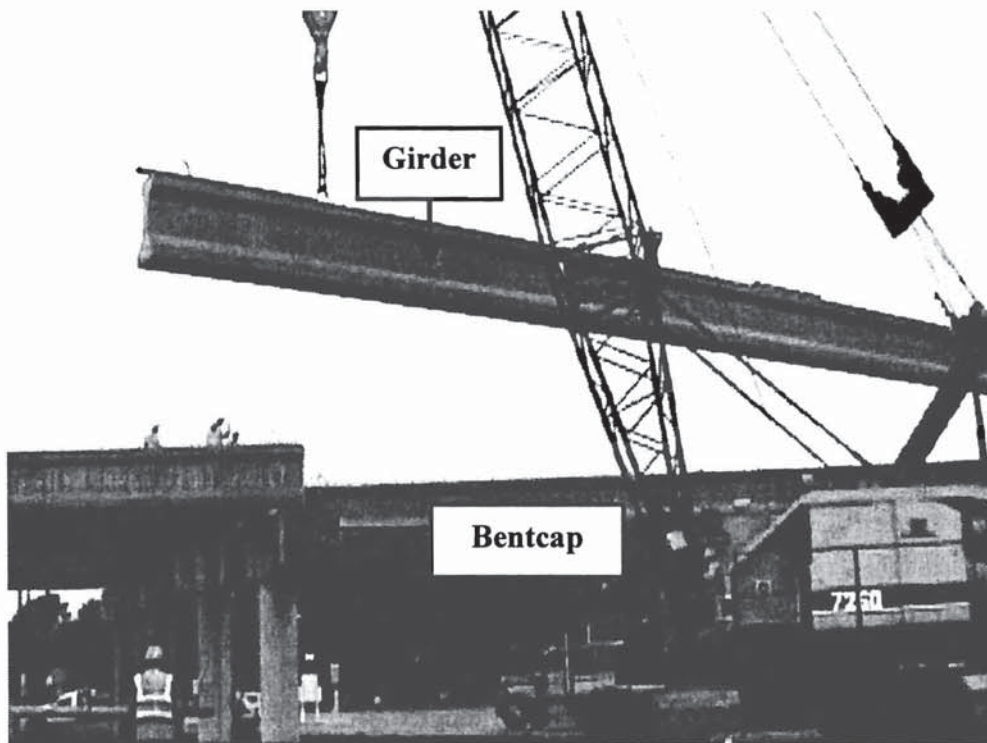


Fig. 5.12. Placing Girders at Krenek Road Bridge Site

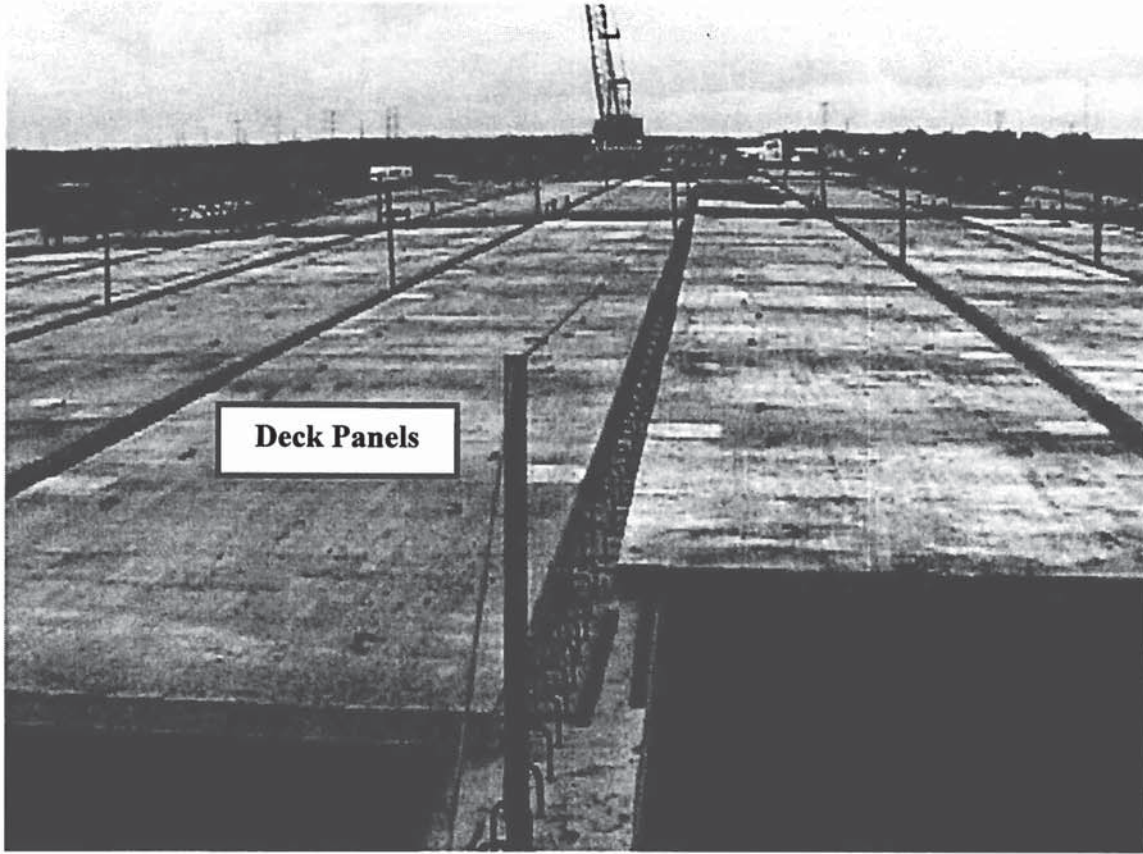


Fig. 5.13. Placement of Deck Panels at Krenek Road Bridge Site

5.2.7 Live Load Simulation

About two months before the bridge went into service, six TxDOT maintenance vehicles (dump trucks) with ballast weighting about 116.6 kN (13.1 ton) each onto two lanes in the South zone of the deck and parking them in such a location that the weights of the trucks produced maximum loads on Footing A and B. The trucks were moved to a position immediately north of the south abutment, which maximized loads on the abutment piles. This process constitutes one phase of loading (live load simulation). The live load simulation by six trucks is as shown in Fig. 5.14. The completed Krenek Road bridge in service on Highway U.S. 90 is shown in Fig. 5.15.



Fig. 5.14. Live Load Simulation with Six Trucks at Krenek Road Bridge Site

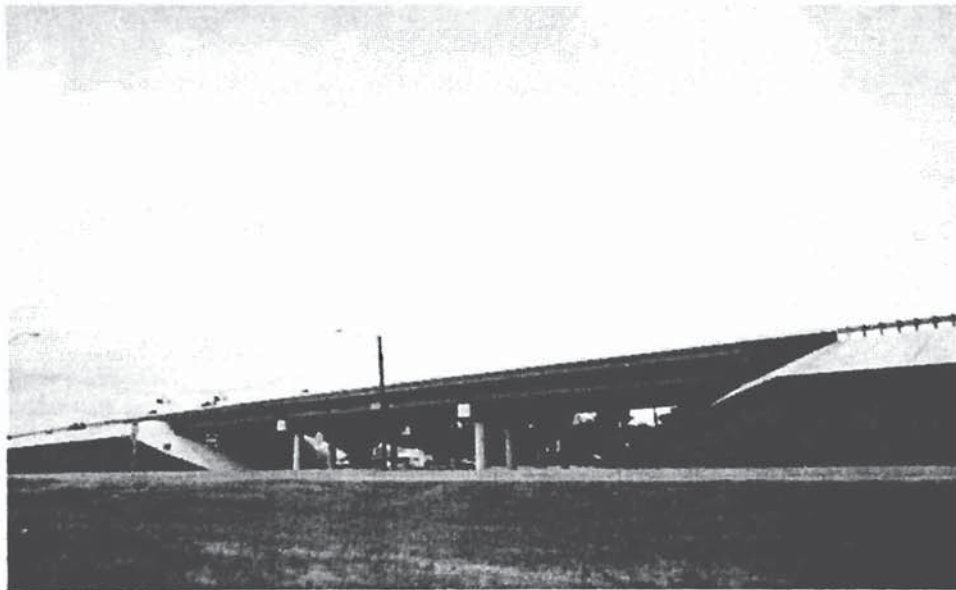


Fig. 5.15. Completed Krenek Road Bridge

5.3. Bid Evaluation and Cost Effectiveness of ACIP Piles Versus Driven Piles

As stated earlier, the bid price for the 0.457 m diameter ACIP piles was \$20.00 per linear 0.3 m. This included the placement of full-depth reinforcing cages, half of them on a batter, which undoubtedly added to the unit cost. *[The reason for the full-depth cages on this specific project was that the UH implementation team required them in order to place instruments on the piles to monitor load transfer into the soil all the way to the bottoms of the piles. Thrusting the long cages into the grout to full penetration is highly unusual and was perceived to be a challenge by the contractor, which added to the cost. Had instruments not been used, as would be the case for a normal bridge foundation, the cages could have been about half-length (about 9.1 m), which is common practice in ACIP pile construction unless large bending moments are present. This would have made them cheaper to construct and materially reduced the risk in not installed the cages to the planned depth. In turn, this would have reduced the cost by about \$2.00 per 0.3 m].* TxDOT's current design method results in 30 % less side shear capacity for ACIP piles (or drilled shafts, for that matter) than for driven piles. Therefore, the cost of the ACIP pile system was actually higher than for a driven pile system on a pile-for-pile basis.

Load tests conducted on both the ACIP test pile and a driven, prestressed concrete pile as part of the implementation project being reported here (Chapter 8) did not corroborate the use of significantly higher side resistance in the driven piles relative to the ACIP piles. In fact, comparison of the loading tests on the two types of piles showed the opposite effect. The ACIP test pile actually had a higher factor of safety than it was designed for. The driven test pile, on the other hand, actually had a lower factor of safety than it was designed for. If the driven pile had been lengthened so that it had the same

side shear capacity as the ACIP pile, resulting in the same factor of safety as the ACIP pile (2.4), the driven piles for the Runneburg Road bridge foundations would have cost \$1238 per pile based on a \$22.00 per linear 0.3 m unit cost, while the ACIP piles for the central bents at Krenek Road cost \$1140 per pile. Installation cycle times for driven piles and ACIP piles were essentially identical for the abutments for the structures at both Krenek and Runneburg Roads (45 minutes). Pre-drilling of pilot holes through the header banks was required for driven piles by TxDOT, which took about 1/3 of the cycle time. There are no reliable data for cycle times for the central bent piles at Runneburg Road because the contractor experienced delays due to the need to reposition equipment.

In addition to the cost of ACIP piles having been influenced by the need to use full-depth reinforcing cages on a batter, one other construction factor had an important impact of the cost of the ACIP piles: the TxDOT rule restricting the distance between piles installed in one 24-hour period (6 pile diameters). This rule was apparently developed for drilled shafts, but it was applied to the ACIP piles on the Krenek Road project. ACIP piles are most economical when many piles can be installed in one area in a short time without moving the drilling rig and grout pump. At Krenek Road, which had a pile layout similar to many grade separations in the Houston area, the contractor was able install only one of four piles in any given group of piles supporting an interior bent column on one day. The contractor then had to return to the same group three more times at intervals of one or two days to complete the pile installation. This is inefficient and is more expensive for an ACIP pile contractor than for a pile-driving contractor due to the set up and movement of the ancillary equipment (hydraulic pumps, grout pumps, pump lines). By allowing construction sequencing to proceed in a manner more favorable to

ACIP piles by reducing the minimum spacing between piles installed in a 24-hour period (or by reducing that period), considerable future cost savings could accrue.

A final factor that affected the cost of the ACIP piles at this project, by an unknown amount, was the requirement to place the abutment piles on a batter. Although this is common practice for TxDOT bridges in which abutments are placed in header banks, it may be less expensive to use slightly larger-diameter piles and place them vertically. This issue will require additional research but should be considered.

5.4 Settlement Data

5.4.1 Fill Settlement

As the fill was placed settlements of the fill were monitored continuously until the central bent piles were installed. All settlement readings with an accuracy of 0.3 mm (0.001 ft) were made optically with reference to a temporary benchmark on the southwest shoulder of Krenek Road at its intersection with the U. S. 90 frontage road. Three settlement stakes were set at the right side, center and left side of the right-of-way at the mid-height and top of the south embankment and had been read off from temporary benchmark. Fig. 5.16 shows the settlement vs. time at the top of the fill (average of three settlement monuments). Fill settlement measurements were corrected and extrapolated with the help of a theoretical time-dependent consolidation settlement curve predicting the time vs. settlement of the softer clay in the 1.5 m (5 ft) of soil below the compacted soils beneath the header bank. All other soils, including the fill were considered to be incompressible. Fill settlement readings began when the fill height was about 4 m (13 ft), just below the heads of the abutment piles, which occurred on Day 73. The settlement

monuments were placed about 0.3 m (1 ft) into the fill and not at the contact between the fill and the subgrade, so that settlement readings were not obtained with respect to Day 0 (commencement of construction of the fill). Settlement readings continued until about three weeks after the abutment piles were installed, at which time a concrete slab (“rip-rap”) was placed on the fill slope, which then blocked access to the fill itself to make settlement measurements. Settlement measurements were made for several months longer on the surface of the rip-rap, but no settlements were observed there. It is speculated that the fill continued to settle, however, well beyond the time the abutment piles were installed.

5.4.2 Footing and Abutment Settlements

At the time the southern central bent piles were capped, settlement monuments were placed on the corners of the square caps (as shown in Fig. 5.17) to allow for measurement of the settlement of the four “footings” in this bent (just south of Krenek Road) and rotation of two of them. Rotation would be an indicator of problems with construction.

At the time abutment piles were capped, settlement monuments were also placed in the abutment wall cap and read with reference to the permanent benchmark described previously. These settlement points allowed for measurement of settlement of abutment piles and for cross-abutment rotation. The results of the footing settlements at the central bent and the abutment will be reported in Chapters 10 and 11, respectively.

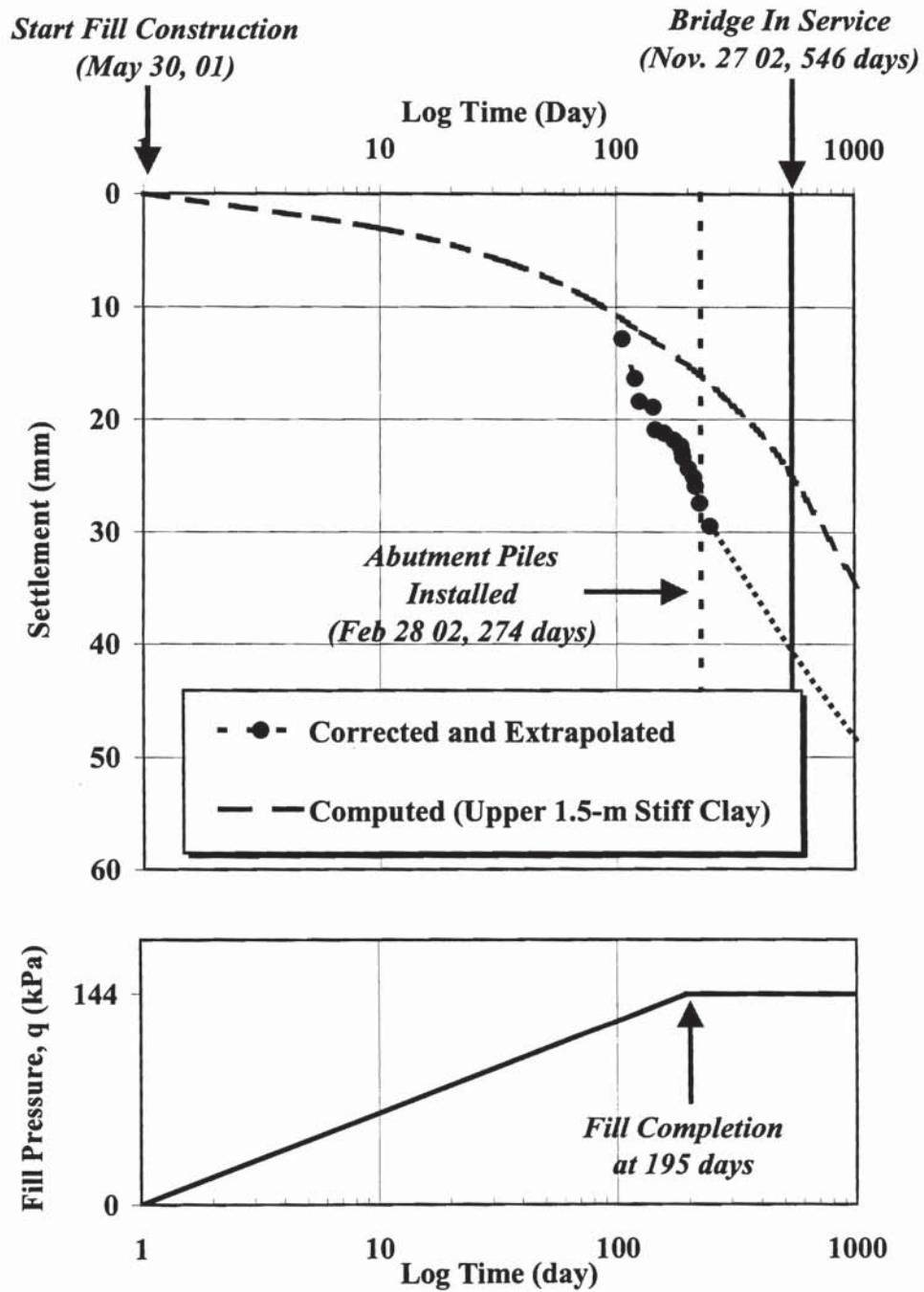


Fig. 5.16. Fill Settlement vs. Time

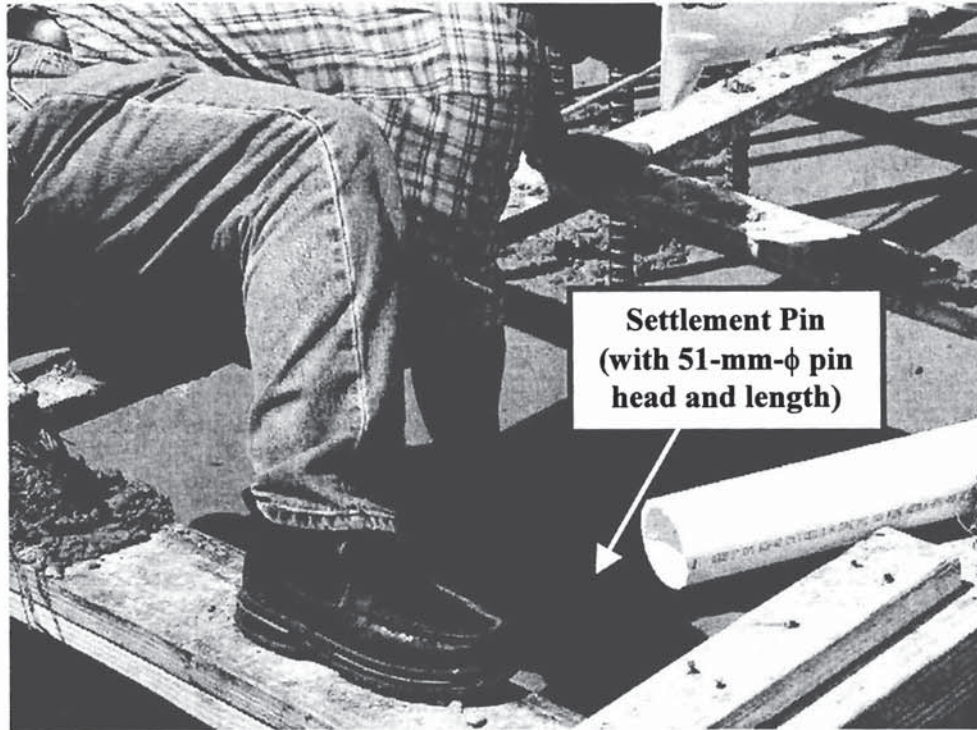


Fig. 5.17. Placement of Settlement Pin on the Corner of the Square Cap

5.5 Summary

ACIP piles did not cost less than driven piles in this implementation project based on the bid evaluation – for the specific structure considered. The reasons have been explained. With some changes in the design procedures to reflect actual pile performance and permissible construction practices (including allowing piles to be placed adjacent to each other within 4.5 diameters in the same 24-hour period and not requiring full-depth cages), based on lessons learned from the project, ACIP piles could be clearly less expensive than driven piles in a setting similar to the one considered here. If they are only cost-competitive, the marketplace will drive down the cost of the foundation whether ACIP piles or driven piles are chosen.

CHAPTER 6

INSTRUMENTATION

6.1 General

In order to develop a clear understanding of how the ACIP piling system performs in a typical bridge, a test pile and twelve production piles (eight central bent and four abutment piles) were instrumented using calibrated vibrating wire sister bars. At the bottoms of the pile caps (footings) and the abutment cap, calibrated vibrating wire contact pressure cells were placed in order to obtain measurements of loads carried by the footings rather than the piles so as to allow for the assessment of load sharing between group piles and pile cap. Fig. 6.1 shows the general instrumentation plan. A total of 144 vibrating wire sister bars, including 16 for test pile, and 11 contact pressure cells were used in this project.

6.2 Vibrating Wire Sister Bars

Vibrating wire sister bars are essentially strain gauges that operate on the vibrating wire principle rather than the electric resistance principle common to most strain gauges. The vibrating wire sister bars measures strain in a member by measuring the change in frequency of a tensioned piano wire clamped in a fixture securely attached to the member (McRae and Simmonds, 1991). This gauging system was used because it is very stable over a long period of time, whereas resistance-type gauges tend to drift

The vibrating wire sister bar consists of a short length of high strength steel, containing the vibrating wire element, a plucking magnet and a frequency sensor, welded between two 594-mm long sections of #4 deformed reinforcing bar (Geokon, Inc., 1999). It is designed to be tied using plastic or steel ties in parallel with the longitudinal structural rebar in the reinforcing cage. The small diameter of the bar minimizes its affect on of the section modulus of the reinforced concrete. Each sister bar was 1378 mm long, which allows for enough embedment of the rebar on either side of the sensing element to ensure that the bar does not de-bond from the grout and thus carries the same strain as the grout.

A cable exits from the sensing element through a small grommet of protective epoxy. This cable was run up the reinforcing cage to the ground surface and thereafter to an electronic readout box. Each vibrating wire sister bar was also equipped with a thermistor for reading temperature. Typical vibrating wire sister bar is shown in Fig. 6.2 and Fig. 6.3 shows the sister bars attached to the reinforcing cage with plastic ties.

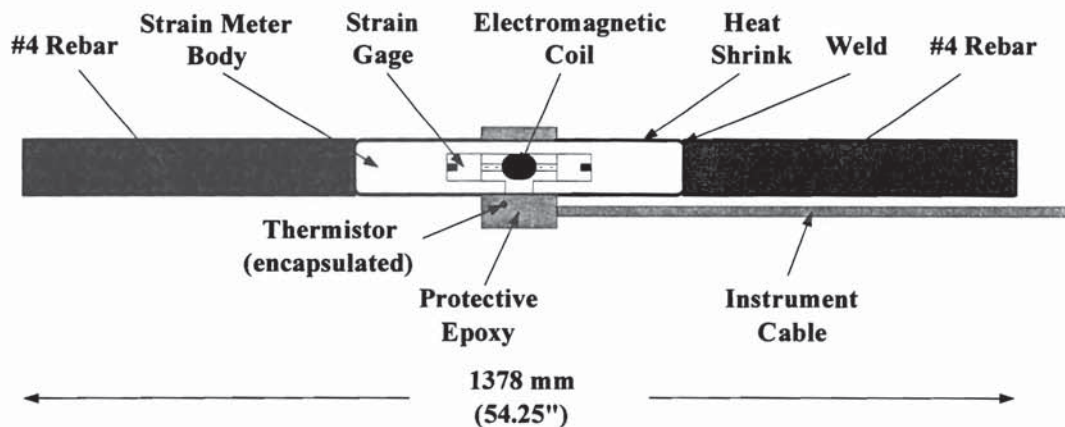


Fig. 6.2. Sketch of Typical Vibrating Wire Sister Bar

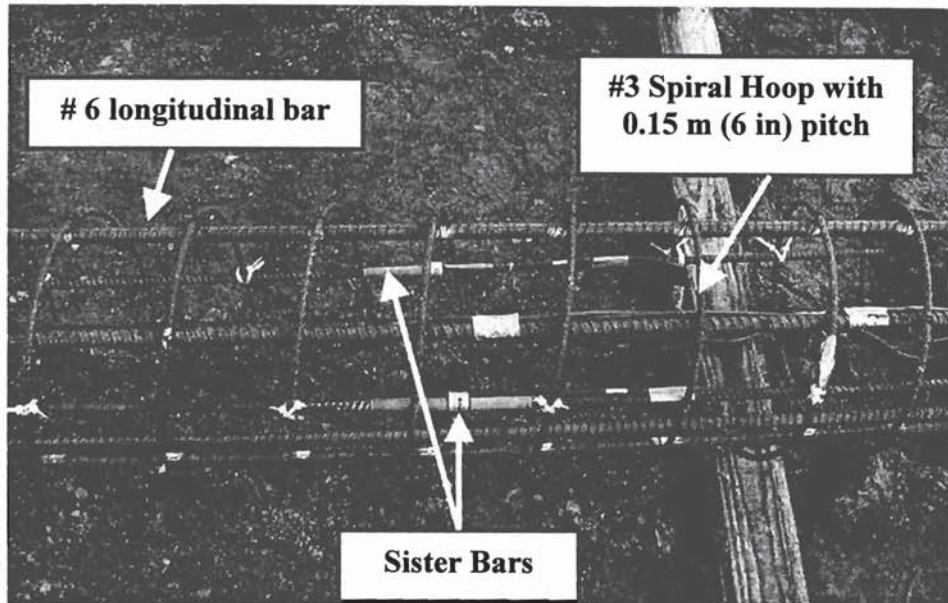


Fig. 6.3. Vibrating Wire Sister Bars Attached to Cage with Plastic Ties

Each vibrating wire sister bar was calibrated by manufacturer (Geokon, Inc.) using the linear regression method. These calibrated instruments were installed on rebar cages prior to insertion of the cages into the grout columns.

A test pile and twelve production piles (eight central bent and four abutment piles) were instrumented using the calibrated vibrating wire sister bars. The test pile was instrumented with 16 vibrating wire sister bars at various levels along the pile length. Instrumentation details for the test pile are shown in Fig. 6.4. Central bent piles were instrumented with 14 sister bars at six different locations (Type A – FA/P1, FA/P3, FB/P1, and FB/P3), with 8 sister bars with three different locations (Type B – FA/P2, FB/P2, and FB/P4), and with 12 sister bars with five locations (Type C – FA/P4) along the pile length as shown in Fig. 6.5. Abutment piles were instrumented with 10 sister bars at five different levels (Type I - GA/PF, GA/PB, and GB/PF) and with 6 sister bars at three top levels (Type II – GB/PB) as shown in Fig. 6.6. The sister bars were read

continually throughout the project, especially at critical construction steps such as placing pile caps and the abutment cap and wall, placing columns, placing girders, placing deck, placing a simulated live load, and operating the bridge under traffic.

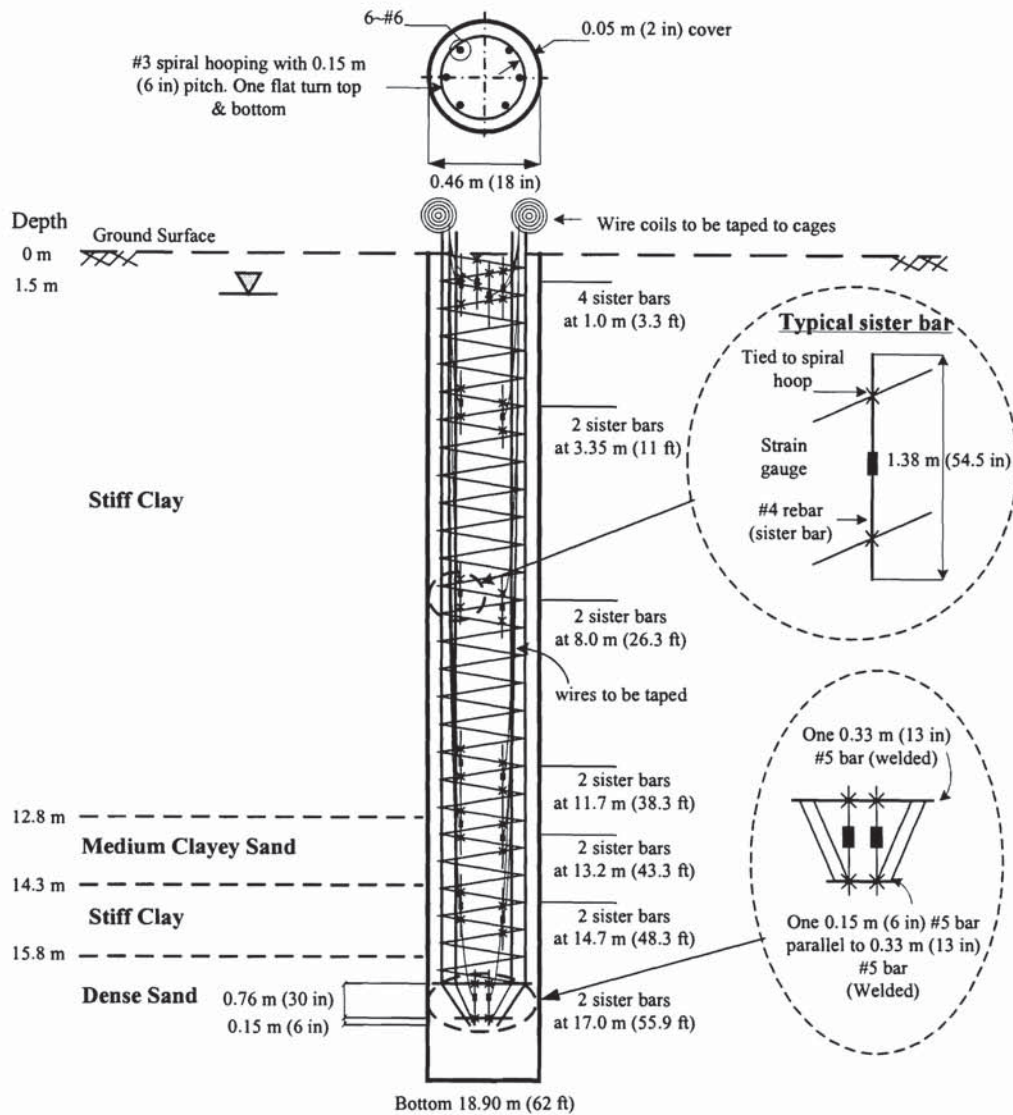


Fig. 6.4. Instrumentation Details for Test Pile

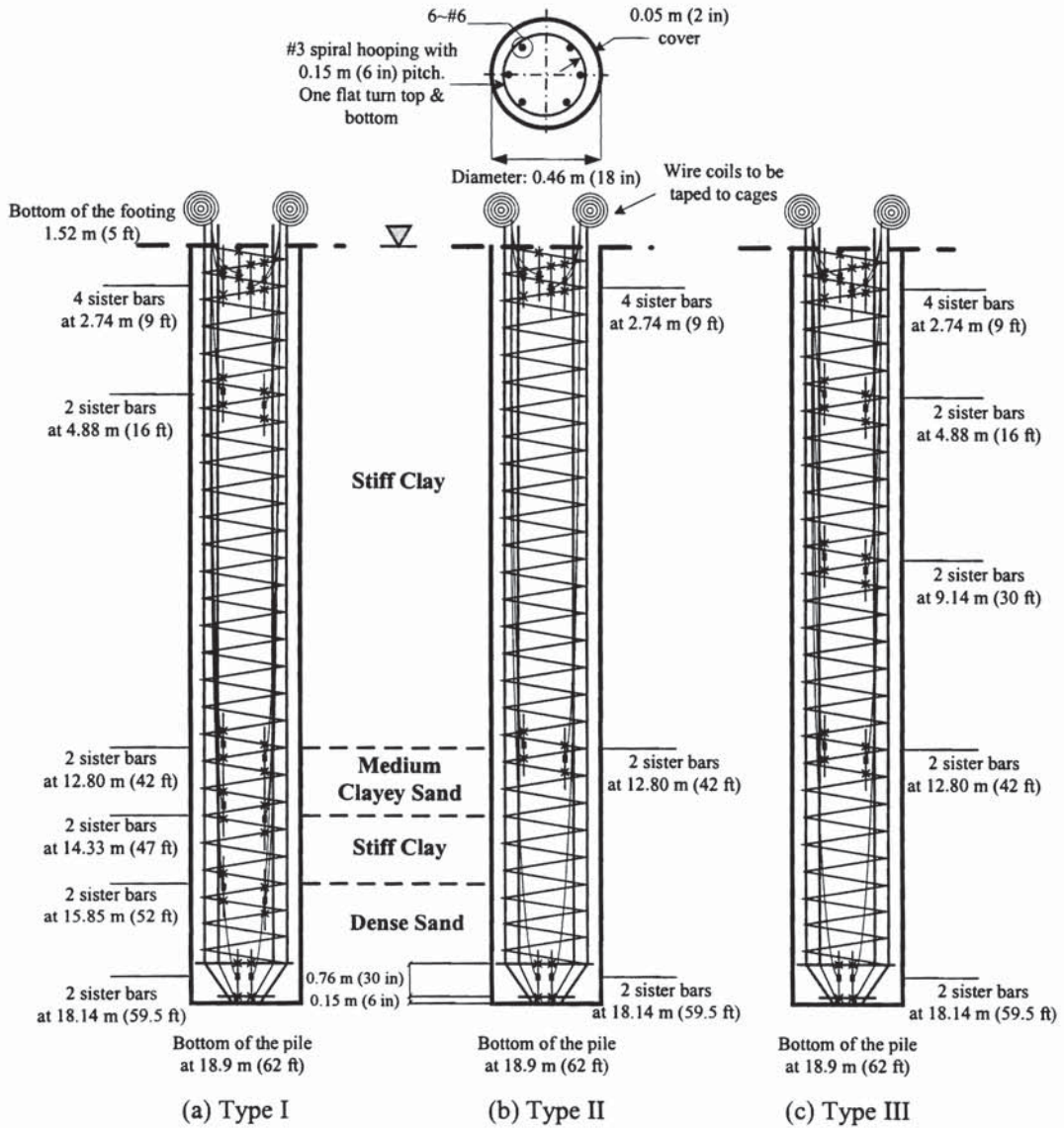
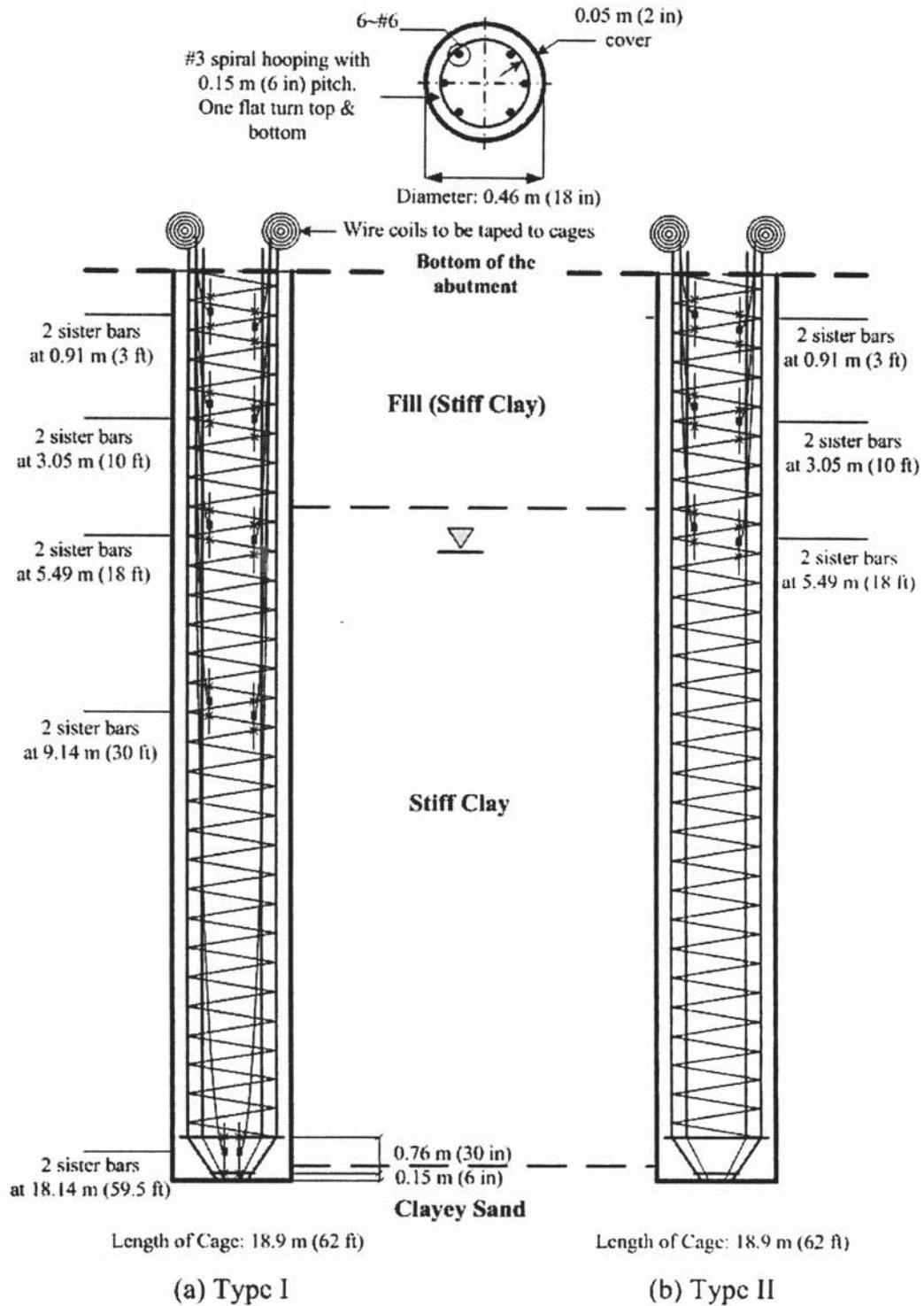


Fig. 6.5. Instrumentation Details for Central Bent Piles:

(a) Type I (b) Type II (c) Type III



Note: Abutment piles are installed in a 4:1 batter through the stiff clay fill. Levels of sister bars shown here are those below the bottom of the abutment along the pile length.

Fig. 6.6. Instrumentation Details for Abutment Piles:

(a) Type I (b) Type II

The sister bar gauges served to determine whether any drag loads were induced in the piles by settlement of the embankment; the magnitude of any bending moments that may be produced in the piles due to rotation of the abutments or central pier footings or to lateral squeeze of the embankment material; the uniformity of distribution of loads to the heads of the piles, and the rate of transfer of load into the piles through the various soil strata at the site. Four gauges were placed near the head of the instrumented test pile and each central bent pile in order to ascertain both axial loads and bending moments in two directions. These gauges also served to indicate whether load had been shed from shaft to toe (or vice versa) over a long period of time. These data are complementary information to the continual, time-dependent settlement that was observed. The information that was obtained from this monitoring process can also be considered in establishing design procedures for ACIP pile foundations on future projects by answering questions concerning whether drag loads develop on the piles installed through embankment fills and the magnitude of the moments that actually occur in the piles due to fill settlement that has a component transverse to the axis of the pile. In current practice, abutment piles are generally considered to be moment free for design purposes.

6.3. Vibrating Wire Contact Pressure Cells

Vibrating wire contact pressure cells are constructed from two stainless steel plates welded together around the periphery and spaced apart by a narrow cavity filled with antifreeze solution (Geokon, Inc., 1998). A length of high-pressure strain steel tubing connects the cavity to a pressure transducer (Geokon, Inc., 1998). External pressures acting on the cell are balanced by an equal pressure induced in the internal fluid

(Geokon, Inc. 1998). This pressure is converted into an electrical signal which is transmitted by a four conductor shielded cable to the readout location (Geokon, Inc, 1998). The pressure cell is shown in Fig. 6.7.

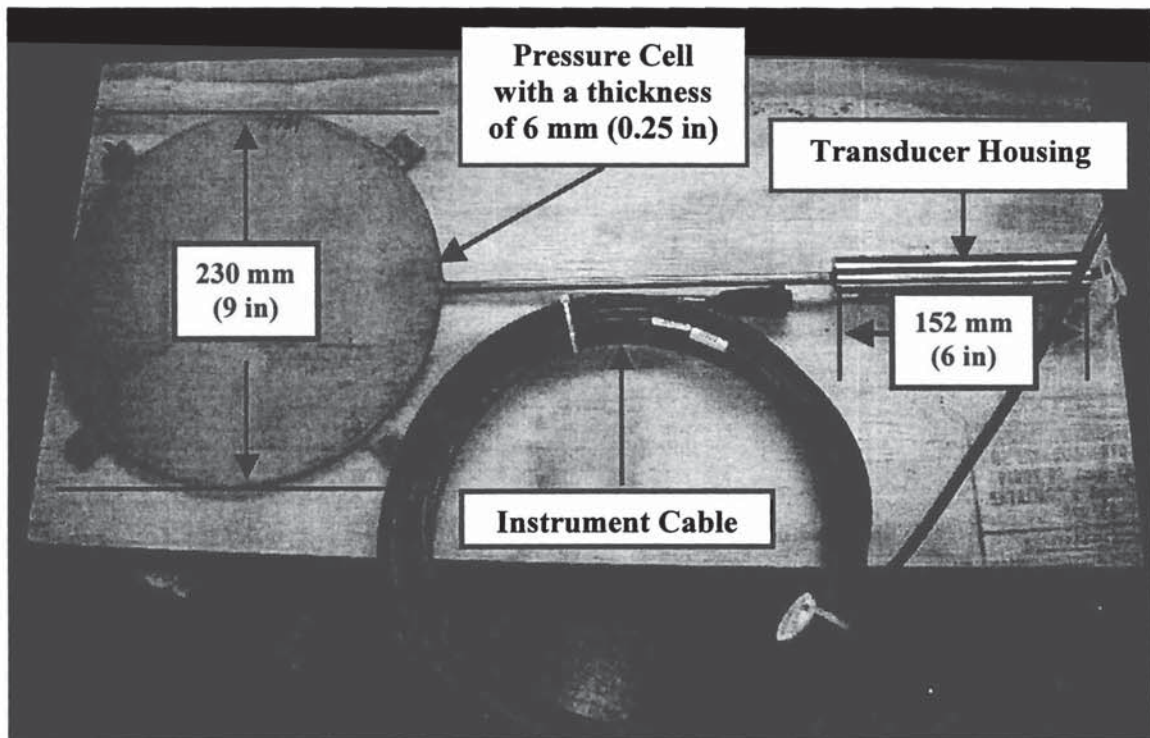


Fig. 6.7. Vibrating Wire Contact Pressure Cell

Calibrated eleven vibrating wire contact pressure cells were installed as shown in Fig. 6.1. Six pressure cells were placed under the two central bent pile caps that contained instrumented piles. Three pressure cells were installed under each pile cap. The others were installed under the abutment footing. In Fig. 6.8, the placement of the contact pressure cell at the bottom of the footing is shown. The purpose of these pressure cells was to determine how much of the applied load is taken by the pile cap (footing) as compared to how much load is resisted by the piles, which were determined by reading

the sister bars at the tops of the piles. Pile cap resistance could be substantial and may lead to reduce design loads on the piles, which has implications with respect to future design procedures. However, as already described, the subgrade for the footings was not compacted, and consisted of perhaps 0.3 m (12 in.) of soft clay over relatively undisturbed soil. Whether significant long-term load will be shared by the cap with this soil condition is a specific subject of this study.

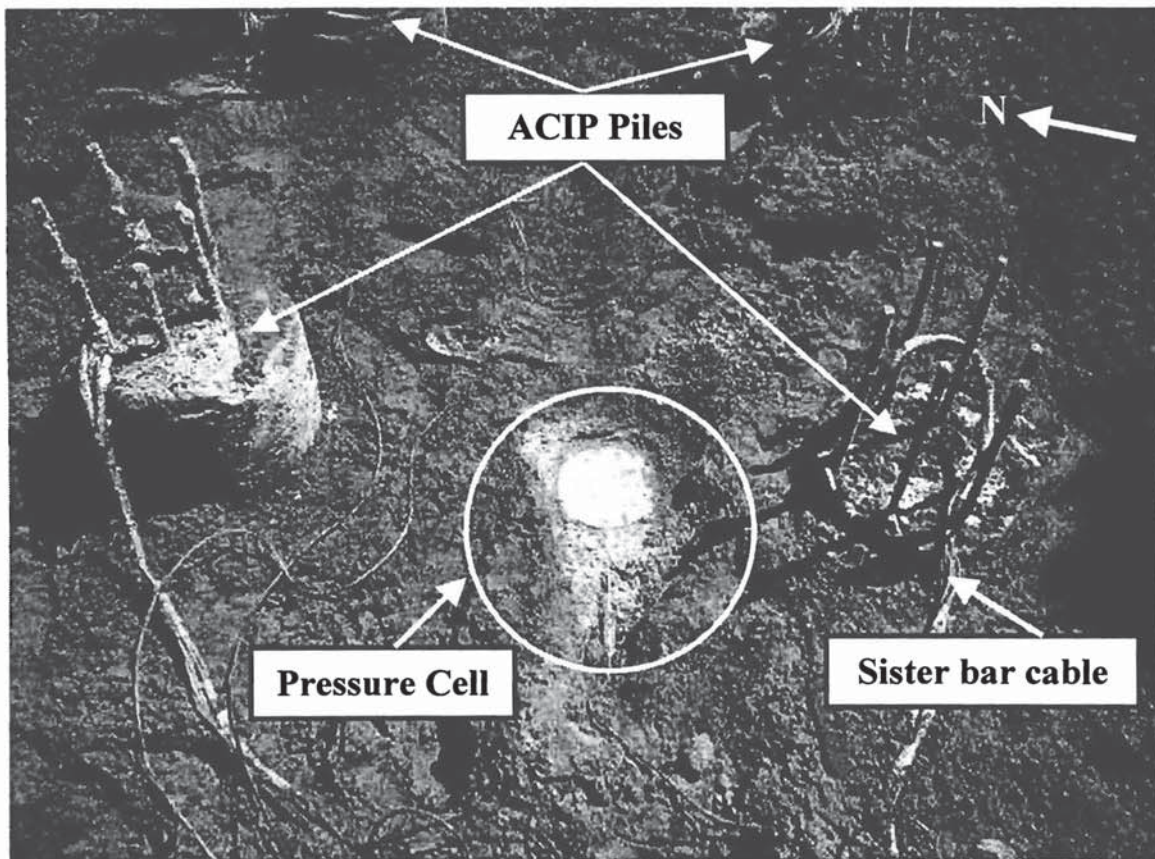


Fig. 6.8. Placement of Contact Pressure Cell at the Bottom of Footing A

6.4 Data Acquisition Methods (Readout Devices) and Preliminary Reduction

A 32-channel terminal switch box was used for easy connection and disconnection of the lead wires (cables) from the sensors to a readout device. The readout device sensed the frequency of the vibrating wire in each gauge sensor to which it was connected through the switch box. In this manner it was used to monitor both the sister bars and pressure cells. Up to 256 readings can be stored in this device, along with reference number, time, date, and temperature. Stored readings were later easily imported to a laptop personal computer with the 25 pin RS-232 connector using PROCOMMTM communications software, provided by the manufacturer. These imported readings (ACIII format) were thereafter transferred to Excel spreadsheets.

The unit for readings of vibrating wire sister bars using the readout device is digits. The digit was calculated using the following Equation (6.1).

$$Digits = \left(\frac{1}{T}\right)^2 \times 10^{-3}, \text{ or } Digits = \frac{Hz^2}{1000}, \quad (6.1)$$

where

T = the period in seconds,

Hz = the frequency in cycles per second.

Vibrating wire readings (digits) from the readout device were converted to strain by multiplying by each strain gauge factor.

In order to convert readings (digits) to strain, considering temperature changes during the period of the readings, the Equation (6.2) was used.

$$\epsilon_{corrected} = (R_1 - R_0) X C_s + (T_1 - T_0) X K , \quad (6.2)$$

where

- R_0 = Initial or previous reading (digits),
 R_1 = Current reading (digits),
 C_s = Calibration factor (microinches/inch/digit),
 Strain (ϵ) = Compression (-) and Tension (+) (microinches/inch),
 T_0 = Initial or previous temperature reading ($^{\circ}$ C),
 T_1 = Current temperature reading ($^{\circ}$ C), and
 K = Thermal coefficient, 2.2 microinches/inch/ $^{\circ}$ C (suggested by GeoKon, Inc).

$\epsilon_{corrected}$ was then multiplied by the product of the equivalent elastic modulus for the cross section and the nominal cross-sectional area to obtain load in the pile at the depth of the strain gauge for the particular event being monitored. This process will be discussed further in a later chapter (Chapter 7).

For the contact pressure cells, digits from the readout device were converted to pressure in a manner similar to that used for the sister bars, except that a pressure gauge factor, C_p , was used in lieu of C_s . In order to convert readings to pressure considering temperature changes during the following Equation (6.3) was used.

$$P_{corrected} = (R_0 - R_1) X C_p + (T_1 - T_0) X K , \quad (6.3)$$

where

P = Pressure (psi),

R_0 = Initial or previous reading (digits),

R_1 = Current reading (digits),

C_p = Calibration factor (psi/digit),

T_0 = Initial or previous temperature reading ($^{\circ}\text{C}$),

T_1 = Current temperature reading ($^{\circ}\text{C}$), and

K = Thermal factor of $-0.02814/^{\circ}\text{C}$.

CHAPTER 7

GROUT PROPERTIES AND PILE STIFFNESS

7.1 General

The major structural constituent in the ACIP pile is grout. The grout must have good working properties so that it can be pumped into place, and the steel cage can be easily inserted into the grout after filling the borehole. Flow cone tests were carried out to check the workability of the grout in the field prior to pumping the grout into each pile. Mechanical properties (compressive strength and Young's modulus) of the grout were determined in the laboratory by conducting unconfined compression tests on samples recovered from the field during pile installation, with and without attaching strain gauges. According to TxDOT special specification for ACIP piling (O'Neill et al., 1999), the grout samples tested at 28 days after casting shall exhibit a minimum compressive strength of at least 27.6 MPa (4,000 psi) for cylinders or 30.3 MPa (4,400 psi) for cubes. Splitting tension tests were also performed on sample of grout in order to check if tensile residual loads or stresses induced by bending that might occur on an ACIP pile exceed the tensile strength of grout. The test data were used for field data reduction.

7.2 Mix Design

The constituents of the grout mix used in this project are Portland cement (Type II), fine aggregate meeting the requirements of TxDOT Item 421.2 (0 + #16 sieve), water, fly ash, and an additive ("fluidifier"). The mix design for the grout used is shown in

Table 7.1. The fluidifier is a proprietary product but serves the same purpose as a high-range water reducer in a concrete mix.

Table 7.1. Grout Mix Design

Constituents	Amount by Weight (%)
Portland Cement (Type II)	20.3
Fine aggregate	61.4
Water	12.1
Fly ash (Class F)	6.1
Additive (Fluidifier)	0.05

7.3 Flow Cone Test (ASTM C 939)

The flow cone test was used for routine quality control of grout in the field. It is a static instrument that indirectly measures the viscosity of the grout. The variable measured is the time, in second (s), required for a given quantity of grout to pass through the orifice of a standardized funnel. The flow time was measured for the first 950 mL (32 oz, or 1 quart) of the grout to flow through the 19 mm (0.75 in)- ϕ orifice. The measurement obtained is influenced considerably by the rate of gellation and by the density, which varies the hydrostatic head of the column of the grout in the funnel. The flow cone measuring the viscosity gives a measure of the fluidity of the grout by virtue of the “time of efflux” through the orifice, with an orifice diameter of 19 mm (0.75 in). The field efflux value for grout mixes were in the range of 8-18 seconds. Based on the field observation, it is not recommended using grout for an ACIP pile with a field efflux value

higher than 18 sec, since the grout was too viscous to push the cage into. Flow cone test results were summarized in Table 7.2 for the instrumented piles and the test and reaction piles. See Fig. 6.1.

Table 7.2. Flow Cone Test Results for Instrumented Piles, and Test and Reaction Piles

Pile Name	Efflux Time (sec)	Remarks Recommended efflux time (18 sec)
Test Pile	10	O.K
FD/P4 (Reaction Pile 1)	10	O.K
FD/P3 (Reaction Pile 2)	19	Higher than recommended time
FC/P2 (Reaction Pile 3)	10	O.K
FC/P1 (Reaction Pile 4)	15	O.K
FA/P1	14	O.K
FA/P2	11	O.K
FA/P3	12	O.K
FA/P4	11	O.K
FB/P1	10	O.K
FB/P2	11	O.K
FB/P3	14	O.K
FB/P4	14	O.K
GA/PF	8	O.K
GA/PB	8	O.K
GB/PF	17	O.K
GB/PB	>20	Higher than recommended time

7.4 Grout Strength and Modulus Tests

In order to deduce loads from sister bar readings, strains were converted to stresses using appropriate moduli for the grout and steel. Cylindrical plastic mold specimens of grout (76-mm- ϕ X 152-mm) were collected from the field and tested in compression in the laboratory at various curing times of the grout in accordance with ASTM C 109. The specimens were cured in the mold till the time of testing. The testing machine was operated at a constant displacement rate of 0.03 mm/min. Sets of at least three compression tests were conducted at various times after pile installation using the samples collected (4 days, 7 days, 14 days). A final set of tests was performed at 18 days for the test pile and 28 days for the production piles. Five tests for the test pile and 11 tests for the production piles were conducted at that time. The objective of the grout tests was to obtain a relation between the low-strain secant modulus of the grout and time. This was accomplished by placing bonded electrical resistance strain gauges on two opposite sides of the five reference samples for the test pile, and of eleven samples from the production piles, collected from the field during pile installation. These samples were tested on the day of the load test (test pile) or capping of the production piles, after curing and storing the samples in humid room until the time of testing. The samples were loaded in compression in a compression testing machine (servo-hydraulic Tinius-Olsen machine) with a capacity of 1.7 MN (400 kips) while simultaneously making strain readings from the bonded strain gauges on the specimens. It is noted that all samples were trimmed and capped to ensure parallel surface. Stress-strain curves for samples are shown in Appendix B. Ratios of initial, small-strain secant modulus (ISM) to compressive strength

(f_{cr}) were computed from these tests, where f_{cr} refers to the compressive strength of the reference grout samples (on the day of test).

The sets of grout samples tested at intermediate times ($t = 4, 7, 14$ days after casting) were not strain-gauged but instead were subjected to compression tests to failure. ISM's corresponding to these intermediate times were determined for the test pile and for the production piles (separately) by multiplying the ratio of measured intermediate compressive strength, f_{ci} (4, 7, 14 days), to the compressive strength of the reference specimen, f_{cr} , times the mean ISM of the instrumented reference specimen, on the assumption that average ISM/f_c was nearly constant over time in a given grout batch. Separate ISM/f_{cr} values were employed for the test and production piles because the grout was batched at different times and by different suppliers.

The ISM and f_{cr} for the test pile at the time of the load test (18 days after pile installation) are summarized in Table 7.3. The mean values of f_{cr} (18 days) and ISM for the test pile were 36.0 MPa and 26.2 GPa, respectively. It is noted that the average compressive strength of 36.0 MPa for the test pile at 18 days is higher than minimum compressive strength of 27.6 MPa (4,000 psi) at 28 days for cylinders to meet TxDOT special specification. The mean value of ISM/f_{cr} at 18 days was 598. Table 7.4 summarizes the values of f_{ci} (4, 7, 14 days) measured at various intermediate times (4, 7, 14 days) after casting and values of ISM computed from those values and the measured values of f_{cr} (18 days) and ISM for the reference specimens. The computed values of ISM for the grout were converted to ISM values for the piles by considering the relative moduli of the longitudinal steel and the grout and the relative cross-sectional areas. The

Young's modulus of the longitudinal reinforcing steel was taken to be 200,000 MPa, which is usually used in drilled shaft design (Reese and O'Neill, 1988).

Table 7.3. Ratio of Initial Secant Modulus (ISM) to Compressive Strength of Grout for Test Pile on the Load Test Day (18 Days After Test Pile Installation)

Grout Sample	Measured Compressive Strength (MPa)	Measured ISM (GPa)	Ratio
TP-1	36.6	22.8	622
TP-2	36.6	20.7	565
TP-3	36.5	22.1	604
TP-4	37.0	20.7	560
TP-5	33.4	21.4	640
Mean	36.0	21.5	598
St. Dev.	1.5	0.9	35
C.O.V.	0.04	0.04	0.06

Table 7.4. Summary of Compressive Strength of Grout, Initial Secant Modulus (ISM) of Grout, and ISM of Pile at Various Times after Casting Test Pile

Time after Casting (days)	Measured Compressive Strength (MPa)	Computed ISM of Grout (GPa)	Computed Composite ISM of Pile (GPa)
0	0.0	0.0	0.0
4	28.7	17.2	19.1
7	30.4	18.2	20.1
14	32.6	19.5	21.4
18 (Load Test)	36.0	21.6	23.4

The ISM's of the grout and production piles were determined in a similar manner.

Table 7.5 shows the $f_{cr(28 \text{ days})}$ and ISM values measured for these piles. The mean value

of f_{cr} (28 days) and ISM for the production piles was 38.6 MPa and 26.2 GPa, respectively. It is noted that the average compressive strength of 36.0 MPa for the test pile at 18 days is higher than minimum compressive strength of 27.6 MPa (4,000 psi) at 28 days for cylinders to meet TxDOT special specification for ACIP piling. The average value of ISM/f_{cr} (28 days) was 683 at 28 days after pile installation, which corresponded to the time at which loads were evaluated in the production piles. Table 7.6 summarizes information for the production piles that is similar to that in Table 7.4 for the test pile.

Table 7.5. Ratio of Initial Secant Modulus (ISM) and Compressive Strength of Grout for Production Piles at Age 28 Days (11 samples)

Grout Sample	Measured Compressive Strength (MPa)	Measured ISM (GPa)	Ratio
B-23	41.7	24.2	580
B-24	41.7	24.2	579
B-25	40.7	29.3	720
B-26	36.0	27.9	776
B-31	38.4	27.6	718
B-32	38.5	22.1	573
B-34	35.4	29.0	820
A-15	42.4	24.2	570
A-16	41.5	28.3	682
A-17	36.7	26.9	733
A-18	31.8	24.2	759
Mean	38.6	26.2	683
St.Dev	3.4	2.5	92
C.O.V.	0.09	0.09	0.13

Table 7.6. Summary of Compressive Strength of Grout, Initial Secant Modulus (ISM) of Grout, and ISM of Pile at Various Days for Production Piles

Time (day)	Measured Compressive Strength (MPa)	Computed ISM of Grout (GPa)	Computed Composite ISM of Pile (GPa)
0	0.0	0.0	0.0
4	28.7	19.6	21.5
7	30.4	20.7	22.6
14	32.6	22.3	24.1
28	38.6	26.4	28.2

7.5 Splitting Tension Test (ASTM D-3967)

Tests were performed on specimens of grout with a diameter of 76.2 mm (3 in) and a height of 50.8 mm (2 in) to determine their tensile strength at a time of 18 days (load test) for the test pile and 28 days for the production piles. A screw-type loading machine with a capacity of 44.5 kN (10 kips) was used for determining the splitting tensile strength of grouts. Six specimens were tested for the test pile and seven for instrumented production piles. Tables 7.7 and 7.8 shows the results of the splitting tension tests for the test pile and the production piles.

7.6 Procedure for Converting Strain to Load

Vibrating wire strain gauges were read at various times after casting the piles. Initial strain readings, used as zero readings, were made when the grout was fluid with the sister bars attached to the rebar cage immediately after the cage had been thrust into the grout column.

Table 7.7. Summary of Splitting Tension Test Results for Test Pile

Specimen	Tensile Strength (MPa)
T-1	2.6
T-2	6.3
T-3	2.8
T-4	5.3
T-5	2.4
T-6	4.5
Average	4.0
St. Dev.	1.63
C.O.V.	0.41

Table 7.8. Summary of Tension Test Results for Production Piles

Specimen	Tensile Strength (MPa)
FA/P1	4.0
FA/P2	5.6
FA/P3	3.1
FA/P4	5.4
FB/P1	4.9
FB/P4	3.5
FB/P2	4.2
Average	4.4
St. Dev.	0.96
C.O.V.	0.22

Small strains were measured throughout the curing process; therefore the stress-strain curve for the grout was assumed to be linear (expressed using the ISM, as

suggested in the preceding section) but time dependent due to curing. The pile ISM values from either Table 7.4 (test pile) or Table 7.6 (production piles) were plotted against time, as illustrated in Fig. 7.1. Axial stress, σ_a , in the pile at each level of instrumentation was then computed incrementally in time from Equation (7.1).

$$\sigma_a = \sum_{t=1}^{t=t_{max}} (\varepsilon_t - \varepsilon_{t-1}) \left[\frac{(\text{ISM}_t + \text{ISM}_{t-1}) A_g + E_s A_s}{2(A_g + A_s)} \right], \quad (7.1)$$

in which ε_t and ε_{t-1} are the measured strains (average of all gauges at a level), considered positive in extension, at discrete times t and $t-1$, respectively, The ISM's are the ISM's of the grout at the appropriate times after casting (t). A_g and A_s are the nominal areas of grout and steel in the cross section, respectively (164,173 mm² and 1,703 mm²), respectively) and E_s is the Young's modulus of the longitudinal steel (200,000 MPa).

Stresses were summed from time increment to time increment because the ISM changes with time. Within any time increment, the ISM was taken to be constant, as ISM _{t} , shown in Fig. 7.1.

The resulting value of σ_a was a composite value, considering both steel and grout, and was therefore multiplied by the nominal gross cross-sectional area of each pile (0.164 m² or 254 in.²) to obtain the load in the pile at time t .

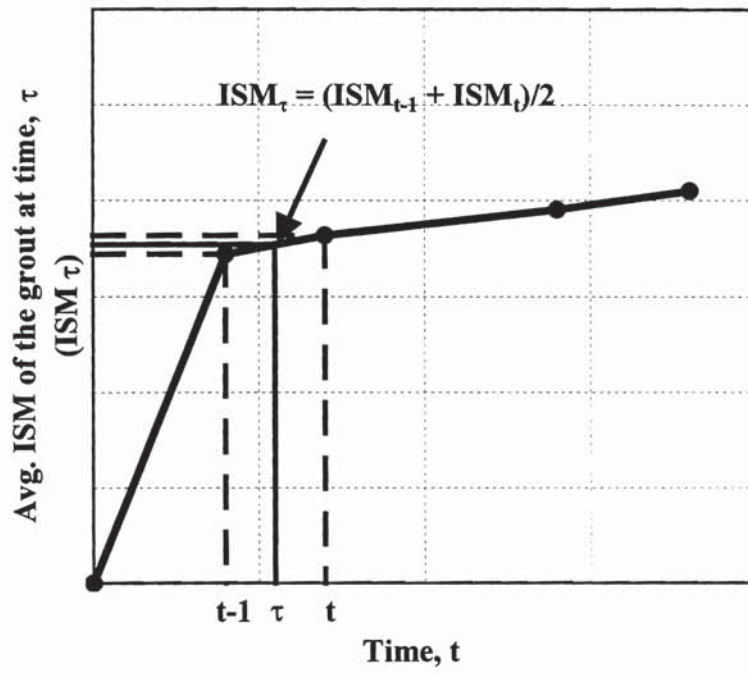


Fig. 7.1. ISM vs. Curing Time

CHAPTER 8

FULL-SCALE LOAD TESTS

8.1 General

This chapter presents the details of full-scale load tests on an instrumented ACIP pile at U.S. 90 at Krenek Road and a driven prestressed concrete (PC) pile at U.S. 90 and Runneburg Road. The two test sites (hereafter called Krenek and Runneburg) are at adjacent bridges, both grade separations and both nearly identical structurally, along a new highway. The location of the two sites is marked in Fig. 3.1. An instrumented ACIP pile was load-tested before installing production piles at the Krenek Road site to monitor the single ACIP pile load transfer behavior and to verify the pile capacity estimated in the design stage. This process was repeated for a conventional driven PC pile at the adjacent bridge at Runneburg Road. The results of load tests were used to compare side shear resistances of ACIP and driven PC piles as a means of evaluating the relative load-carrying efficiencies of the two pile types in the overconsolidated Pleistocene soil formations of the area. In order to make a fair comparison of the side resistances for the two piles, which were situated in similar geologic materials, but in which the undrained shear strengths varied slightly, the ratio of average unit side resistance to average undrained shear strength, commonly termed the “ α factor” were compared for the two test piles.

Prior to the load tests, residual tension loads were found to exist in the ACIP test pile. These tension loads increased with time during grout curing. Generally, these

residual loads were found to be relatively small, but not insignificant, and appear to have been related to site-specific soil profile characteristics. The PC pile at the Runneburg site was not instrumented, so it was not possible to determine residual loads, if any, in that pile.

8.2 Residual Loads

The existence of post-driving residual loads in driven piles has long been known (Vesic, 1977; Holloway et al., 1978; Poulos & Davis, 1980; Briaud & Tucker, 1984; Fleming et al., 1985). The “capture” of stress waves, particularly in flexible piles, produces these residual loads. Fellenius (2002) and Falconio and Mandolini (2003) have recently suggested that residual loads may also develop in drilled shafts and that part of the residual or “locked-in” load in a deep foundation is caused by post-construction volume change of the ambient soil and other time-dependent phenomena. Fellenius also stressed that the residual loads must be considered in the analysis of load test data to avoid erroneous conclusions, for example, regarding ratios of developed unit side resistance to the shear strength of the soil at various points along the pile.

In the past, it has generally been assumed that residual loads do not develop in cast-*in-situ* piles such as drilled shafts and ACIP piles, in the overconsolidated, Pleistocene soils of the Texas Gulf Coast, since there are no stress waves to capture and since reconsolidation of the overconsolidated soil should be minimal. Therefore, when conducting a load test on an instrumented cast-*in-situ* pile, the zero readings in the strain gauges at the beginning of the load test have always been assumed to represent an unstressed condition, and load transfer patterns have been derived from the test data

based on that assumption. The implementation of ACIP piles in the Krenek Road bridge foundation has allowed for the measurement of residual loads in several ACIP piles to test the validity of this assumption. Later, distributions of measured residual loads are considered in the test pile (in this chapter) when interpreting load transfer phenomena in the ACIP piles.

8.3 Full-Scale Load Tests

8.3.1 Krenek Road Site

The Krenek Road bridge site consists of a mixed soil profile of generally stiff clays and medium dense sands, as shown in Fig. 3.2 in Chapter 3. The 0.457-m-diameter ACIP test pile along with 4 reaction piles were installed. The location of test pile and reaction piles are shown in Fig. 3.3 in Chapter 3. The test pile was installed between footing C and footing D. Detailed layout for the test pile and reaction piles is shown in Fig. 5.2. The reaction piles were used as production piles (central bent piles) after load testing was done. The order of installation was FD/P4, FC/P2, the test pile (TP), FD/P3, and FC/P1 in Fig. 5.2. Installation dates for the piles were shown in Table 5.1.

The axial load test was performed on the instrumented ACIP test pile (Fig. 6.4), which penetrated 18.9 m below the surface of the ground. The test was performed by jacking the head of the test pile against reaction beams anchored by four reaction piles using a pneumatically powered jacking system. The jacking system consisted of a hydraulic jack and an electronic load cell with a capacity of 4.5 MN (500 tons). Both the load cell and the hydraulic jack were placed inside a reaction strut supported by the reaction beam. The load cell with the jacking system was calibrated prior to the loading

test. The load cell met the accuracy standards of ASTM E-4-99 (+/- 1% of reading) up to 4.5 MN (500 tons). Both the jack pressure, which was correlated to load during calibration of the jack and the load cell were read during the loading tests. The load readings never varied between these two load monitors by more than one percent. Four mechanical dial gauges having a precision of 0.0254 mm (0.001 inches) attached to the top of the test pile and suspended from reference beams were used to monitor the axial settlement of the test pile. Dial gauges were equally spaced around the test pile and readings were averaged to correct for any pile top tilting during the test. Supports for reference beams were located at a distance of 2.7 m (9 ft) from the application of each new load increment and decrement. The loading arrangements for both the Krenek and Runneburg test piles were essentially identical. Fig. 8.1 shows the load test arrangements for both the Krenek and Runneburg bridge sites.

The axial compressive load test was designed to produce compressive axial forces in the piles by applying axial loads to the heads of the pile. The load test was performed in general accordance with the TxDOT Specification (1993) Item 405 "Foundation Test Load" and ASTM D1143, "Standard Method of Testing Piles under Static Axial Compression load". The pile was loaded in 222 kN (25 tons) increments up to 1779 kN (200 tons). Load increments above 1779 kN were then reduced to 89 kN (10 tons) to failure, due to the rate of pile head deflection that was observed for loads in excess of 1557 kN (175 tons). The failure load was determined by the Davisson failure criterion (Davisson, 1972) which was 1913 kN (215 tons).

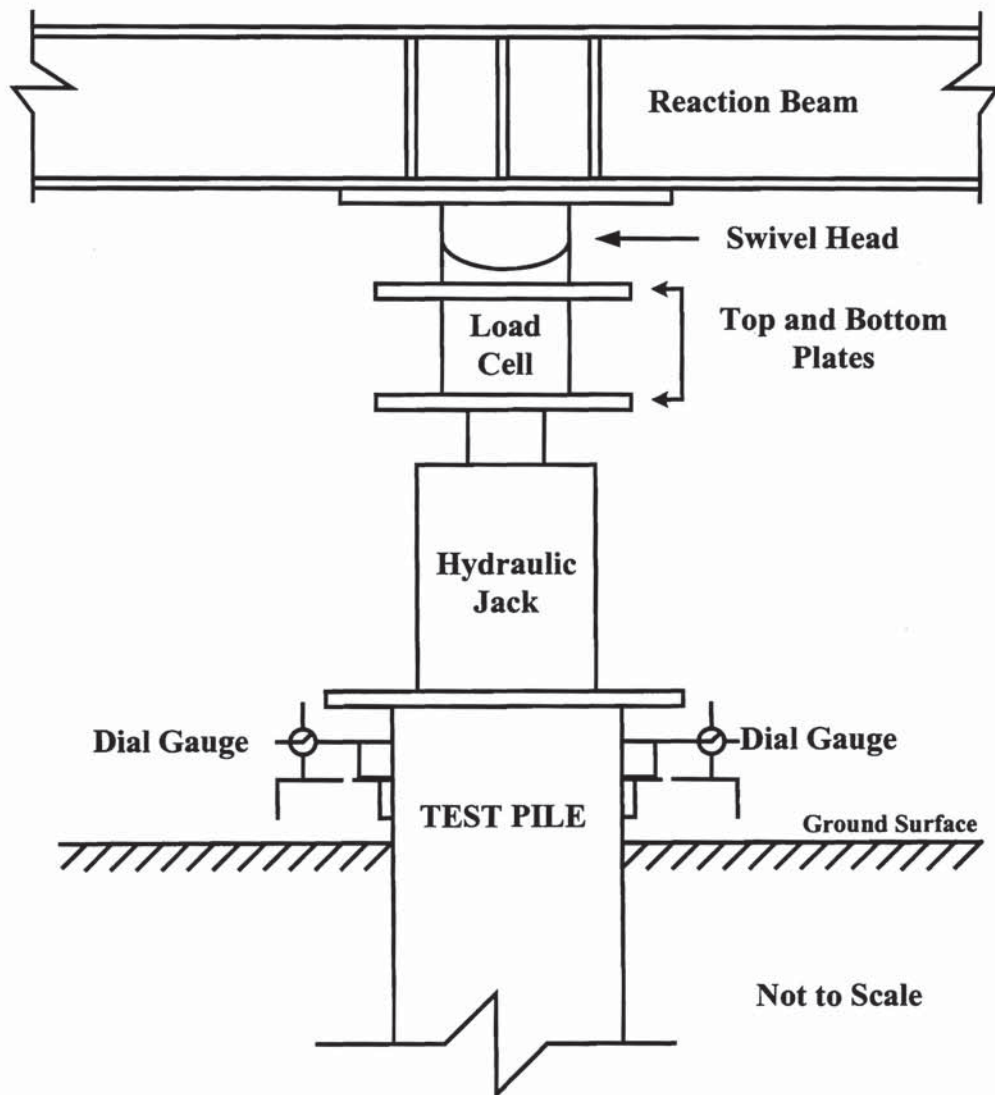


Fig. 8.1. Load Test Arrangement

Each new load increment was applied and held for 20 minutes. Load, sister bar and settlement readings were taken at 10 minutes and 20 minutes after each new load was applied. After reaching failure, the test pile was unloaded in 512 kN (57.5 tons) decrements until the head load was zero. Each new decrement was also held for 20

minutes, and load, sister bar and settlement readings were taken at 10 minutes and 20 minutes after each new decrement was applied. Loading was monotonic. That is, no unloading cycles were applied until the pile had failed geotechnically. Fig. 8.2 shows the load-settlement results for the ACIP test pile using readings taken 20 minutes after each increment/decrement was applied.

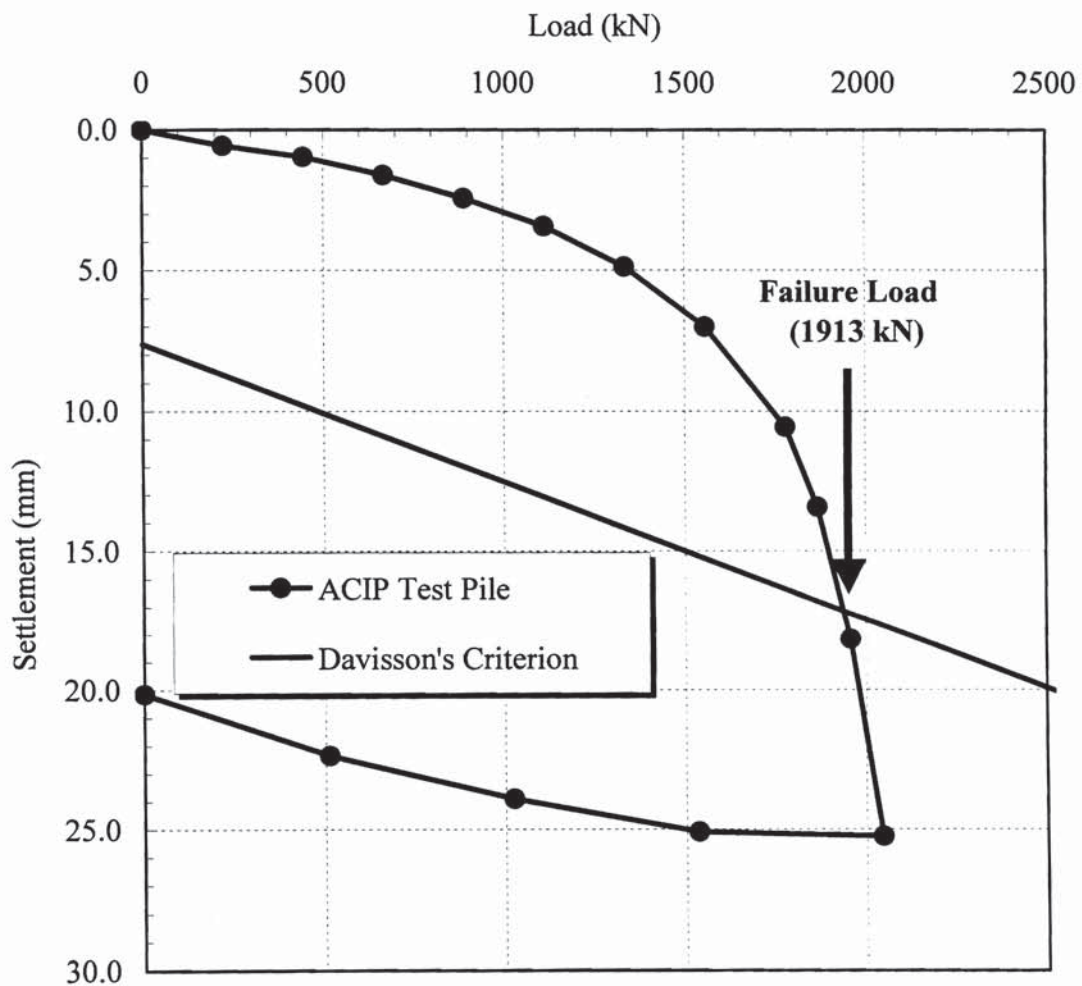


Fig. 8.2. Load-Settlement Curve for ACIP Test Pile

In Fig 8.3, load vs. depth relationships measured at various applied loads are compared. The load at the tip of the pile at failure load (1913 kN) is very small (40 kN - only about 2% of the total load) indicating little load is transferred from pile to soils at the tip of the pile. For this figure the loads on the pile at the beginning of the test were assumed to be zero. That is, it was assumed that the pile had no residual loads. Load vs. depth curves here were drawn using third-order least-squares fits.

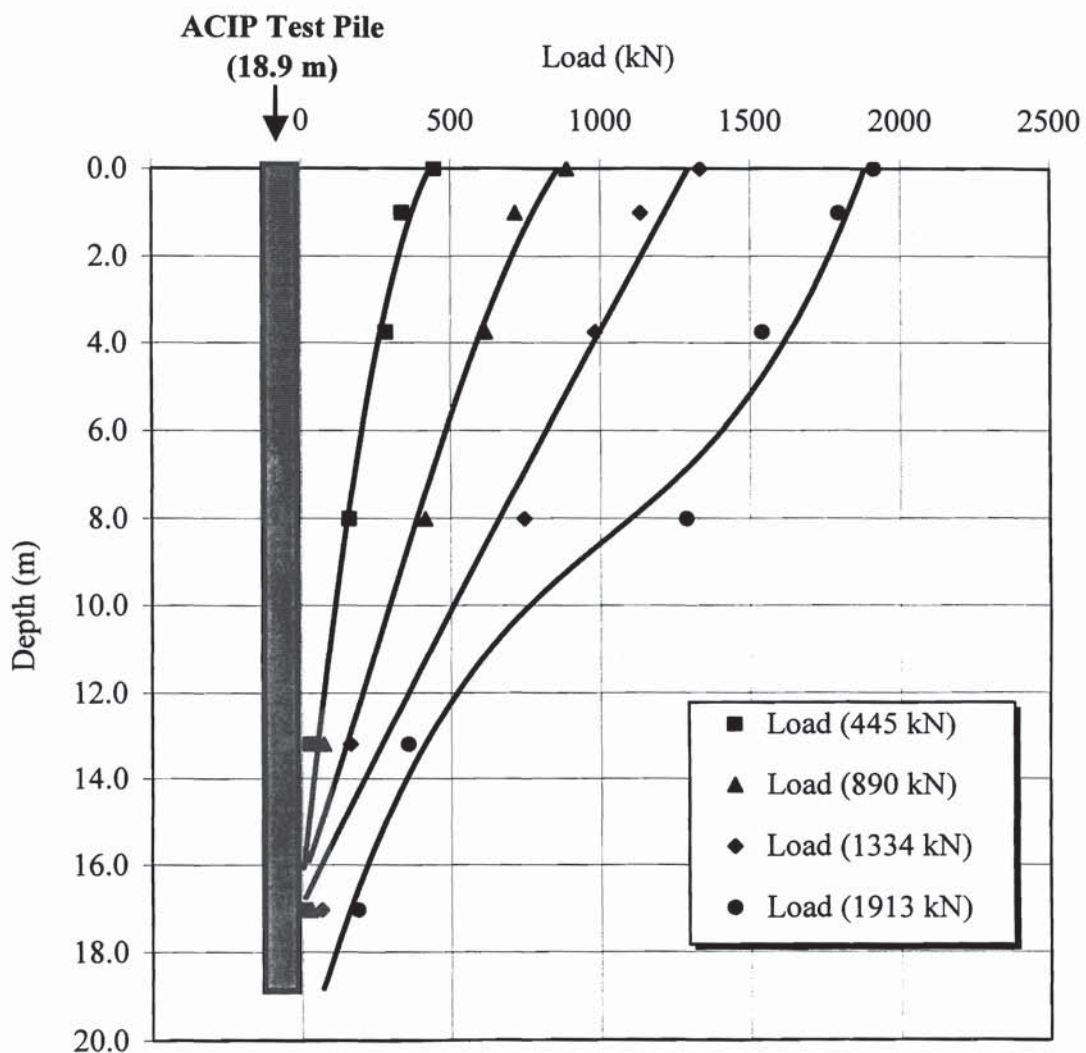


Fig. 8.3. Load vs. Depth Curves for Test Pile (Zeroing at the Start of Test)

Fig. 8.4 shows load vs. depth relationships measured at various value of applied load. For this figure the loads at the start of installation were assumed to be zero (considering residual loads prior to loading). Load vs. depth curves here were drawn using third-order least-squares fits.

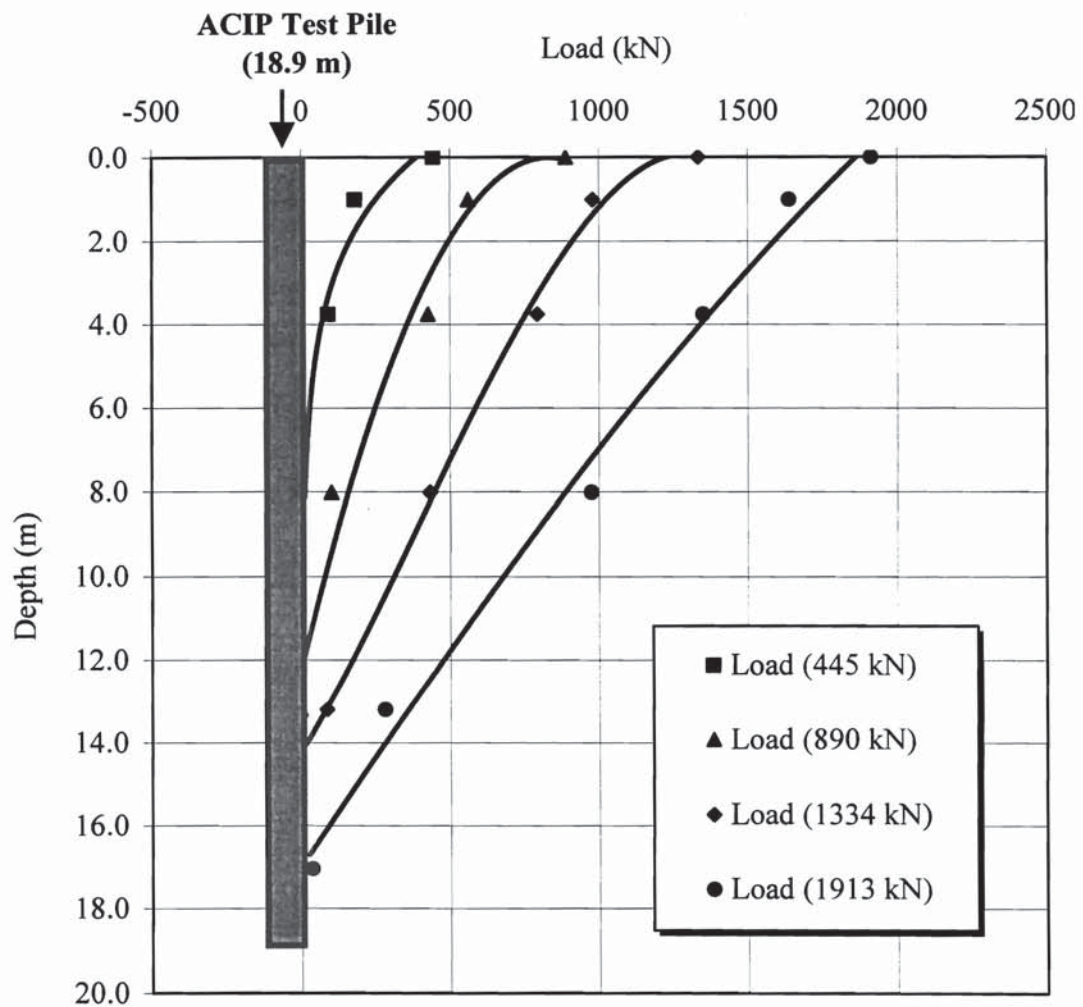


Fig. 8.4. Load vs. Depth Curves for Test Pile
(Assuming Initial Zero Readings Correspond to Unstressed Pile)

Load Transfer Curves (t-z curves)

Once the load-settlement curve was determined and a family of load vs. depth relationships was generated, unit load transfer curves, sometimes called “t-z” curves, were derived from the loading test using a simple procedure.

- At selected depths along the pile, the slope of the load vs. depth relationship was determined from each of the load-depth curves. Each of the resulting values was divided by the nominal circumference of the pile to give unit side (shearing) resistance.
- At the same depths the settlements at that depth (local settlements) corresponding to the unit side resistances computed in the above step were determined by subtracting from the settlement measured at the pile head the area under the load vs. depth relationship from the pile head to the depth of interest divided by the composite Young’s modulus of the pile material times the nominal cross-sectional area of the pile.
- The resulting number pairs (unit side resistance, f , and local settlement, w) were then plotted for the loading portion of the test.
- At the pile toe the procedure is usually similar except that the extrapolated toe load is used directly. This load is then divided by the nominal cross-sectional area of the pile to give the net unit soil reaction stress at the toe of the pile, q , and the relationship between q and w (local settlement at the pile toe) can be plotted. However, the q - w for the test pile was plotted because toe loads with and without consideration of residual loads at various values of applied load were almost zero

as shown in Fig. 8.3 and 8.4. In other words, the plot of $q-w$ is negligible. It is noted that maximum toe load at failure load was only about 40 kN (2% of failure load) in Fig. 8.3.

Load Transfer Considering Residual Loads

Load vs. depth curves at various loads, considering residual loads, are plotted in Fig. 8.4. Fig. 8.5 shows residual loads that were computed from the residual strains that were measured (strains registered by the sister bars 18 days after casting the piles) by the procedure described in Chapter 7, and load-depth curves considering and ignoring residual loads. In Fig. 8.5, the load vs. depth relationship at compressional failure (1913 kN or 215 tons) in the loading test is also shown based on (1) pre-test zeros and (2) zeros taken when the instruments were first placed in the grout (reflecting residual loads).

The pattern of residual load in the test pile (Fig. 8.5) suggests in general that the clay soils at the site were exerting upward-directed shear stresses on the upper sections of the pile (generally above 7 m depth) when it was in the unloaded condition and that below that depth the side shear stresses were generally directed downwards, with some local variations. One would expect the opposite pattern of developed side shear during curing if the ACIP piles were expanding (downward directed shear stresses near the head and upward directed shear stresses near the toe of the pile to restrain movement). It is speculated that the grouting process enhanced minor fractures in the overconsolidated clay that allowed free water to intrude into the near-surface clay and cause portions of the clay layers near the pile to swell.

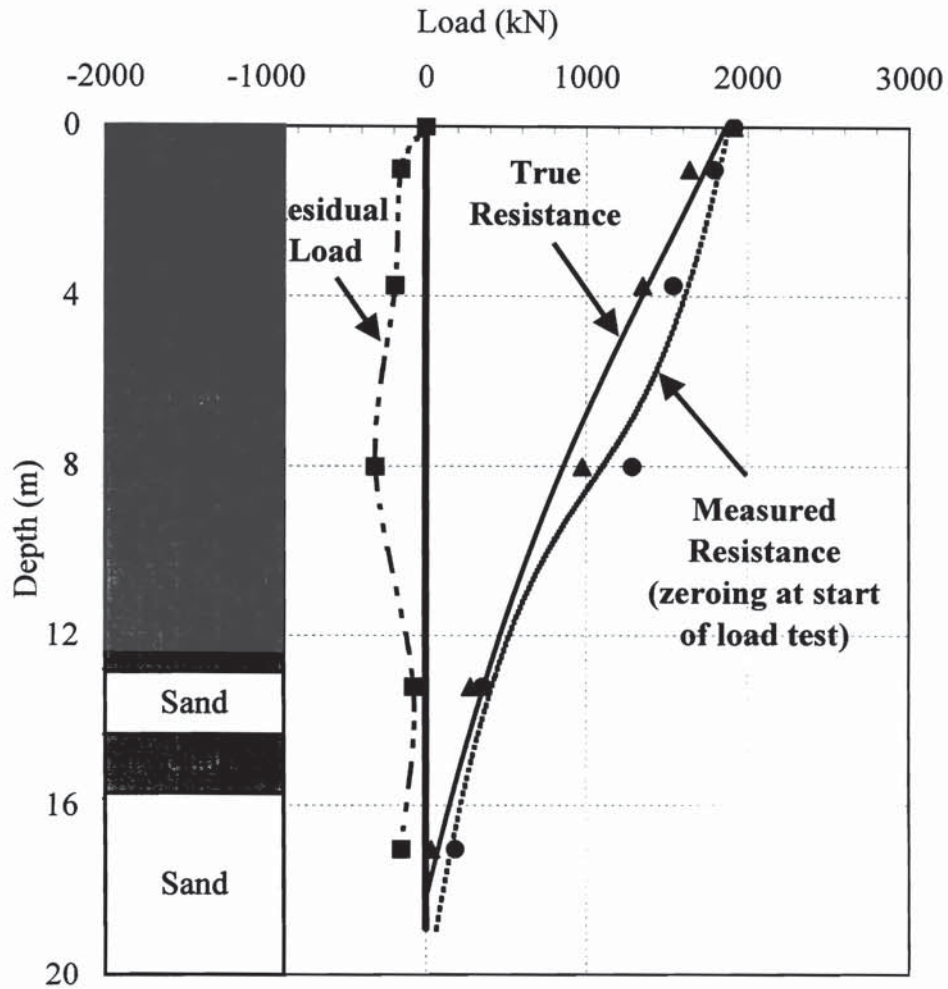


Fig. 8.5. Residual Load, True Resistance, and Measured Resistance for Test Pile

The source of free water to produce such a phenomenon is suggested in Fig. 8.5. Very little load was transferred from the pile to the soil within the bottom 2 m (initially dense, clean sand). This suggests that during construction the density of this waterbearing sand decreased dramatically, possibly because of a rapid depressurization

of the sand layer as the auger broke through the overlying clay. This phenomenon is strengthened by the comparison of CPT records immediately adjacent to the test pile (CPT 1) and 4.3 m (14 ft) away from the test pile (CPT) toward Krenek Road as shown in Fig. 3.5. The CPT records clearly show the loosening of sand around the toe of the test pile. This would have caused a flow of sand upward through the auger, reducing the density of the dense sand layer and producing a corresponding upward flow of groundwater prior to the time grouting through the hollow stem of the auger began. This speculation is strengthened by the fact that a column of free water, about 3 m high, was observed rising on top of the grout column for all nine instrumented plumb piles as grouting proceeded.

It must be noted that the largest residual tensile force in the test pile was about 325 kN, giving a maximum tensile stress of approximately 1980 kPa (287 psi). It is further noted that temperature effects in the vibrating wire gauges and their circuitry account for a maximum of only about 50 kPa (7 psi) of the measured residual stress. Even considering the pseudo stress indicated by temperature changes, 1980 kPa (287 psi) was well below the mean tensile strength of the grout, which was measured in splitting tension on seven grout samples to be 4380 kPa (635 psi) at an age of 18 days [with a minimum value of 3120 kPa (452 psi)]. Therefore, the residual strain readings should represent values from continuous, not cracked, structural elements, making the assumptions regarding computation and application of ISM for the piles valid (which may not have been true had the piles been cracked).

Comparison of t-z Curves Considering and Ignoring Residual Loads

Figs. 8.6 through 8.8 show f-w curves (“t-z curves”) for three representative depths (at 2.4 m, 10.6 m and 15.1 m, respectively) using instrument zeros prior to the load test (ignoring residual stresses) and at the time of installation in the fluid grout (“true” relationship considering residual stresses). As with compressible driven piles, the effects of the residual loads are evident in the t-z curves. Near the head of the pile (Fig. 8.6), the true values of f are higher than those for the pre-test zero values at all values of w, whereas in the middle of the pile and near the toe of the pile (Figs. 8.7 and 8.8), the opposite is true. The differences in the true and pre-test-zero curves carry the implication that the shear stiffness of the soil is higher near the surface and lower farther down the pile than is implied using pre-test zero curves. This, in turn may have some implications in the modeling of the load-settlement behavior of the pile. Mean undrained shear strength values for the clay at the three levels at which f-w curves are shown are also plotted in Figs. 8.6 through 8.8 to provide a general indication of the error involved in neglecting residual loads in an ACIP pile during a load test in establishing α factors for design purposes.

8.3.2 Runneburg Road Site

The Runneburg bridge site also consists of a soil profile of generally stiff clays with a few seams of medium dense sand, which is geologically similar with Krenok site. However, stiff clay layers are predominant along the entire pile length and (unlike the Krenok site) under the pile toe. Fig. 8.9 shows the soil profile at Runneburg Road.

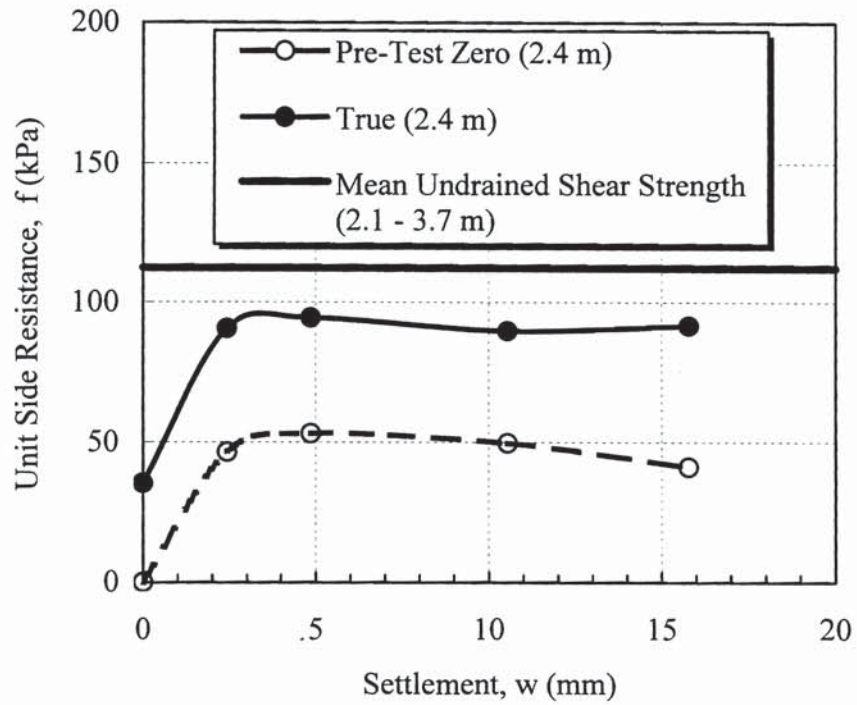


Fig. 8.6. f - w Curves at 2.4 m

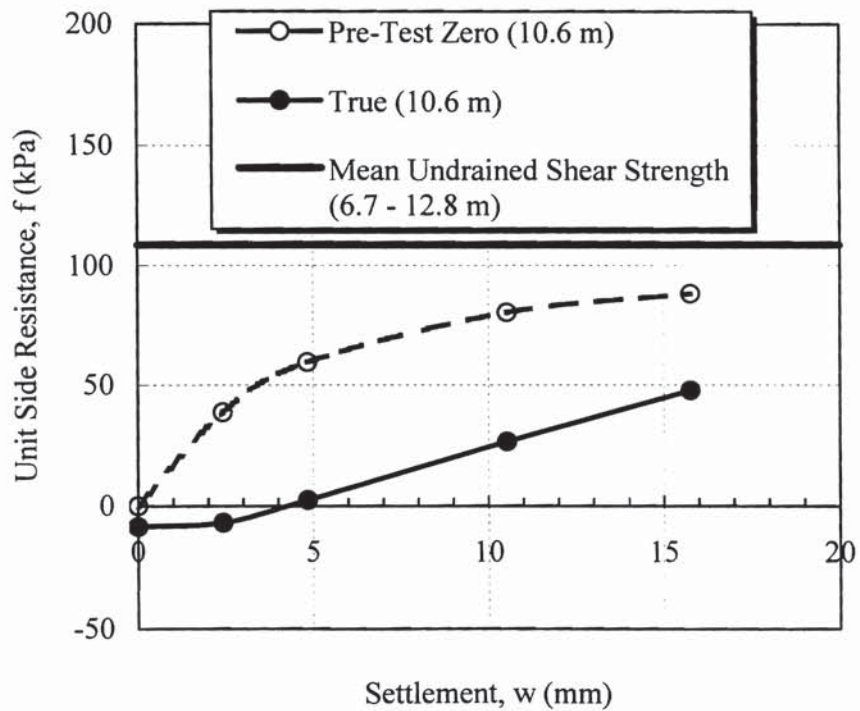


Fig. 8.7. f - w Curves at 10.6 m

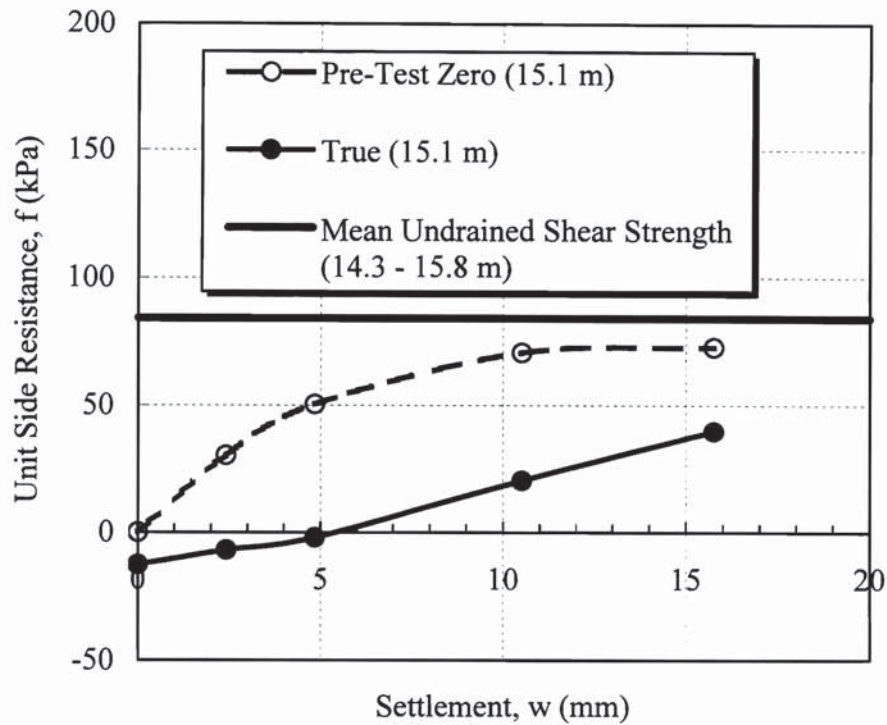


Fig. 8.8. f-w Curves at 15.1 m

A 0.406 m (16 in.) square, driven pre-stressed concrete (PC) test pile was installed in order to compare the behavior of this TxDOT standard foundation pile to that of the non-standard ACIP pile. The length of pile was 14.0 m (46 ft). Penetration length below the level of the ground was 13.1 m (43 ft). This test pile was driven with a Delmag D-30 open-ended-diesel hammer using a plywood pile cushion. It was driven to the penetration that the TxDOT static design procedure indicated would give an ultimate capacity of 1.6 MN [180 tons (2 X design load)]. This shallow depth, relative to the depth of the ACIP pile at Krenok Road, was due primarily to the fact that the soil along the sides of both types of piles was mainly overconsolidated clay and that the TxDOT design procedure allows for the use of the full undrained shear strength of that clay when computing the

shearing resistance along a driven concrete pile ($f = \alpha s_u$). That is, $\alpha = 1$. However, for an ACIP pile, which was treated as a drilled shaft for design purposes, TxDOT requires that the side shear resistance in clay be limited to 0.7 times the undrained shear strength of the clay. That is $\alpha = 0.7$.

The loading test on the driven PC pile was performed using the same procedure as that used on the ACIP test pile at Krenek Road except that strain readings from sister bars were not taken during the test since the pile was not instrumented. The pile was loaded in 222 kN (25 tons) increments to failure. Each load was held for 20 minutes. Load and settlement readings were taken 10 minutes and 20 minutes after each new load was applied. The test pile was unloaded in 389 kN (43.8 tons) decrements until the head load was zero. Each new load decrement was held for 20 minutes. Readings were taken at 10 minutes and 20 minutes after each new decrement was applied.

As with the ACIP pile, only one cycle of loading was applied. Fig. 8.10 shows the load-settlement results for the test pile using the 20-minute readings. The Davisson failure load was 1468 kN (165 tons).

Note is made of the fact that failure load of 1468 kN (165 tons) is less than twice the design load of 0.8 MN (90 tons), which means the actual factor of safety for the driven pile was less than the standard TxDOT value of 2.0. However, the reduced factor of safety is acceptable because the load test will reduce the level of uncertainty in the design, relative to the strength of the soil, the effects of soil disturbance during driving and set-up after driving. A portion of the geotechnical factor of safety is applied in the design phase to reflect geotechnical uncertainty.

Depth m (ft)	Log	N _{TxDOT} blows/ 0.30 m	Avg. s _u kPa (psi)	Avg. γ _t kN/m ³ (pcf)	Soil Classification
1.5 (5)	▽	12	105.2 (15.3)	20.2 (128.6)	CLAY, brown, tan, stiff
3.0 (10)		12	137.0 (19.9)	20.7 (131.5)	CLAY, w/little sand, tan, stiff
4.6 (15)		13	71.1 (10.3)	20.1 (128.0)	CLAY, sandy, tan, gray, stiff
6.1 (20)		15	115.6 (16.8)	20.7 (131.8)	
7.6 (25)		15	70.7 (10.3)	21.2 (134.6)	CLAY, brown, gray, stiff
9.1 (30)		20	151.8 (22.0)	20.2 (128.3)	
10.7 (35)		38	140.8 (20.4)	21.0 (133.4)	
12.2 (40)		63	114.8 (16.6)	21.2 (135.2)	SAND, light brown, clayey @ 11.9~12.2 m
13.5 (45)		28	116.8 (16.9)	21.3 (135.4)	CLAY, gray, brown, organic, stiff
15.0 (50)		84	69.0 (10.0)	21.5 (136.9)	SAND, brown, clayey @ 14.9~15.2 m
16.5 (55)					CLAY, very stiff

Fig. 8.9. Soil Profile for Runneburg Road Bridge Site

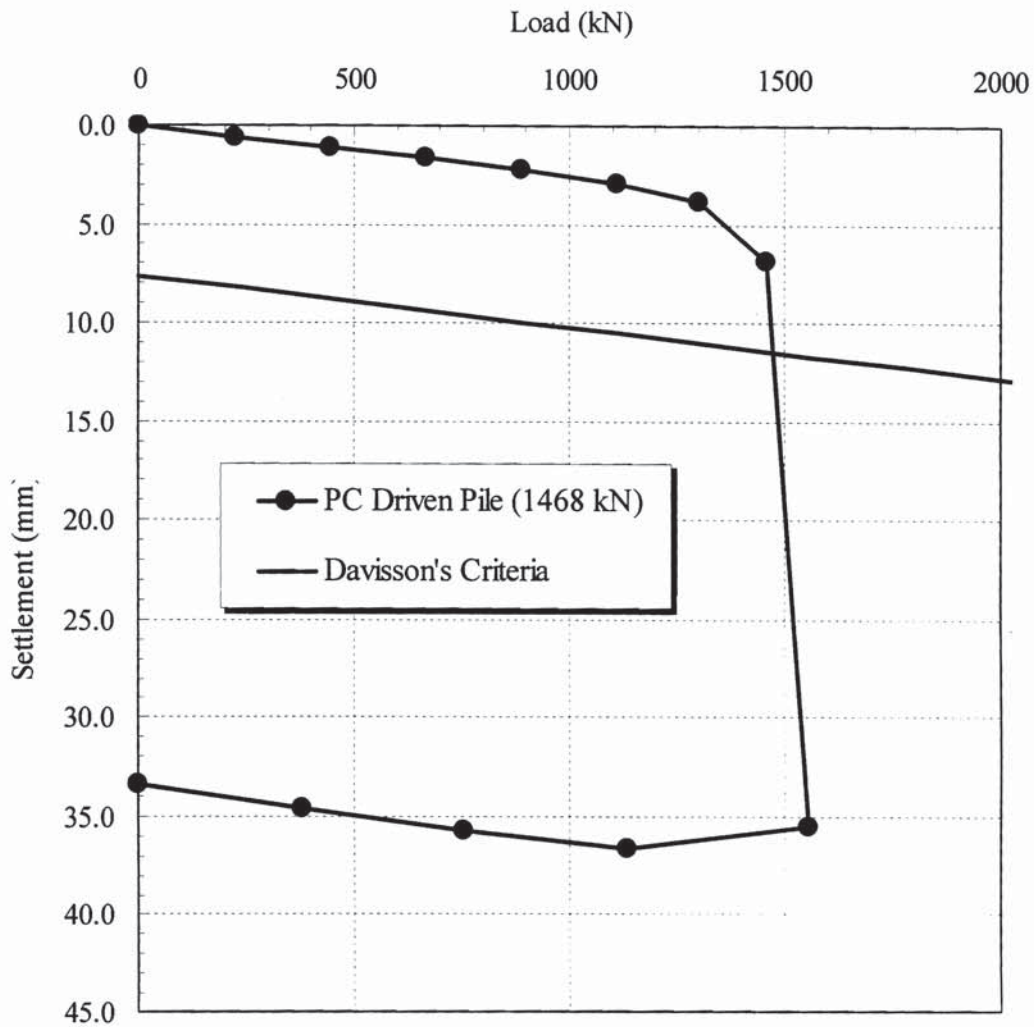


Fig. 8.10. Load-Settlement Curve for PC Driven Test Pile at Runneburg Site

8.4 Comparative Behavior of ACIP and Driven Piles

The issue of comparative resistance of driven and augered piles arises in assessing which system is economically more attractive for a specific project. In the soils of the Texas Gulf Coast, side resistance is the predominant mode of pile support, and this aspect of resistance will be emphasized. Information for both piles is shown in Table 8.1. UU

triaxial compression tests were performed for each site. The results are plotted in Figs. 8.11 and 8.12 for the Krenek and Runneburg sites, respectively. When the average maximum unit side load resistance along each type of pile was divided by the average undrained shear strength at each test site, the ratio (“ α ” factor) for the ACIP pile was considerably higher than that for the driven PC pile. The cost comparison given earlier (chapter 5) indicated that if the piles had been installed so that they had the same ultimate head resistance as that measured for the ACIP pile, the ACIP pile would likely have been slightly less expensive for this particular project.

Table 8.1. Pile Information

Pile Type	ACIP	Driven PC
Pile Diameter (m)	0.46	0.41
Total Pile Length (m)	19.2	14.0
Embedded Pile Length (m)	18.9	13.1
Hammer Type / Weight (kg)	-	Delmag D30 / 2977 OED
Length of Hammer (m)	-	2.44
Average Penetration per 20 Blows (m)	-	0.18
Cushion Type / Thickness (m)	-	Plywood / 0.27
Blow Counts per Avg. 0.30 m for Last 0.91 m	-	33
Resistance upon Completion of Driving from Wave Equation (GRL WEAP TM) (kN)	-	1001

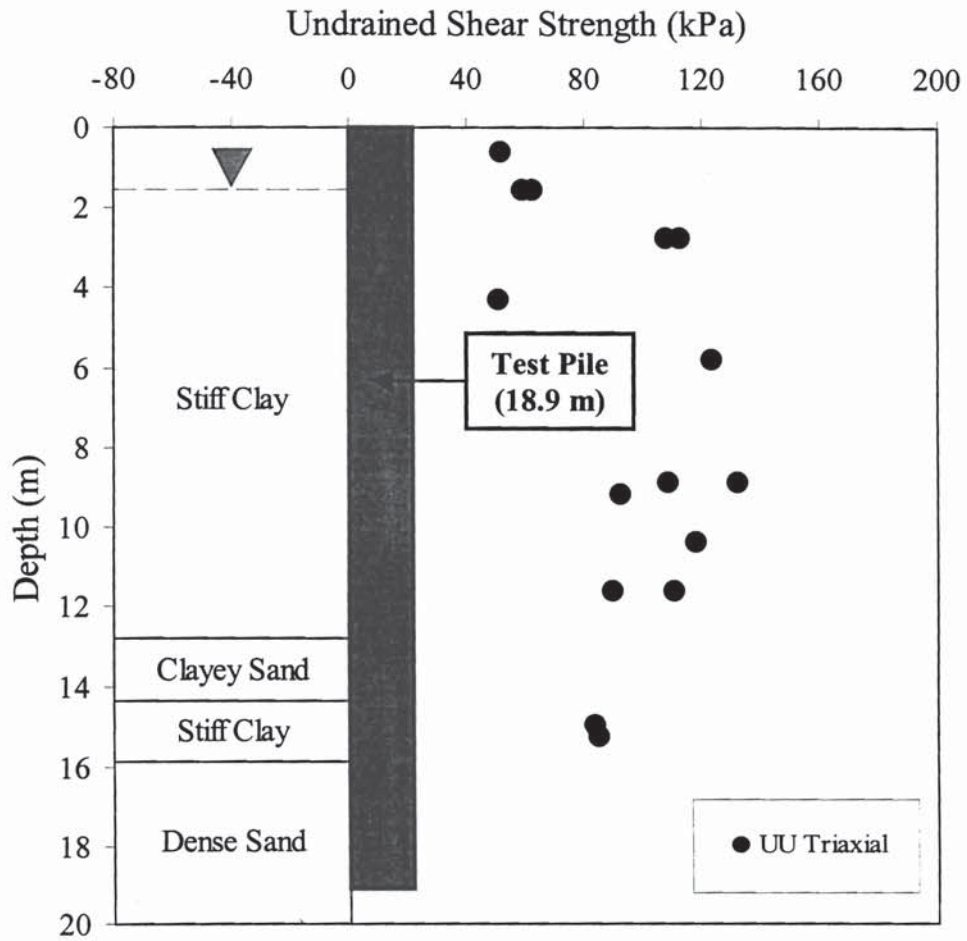


Fig. 8.11. Undrained Shear Strength vs. Depth for Krenok Road Bridge

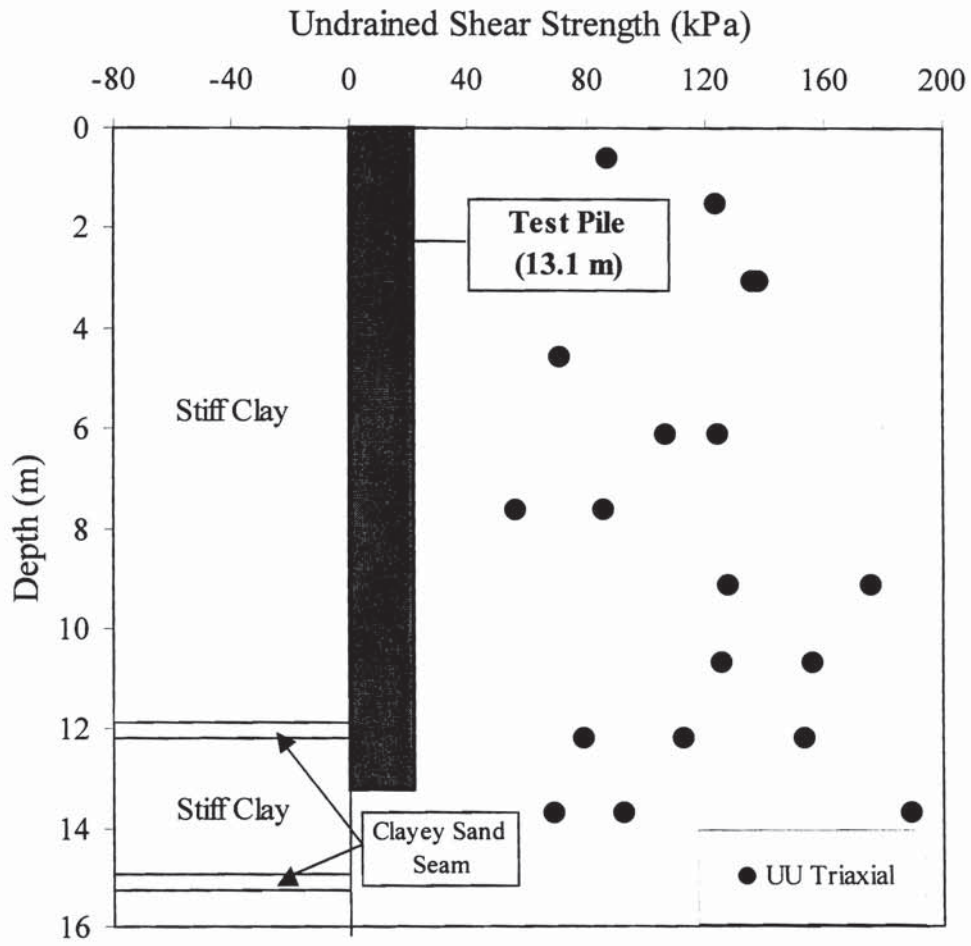


Fig. 8.12. Undrained Shear Strength vs. Depth for Runneburg Road Bridge

The α factor for the ACIP pile was determined for the clay soils from the surface to a depth of 12.8 m (bottom of upper layer of clay) from the data given in Fig. 8.5 and the nominal peripheral area of the pile. The α factor for the driven pile was determined over its full embedded length (13.1 m) by subtracting from the Davisson failure load the load carried by the toe, which is equal to $9 s_{u (toe)} A_{(toe)}$, in which A is the cross-sectional area of the pile, s_u is the operational undrained shear strength and (toe) indicates values appropriate for the pile toe. The calculated toe resistance was 172 kN, about 12 % of the ultimate (failure) load. The α factors deduced from this process for both piles are summarized in Table 8.2. This process implicitly includes the effects of residual loads, as long as the end-bearing formula, above, and the interpreted shear strength of the clay near the pile toe is correct.

The α factor for the ACIP pile was considerably higher within the clay to a depth of about 13 m than that for the driven pile to a corresponding depth. The reasons are not entirely clear; however, the actual diameter of the ACIP pile was likely greater than the nominal diameter of 0.457 m, and the interface between pile and soil was likely rougher in the ACIP pile. The average α value for the driven pile was comparable to that of drilled shafts in the Beaumont formation (O'Neill and Reese, 1972), and the measured resistance appears reasonable because the static capacity during load testing was measured to be 1468 kN, whereas the static capacity at end of driving was deduced through wave equation analysis to be 1001 kN. This observation implies a set-up factor of 1.47, which is typical for the clay soils of the Beaumont formation. Because of cost and time limitations the driven PC test pile was not restruck to confirm the exact value of the set-up factor.

The conclusions obtained by comparing the results of the two load tests has important implications for pile design in the Texas Gulf Coastal clays.

Table 8.2. α Factors for ACIP and Driven Prestressed Concrete (PC) Piles from Static Load Tests

Pile Type	ACIP		Driven PC
	Yes	No	N/A
Consideration of Residual Loads	Yes	No	N/A
Measured Davisson Failure Load (kN)	1913	1913	1468
Measured Side Shearing Resistance in Pile from Surface to 13.1 m (kN)	1517	1486	1296
Calculated Toe Resistance (kN)	N/A	N/A	172
Average s_u (kPa)	94	94	116
Shearing Resistance of Undisturbed Soil to Depth of 13.1 m (kN)	1721	1721	2468
α (0 to 13.1 m)	0.88	0.86	0.53

CHAPTER 9

CONSTRUCTION QUALITY CONTROL

9.1 General

It is recognized that the integrity of an ACIP pile foundation system is highly dependent on the skill and experience of the contractor (Booth and McIntosh, 1994; O'Neill et al., 1999). Quality control during the ACIP pile installation is crucial to the success of an ACIP pile project (O'Neill et al., 1999). As a minimum, incremental grout ratios and systolic and diastolic grout pressures along the piles should be monitored to assure the quality of the piles during the pile installation during the grouting phase of installation. These factors can be monitored in an automated manner in such a way that accurate electronic records are available for later forensic analysis, if necessary. With computer-based techniques, the values for these factors can be displayed on a screen in bar-chart form in the cab of the drilling rig (as shown in Fig. 9.1) to allow the operator to view the progress of the grouting operation and to make immediate corrections to the grouting process if grout take and pressure criteria are not met and some elevation within the borehole. For example, if the grout supplied to a specific segment of the pile is less than the theoretical volume, or if the systolic pressure in the grout is too low, the operator, can immediately drill back down into the grout for one or two meters and re-grout the segment in question.

Other, visual, quality control and quality assurance procedures should also be followed. For example, it is desirable that a head of grout within the auger but outside of

the hollow stem, be maintained at about 4.5 m (15 ft), based on empirical evidence. The amount of grout initially pumped into the hole can be measured with a flowmeter and calibrated to this value of grout head, knowing the physical dimensions of the auger. At the end of the grouting process, grout should be observed visually returning to the surface when the tip of the auger is still about 4.5 m (15 ft) in the ground. It is also important that free water or soil not be floating on top of the rising grout column, as this indicates a blow-out condition. Although the 4.5-m (15-ft.) criterion was met for every ACIP pile in this project, water was observed preceding the grout column in most of the piles supporting the central bents, but not those at the abutments, presumably because the central bent piles penetrated the lower, clean waterbearing sand layer.

Other quality control procedures included the acquisition and testing of grout samples, as described in Chapter 7, and possibly the automated measurement of torque and auger inclination during drilling. Although equipment currently exists to make the latter two measurements, such equipment is not common and was not used on this project.

9.2 Quality Assurance Data

9.2.1 Pile Installation Recorder for ACIP Piles (PIR-A)

Pile installation was monitored using a Pile Installation Recorder™ (proprietary product of Pile Dynamics, Incorporated, of Cleveland, Ohio) for Augercast piles (PIR-A). PIR-A monitoring included continuous measurement of the volume of grout placed versus auger tip elevation, in segments of 0.61 m (2 ft), using a magnetic flowmeter (as shown in Fig. 9.2) and a rotational potentiometer (to measure auger depth, Fig.9.3), and

continuous measurement of the pressure in the grout line at either the pump outlet on the ground surface or at the tip of the auger. Fig. 9.4 shows the ACIP drilling rig with PIR system.

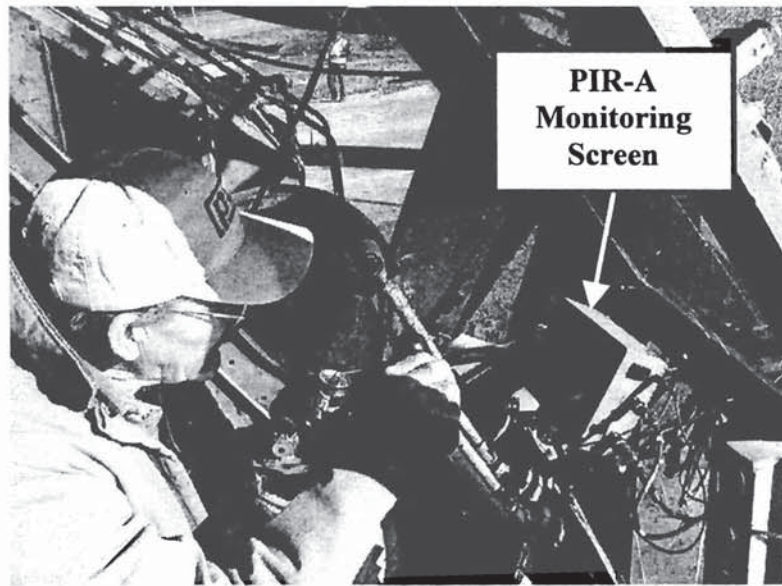


Fig. 9.1. PIR-A Monitoring in the Cab of the Drilling Rig

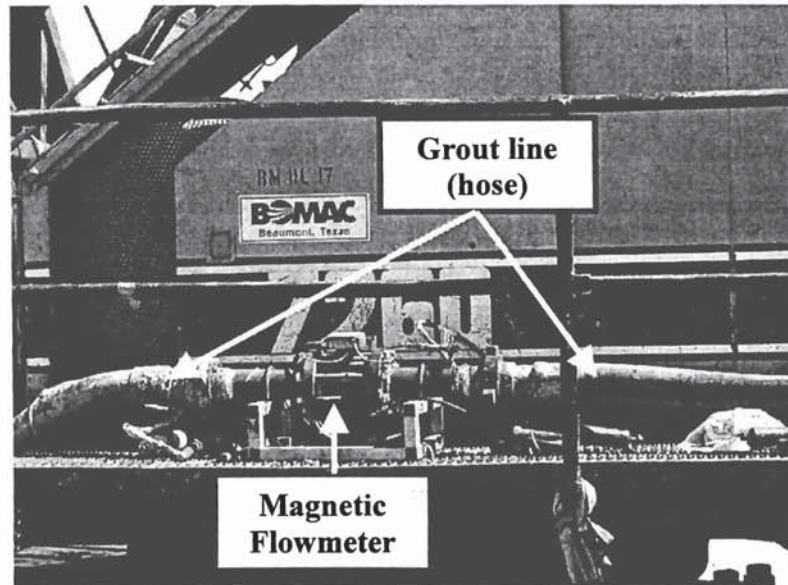


Fig. 9.2. Magnetic Flowmeter Attached in ACIP Pile Drilling Rig

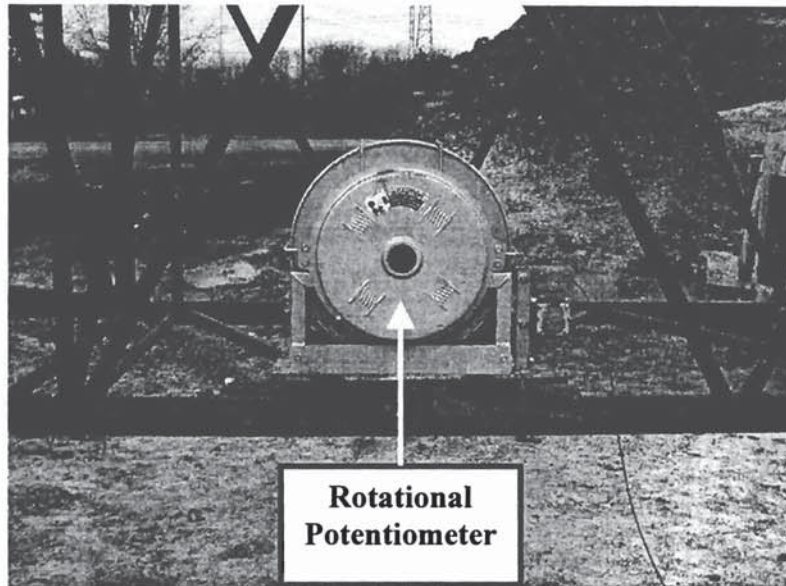


Fig. 9.3. Rotational Potentiometer in PIR System to Measure Auger Depth

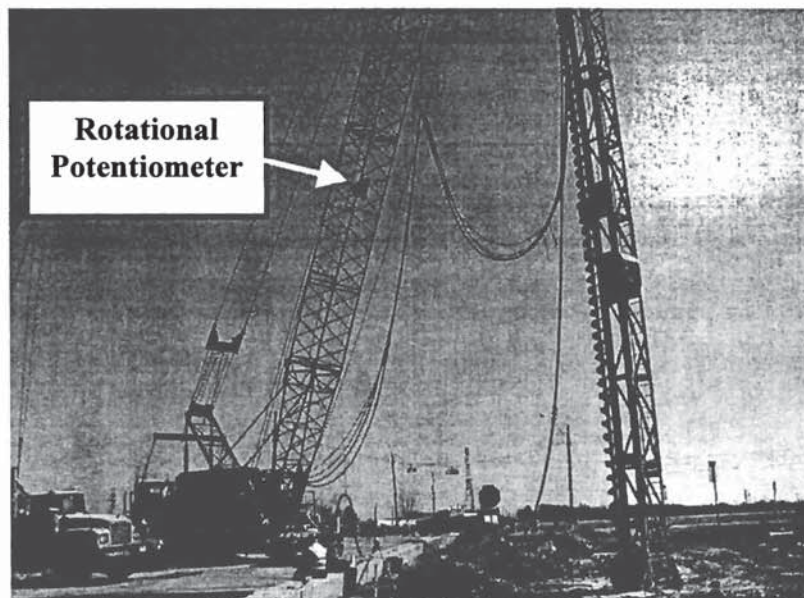


Fig. 9.4. ACIP Pile Drilling Rig with PIR System

The appropriate place to measure grout pressure is at the bottom of the auger, at the point at which it is released into the borehole. However, appropriate instrumentation was not available to measure grout pressures at this location at the time of this project. The grout pressure measurements that were made at the ground surface are likely to be lower than the pressures at the grout outlet orifice at the tip of the auger. Hassan et al. (1997) suggested that a reasonable criterion was to specify a minimum diastolic grout pressure equal to the total vertical stress in the soil at the elevation of the auger tip at the time the measurement is made. This would prevent hole collapse once the grout is in the hole. Using this criterion, any factor of safety would be provided by the additional pressure from the head of grout in the auger.

The PIR-A measurements automatically document the augering and grouting processes and result in a profile of grout volume pumped versus auger tip depth. The PIR-A was used on the test pile and all production piles used as bridge foundations.

The ratio of the actual volume of grout pumped to the theoretical volume of the pile is defined as the grout ratio. Hassan et al. (1997) recommended that in the overconsolidated clays of the Texas Gulf Coast the average grout ratio be at least 1.15 for any one pile. However, they did not make clear whether any incremental grout ratios can be less than this value. The grout ratios vs. elevation of the auger tip for test and reaction piles are shown in Fig. 9.5. The maximum and minimum grout pressures at the pump vs. elevation of the auger tip for the test pile are shown in Fig. 9.6.

Figures 9.7 and 9.8 show the grout ratios vs. elevation of the auger tip for central bent piles under Footing A and under Footing B, respectively. Figures 9.9 and 9.10 show the grout ratios vs. elevation of the auger tip for abutment piles under Group A and for

abutment piles under Group B, respectively. The grout ratios along the pile length for every pile were also monitored and are attached in Appendix C.

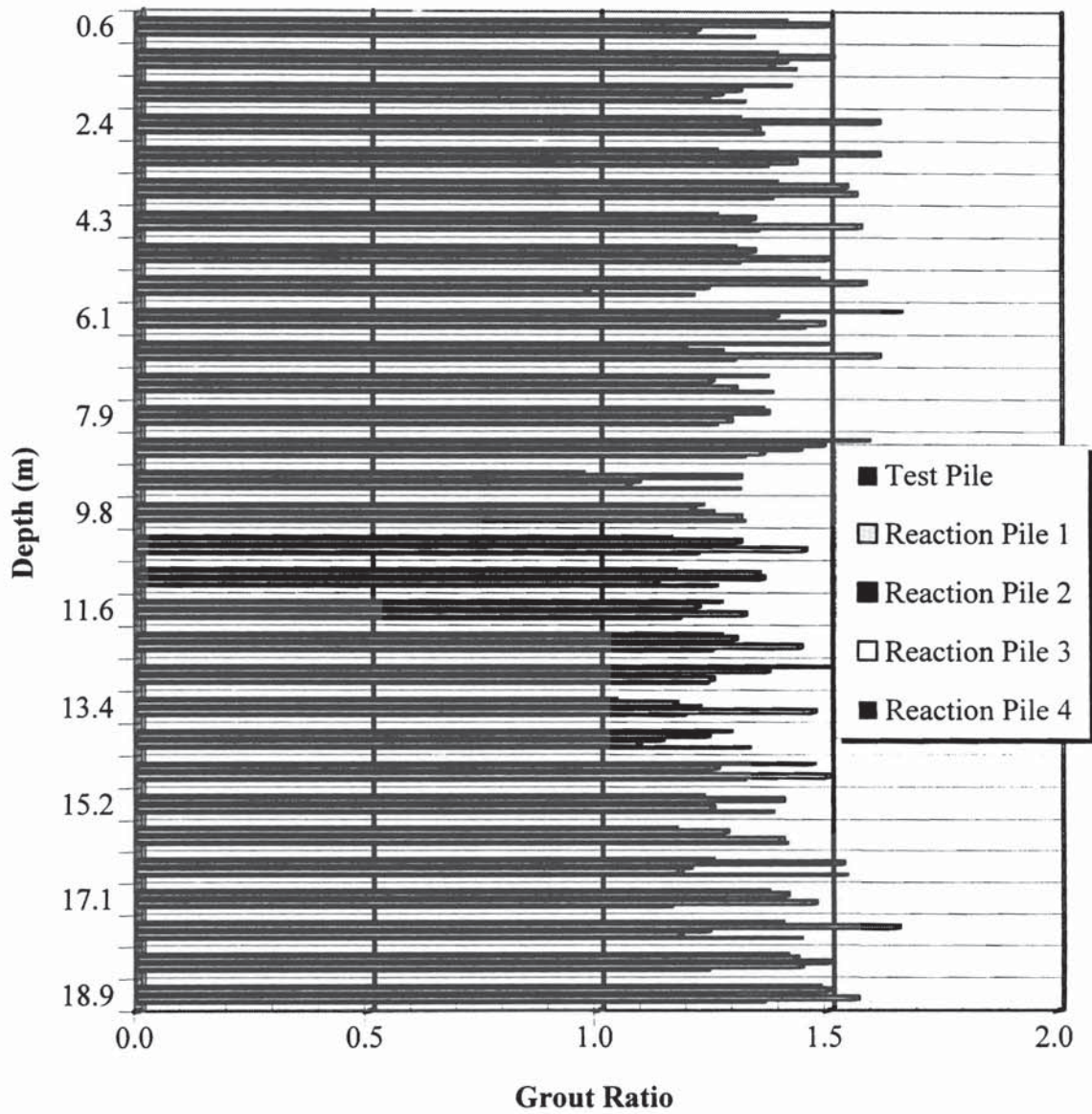


Fig. 9.5. Grout Ratios for Test and Reaction Piles

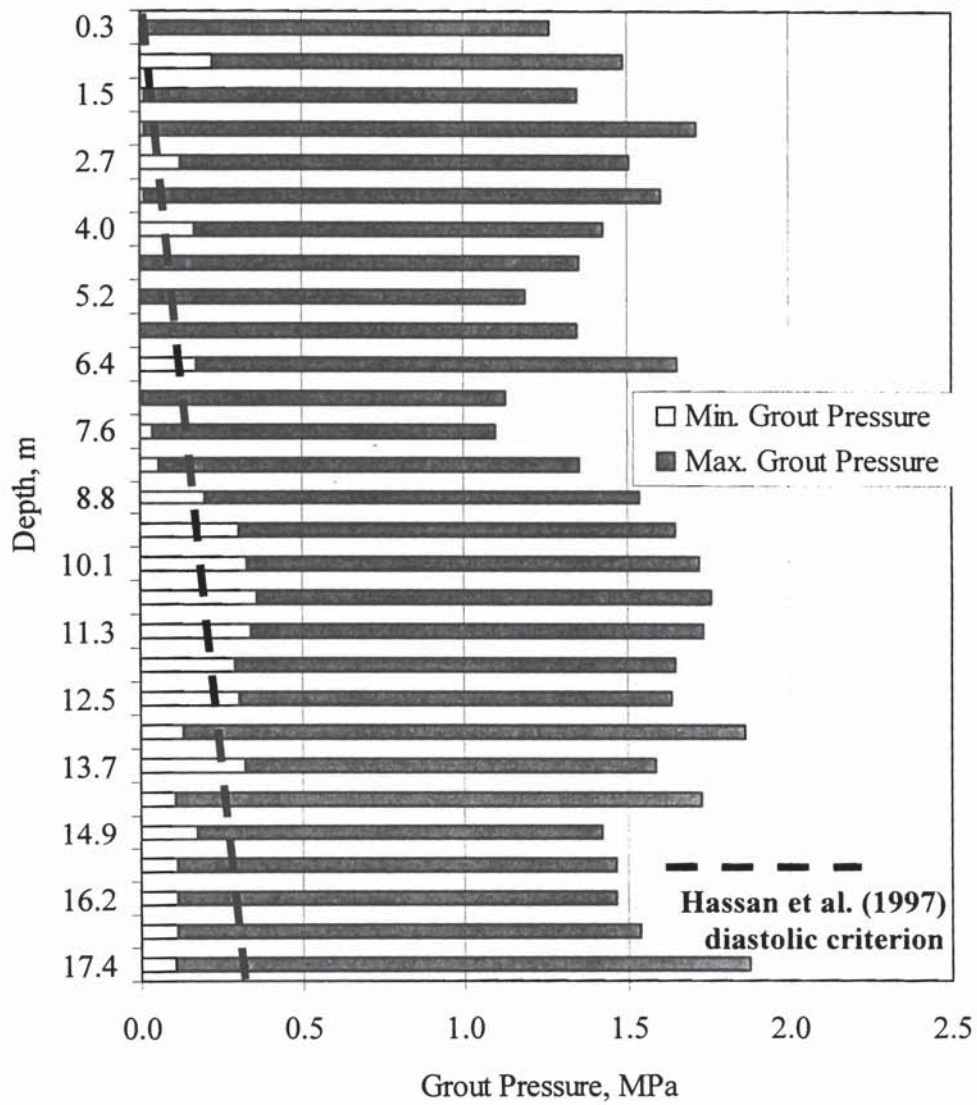


Fig. 9.6. Maximum (Systolic) and Minimum (Diastolic) Grout Pressures for Test Pile

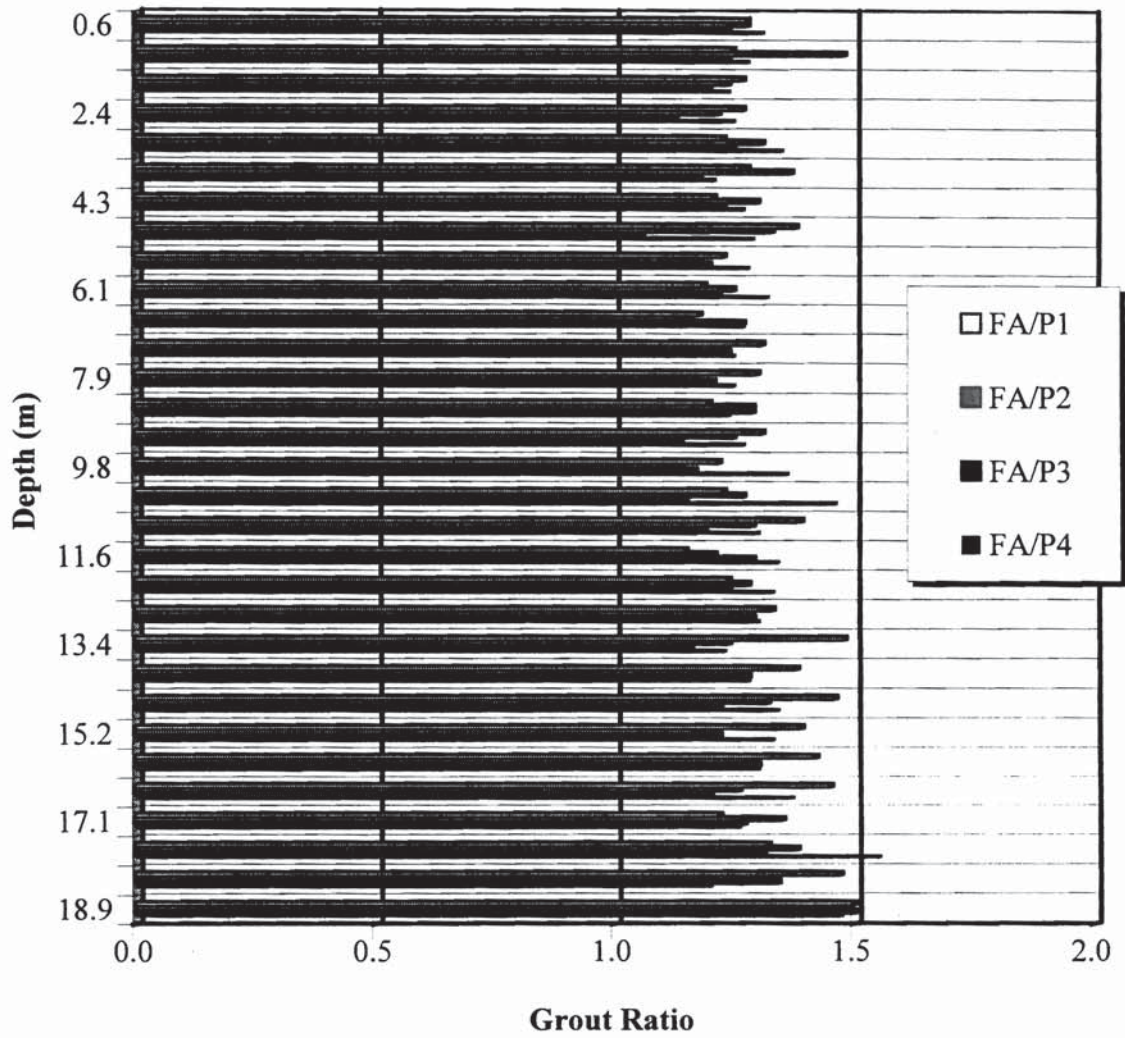


Fig. 9.7. Grout Ratio vs. Auger Elevation for Central Bent Piles Under Footing A

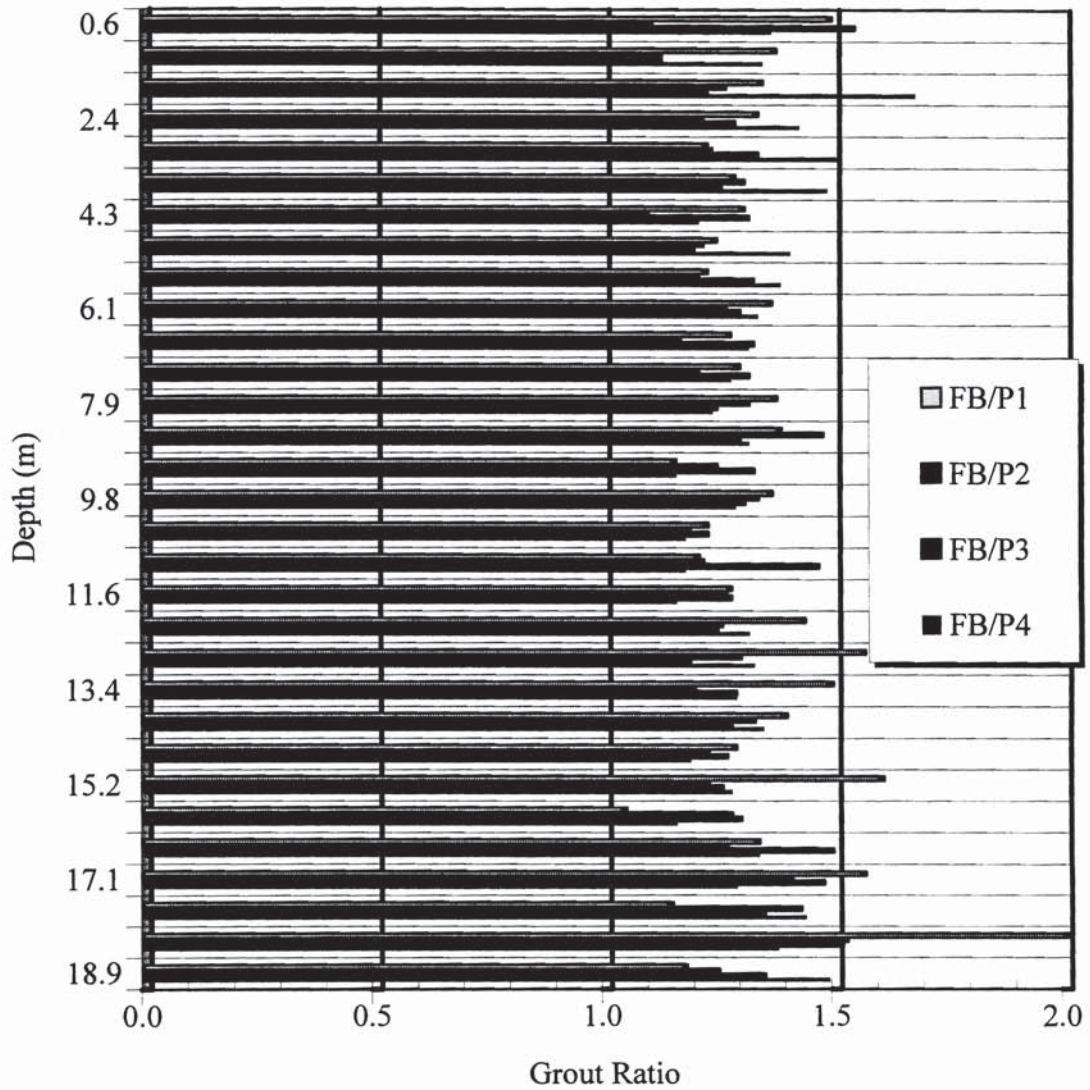


Fig. 9.8. Grout Ratio vs. Auger Elevation for Central Bent Piles Under Footing B

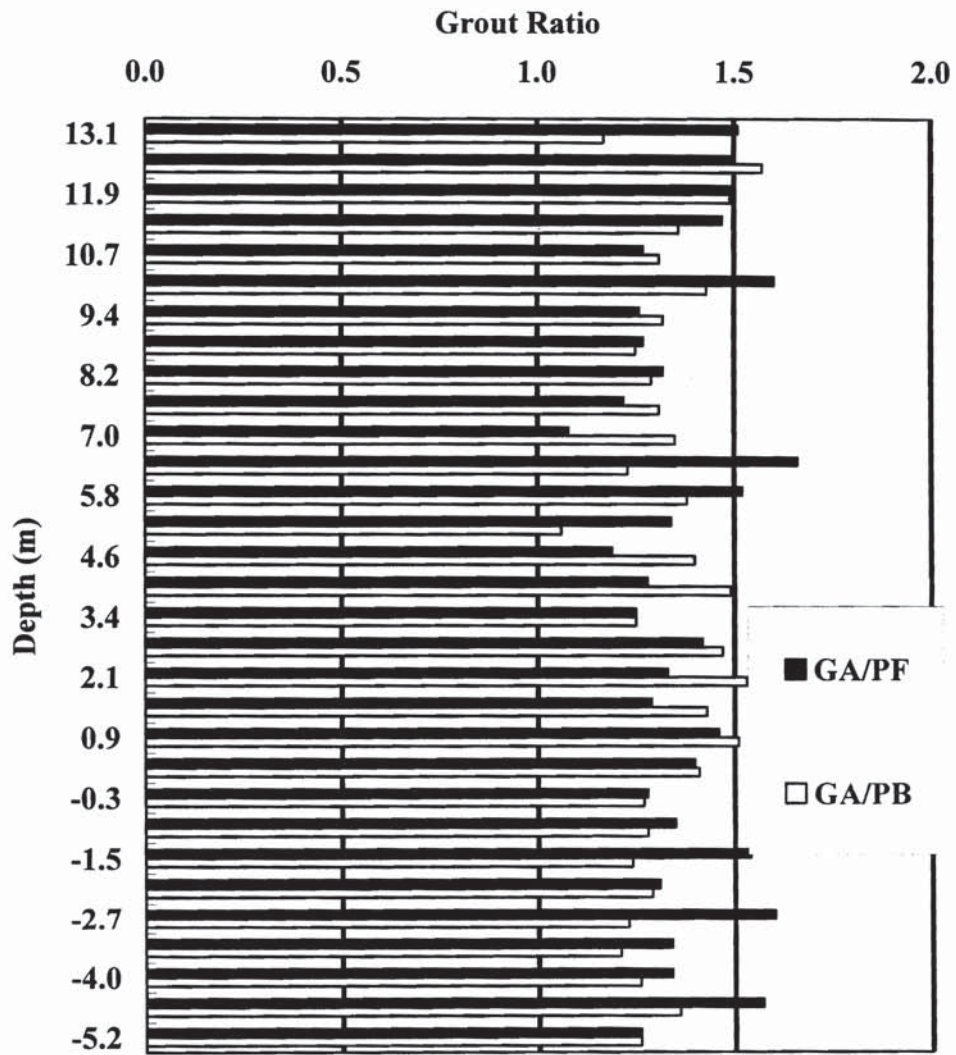


Fig. 9.9. Grout Ratio vs. Auger Elevation for Abutment Piles Under Group A

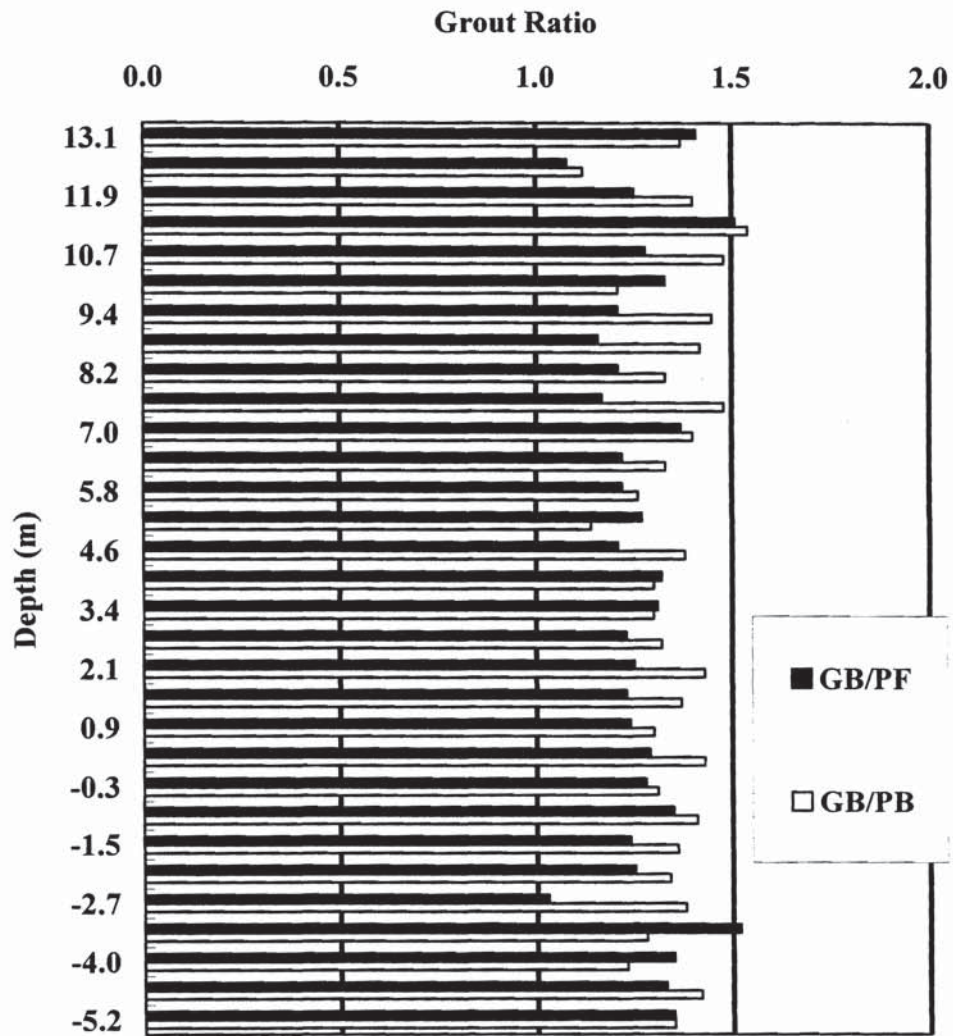


Fig. 9.10. Grout Ratio vs. Auger Elevation for Abutment Piles Under Group B

Based on the quality control procedures adopted in this study following can be concluded:

- Some segments along the piles had incremental grout ratios less than 1.15, for example, at depths of 9.1 and 12.8 m in the test pile (Fig. 9.1). In fact, at the depth of 9.1 m, the incremental grout ratio was less than 1.0 in the test pile. However, the incremental grout ratios were well in excess of 1.15 for the segments just above and below these depths. A logical explanation for the incremental under-run is that the volume of grout required to fill a 0.61-m (2-ft) segment of the 0.457-m (18-in.) diameter pile was provided by only 5 strokes of the grout pump. Depending upon where the grout volume measurement started in any segment, the value of volume registered was between 4.5 and 5.5 times the volume of the positive displacement pump. Because of this inherent error, it was therefore more logical to determine acceptable incremental grout volume over a series of strokes (e.g. three segments). Considering this logic, the incremental grout volume for the test pile, and all other piles, was satisfactory.
- The systolic grout pressure averaged about 1.5 MPa (220 psi) along the test pile. However, the diastolic grout pressure was less than the value recommended by Hassan et al. (1997) along part of the pile. At the Krenek Road site the diastolic grout pressure should have been about 0.34 MPa (49 psi) at the bottom of the pile by this criterion, varying linearly with depth to zero at the ground surface. Hassan's criterion is shown in Fig. 9.6. It can be clearly seen that the diastolic grout pressures were below the total vertical pressures in the soil below a depth of about 13 m. This generally coincides with the depth of lower load transfer (lower

sand strata) that can be seen in Fig. 8.6. Above 13 m, it is probably of little consequence that Hassan's criterion was not met because the soil there was stiff clay that was capable of standing on vertical slopes unsupported. Both the loading test and a structural integrity test described later, performed after the loading test, verified that the test pile was sound structurally. There was some loss of geotechnical capacity below about 13 m. How or whether this relates to the low diastolic pressures in the grout is unknown.

9.2.2 Low Strain Integrity Testing

Low strain integrity testing was performed on the test pile at Krenek Road as shown in Fig. 9.11 to ascertain whether the pile had a neck or variation in cross sectional area along the pile length, especially at depths of 9.1 and 12.8 m. The particular test performed was a pulse-echo test, in which a low-strain impulse is sent down the pile by striking the head of the pile. Energy is reflected from depths at which there is a change in the EA value of the pile (e. g., change in cross-sectional area, A if the grout modulus is constant with depth), and this reflected energy is sensed by an accelerometer at the head of the pile (Roberts, 1994). By knowing the velocity of the compression wave in the pile, the depth of any anomalies, such as necks, can be identified (Rausche et al, 1994; Roberts, 1994). The test results are shown in Fig. 9.12. Grout wave speed of the grout was assumed to be 3657 m/sec (12,000 ft/sec) in this test. There was no evidence that there was any defect in the pile. It was indicated, however, that there was some bulging at the depth of about 13.7 m where a clayey sand layer is located. However, the evaluation of the pile was not conclusive since the impact wave reflection from the pile

tip was not evident. Experience indicates, however, that reflected waves can be seen in slender piles, only above relative depths of about $30 D$, where D is the pile diameter. The test pile had a depth of $41.3 (= 18.9 \text{ m} / 0.46 \text{ m}) D$.

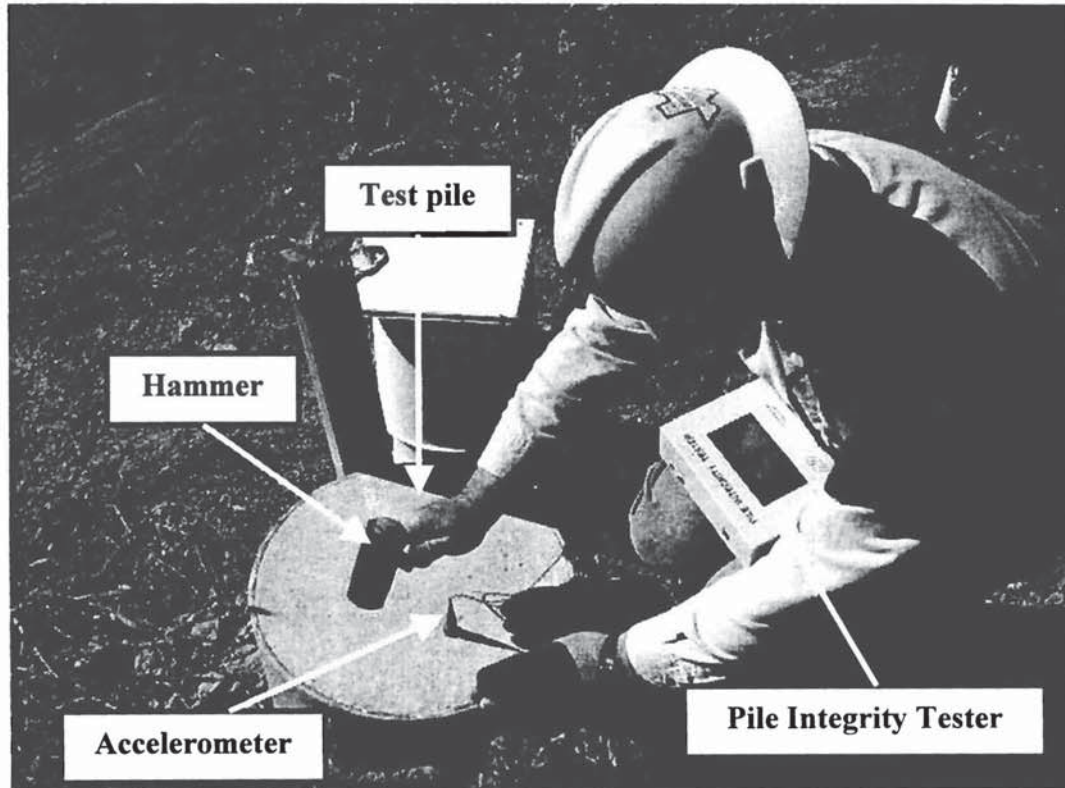


Fig. 9.11. Pulse-Echo Test for Krenek Road Test Pile

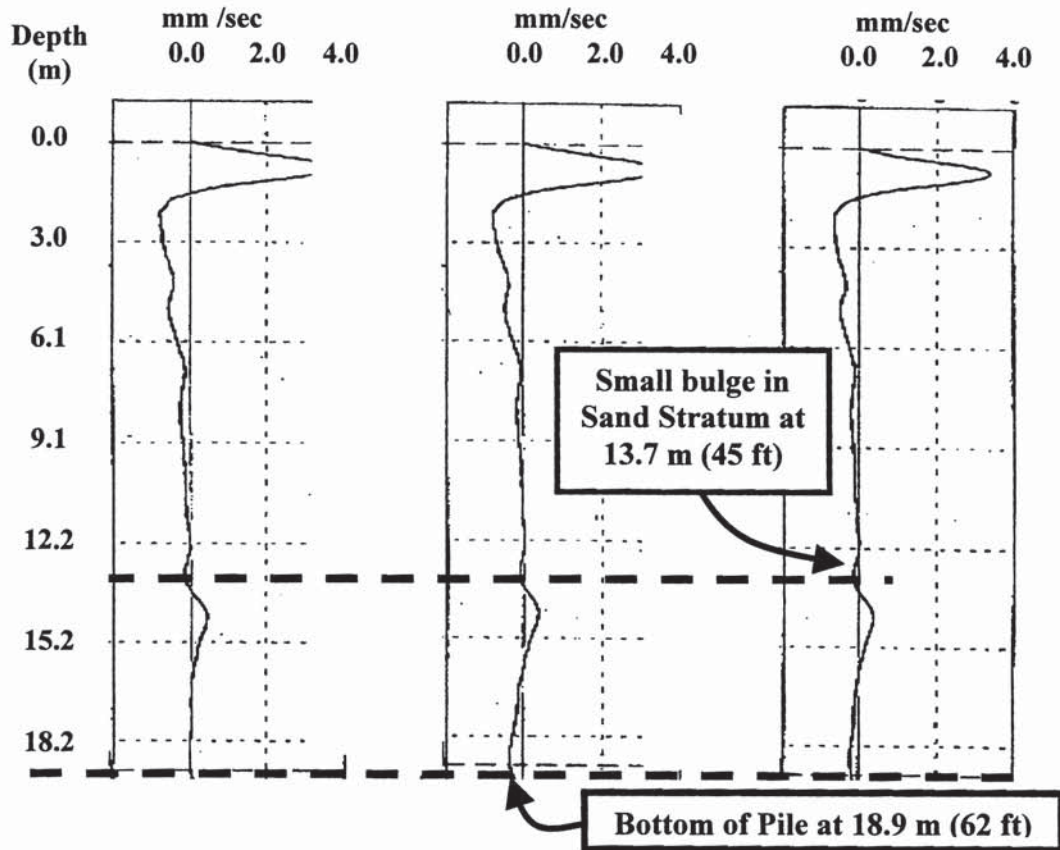


Fig. 9.12. Low Strain Integrity Testing (Pulse-Echo) Results on ACIP Test Pile (3 Separate Hammer Blows)

9.3 Construction Issues

9.3.1 Thrusting Cages into the Grout

Full-depth cages were designed for the test pile and all sixty-four production piles. The reason for the full-depth cages on the project was that the UH implementation team required them so that instruments could be placed on the piles to monitor load transfer into the soil all the way to the toes of the piles. TxDOT, however, requires full-depth cages for drilled shafts and by implication for ACIP piles. Where the cage is very

long, TxDOT allows part of the longitudinal reinforcing steel for a drilled shaft cage to be dropped off below a depth of about 10 m, or where the theoretical bending moment goes to zero, whichever is deepest. That is, currently, full-depth cages of some sort will be required for ACIP piles by TxDOT. Thrusting the long cages into the grout to full penetration is highly unusual in private sector work and was perceived to be a challenge by the contractor. Had instruments not been used, as would be the case for a normal bridge foundation, the full cages could have been about half-length [10 m long] with minimal longitudinal steel with stabilizing hoops to hold the bars in place to the pile toes, which would have made the insertion of cages much easier. For the central bent piles, three or four plastic rollers were used at every 3 m (10 ft) along the cage to aid in pushing the cage into the grout without the cage buckling and to keep the cage centered. Despite the long cage lengths, no significant construction problems were encountered inserting the cages in the central bent piles, which were all vertical.

For the battered abutment piles, instead of using rollers, three PVC pipes were attached to each cage so that the cage could easily slide down the side of the borehole into the wet grout. Ninety-two percent (60 out of 65) of full cages for the test and production piles were successfully inserted into the grout top the bottoms of the grout-filled boreholes. Cases in which the cage could not be thrust to full depth (5 / 65) were all in the abutment piles and were due to one of the followings.

- The grout was too viscous (the efflux time of the grout was more than 18 sec) – 3 cases in this project (one case – 19 sec, and two cases - > 20 sec).

- Discontinuous work or lack of timely availability of piling crews to place the cage. In two cases, the piling crew was busy preparing the next pile for installation and was late in thrusting the cage. (The cage should be inserted within 5 minutes after augering and grouting processes are complete.) - 2 cases in this project

While 5 cages could not be inserted to their full depth, those cages were nevertheless inserted to within about 2 m (or less) of their full depth. It is not likely that this posed any structural problems for the foundation of the Krenek Road bridge.

9.3.2 Spacing Between Piles in Group

ACIP piling installation was delayed because the piling contractor had to avoid installing the piles in a group in same day unless the pile spacing between the pile to be installed and any pile installed within at least 24 hours was higher than 6 times the pile diameter. If the spacing had been reduced for this project to 4.5 times the pile diameter, the contractor could have expedited the piling work by doubling the rate of production for the central bent piles. In this project, central bent piles under the eight central bent footings were installed in four days. If the specification on the pile spacing is revised, that duration could be reduced to two days for piles with a geometrical layout similar to that for the Krenek Road bridge, since the diagonal piles with a spacing of 2.16 m (7.07 ft) in each four-pile group could be installed at the same time. The ratio of spacing and diameter for diagonal piles was about 4.7.

If the spacing is reduced, consideration should be given to the possibility that augering one pile can open seams of soil (for example, waterbearing sands) and allow unset grout from a neighboring pile to drain into the excavation for the new pile. This phenomenon is entirely dependent on the stratigraphy at the project site. For sites that have massive clay soils, it is likely that a four and half diameter criterion could be used without further debate. Where clean, waterbearing sand layers are present between clay layers of low permeability, it may be prudent to keep the six-diameter criterion. This issue is a subject for future study. If the spacing is reduced, the inspector should verify that there is no drop in the level of grout at the head of any newly installed pile within six diameters of a pile currently being installed.

9.3.3 Bearing in Cohesionless Soil Layer Under Water Table

Central bent piles were designed to be tipped in a dense, waterbearing sand layer through stiff, relatively impermeable clay. Pile toe resistance was measured to be almost zero because of the blow-out phenomenon discussed earlier. In hindsight, it would have been preferable to tip the piles in the stiff clay overlying the lower sand by increasing the pile diameter and shortening the pile length. Such action by the designers would be desirable for other bridge foundations located in geologic profiles similar to that found at Krenek Road.

9.3.4 Inappropriate Installation Procedures

On relatively numerous occasions, the contractor was observed slowly turning the auger with the auger in the borehole without either excavating soil or pumping grout and

extracting the auger (either with its tip at the bottom of the hole, or with its tip farther up the hole after some amount of grout had been placed). This operation was carried out because there was no grout truck momentarily at the site, and the contractor could not stop turning the auger and wait for grout to be delivered because of the possibility that the auger would freeze in the ground and become un-extractable. This practice only serves to increase mining of waterbearing sands. Clearly, changing grout trucks during the grout session may cause over-rotation and soil mining, especially in cohesionless soils. The next generation of construction specifications should require that the contractor not begin augering until a full grout truck containing at least the volume of grout required in the borehole is on the site filled with grout that is ready to be placed in the borehole. In the event that the volume of grout required in the pile is larger than the volume of grout that can be carried by one truck, more than one truck containing the full volume of grout for the borehole should be present on the site prior to beginning augering, except in rare circumstances (e. g., drilling in soft rock) where much time (more than the time required for the grout in the ready-mix truck to begin gaining viscosity) will be needed to excavate the borehole.

9.4 Summary

- The grout was too viscous to place (insert) the full-length cage into the hole filled with the grout if the efflux time of the grout was more than 18 sec.
- The cage should be inserted within 5 minutes after augering and grouting processes are complete in order to insert the full-length cage without any problem.

- If the pile spacing had been reduced for this project to 4.5 times the pile diameter, the piling work could have been expedited by doubling the rate of production for the central bent piles.
- ACIP pile should not be tipped in a dense, waterbearing sand layer through stiff, relatively impermeable clay.
- ACIP pile construction specification should require that the contractor not begin augering until the full grout truck containing at least the volume of grout required in the borehole is on the site filled with grout that is ready to be placed in the borehole.

CHAPTER 10

LONG TERM BEHAVIOR AND PERFORMANCE OF CENTRAL BENT PILES

10.1 General

This chapter describes the long-term behavior and performance of central bent ACIP piles under Footings A and B in the South Zone of the Krenek Road bridge. Vibrating wire strain gauge and contact pressure cell outputs were acquired over an extended period time and at different levels along the piles with the data acquisition system described in Chapter 6. Settlements were continuously measured including sets of measurements for each major loading event, such as placement of girders, deck, live load simulation, initial service load and service loads six months after the bridge went into service.

The load distribution and settlement behaviors, and load sharing within piles and between the piles and pile cap were studied as the structural loads were being applied for six months after the bridge went into service. The effects of group action within central bent piles installed in a group on the load distribution and settlement behaviors were also investigated.

Similar studies were performed for the abutment piles and are described in Chapter 11.

10.2 Process of Analysis

10.2.1 Sister Bars

Eight central bent piles (FA/P1 through P4 and FB/P1 through P4) were instrumented with vibrating wire strain gauges at various levels along the pile length in South Zone of the Krenek Road bridge as shown in Figs. 6.1 and 6.5. Vibrating wire strain gauge outputs were acquired over an extended period time and at different levels along the piles with the data acquisition system as described in Chapter 6. These outputs were converted to strains by multiplying a calibration factor for each gauge and converted to loads in the pile in a spreadsheet by multiplying the average of the strains in the two or four sister bars at each level by composite initial secant modulus of the pile and pile's cross-sectional area as discussed in Chapter 7. Note that no change in composite pile modulus was assumed to occur beyond 28 days after each pile was cast.

The initial modulus of grout in a pile tends to increase with time, but once the pile is loaded the grout modulus tends to decrease slightly due to the creep behavior of the grout, depending on elapsed time after loading and stress level according to Wooley and Reese (1974). Attempts to measure precisely the creep strain in the grout at various levels of stress in the laboratory were unsuccessful, so that a precise modulus based on time after casting and long-term stress level could not be evaluated precisely. Therefore, it was assumed that the initial modulus of the grout in any pile at every loading event (e. g., placing column, bentcap, girder, deck, simulated live loads, initial service loads, and service loads six months after service) was same as the initial composite modulus obtained at the time of 28 days (Chapter 7) as routinely done in the short-term test pile analysis, for the purpose of long-term analysis. Specifically, this was the grout modulus

in the piles at the time the footings were placed. No special consideration was given to any differences between the moduli of the grout measured in the laboratory and in the piles due to any differences in curing environment.

10.2.2 Calibration of Cross-Sectional Area

The cross-sectional area of each central bent pile needed to be determined precisely in order to convert measured average strains at each level in the piles into relationships of load vs. depth. This task was accomplished by comparing accumulated loads taken by the piles under the footing and by the footing itself (through the measurement of contact pressures), immediately before and after the girders were placed. In this process, it was assumed that during the short period of time required to place the girders (one day) there were no critical effects such as development of further residual loads or creep of the grout. The differences in the sister bar strain gauge readings, immediately before and after girder placement were converted to corresponding stress increments on the section of the pile at which the uppermost level of sister bars was 1.22 m (4 ft) below the bases of the footings located as shown in Fig. 6.5. In the conversion of strain to stress, the initial composite modulus obtained at the time of 28 days was used for the grout in the piles.

Since the girder loads applied to each column were known, based on the known weights of the girders and the locations of the central bent footings, it was possible to use simple statics to compute the load increment applied to each footing, as the superstructure was designed with simple, statically determinate spans. The increment of the girder load that was transferred from each footing to the soil was then determined from differences in

computed soil reaction against the footing acting on the contact area of the footing by multiplying the average incremental contact pressure cell reading beneath each footing times the contact area between the footing and the soil. The incremental soil reactions obtained in this way were quite small. These soil reaction loads were then subtracted from the computed column loads and then distributed equally to each of the four piles in the footing. The average load increment in any one pile based on incremental strain measurements at the upper level of sister bars was then computed as the incremental composite stress obtained from the strain gauges times the cross-sectional area of the pile, which was to be determined. This was set equal to the computed load increment in the pile allowing for the computation of the cross-sectional area. The actual diameter of the pile at the top level of sister bars was then computed from the cross-sectional area determined in the process documented above. Finally, because it was necessary to distribute the computed load equally among the piles in the calibration process, it was judged necessary to compute an average pile diameter for all eight central bent piles for use in further computations for all central bent piles.

Since this process cannot be applied to sister bar levels farther down the pile because of load transfer from the pile to the soil, it was assumed that the pile diameter deduced from this calibration process applied to all levels along the pile. From this process a diameter of 0.495 m (19.5 in.) instead of the nominal value of 0.457 m (18 in.) was used in converting stress to load for all the central bent piles.

10.2.3 Development of Load vs. Depth Curves

Load vs. depth curves were developed for each pile at various loading events without consideration of residual loads. Sister bar readings taken at the time of placing concrete for the footings were considered as zero readings for load-depth curves. Such readings correspond to readings taken in the test pile just prior to the load test (Chapter 8) and do not reflect any residual strains that developed between casting and the application of external load. Note that sister bar readings for the central bent piles taken just after the footings were placed do not truly reflect any loads, since it can readily be assumed that the weight of the fluid concrete in each footing was carried entirely by the soil beneath the footing. Therefore, there was no transfer of load from the wet concrete to the piles. The first actual external loading event for the piles was the construction of the columns. Various other loading events included placement of the bent caps, deck, simulated live loads (loaded trucks), immediate service load, and service loads up to six months after the bridge went into service. The latter loads contain the effects of cyclic loads from traffic.

10.2.4 Simulated Live Load

In order to assess whether the piles would perform properly under dead plus live loading before the bridge went into service, live load was simulated on the structure to bring the axial loads on the piles to a value near their design load [0.80 MN (90 tons) for central bent piles and 0.49 MN (55 tons) for abutment piles]. Actual simulated live load per pile for central bent piles was 0.64 MN and 0.29 MN for abutment piles. This was accomplished by driving six TxDOT maintenance vehicles (dump trucks) loaded with ballast weighting about 116.6 kN (13.1 ton) each (including ballast) onto two lanes in the

South zone of the deck and parking them in such a location that the weights of the trucks produced maximum loads on Footings A and B. After sister bars, contact pressure cells and settlements of these footings were read, the trucks were moved to a position immediately north of the south abutment, which maximized loads on the instrumented abutment piles, and the sister bars, contact pressure cells and settlements were then read for the instrumented abutment piles. This process constituted one phase of loading.

10.2.5 Contact Pressure Cells

In order to study load-sharing behavior of ACIP piles and the pile caps, a total of six contact pressure cells were placed under the pile caps as shown in Figs. 6.1 and 6.8. Three pressure cells were placed at the bottom of the Footing A to measure load resisted by the soil beneath the pile cap, and the other three were placed beneath Footing B. The bearing surface for each cell was prepared by flattening the surface of the soil, placing about 15 mm of dry, clean sand on the flattened soil surface, seating the plate of the pressure cell into the sand by pushing and rotating, placing a small thickness of concrete on top of the cell to keep it in position, and finally placing the concrete for the footing within a short period of time after seating the cell. Pressure cell outputs were converted to pressure using Equation 6.2 and then to load by multiplying the average indicated pressure by the area of footing less the area occupied by the piles.

10.2.6 Settlements

Settlements of the footings were monitored by placing settlement points (steel pins) in each corner (directly above the top of each pile) of the top of each footing at the

time of placing concrete for footings. Settlements were continuously measured from the permanent benchmark noted in Fig. 3.3, including sets of measurements for each major loading event, such as placement of girders, deck, live load simulation, initial service load and service loads six months after the bridge went in service. Measurements were made using optical levels and Philadelphia rods, which allowed readings to be made to a precision of about 0.3 mm (0.001 ft).

10.3 Residual Loads in Central Bent Piles

Residual loads were calculated using the data obtained at the time of placing concrete for footings assuming that there was no load transfer from weight of wet concrete for footings to the piles. That is, the weight of the footing did not load the piles, except perhaps in some minor way through cap-soil-pile interaction, which was neglected. The residual loads were computed using the same algorithm that was used for the test pile, as described in Chapter 8. The residual load distribution curves for the ACIP piles under Footings A and B after placement of the footings are plotted in Figs. 10.1 and 10.2, respectively. The average residual load distribution along the eight central bent piles under the two footings is shown in Fig. 10.3.

It can be observed that the trend of residual load distribution in the central bent piles was similar to that of residual load distribution for the test pile in that loads are generally tensile along the entire pile length. The average value of residual load ranged approximately from 77 kN to 187 kN (8.6 to 21 ton) along the pile length, where tension is represented by negative values in Figs. 10.1 - 10.3. It is noted that the largest residual tensile force in any pile was only about 350 kN, giving a maximum tensile stress of 2135

kPa. This value was well below the mean tensile strength of the grout, which was measured in splitting tension tests on seven grout samples (as summarized in Table 7.8) to be 4400 kPa. Therefore, residual strain readings should represent values from continuous, not cracked, structural elements.

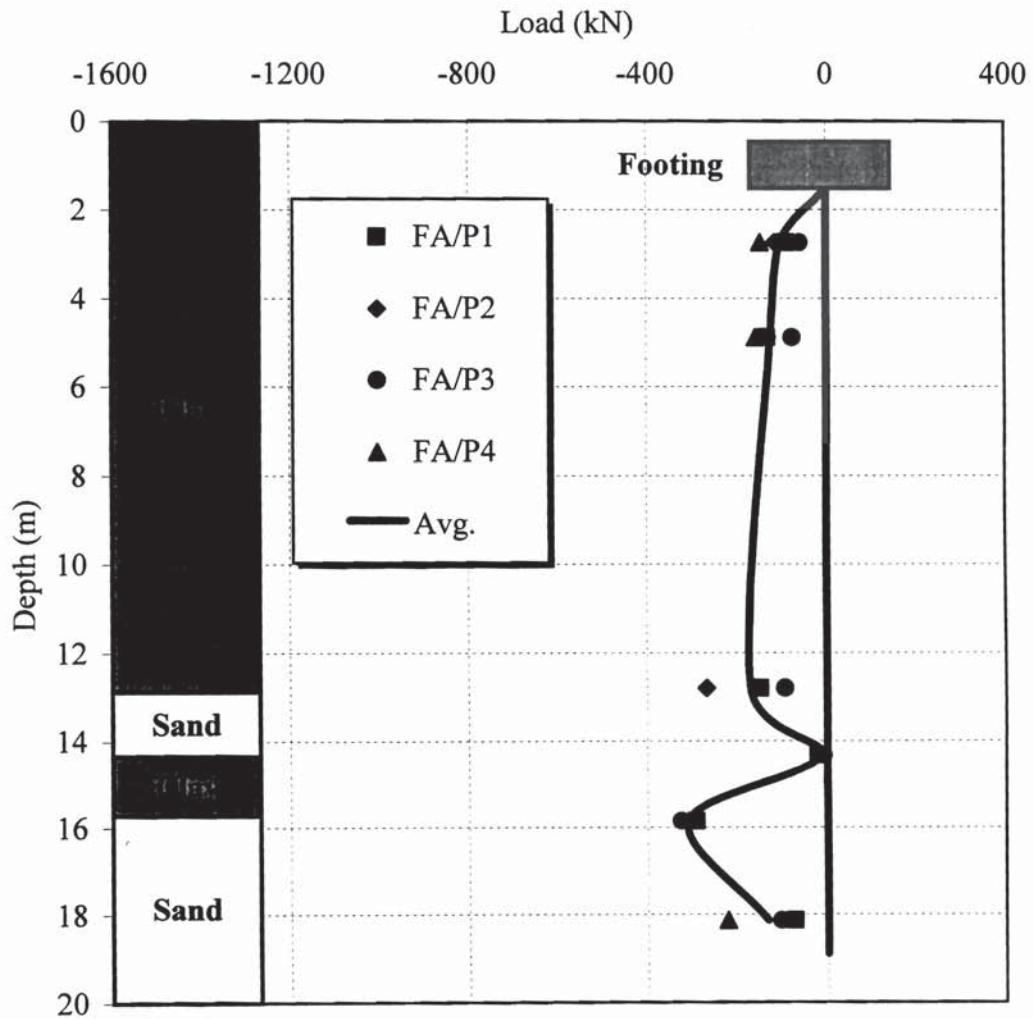


Fig. 10.1. Residual Load Distribution for Central Bent Piles Under Footing A

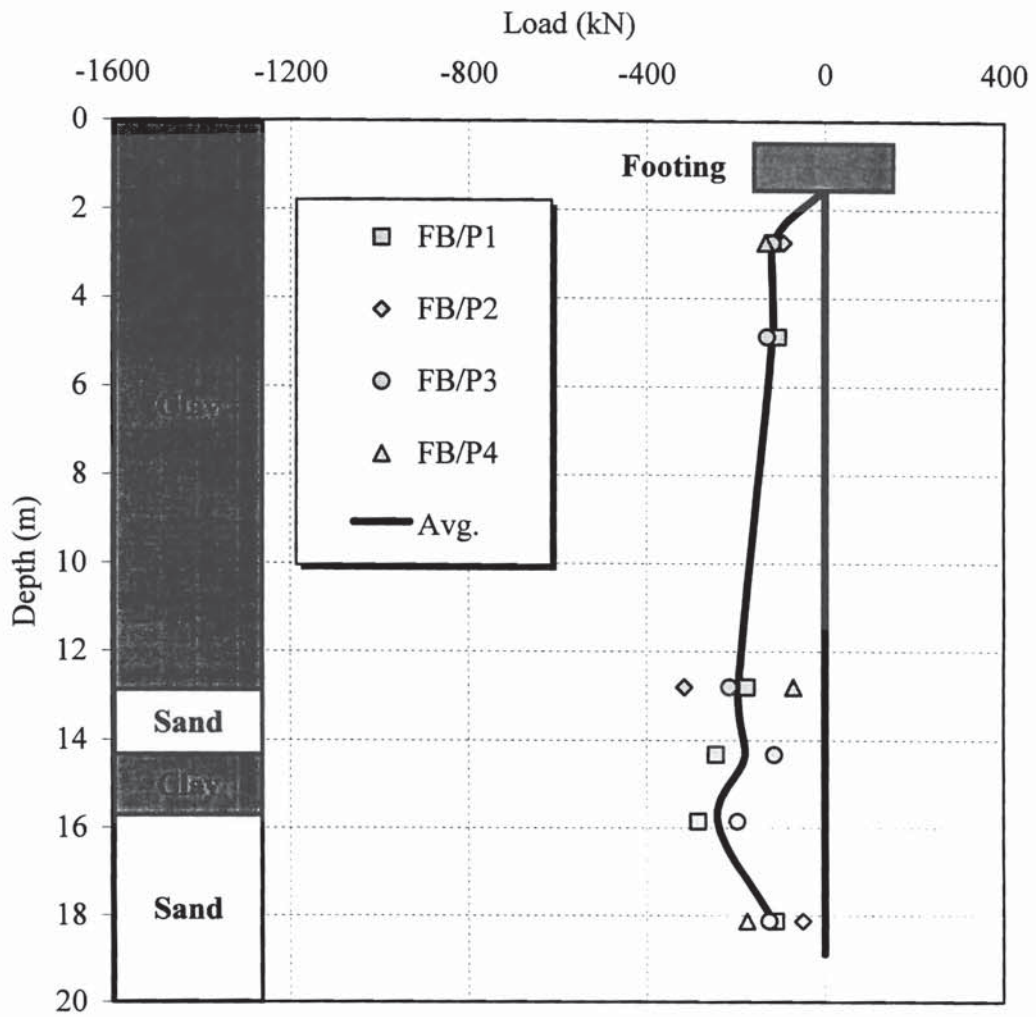


Fig. 10.2. Residual Load Distribution for Central Bent Piles Under Footing B

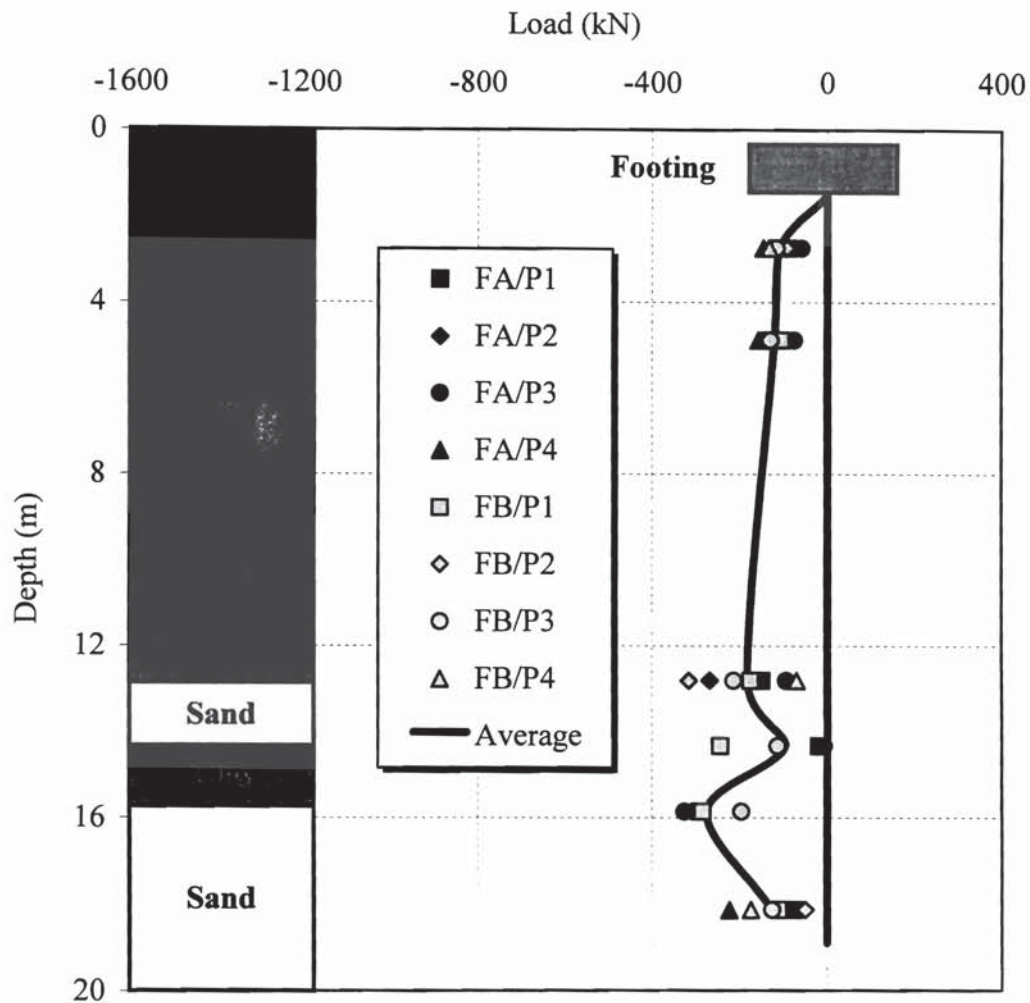


Fig. 10.3. Average Residual Load Distribution for All Central Bent Piles

The progression of loading events is chronicled in Fig. 10.4. The loads that are shown are computed loads, not measured loads. Example calculations for the pile loads are shown in Appendix C. It was observed from sister bar readings taken between loading events that residual tensile strains along the pile length were generally developing not only during curing (first 28 days) but also during every loading event and even after the bridge went into service. Residual loads can occur in ACIP piles because of the

expansion of grout from excess water and/or swelling of clay soils surrounding the upper part of the pile. Recently, Falconio and Mandolini (2003) showed that either expansion or shrinkage in the grout could occur after grouting the piles, according to external environmental conditions (drying or wetting of the ambient soil). They concluded that significant strains develop in the pile after the placement of the grout in the borehole resulting from complex pile-soil interaction. At the Krenek Road bridge site, copious amounts of water were available to the clay soil near the surface from flooding of the footing excavations between the time the piles were installed and the concrete for the footings was poured. This flood water was not pumped out of the footing excavations until just before the footings were poured. Undoubtedly, some of this free water found its way into the upper clay soils surrounding the piles and produced uplift (residual tensile stresses). Swelling of clay soils is a time-dependent process that can take months to years to develop fully. More information on the process for ground wetting around drilled shafts given by Kim and O'Neill (1998).

10.4 Load Distribution of Central Bent Piles

10.4.1 Load-Depth Curves

Load vs. depth curves without consideration of residual loads for each instrumented central bent pile at various loading events are given in the figures following Fig. 10.4. In each plot (Figs. 10.5 through 10.9), solid symbols represent points that were given the highest weight for plotting the fitted curves. Open symbols represent points that were given lower weights in plotting the fitted curves than the solid symbols because they were within the zone below 13 m that appeared to give somewhat erratic residual loads.

The various points within the zone below 13 m suggest a complex variation in the load-depth relations. It is reasoned that this variation reflects long-term development of tensile stresses in the piles due to expansion of grout and may also reflect long-term localized strain changes due to the presence of non-uniformities in the pile cross-section.

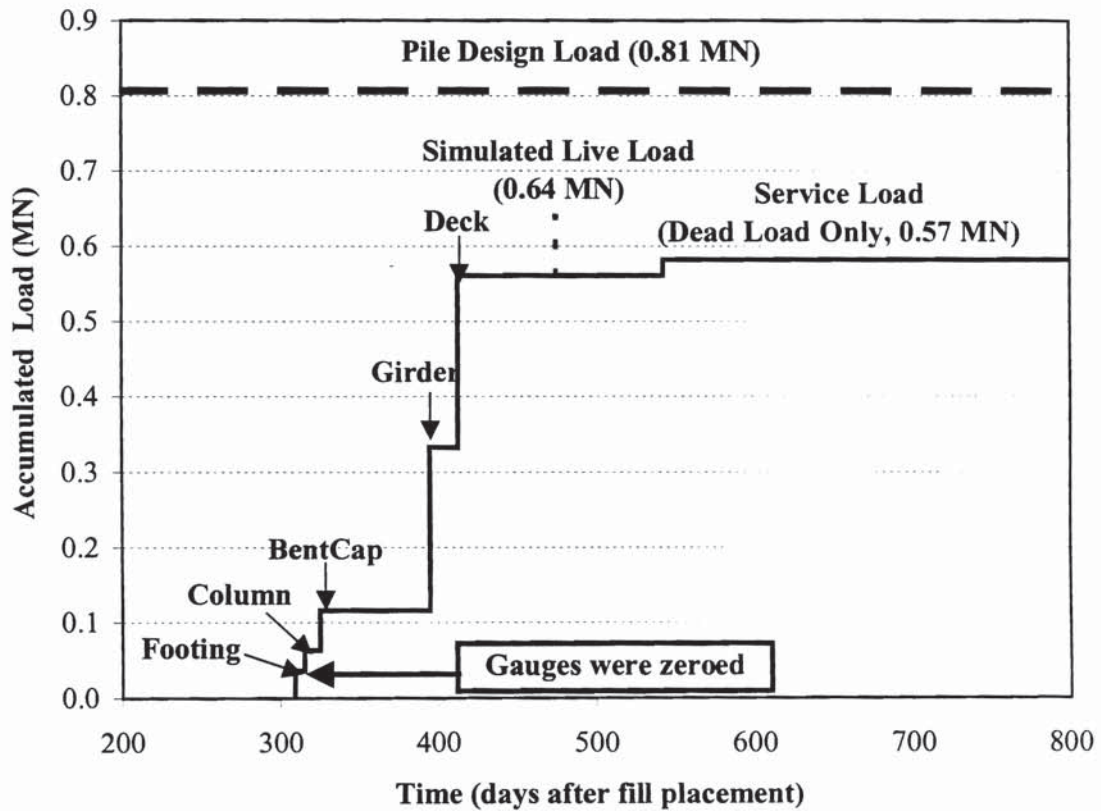


Fig. 10.4. Applied Load on Each Central Bent Pile vs. Time

Figures 10.5 through 10.8 show graphs of loads along the piles in Footing A at various loading stages including placement of deck, live load simulation, initial service load, and six months after bridge went into service indicated on the figures. Figure 10.9

compares load distribution curves along the piles in Footing A at initial service load and six months after going into service. The fitted curves were drawn by judgment using the point weighting system described above. That is, they were not drawn using any formal curve fitting scheme.

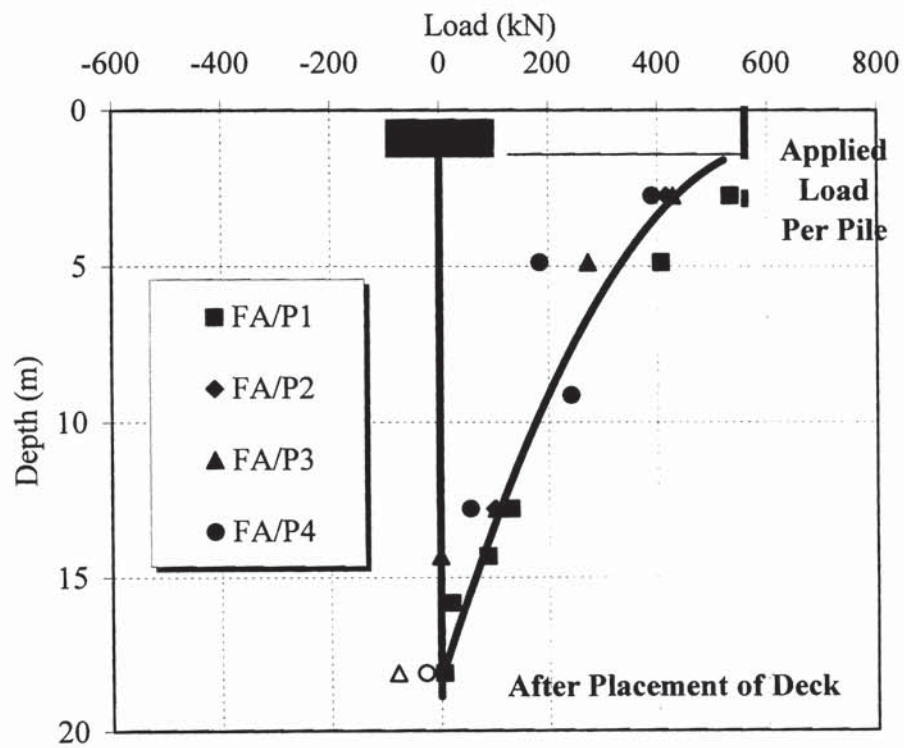


Fig. 10.5. Load vs. Depth Curve for Piles Under Footing A After Placement of Deck

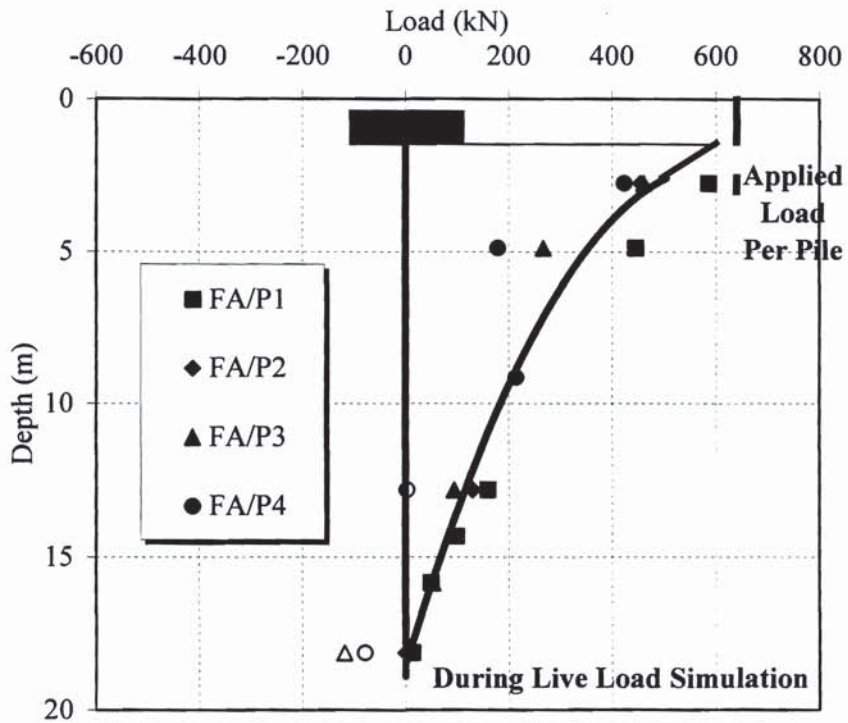


Fig. 10.6. Load vs. Depth Curve for Piles Under Footing A During Live Load Simulation

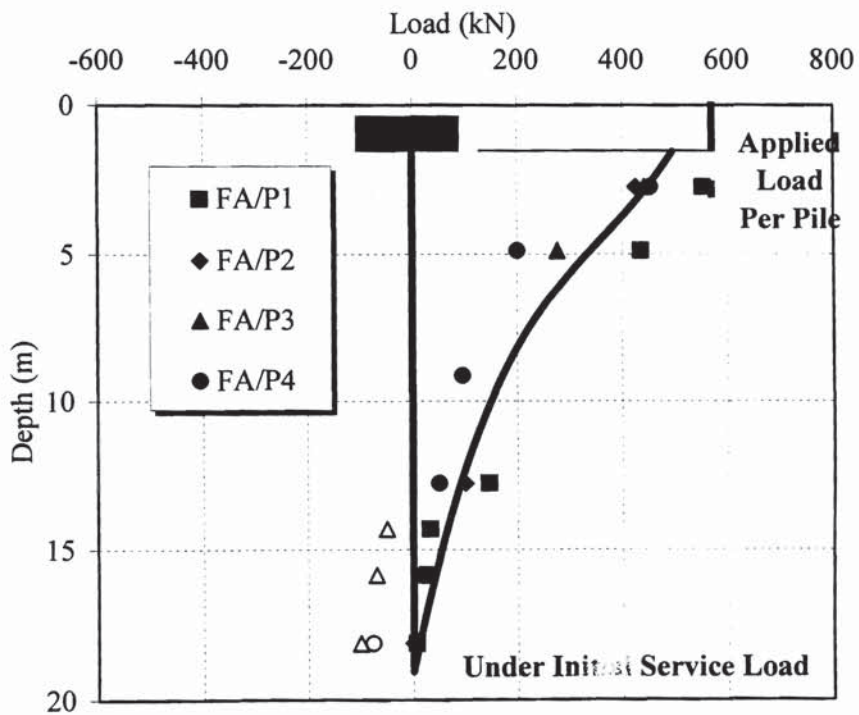


Fig. 10.7. Load vs. Depth Curve for Piles Under Footing A Under Initial Service Load

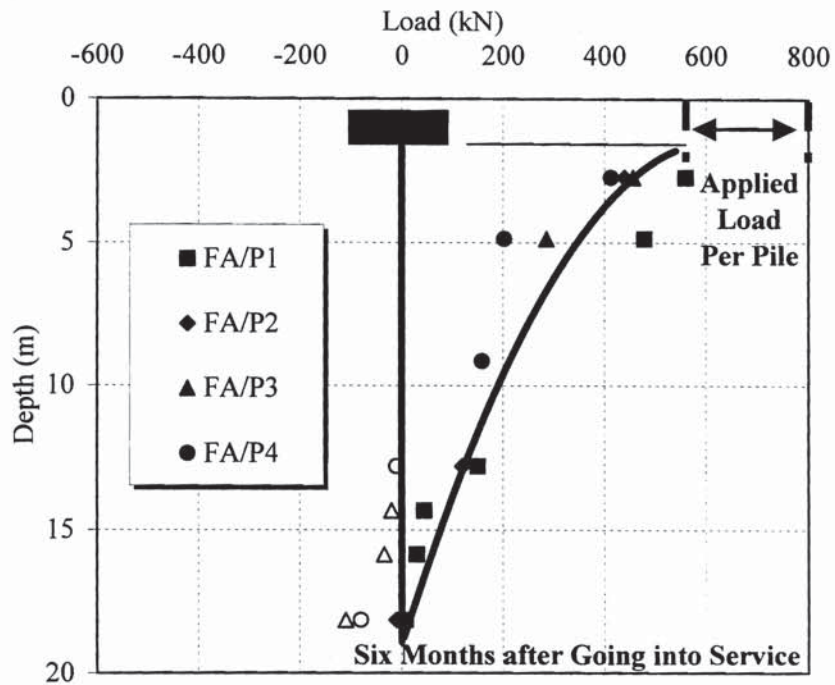


Fig. 10.8. Load vs. Depth Curve for Piles Under Footing A Six Months After Going into Service

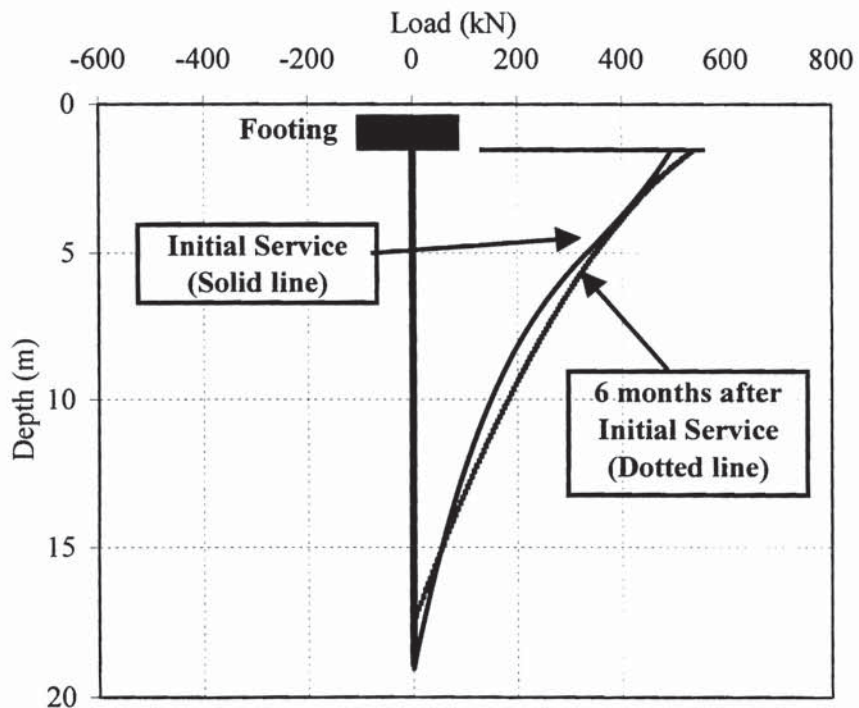


Fig. 10.9. Load vs. Depth Curves for Piles Under Footing A During Initial Service Load and Six Months After Going into Service

Figs. 10.10 through 10.13 show graphs of loads along the piles in Footing B at various loading stages including placement of deck, live load simulation, initial service loading, and six months after bridge went into service indicated on the figures. Figure 10.14 compares average load distribution for the piles in Footing B at initial service load and six months after bridge went into service. Again, the fitted curves were drawn by judgment using the point weighting system as described earlier.

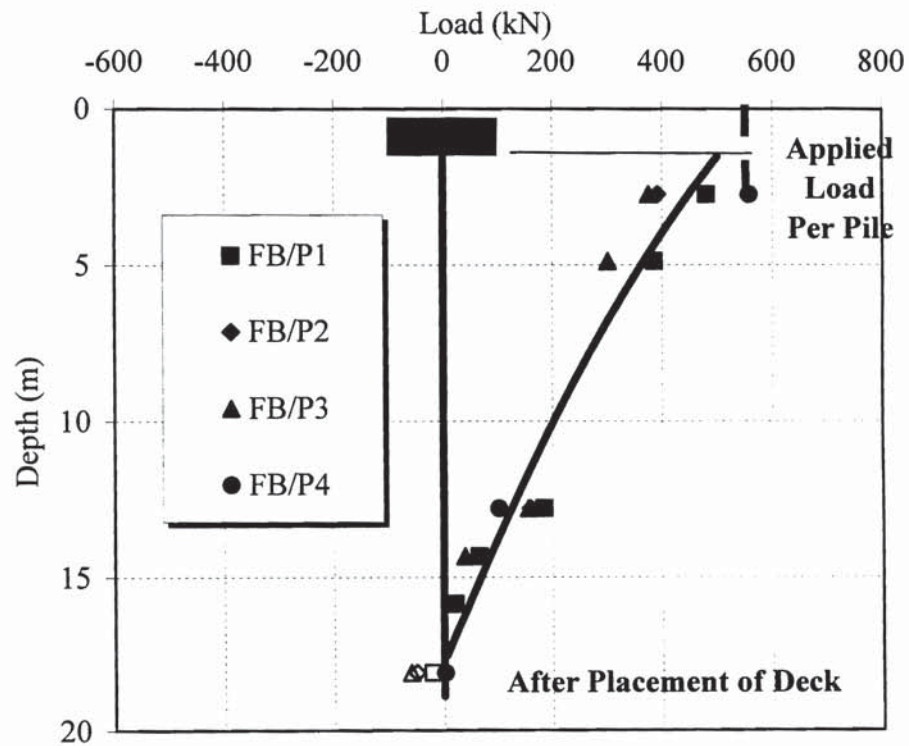


Fig. 10.10. Load vs. Depth Curve for Piles Under Footing B After Placement of Deck

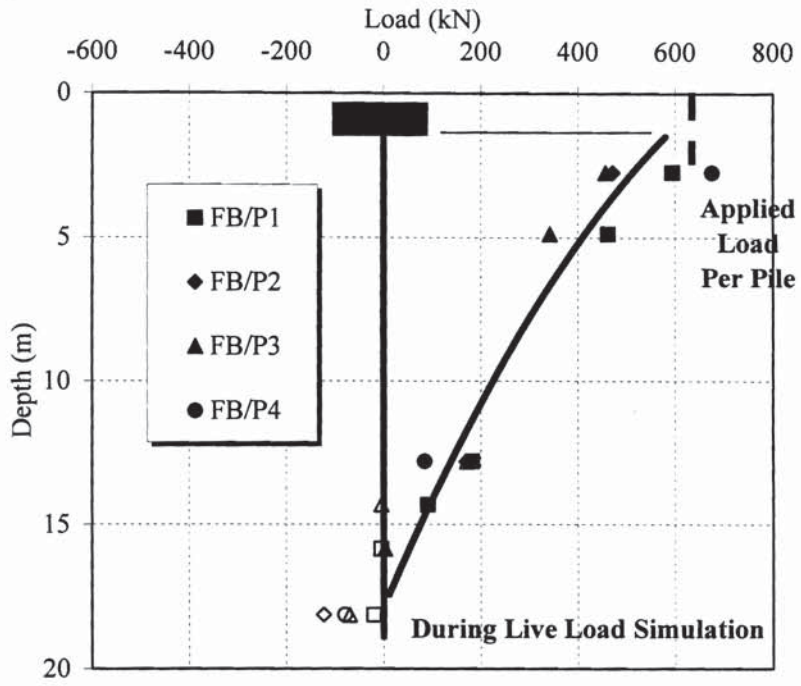


Fig. 10.11. Load vs. Depth Curve for Piles Under Footing B During Live Load Simulation

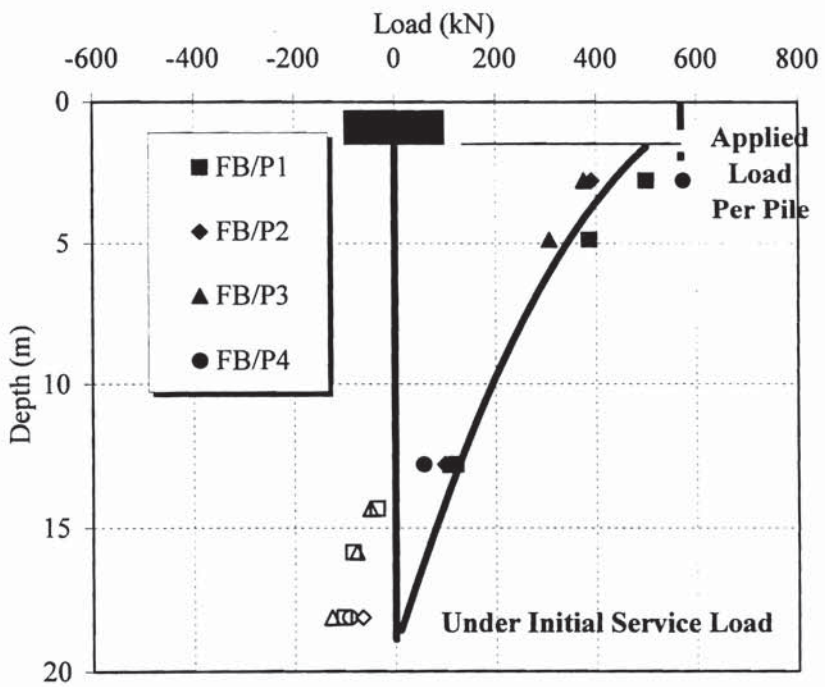


Fig. 10.12. Load vs. Depth Curve for Piles Under Footing B Under Initial Service Load

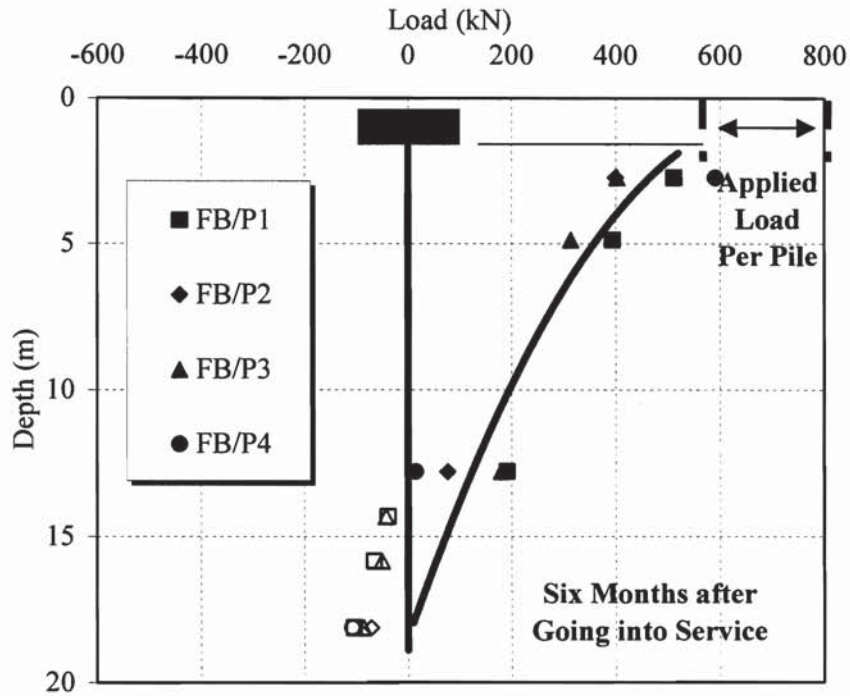


Fig. 10.13. Load vs. Depth Curve for Piles Under Footing B Six Months After Going into Service

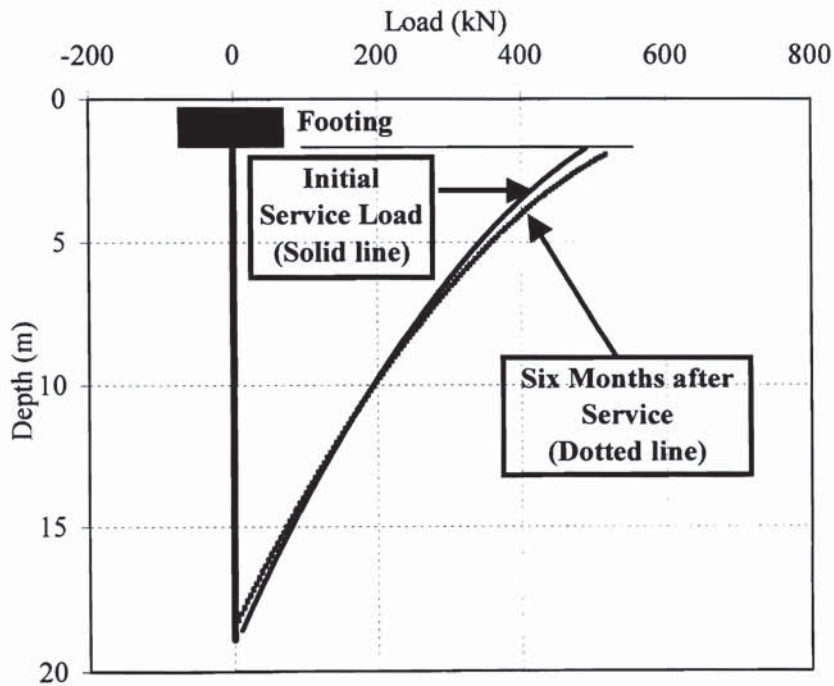


Fig. 10.14. Load vs. Depth Curves for Piles Under Footing B During Initial Service Load and Six Months After Going into Service

The time-dependent increase in tension in the lower parts of the piles that can be inferred in load distributions shown in Figs. 10.5 – 10.14 may be due to long-term swelling of the grout, although the cause is not completely known. Sister bar instrument drift is normally reflected in decreasing frequency (decreasing tension) with time, as the vibrating wire slips in the grips. Since the opposite effect was observed here, it is probable that instrument drift was not the cause of the indications of increasing tension.

Inspection of load-depth curves for central bent piles under Footings A and B reveals several apparent findings. Generally, at working load conditions (live load simulation, initial service load, and 6 months after bridge went into service) the patterns of the load-depth curves were similar. For all the load distribution curves, the load at the tip of the ACIP pile was exceptionally small (almost zero) indicating no loads are transferred from pile to soils at the base (tip) of the pile under working load conditions. By 6 months after bridge went into service, there is no evidence of any load shedding taking place. The tip load has been shown to remain zero throughout the period studied in this project.

There is some question as to how long a period of time is required for a substantial amount of load shedding to occur. Because of the load shedding effect is related to creep (Wooley and Reese, 1974), and because the effect of creep is most seriously felt soon after the loading sequence is initiated, if load shedding were to occur, some signs of it should be appeared. The apparent absence of creep is probably due primarily to the low magnitude of load relative to the capacity of ACIP piles.

Little load shedding is anticipated in the future, based on the small settlement and almost zero tip loads, the monitoring field instrumentation should be continued after bridge went into service.

10.4.2 Load Distribution

The distribution of load to the various piles in the central bent pile groups at working load conditions varied from pile to pile within a group. This variation may have been due to the variation in pile stiffness, the quality of the pile-cap connection and the presence of lateral loads on the caps from the bridge superstructure. Tables 10.1 and 10.2 respectively summarize the load distribution to the individual piles in the central bent pile groups, Footings A and B, for various loading events. The loads in Tables 10.1 and 10.2 were determined from the top level of sister bars on each pile.

Table 10.1. Head Load in Piles in Central Bent Footing A

Group A	FA/P1	FA/P2	FA/P3	FA/P4	Total	Avg.
Deck (kN)	534	416	429	390	1768	442
Each Pile / Total (%)	30	24	24	22	100	25
Simulated Live Load (kN)	587	455	461	423	1926	481
Each Pile / Total (%)	30	24	24	22	100	25
Initial Service (kN)	553	426	442	453	1874	469
Each Pile / Total (%)	30	23	24	24	100	25
6 Month (kN)	560	439	456	413	1868	467
Each Pile / Total (%)	30	23	24	22	100	25

Table 10.2. Head Load in Piles in Central Bent Footing B

Group B	FB/P1	FB/P2	FB/P3	FB/P4	Total	Avg.
Deck (kN)	480	392	375	558	1805	451
Each Pile / Total (%)	27	22	21	31	100	25
Simulated Live Load (kN)	594	471	457	676	2198	550
Each Pile / Total (%)	27	21	21	31	100	25
Initial Service (kN)	500	391	375	574	1840	460
Each Pile / Total (%)	27	21	20	31	100	25
6 Month (kN)	512	400	403	591	1906	477
Each Pile / Total (%)	27	21	21	31	100	25

There was no verifiable load distribution trend among the piles in each footing that might be associated with the installation sequence. In each footing, the installation sequence was P1, P2, P3 and P4, in that order. In Footing A, the pile installed first tended to carry more load than the pile installed later, while the opposite trend occurred in Footing B. This may be only coincidence.

10.5 Load Sharing between ACIP Group Piles and Pile Cap

An objective of this study was to determine whether pile caps could be counted upon to carry part of the column loads when the bearing surface was prepared in the standard manner for TxDOT bridge foundations (i. e., no soil compaction and no dewatering except at the time of footing placement). If this were possible, then it might be possible to reduce the number of piles in the foundation and affect further economy. Loads carried into the soil directly by the pile caps at the Krenek Road bridge were

estimated by measuring contact pressures with three vibrating wire pressure cells located as shown in Fig. 6.1. The average contact pressure was then multiplied by the contact area of the footing less the area of the piles to obtain soil resistance acting directly on the footing. These loads were then compared with the loads taken by the piles.

Tables 10.3 and 10.4 summarize load sharing between piles and footing (cap) in Footings A and B, respectively, for various loading events. At working load conditions (such as live load simulation, service and six months after beginning service), the average load resisted by the cap in both footings was about 8 % of total loads. Maximum and maximum load resisted by the cap in both footings were 7.1 % and 8.1 % of total loads, respectively. Again, the pile group loads in Tables 10.3 and 10.4 are determined from the top level of sister bars on each pile. This would not be sufficient to allow for the removal of a pile and to replace the four-pile group with a three-pile, triangular, cluster.

Table 10.3. Load Sharing Between Pile Group A and Cap A for Various Loading Events

Footing A	Deck	Live Load	Service	6 month
Pile Group, MN	1.77	1.93	1.87	1.87
Cap, MN	0.15	0.17	0.16	0.15
Total Load, MN	1.92	2.10	2.03	2.02
Cap/Total Load, %	7.8	8.1	7.8	7.5

Table 10.4. Load Sharing Between Pile Group B and Cap B for Various Loading Events

Footing B	Deck	Live Load	Service	6 month
Pile Group, MN	1.81	2.20	1.84	1.91
Cap, MN	0.15	0.17	0.16	0.15
Total Load, MN	1.95	2.37	2.00	2.06
Cap/Total Load, %	7.6	7.1	7.8	7.3

10.6 Calculated Load vs. Settlement vs. Time for Each Central Bent Pile Group

The settlement readings were used for two primary purposes: (1) To verify that excessive settlement was not occurring in the ACIP piles under dead loading and later dead loading plus live loading. (2) To assess the effect of loading piles in groups of four on pile settlement relative to the settlement of the single test pile at common values of head load.

By 6 months after bridge went into service, there is no evidence of any load shedding taking place. The tip load has been shown to remain zero throughout the period studied in this project. Therefore, it is not expected that there is significant settlement increase occurring in the ACIP piles under each footing. The settlements for each central bent pile at working load conditions (such as simulated live loading, initial service load and at six months after going into service) are shown in Figs. 10.15 through 10.17. Maximum and minimum settlements were 4.57 mm (0.18 in) and 1.52 mm (0.06 in), respectively at working load conditions. During the live load simulation, the average footing settlement was 3.05 mm (0.12 in). When the bridge went into service, the

average footing settlement was 2.67 mm (0.105 in). Six months after the bridge went into service the average footing settlement had increased to 3.05 mm (0.12 in). The additional settlement for 6-month service period was only about 0.38 mm (0.015 in). Considering the fact that optical level for the settlement measurements had an accuracy of 0.30 mm (0.012 in) the additional settlement of 0.38 mm (0.015 in) was not very meaningful. Therefore, it can be concluded that there was no additional settlement occurring in ACIP piles under each footing between the initial service and 6 months after bridge went into service.

From a design perspective, the settlement of the footings (3.05 mm) were not large enough six months after the bridge went into service to result in any performance deficiencies in the structure.

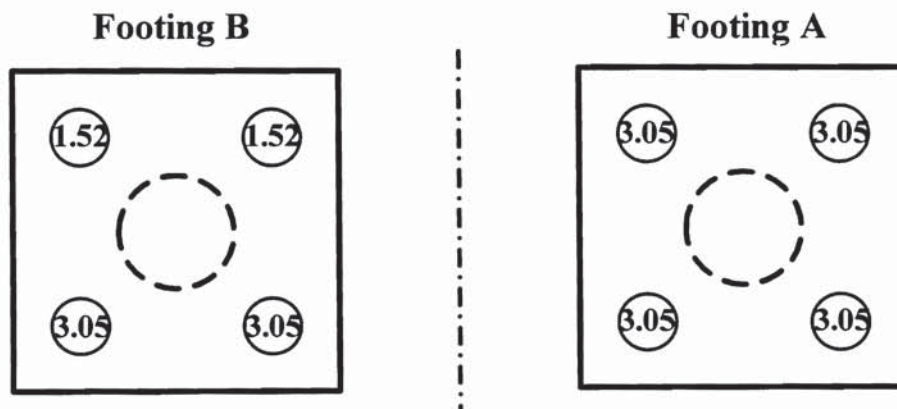


Fig. 10.15. Measured Settlements (mm) Within Central Bent Piles Under Footings A and B During Initial Service Load

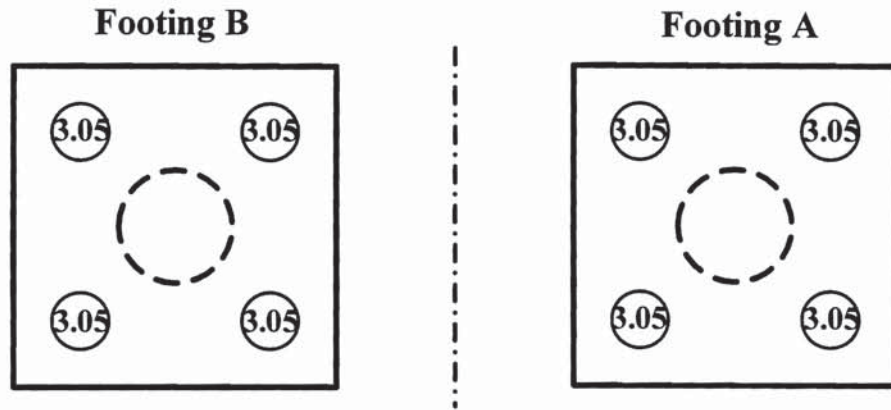


Fig. 10.16. Measured Settlements (mm) Within Central Bent Piles Under Footings A and B 6 Months After Going into Service

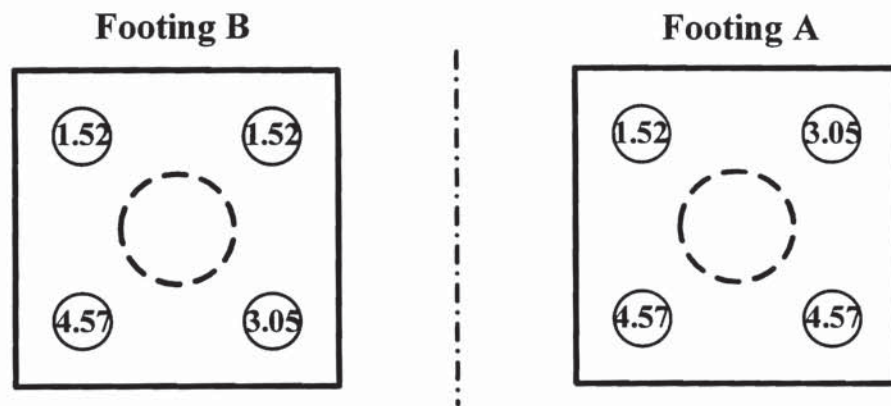


Fig. 10.17. Measured Settlements (mm) Within Central Bent Piles Under Footings A and B During Live Load Simulation

In order to study the effect of loading of piles in groups on load-settlement behavior of the ACIP piles, load-settlement curve for the test pile and settlement points of the central bent piles at working load condition were compared in Fig. 10.18. At the time of working load application, the ratio of average settlement for Footings A and B, and the test pile was about 2.0 at common values of average load per pile, which indicates that there is group action occurring within the central bent ACIP piles under each footing. The group action will be further investigated by finite element analysis in Chapter 12.

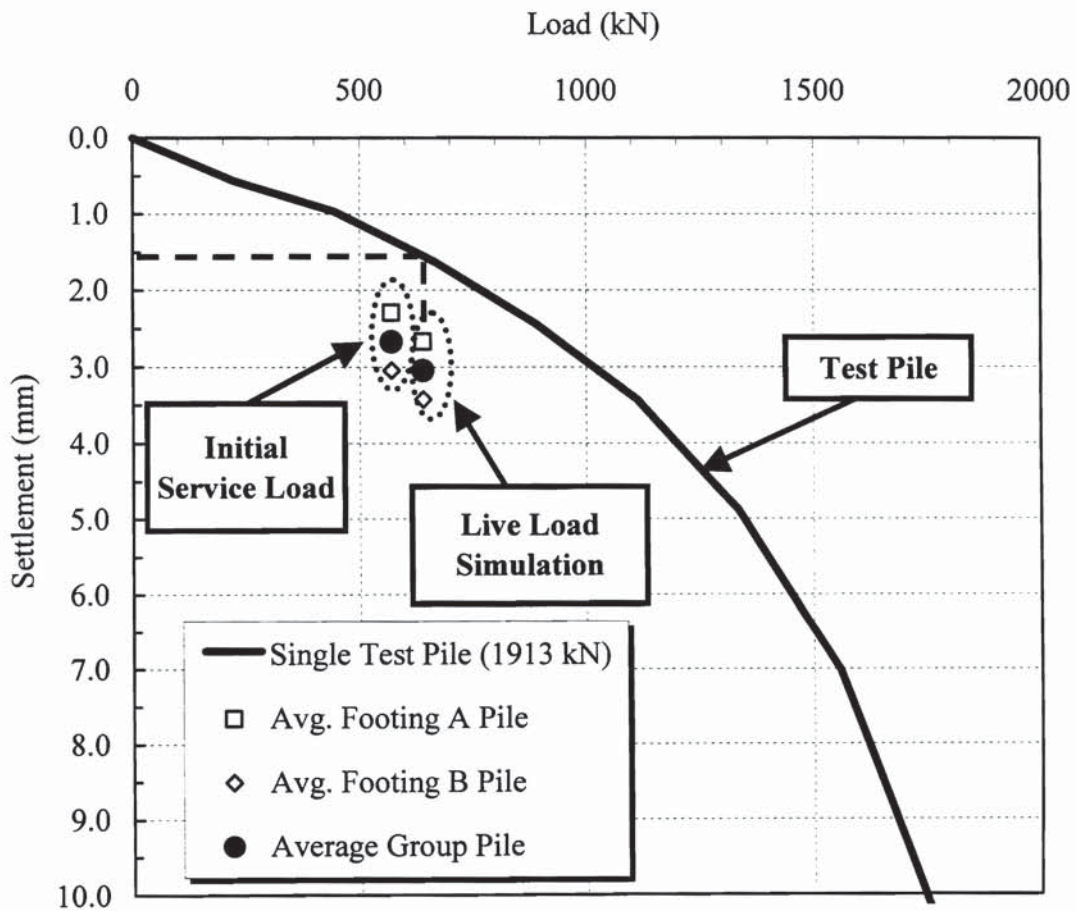


Fig. 10.18. Comparison of Measured Settlements for Single Test Pile and Group Pile (Central Bent Piles) at working Load Conditions

10.7 Summary

- The time-dependent increase in tension in the lower parts of the piles that can be inferred in load distributions may be due to long-term swelling of the grout, although the cause is not completely known.
- The load shedding in central bent ACIP piles did not occur until 6 months after the bridge went into service (under cyclic live load) primarily because the low magnitude of working load was applied relative to the capacity of ACIP piles.
- At working load condition (live load simulation, service and six months after beginning service), the average load resisted by the cap in both footings was only about 8 % of total loads. This would not be sufficient to allow for the removal of a pile and to replace the four-pile group with a three-pile, triangular, cluster.
- Six months after the bridge went into service the average footing settlement was only 3.05 mm. From a design perspective, the settlements of the footings were not large enough six months after the bridge went into service to result in any performance deficiencies in the structure.
- Settlement ratio of the single test pile and the average group pile under Footings A and B at working load condition was about 2.0 indicating the group action occurring within the central bent piles.

CHAPTER 11

LONG TERM BEHAVIOR AND PERFORMANCE OF ABUTMENT PILES

11.1 General

It was expected that the abutment piles would behave differently from the central bent piles:

- The abutment piles were installed on a 4:1 batter. This is a rare application for ACIP piles, even in the private sector, and no information on the issue of performance of ACIP piles constructed on a batter could be found in the literature. For example, since the piles are drilled, the borehole might collapse partially before the grout can be placed, resulting in severe necks within the pile. (The Krenek site contained cohesive soil above the toes of the batter piles, so hole collapse was not considered likely, but, nevertheless, this was an unproven application of ACIP piles.)
- The 4:1 batter piles are loaded vertically at their heads, which, unlike the vertical central bent piles, produces both an axial and a lateral component of loading on the pile head (Fig. 11.1).
- Each group of two battered ACIP piles (Fig. 11.1) had a component of horizontal loading from backfill behind the abutment wall.

The behavior and performance of the ACIP abutment piles in a real field environment (Krenek Road bridge abutment) over an extended period of time were observed and analyzed. Four battered abutment piles were instrumented in Group A and B, as shown in Figs. 6.1 and 6.6 in Chapter 6. Ten vibrating wire strain gages were used for abutment piles (GA/PF, GA/PB, and GB/PF) and six were used for abutment pile, GB/PB.

Load distribution and settlement for the abutment piles were observed for an extended period time. Mean strain readings at each sister bar level were converted to axial loads using appropriate initial composite secant moduli of the pile and the pile's calibrated cross-sectional area. The procedure used was exactly the same as the procedure used for the axial loads, including residual loads, in the central bent piles. At several loading events such as placing the deck, parking trucks for simulating live load, initial service load, and six months after initial service load, axial load distribution curves were developed for each pile. Abutment and fill settlements were monitored for an extended period of time, as well as contact stresses between the abutment cap and the underlying fill.

11.2 Residual Loads of Abutment Piles

Residual loads were calculated using initial secant modulus at 28 days after grouting the piles, just before the abutment cap was placed. At every loading event, the loads were computed using the same initial secant modulus as the one obtained at the time of 28 days after placing grout. Residual load distributions (at 28 days) for in-battered piles and out-battered piles were plotted in Fig. 11.2.

The general trend of residual load distribution for in-battered piles was similar to that of out-battered. Residual loads for the abutment piles along the pile length were generally compressive except for the top 2.5 m of the piles. That is different from those for the test pile and central bent piles, presumably because the external environmental conditions were different from one another. The abutment piles were installed battered 4:1 through compacted fill such that the heads of the piles were about six meters above the water table. The fill was compacted wet of optimum moisture content. Apparently, the suction potential of the embankment soil was not sufficient to cause any significant swelling due to absorption of water from the grout except very near the heads of the piles, the residual compression loads below a depth of about 2.5 m appear to be the result of drag loading from the fill during the first 28 days after the piles were installed.

11.3 Load Distribution and Settlement of Abutment Piles

Axial load vs. depth curves without consideration of residual loads for both instrumented abutment pile groups (in which each group contained one in-battered and one out-battered pile) for various loading events were plotted, as per the central bent piles in Chapter 10. For purpose of definition, an “in-battered” pile is one that slopes toward the fore-slope of the header bank (fill), while an “out-battered” pile slopes away from the fore-slope of the header bank. These terms were developed because of the way the ACIP pile rig was positioned, in which the out-battered piles sloped away from the rig and the in-battered piles sloped in toward the rig.

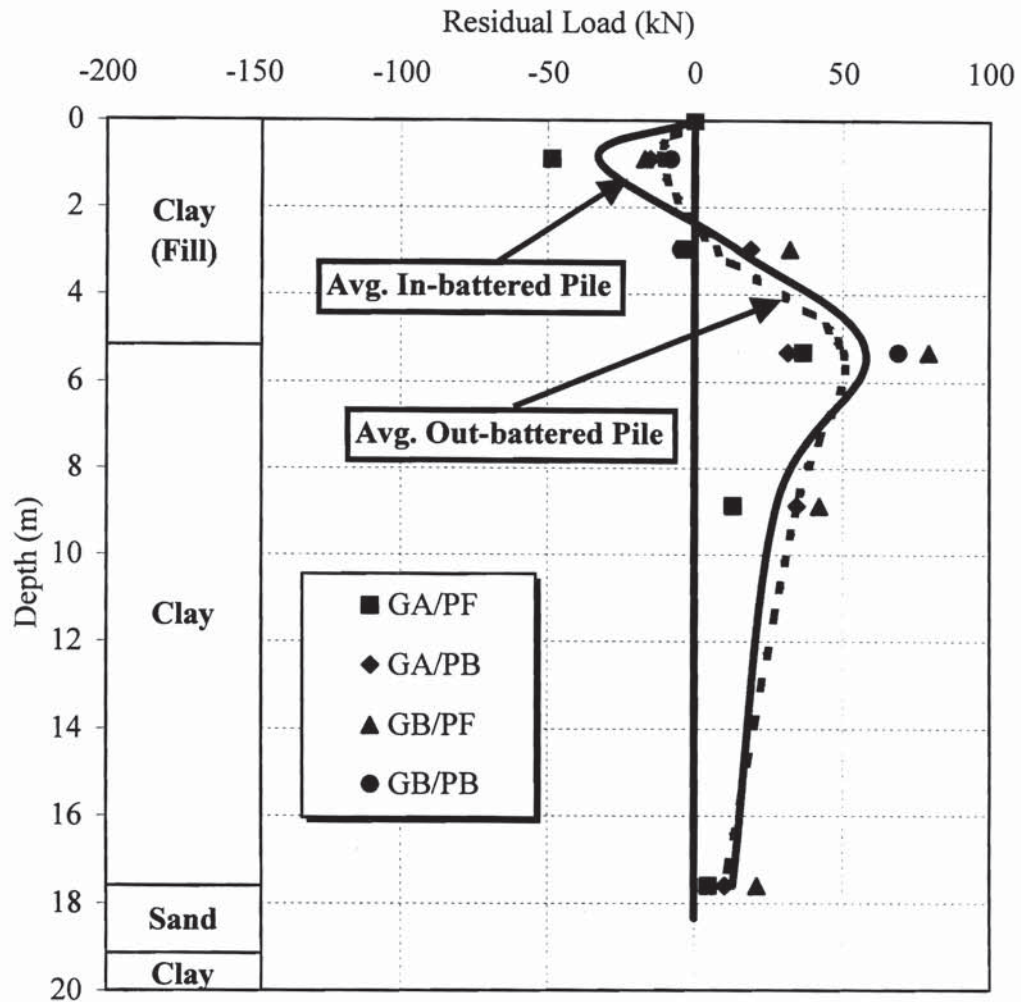


Fig. 11.2. Residual Load Distribution for Abutment Piles

Fig. 11.3 shows load distribution curve for the in-battered abutment piles immediately after the deck was placed. Figs. 11.4 through 11.6 show load distribution curves for in-battered abutment piles at various loading events (working load conditions) including simulated live load, initial service load and 6 months after bridge went into service. The general trend of the load vs. depth curves was similar to one another. Load distribution curve clearly indicate that there are downdrag loads acting on the in-battered

piles down to a depth of about 5 m from the tops of the piles (bottom of the abutment footing). These loads can only be due to fill settlement. Load at the toe in every loading event was almost zero indicating no load is transferred to soil at the toe. The load distribution curves at various loading events are compared in Fig. 11.7. The measured changes in the axial load distribution from deck placement to the time the bridge went into service (a period of about three months) indicates that further drag loading was occurring from the fill. The changes from the time the bridge went into service until a time six months afterwards were small.

Table 11.1. Calculated Pile Load and Settlements at Various Loading Events

Loading Event	Abutment (Cap +Wall)	Girder	Deck	Live Load Simulation	Bridge In Service	Six Months After Going into Service
Accumulated Calculated Average Load Per Pile (MN)	0.04	0.15	0.25	0.29	0.26 ^A	0.26 ^A
Average Abutment Settlement (mm)	0.0 ^B	0.8	1.0	1.8	1.6	2.7

Note: ^A Dead load only; ^B Initial settlement zero was taken at placement of abutment cap.

Table 11.1 shows the estimated (calculated) axial load per pile and settlements for the various milestone loading events. Loads at various times were estimated as demonstrated in Appendix D. The pile load was estimated by dividing 2-pile group loads by 2. The calculated accumulated abutment pile load vs. time at each loading event is

chronicled as shown in Fig. 11.8. These loads are in general agreement with the measurements once the effect of load distribution between the in-batter piles and the out-batter piles are considered. Table 11.1 also shows the settlements of the abutment footing during construction and up to six months after the bridge went into service. Average settlement generally increased with increment of loads and also with time considering the data at service and 6 month after service (See Appendix E). The settlement of the fill was larger than the settlement of the abutment footing, as can be seen by comparing the settlements tabulated in Table 11.1 with the settlements from Fig. 5.16, which reinforces that conclusion that downdrag was occurring. For example, the fill settlement (between installation of abutment and bridge going into service) in Fig. 5.16 was about 10 mm, which is larger than the abutment settlement of 1.6 mm at service load.

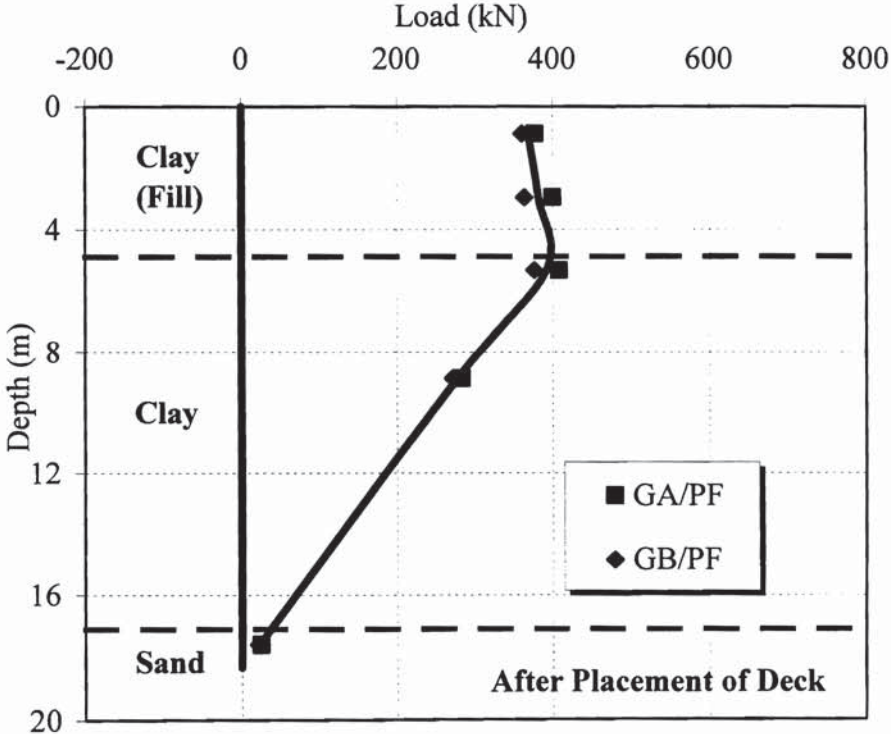


Fig. 11.3. Load vs. Depth Curve for In-Battered Abutment Piles After Placement of Deck

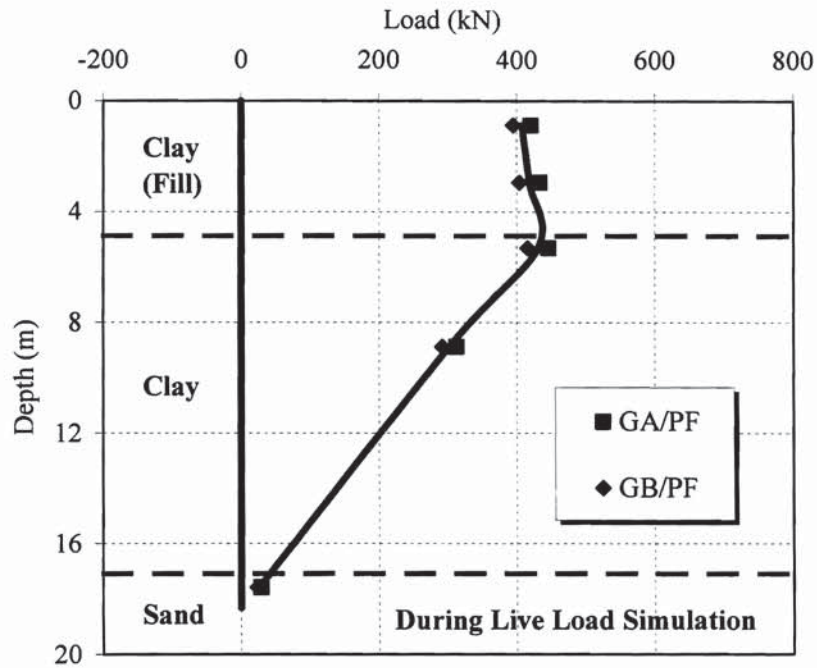


Fig. 11.4. Load vs. Depth Curve for In-Battered Abutment Piles During Live Load Simulation

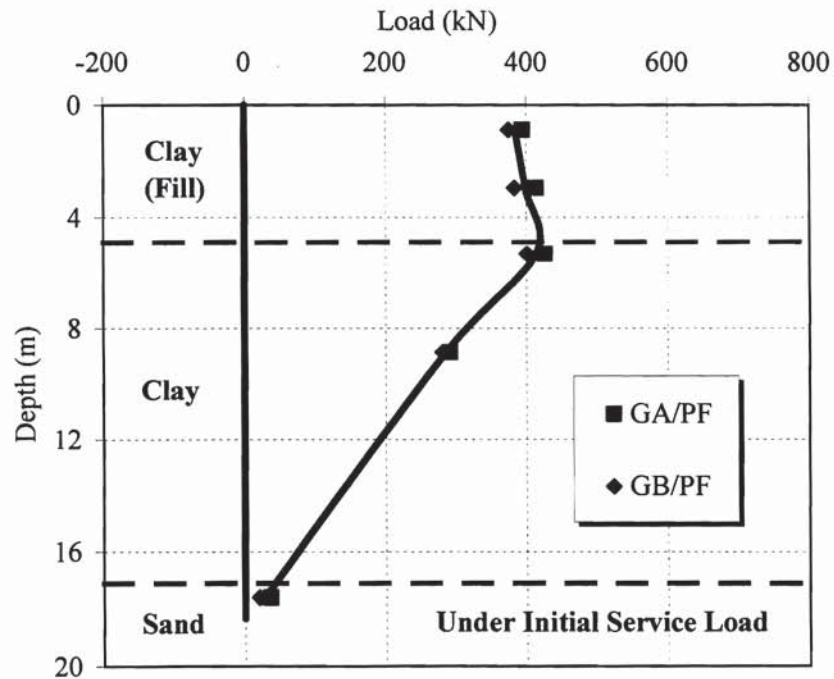


Fig. 11.5. Load vs. Depth Curve for In-Battered Abutment Piles Under Initial Service Load

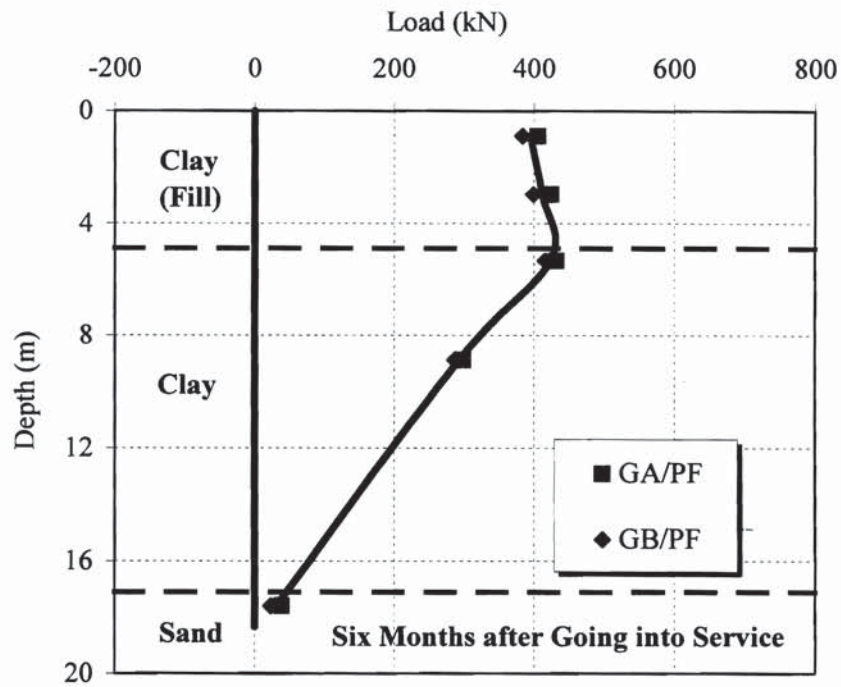


Fig. 11.6. Load vs. Depth Curve for In-Battered Abutment Piles Six Months After Going into Service

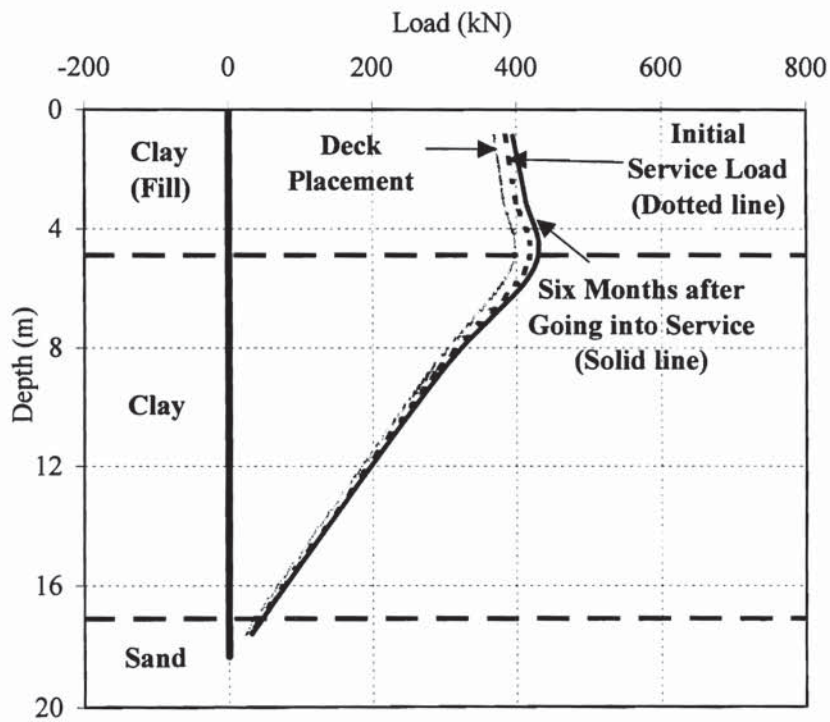


Fig. 11.7. Comparison of Load vs. Depth Curves for In-Battered Abutment Piles

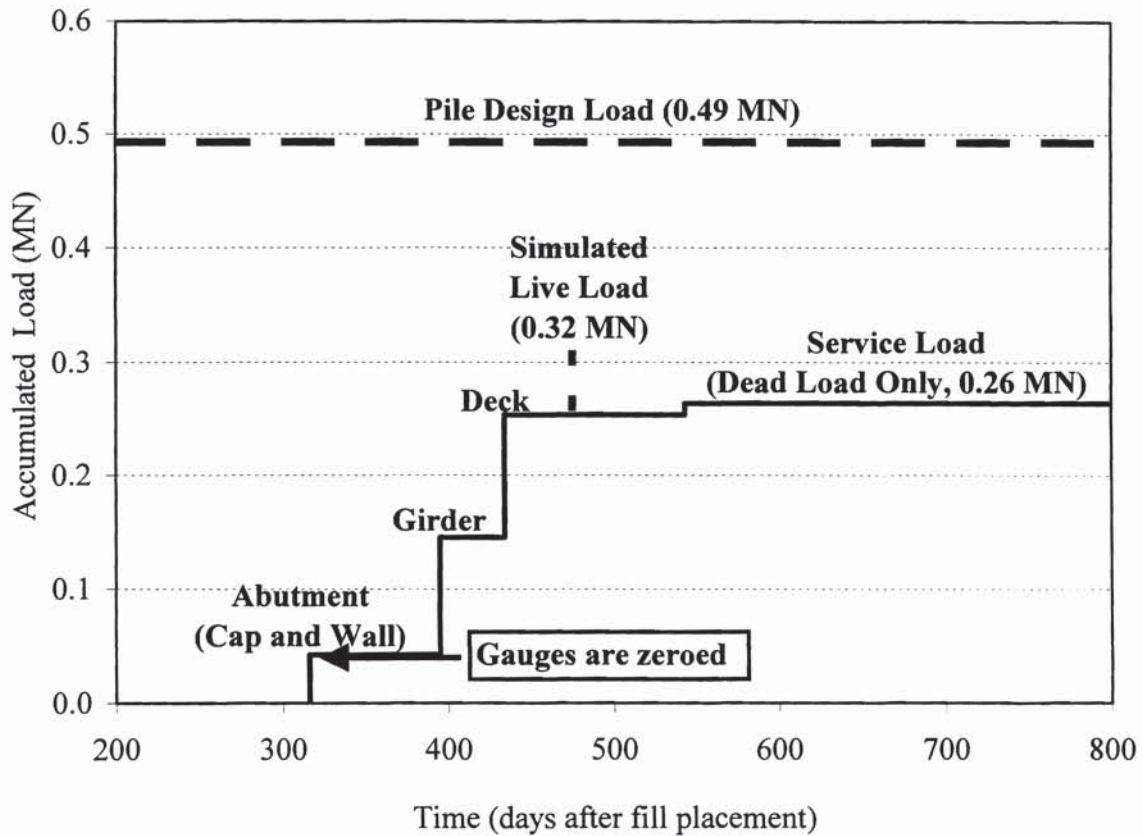


Fig. 11.8. Applied Load (Estimated) on Each Abutment Pile vs. Time

Figs. 11.9 through 11.12 show the load distribution curves for the out-battered abutment piles at various loading events. As with the in-battered piles, there is the indication that load transfer behavior of the piles down to a depth of 5 m is affected by downdrag loads due to the fill settlements. However, the load distribution behavior of the out-battered piles was different from that of the in-battered piles in that the out-battered pile is receiving much smaller compressive loads on the top of the pile coming from the

cap. As with in-battered piles, load at the toe in every loading event is almost zero indicating no load is transferred to soil at the toe.

Load distributions for various loading events are compared in Figs. 11.13. The curves are seen to be generally similar to one another. The measured changes in the axial load distribution from deck placement to the time the bridge went into service (a period of about three months) indicates that further drag loading was occurring from the fill. The changes from the time the bridge went into service until a time six months afterwards were very small.

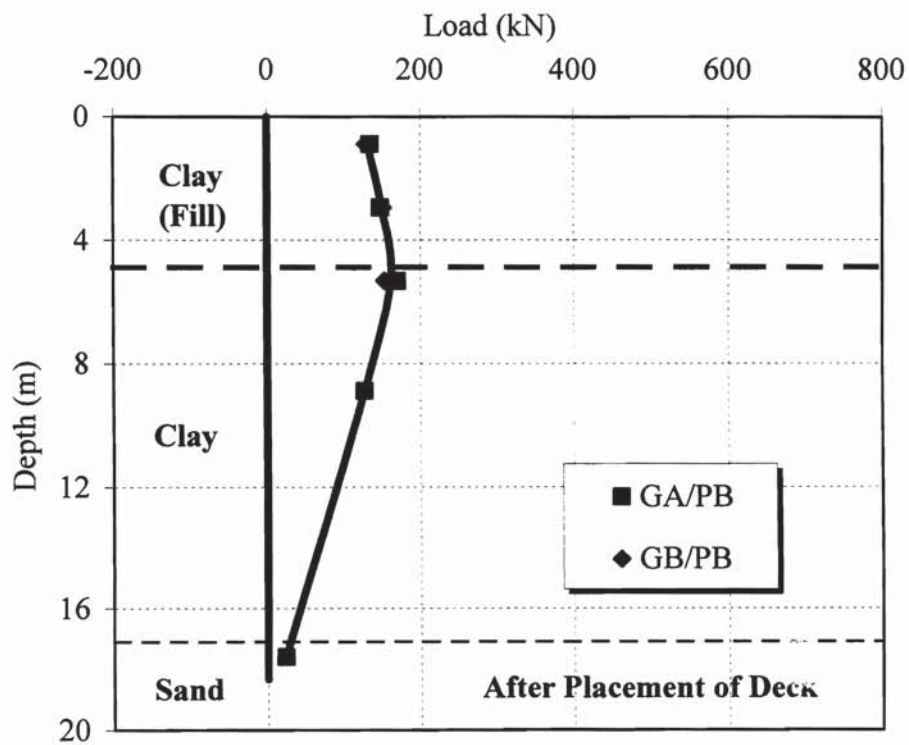


Fig. 11.9. Load vs. Depth Curve for Out-Battered Abutment Piles After Placement of Deck

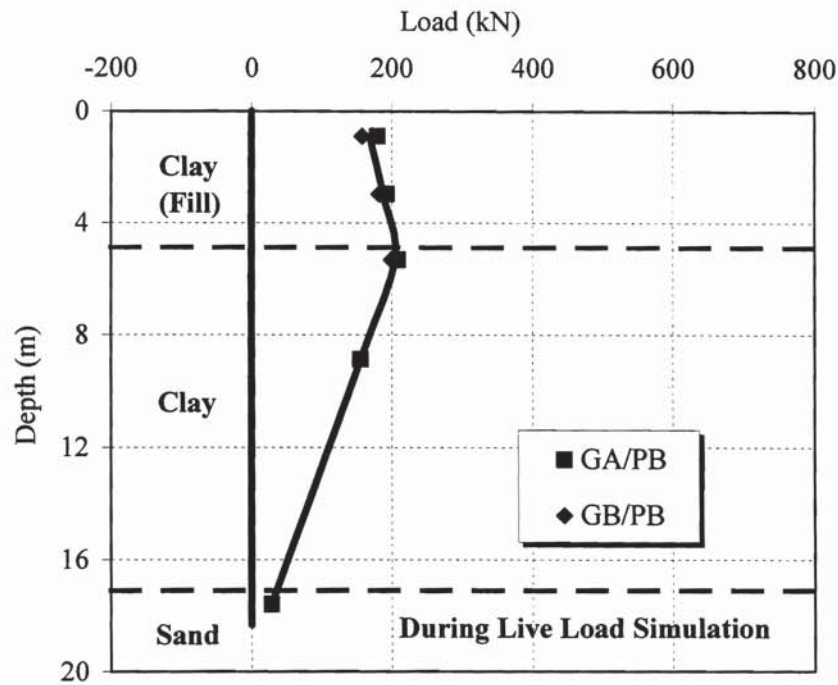


Fig. 11.10. Load vs. Depth Curve for Out-Battered Abutment Piles During Live Load Simulation

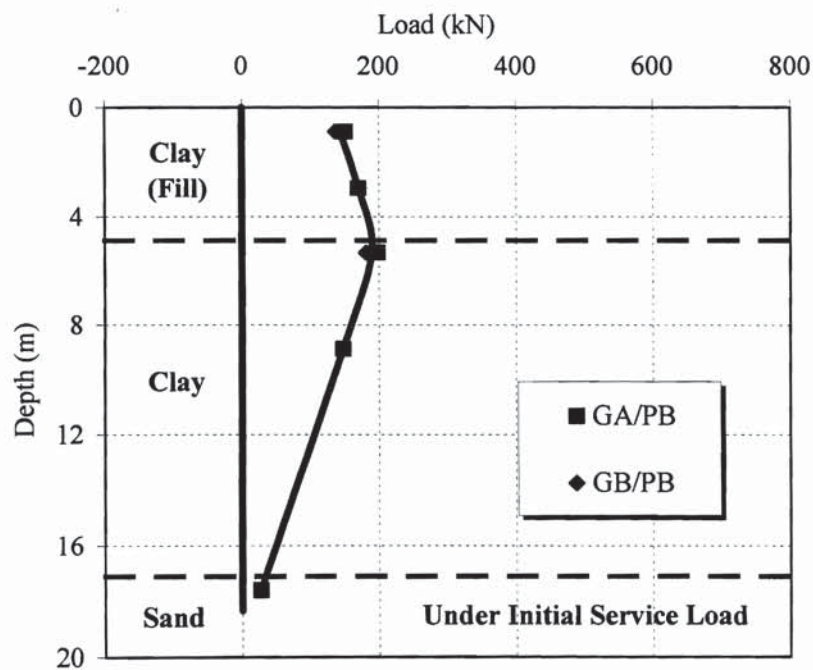


Fig. 11.11. Load vs. Depth Curve for Out-Battered Abutment Piles Under Initial Service Load

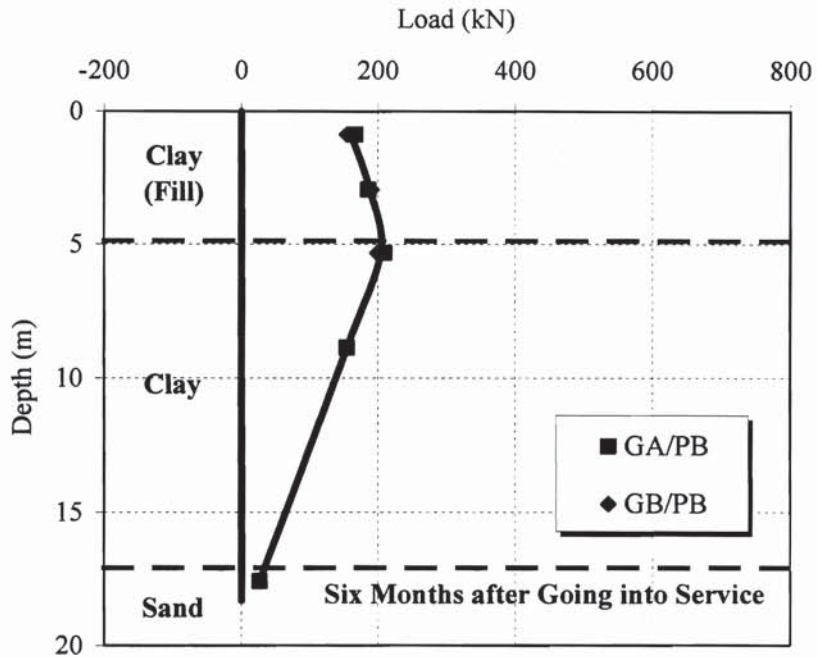


Fig. 11.12. Load vs. Depth Curve for Out-Battered Abutment Piles Six Months After Going into Service

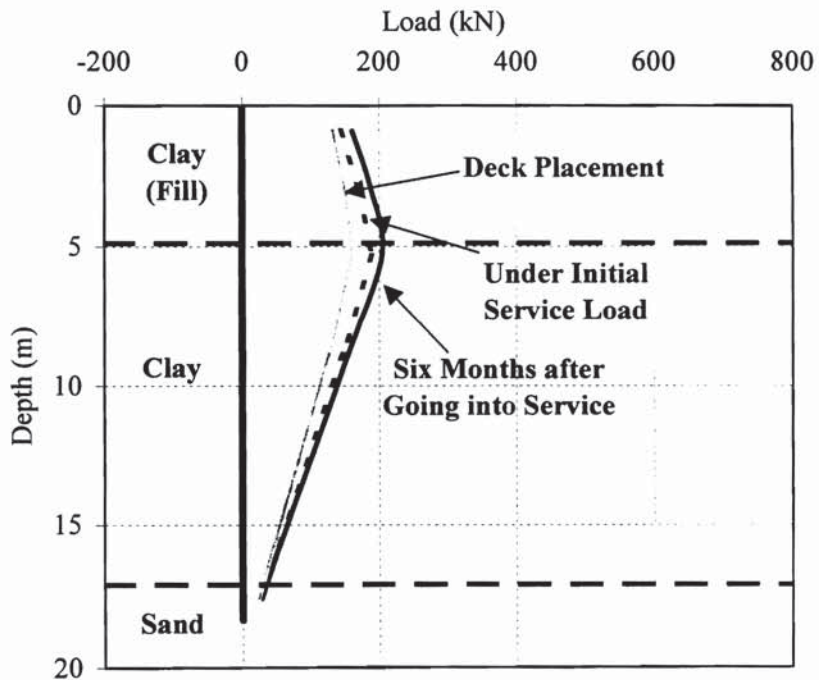


Fig. 11.13. Comparison of Load vs. Depth Curves of Out-Battered Abutment Piles

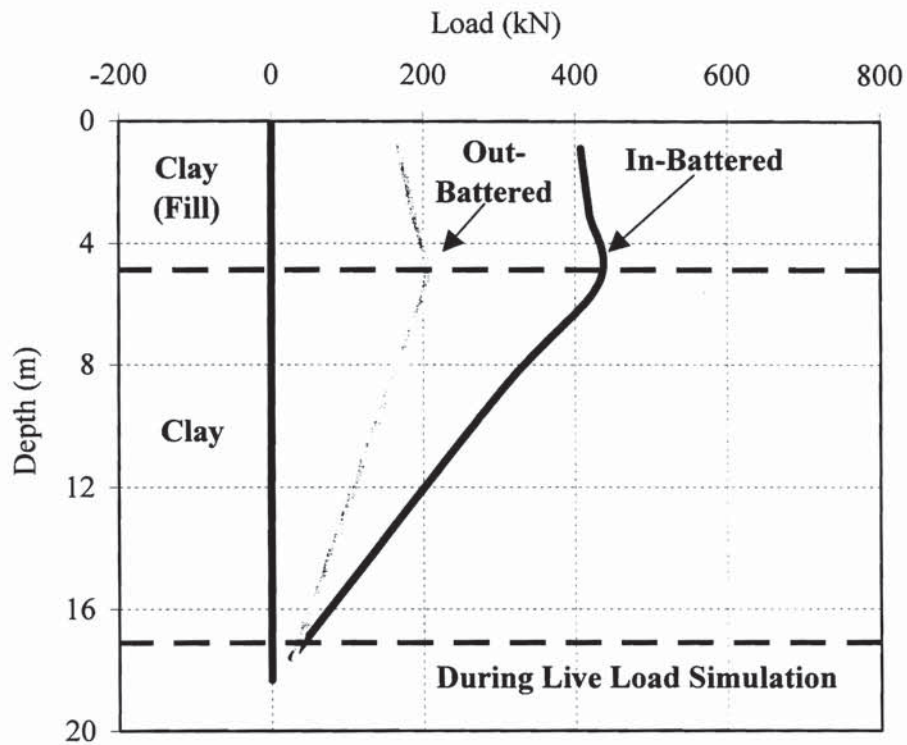


Fig. 11.14. Comparison of Average In-Battered and Out-Battered Pile Load Distribution Curves During Live Load Simulation

Finally, load distribution curves are compared for the average in-battered and out-battered piles during simulated live loading event in Figs. 11.14. There is a striking difference between the load distribution curves for the out-battered piles and the in-battered piles. The striking difference suggests large lateral loads on the heads of the piles due to lateral movement of the fill (perhaps due to lateral pressures on the abutment walls) than were anticipated.

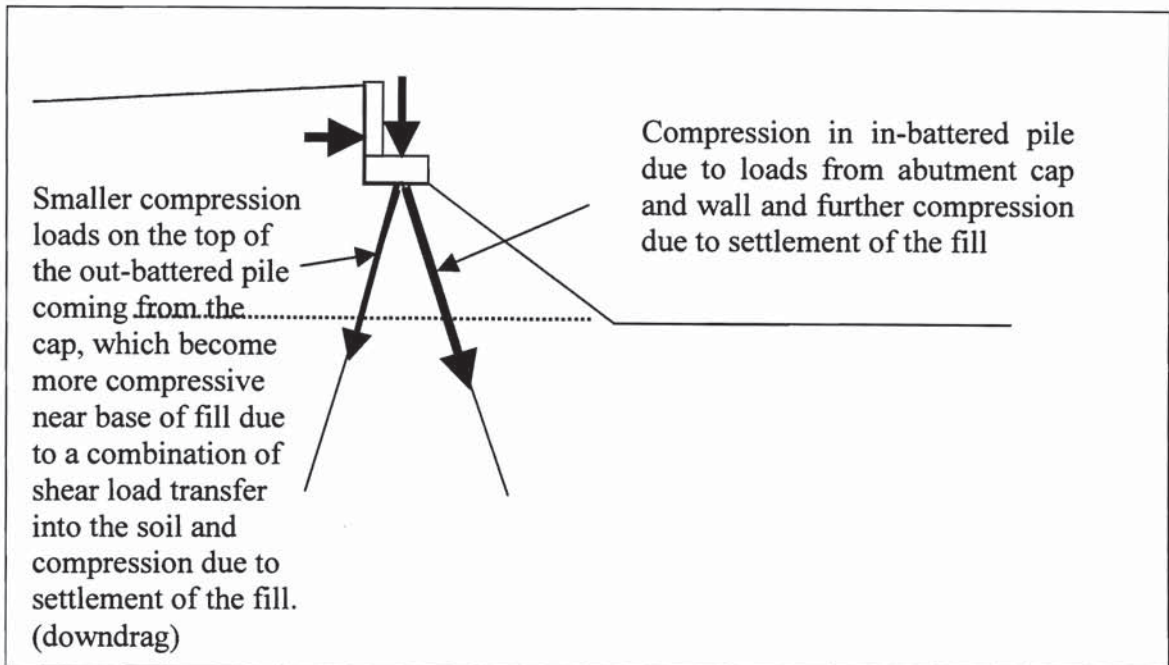


Fig. 11.15. Cartoon for Different Loads Acting on Abutment Piles

A cartoon for different loads acting on abutment piles was drawn in Fig. 11.15. Axial loads, on the average, are about estimated loads (around 0.3 MN compression, for example, during simulated live loading as shown in Fig. 11.14), but one pile (in-battered) is receiving much higher compressive loads plus drag loads from the fill than the out-battered pile. The compression loads on the in-battered pile and out battered pile were about 0.4 MN and 0.2 MN, respectively. One way this behavior can happen is for the fill to be moving both downward (drag loads) and outward, toward the fore-slope of the header bank, so as to put a large load on the abutment wall. This may be due to lateral creep of the fill, which was compacted wet of optimum (See Appendix F), or possibly lateral swelling of the embankment soil (not likely since compacted wet of optimum).

11.4 Load Sharing Between ACIP Group Piles and Abutment

Load carried into the soil directly by the south abutment cap at the Krenek Road bridge were estimated by measuring pressures with five vibrating wire pressure cells located in Fig. 6.1. The average contact pressure was then multiplied by the contact area of the abutment cap to obtain soil resistance acting directly on the abutment cap. These loads were then compared with the loads taken by the piles.

Table 11.2. Load Sharing Between Abutment Pile Group A and Cap at Various Loading Events

Abutment Pile Group A	Deck	Live Load	Service	6 month
Pile Group, kN	512	600	545	572
Abutment Cap, kN	4.5	2.7	1.8	0.9
Total Load, kN	517	603	547	573
Abutment Cap / Total Load, %	0.9	0.4	0.3	0.2

Tables 11.2 and 11.3 summarized load sharing between piles under group A and group B, and abutment cap at various loading events. As can be seen, cap load gradually reduced to almost zero by 6 months after bridge went into service, which suggests that the header bank fill was settling faster than the footing, which was supported by the piles with time. This behavior is consistent with the development of drag loads in the piles that were indicated by the sister bar readings. Had the footing (piles) and fill settled at the same rate, or had the piles settled at a rate faster than the footing, positive contact pressures would have been registered by the pressure cells. For this reason, loads on the

abutment appear to have been taken completely by the piles at working load conditions (such as simulated live load, initial service load, and 6-month service).

Table 11.3. Load Sharing Between Abutment Pile Group B and Cap at Various Loading Events

Abutment Pile Group B	Deck	Live Load	Service	6 month
Pile Group, kN	489	552	511	538
Abutment Cap, kN	4.5	2.7	1.8	0.9
Total Load, MN	494	555	513	539
Abutment Cap / Total Load, %	0.9	0.5	0.3	0.2

11.5 Summary

Based on the behavior and performance study on abutment piles following can be summarized:

- Residual loads (generally compressive along the length of the pile except top 2.5 m) were found in abutment piles, which were different from those for the test and central bent piles.
- Downdrag loads due to the fill settlements were observed on both in-battered and out-battered piles.
- The in-battered pile received much higher compressive loads than the out-battered pile due to the large lateral load on the abutment wall provided by the fill movement (both downward and toward the fore-slope of the header bank).

- From a design prospective, the settlements of abutment piles were not large enough up to six months after the bridge went into service to result in any performance deficiencies in the structure.
- At working load condition, the average load resisted by the abutment cap was almost zero indicating that the loads have been taken completely by the abutment piles.

CHAPTER 12

FINITE ELEMENT ANALYSIS

12.1 General

When dealing with soil-pile interaction behavior, the finite element method may be considered to be the more popular method in comparison with other methods. The behavior of a single pile (test pile) under a vertical load can be modeled using an axisymmetric finite element analysis. In contrast the behavior of a pile group or, more complex, the behavior of piled footings (piled rafts) can only be modeled applying a three-dimensional analysis (El-Mossallamy, 2000).

In order to model the group action within a pile group (4 central bent piles) at Krenek Road relative to the load-settlement behavior of the piled footings, a three-dimensional non-linear, finite element analysis program, Florida Bridge Pier (FB-Pier) program was used. In this model, the piles in each group were supported by nonlinear soil springs that had the properties of the $f-w$ curves and $q-w$ curve ($t-z$ curves). The $f-w$ and $q-w$ curves were derived from the ACIP test pile (Chapter 8). The FB-Pier does not have the capability of including explicitly the effects of residual loads in the piles, so that the $f-w$ and $q-w$ curves that were used were those based on pre-test zeroes. Since the residual loads in the pile were less than the tensile strength of the grout, it is likely that exclusion of residual stresses did not have a major effect on computed settlement.

12.2 Description of FB-PIER

The FB-PIER was developed by the University of Florida, Bridge Software Institute (BSI), with the support of the Florida Department of Transportation (FDOT) and the Federal Highway Administration (FHWA). This program was previously referred to as “Deep” or “Deep Foundations” which was based on the Florida Pier (FLPIER) program (BSI, 2003). The FB-PIER is a three-dimensional computer code that uses a finite element representation for piles and the pile cap (footing) and nonlinear load transfer springs to represent the interaction of the piles with the soil. FB-PIER performs the generation of the finite element model internally given the geometric definition of the structure and foundation system as graphically input by the user.

FB-PIER uses standard finite element procedures for the analysis (Weaver and Johnston, 1984). The major structural components of the system are the piles and pile cap. Each pile is modeled with 16 two-node, three-dimensional discrete element (Mitchell, 1973; El-Assaly, 1994; Andrade, 1994; Hoit et al., 1997). The discrete elements use very simple rigid link sections connected by nonlinear springs. The behavior of springs is derived from the specified stress-strain behavior of the steel and concrete. The more detailed discussion on the three-dimensional discrete element can be found in a paper by Hoit et al. (1996).

The pile cap is modeled using three-dimensional linear nine-node flat shell elements that have special shear integration and normal rotational stiffness added to correctly model the very thick pile cap (Hoit et al., 1997; BSI, 2003). The shell elements are based on Mindlin theory (Hoit et al., 1997). An eight-point reduced integration scheme is used to account for shear deformations and avoids zero energy modes (Hoit, et

al., 1997). In order to transfer torsion of the pile cap to the piles, additional stiffness terms are added to the elements (Hoit et al., 1997). The major modeling components of FB-Pier and 3D view for pile group analysis are shown in Appendix G.

The soil modeling provides the ability to define the layers of soil at various depths. Each layer can be either a sand or clay using different built-in t - z and p - y curves or with the user-defined curves (Hoit et al., 1997). FB-Pier incorporates both the axial and lateral soil-pile interaction. Both axial and lateral soil-pile interactions are modeled by nonlinear soil springs whose axial and lateral stiffness are obtained from the t - z and p - y curves (Hoit et al., 1997). For pile groups, the axial pile-soil-pile interaction is characterized through the use of axial pile group efficiency (t -multiplier). The lateral pile-soil-pile interaction is characterized through the use of lateral pile group efficiency (p -multiplier).

Since the soil and pile models are nonlinear, FB-Pier performs an iterative solution process. The iteration solution process was discussed by Hoit et al. (1997) as the following. To help reduce the work at each iteration, the linear portion of the structure such as the pile cap is statically condensed before the iterative nonlinear solution begins. The iterative method uses a secant method approach for the solution of the nonlinear equations. This approach allows for a more robust solution when using elastic-plastic soil models. FB-Pier uses a Newton-Raphson iteration scheme. When the analysis has converged, each node in the piles will have out-of-balance forces. FB-Pier used the largest value of the out-of-balance forces as the measure of the convergence of the analysis.

12.3 Input Data

Foundation layout for the test pile and central bent piles in a group and input parameters are shown in Fig. 12.1. The test pile had a diameter of 0.457 m (18 in) and a length of 18.9 m (62 ft). As shown in Fig. 12.1, four central bent piles with a diameter of 0.457 m (18 in) and a length of 17.4 m (57 ft) were capped with a 1.2 m (4 ft) thick square footing [2.6 m (8.5 ft) X 2.6 m (8.5 ft)]. The ratio of spacing and pile diameter (s/d) was 3.33. The piles were located in mixed soil profile of clay and sand. The ground water level was about 1.5 m (5 ft) below the natural ground surface. Pile toe for all the piles were located at 18.9 (62 ft) from the natural ground surface in lower sand layer.

The test pile and piles in each group (central bent piles) were supported by nonlinear soil springs that had the properties of the f - w curves and q - w curve. The f - w and q - w curves were derived from the ACIP test pile (Chapter 8). Since the FB-Pier does not have the capability of including explicitly the effects of residual loads in the piles, the f - w and q - w curves that were used were those based on pre-test zeroes. Since the residual loads in the pile were less than the tensile strength of the grout, it is likely that exclusion of residual stresses did not have a major effect on computed settlement.

Input material properties for the test pile, the group pile, pile cap, and soil are summarized in Table 12.1. It is noted that only axial soil-pile interaction (t - z curves) is considered in this study.

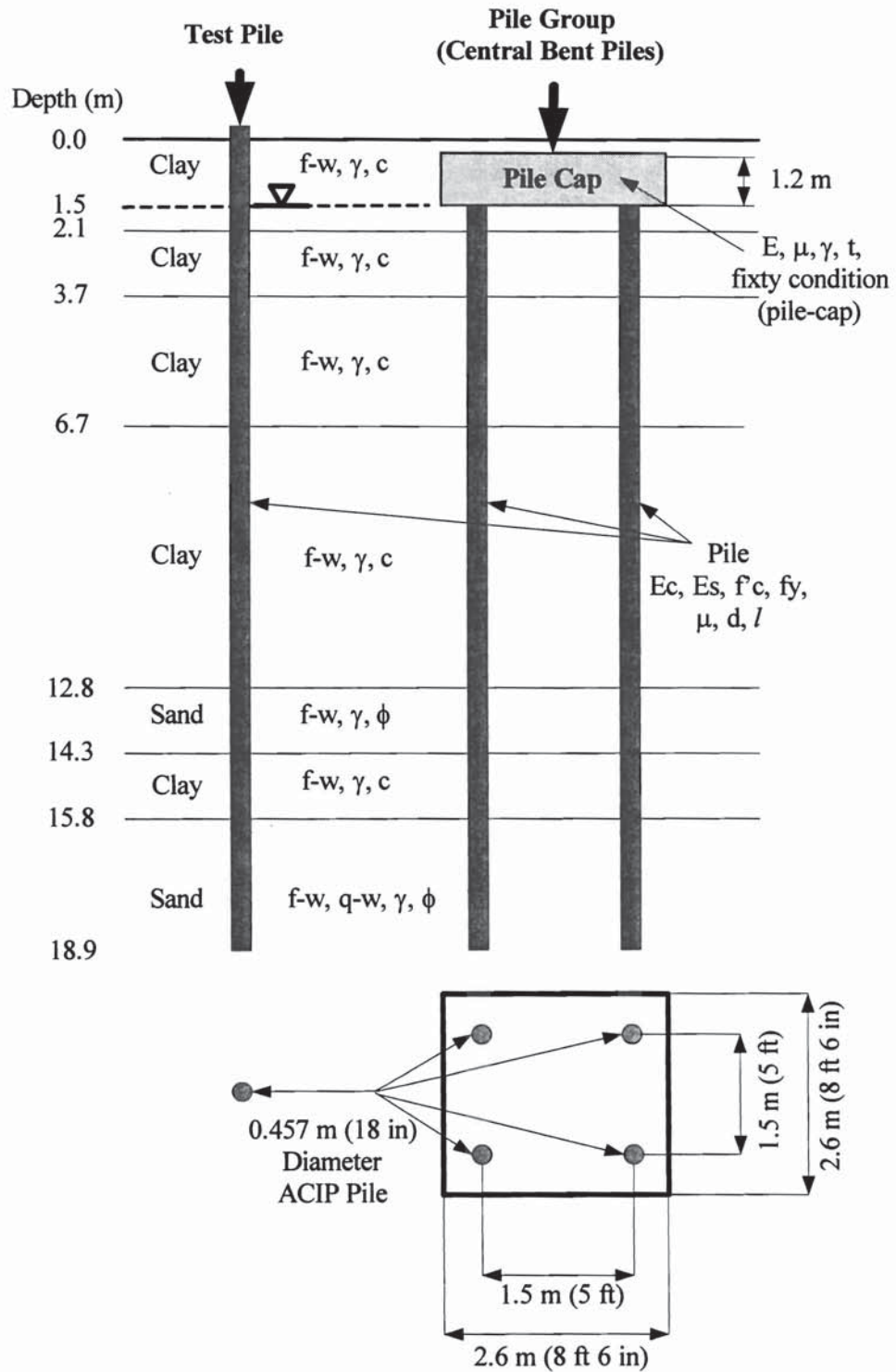


Fig. 12.1. Test Pile and Pile Group Layout and Input Parameters

Table 12.1. Input Properties for FBPIer

Test Pile	Diameter	Tip Depth	Length	Concrete			Steel			
				Elastic Modulus	Comp. Strength	Poisson's ratio	Elastic Modulus	Yield Strength	Poisson's Ratio	Area Ratio
	d	l_{TP}	l	E_c	f_c	μ_c	E_s	f_y	μ_s	A_{steel} / A_{pile}
	in	ft	ft	psi	psi	-	psi	psi	-	-
	18	62	62	3120000	5222	0.20	29,000,000	60,000	0.25	0.01
	Diameter	Tip Depth	Length	Concrete			Steel			
Group Pile	d	l_{TP}	l	E_c	f_c	μ_c	E_s	f_y	μ_s	A_{steel} / A_{pile}
	in	ft	ft	psi	psi	-	psi	psi	-	-
	18	62	57	3120000	5222	0.20	29,000,000	60,000	0.25	0.01
	Thickness	Unit weight	Elastic Modulus	Poisson's ratio						
Cap	t	γ	E_{cap}	μ_{cap}						
	ft	pcf	psi	-						
	4	150	4,000,000	0.20						
	Layer	Bottom	Classification	Shear Strength	Friction Angle	Unit Weight	Water Table			
	Top	ft		s_u	ϕ	γ				
	ft	ft		psf	degree	pcf	ft			
	0	7	Cohesive	1202	0	134				
Soil	7	12	Cohesive	2298	0	134				
	12	22	Cohesive	1819	0	122				
	22	42	Cohesive	2261	0	129	5			
	42	47	Cohesionless	0	40	132				
	47	52	Cohesive	1757	0	123				
	52	65	Cohesionless	0	40	132	Soil-Pile Interaction (Axial)			
							f-w curve			
							f-w curve			
							f-w curve			
							f-w curve			
							f-w curve			
							f-w, q-w curves			

12.4 Prediction of Load-Settlement Behavior for ACIP Test Pile

To examine the validity of this program, load-settlement curve for the ACIP test pile of given dimensions taking into account the non-linear soil and pile response was predicted by using the program “FB-Pier” and compared with the measured load-settlement curve obtained from the load test (Chapter 8). As shown in Fig. 12.2, very good agreement between measurements and analysis can be recognized.

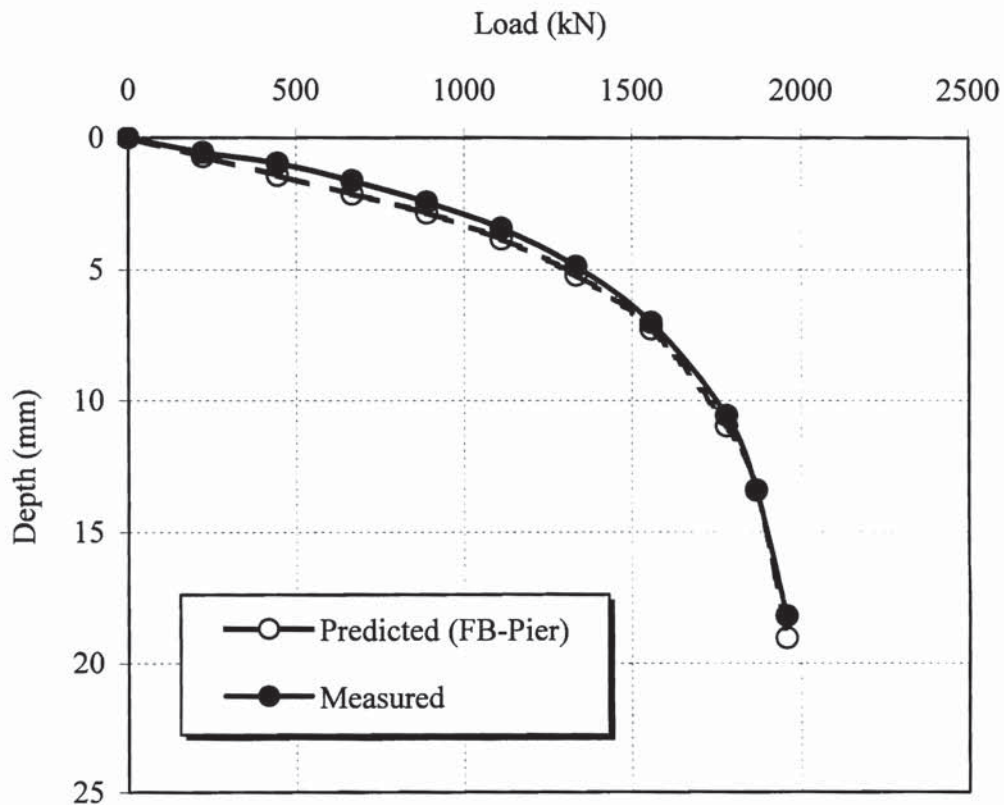


Fig. 12.2. Comparison Between Predicted and Measured Load-Settlement Curves for ACIP Test Pile

12.5 Group Action

The footing settlements computed by FB-Pier were compared with the average footing settlement measurements of two central bent pile groups under Footing A and B in a mixed soil profile of stiff clay and medium to dense sand at working condition such as simulated live load and service load. Each footing settlement is the average of settlements at the four corners. The computed settlement of the pile group using f - w and q - w curves derived from the single test pile was less than the average measured settlement at working load condition, which indicated that pile-soil-pile interaction (group action, or overlap of strain fields around the piles) was occurring within central bent piles. In order to model the group action, the authors of FB-Pier suggest the use of an axial group pile efficiency (t -multiplier) which reduces the f and q values on all load transfer curves along the piles at every value of relative pile-soil deflection. By varying the t -multiplier and matching computed and measured settlements, the value of the t -multiplier for the pile groups in question was obtained. Predicted settlements using various t -multipliers were compared with average settlement measurements at working load conditions (initial service load and simulated live load). Results of this comparison are shown in Fig. 12.3. The results suggest that the use of axial pile group efficiency of 0.65 predicts the load-settlement behavior of average ACIP pile group (2 X 2) at working load condition.

12.6 Summary

The group action within central bent ACIP piles (4 piles) installed in a group in a mixed soil profile of stiff clay and medium to dense sand was investigated by comparing

average footing settlement measurements of two central bent pile groups and predicted settlements by performing the finite element analysis using FB-Pier program. The load-settlement behavior of the central bent piles in a pile group was totally different from the behavior of the single test pile. In order to model the load-settlement behavior of the central bent ACIP piles in a pile group at working load condition in such soil profile, the use of axial group pile efficiency (t -multiplier) of 0.65 was suggested.

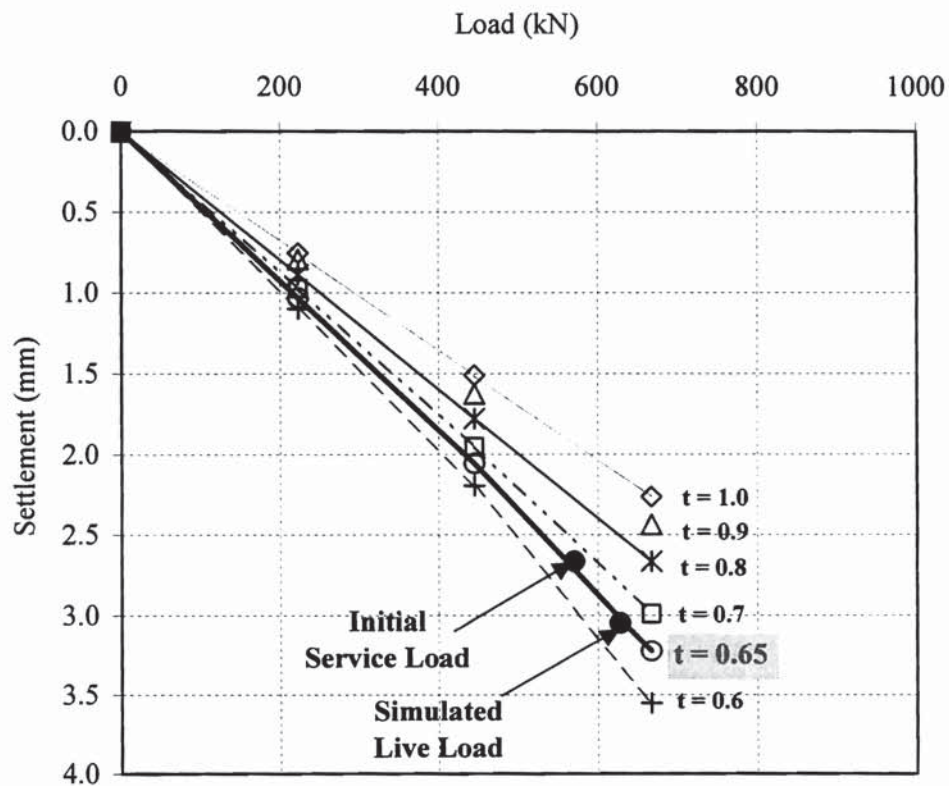


Fig. 12.3. Load-Settlement Curves Using Various t -Multipliers (Axial Group Pile Efficiency)

CHAPTER 13

CONCLUSIONS AND RECOMMENDATIONS

13.1 Conclusions

The overall objective of this study was to determine whether ACIP piles could be designed and constructed with acceptable in-service performance for bridge foundations in the Pleistocene soils of the Texas Gulf Coast region. A new bridge at the Krenek Road and highway U.S. 90 intersection was designed and constructed with 64 ACIP piles for the first time in the State of Texas. One load test was performed on an instrumented ACIP pile before installing production piles on Highway U.S. 90 at Krenek Road site. Another load test was performed on a driven prestressed concrete pile on an adjacent bridge (at Runneburg Road site) with similar soil condition for comparative study. In order to study the long-term behavior and performance of the ACIP piles as bridge foundations, representative ACIP piles, central bent footings, abutment instrumented with calibrated vibrating wire sister bars and contact pressure cells were monitored up to 6 months after bridge went into service. All aspects of bridge construction were carefully monitored including the installation process for every pile, the use of automated system for the purpose of quality control, fill settlement and, footing and abutment settlements. Finite element analysis using FB-PIER was performed to mainly investigate the group action within the central bent piles installed in a group.

The following are the conclusions drawn from this study:

1. The highway bridge constructed with 64 ACIP piles, 0.46 m (18 in) diameter, has performed well with minimal deflection measured (pile caps and abutments) during the first 6 months of operation. The maximum settlement measured after 6 months in services was less than 3.05 mm (0.12 in).
2. Both battered and non-battered ACIP piles were constructed with ease. Each 0.46 m (18 in) diameter ACIP pile (vertical piles) with an average length of 18.3 m (60 ft) was constructed in less than 15 minutes with all the necessary monitoring to ensure quality. Based on ultimate bearing capacity, ACIP pile was cost-effective compared to a driven pile in similar soil conditions.
3. The grout ratio (grout volume pumped/theoretical volume of borehole) and line pressure at ground level were monitored for each pile as outlined in the TxDOT specification.
4. Residual tensile axial strains were measured in non-battered ACIP piles most likely because of expansion of the clay soils. While, residual strains in the abutment piles (battered) were generally compressive, presumably because the settlement of the fill materials.
5. Based on the construction practice and ACIP piling equipment, waterbearing clean sands can be mined, causing loss of ground. ACIP piles should not be tipped in water bearing sand layer.
6. In the soils of the Texas Gulf Coast, side resistance is the predominant mode of pile support. The ratio of average unit side resistance to average undrained shear strength, α factor, for the ACIP pile was considerably higher than that was used in

the design of the ACIP pile and the driven PC pile by comparing the results of the two load tests in cohesive soils.

7. At the service loading condition, the average load carried by the footing supported by the 4 ACIP piles was less than 8 % of the total load.
8. At the service loading condition, the average load carried by the abutment cap was almost zero indicating that the loads have been taken completely by the abutment piles.
9. The load distribution between the piles in the central bent pile groups varied from pile to pile within a group. This variation may have been due to the variation in pile stiffness, the quality of the pile-cap connection and the presence of lateral loads on the caps from the bridge superstructure.
10. The in-battered pile carried much higher compressive loads than the out-battered pile possibly due to the lateral load on the abutment wall provided by the fill movement (both downward and toward the fore-slope of the header bank).
11. Group action within central bent ACIP piles (4 piles in a group) was investigated at working load condition using the finite element analysis. Based on the analysis, the use of axial group efficiency factor (t-multiplier) of 0.65 to model axial group action within central bent ACIP piles (2 x 2 configuration) under working load condition was suggested.

13.2 Recommendations

The following are recommended for future research:

1. The construction sequence of ACIP piles must be investigated. Current TxDOT practice limits the construction a pile within 6-diameter in 24 hours. With ACIP piles this distance could be reduced to make the ACIP construction even faster and efficient.
2. The behavior (load capacity and load-settlement) of ACIP pile groups must be investigated. The contribution of pile cap and pile configuration in the group must be investigated.
3. The constructability and behavior of ACIP piles for bridges that are supported in hard clay or soft rock (clay shale) must be studied. Performance of ACIP piles should be compared to drilled shafts.
4. The forces introduced by the fill soils must be investigated. Contact pressure cells on the abutment wall should be installed to check pressures on the abutment walls by the fill soils.
5. The movement in the fill soil must be monitored by installing inclinometers.
6. ACIP piles constructed in Texas costal soils with stratigraphies similar to those at the Krenek site should not be tipped in a dense, waterbearing sand strata (if the sand strata function as confined aquifers) through stiff, relatively impermeable clay. ACIP piles should terminate in stiff clay strata overlaying sand strata.
7. Changing grout trucks during grouting a single ACIP pile may cause over-rotation and soil mining, especially in cohesionless soils. The construction specification

should require that the contractor not begin augering until a grout truck containing at least the volume of grout required to fill the borehole is on site.

REFERENCES

American Petroleum Institute (1993). *API Recommended Practice RP2A – LRFD*, Recommended Practice for Planning, Designing and Constructing Fixed Offshore Platforms Load and Resistance Factor Design, First Edition, API, Washington D.C.

Andrade, P. (1994). "Materially and Geomechanically Non-linear Analysis of Laterally Loaded Piles Using a Discrete Element Technique, *Master's Report*, University of Florida, Gainesville, FL.

Booth, A. T., and McIntosh, K. A. (1994). "Utilization and Quality Control of Augercast Piles," *In Proceedings*, the International Conference on Design and Construction of Deep Foundations, FHWA, pp. 385-400.

Brettmann, T., and Frank, M. (1996). "Comparison of Cross Hole and Single Hole Sonic Integrity Logging Methods," *In Proceedings*, the Fifth International Conference on the Application of Stress Wave Theory to Piles, Orlando, FL, University of Florida, pp. 698-707.

Brettmann, T., Frank, M., and Berry B. (1996). "Evaluation of Defect Detection During Pile Curing Using Sonic Integrity Logging Methods," *In Proceedings*, the Fifth

International Conference on the Application of Stress Wave Theory to Piles, Orlando, FL, University of Florida, pp. 708-720.

Briaud, J-L. and Tucker, L. (1984). "Piles in Sand: A Method Including Residual Stresses," *Journal of Geotechnical Engineering*, Vol. 110, No. 11, ASCE, pp. 1666-1680.

Bridge Software Institute (2003). "FB-Pier V3 Online Help Manual – Printable PDF Version," www.bsi-web.ce.ufl.edu, April.

Bustamante, M., and Gianceselli, L. (1981). "Portance Reele et Portance Calculee des Pieux Isoles, Sollicites Verticalement," *Revue Francaise de Geotechnique No. 16*.

Bustamante, M., and Gianceselli, L. (1993). "Design of Auger Displacement Piles from In situ Tests," *In Proceedings, Deep Foundations on Bored and Auger Piles*, Balkema, Rotterdam, pp. 21 - 34.

Bustamante, M., and Gianceselli, L. (1998). "Installation Parameters and Capacity of Screwed Piles," *In Proceedings, Deep Foundations on Bored and Auger Piles*, Balkema, Rotterdam, pp. 95 - 108.

Coyle, H. M., and Castello, R. (1981). "New Design Correlations for Piles in Sand," *Journal of the Geotechnical Engineering*, ASCE, Vol. 107, No. GT 7, pp. 965 – 986.

Cutter, W. A., and Warder, D. L. (1998). "The use of ACIP Piles Adjacent to Existing Structures: Lessons Learned," *In Proceedings, Great Lakes Geotechnical Engineering Conference, University of Toledo.*

Davisson, M. T. (1972). "High Capacity Piles," *In Proceedings, Soil Mechanics Lecture Series on Innovations in Foundation Construction, ASCE, Illinois Section, Chicago, IL,* pp. 81 – 112.

Decourt, L. (1993). "Predicted and Measured Behavior of Non-Displacement Piles in Residual Soils," *In Proceedings, Deep Foundations on Bored and Auger Piles, Balkema, Rotterdam,* pp. 369 - 376.

DFI (1994). "*Augered Cast-In-Place Piles Manual,*" Deep Foundations Institute, Sparta, NJ.

DIN 4014 (1987), Entwurf, Federal Republic of Germany.

El-Assaly, A. (1994). "Geometrically Non-Linear Analysis of Framed Structures Using a Discrete Element Model," *Master's Thesis, University of Florida, Gainesville, FL.*

El-Mossallamy, Yasser (2000). "Behavior of Large Diameter Single Pile and Pile Groups in Overconsolidated Clay," *In Proceedings, the Fourth International Geotechnical Engineering Conference, Cairo, Egypt*, pp. 451-463

Esrig, M. I., Leznocki, J. K., and Gaibrois, R. G. (1991). "Building Displacements Resulting from Pile Installation in New York City," *In Proceedings, International Conferences on Deep Foundations, Ecole Nationale des Ponts et Chaussées*, pp. 559-565.

Esrig, M. I., Leznocki, J. K., and Gaibrois, R. G. (1994). "Managing the Installation of Auger Cast-In Place Piles," *Transportation Research Record No. 1447, TRB, Washington D. C.*, pp. 27-29.

Falconio, G., and Mandolini, A. (2003). "Influence of Residual Stresses for Non-Displacement Cast In Situ Piles," *In Proceedings, Deep Foundations on Bored and Auger Piles, Balkema, Rotterdam*, pp. 145-152.

Fellenius, B. H. (2002). "Determining the True Distributions of Load in Instrumented Piles," *Deep Foundations Congress 2002, Geotechnical Special Technical Publication No. 116, Volume 2, ASCE, Orlando, FL*, pp. 1455-1470.

Fleming, W. G. K., Weltman, A. J., Randolph, M. F., and Elson, W. K. (1985). "*Piling Engineering*," Surrey University Press, Glasgow.

Geokon, Inc., (1998). "*Instruction Manual-Models 4800/4810/4820 VW Earth Pressure Cells*," 48 Spencer Street, Lebanon, NH 03766.

Geokon, Inc. (1999). "*Instruction Manual-Models 4911A/4911 VW Rebar Strain Meters*," 48 Spencer Street, Lebanon, NH 03766.

Goble Rausche Likins and Associates, Inc. (1998). "*GRLWEAP Program, Procedures and Models*," Pile Dynamics, Inc., Cleveland, Ohio.

Hassan, K. M., O'Neill, M. W., and Vipulanandan, C. (1997). "Specification and Design Criteria for the Construction of Continuous Flight Auger Piles in the Houston Area," TxDOT Project No. 7-3940, University of Houston, Houston, Texas.

Hayes, J. and Simmonds, T. (2002). "Interpreting Strain Measurements from Load Tests in Bored Piles," *In Proceedings, The Ninth International Conference on Piling and Deep Foundations*, Deep Foundations Institute, Nice, France, June, pp. 663-669.

Hoit, M., Hays, C., and McVay, M. (1997). "The Florida Pier Analysis Program: Methods and Models for Pier Analysis and Design," *Transportation Research Record No. 1569*, TRB, Washington D. C, pp. 1-7.

Hoit, M. I., McVay, M., Hays, C., and Andrade, P. W. (1996). " Nonlinear Pile Foundation Analysis Using Florida-Pier," *Journal of Bridge Engineering*, ASCE, Vol. 1, No. 4, November, pp. 135-142.

Holloway, D. M. and Vesic, A. S. (1978). "The effects of Residual Driving Stresses on Pile Performance Under Axial Loads," *In Proceedings*, the 10th OTC Conference, Houston, Paper OTC 3306, pp. 2225–2236.

Kenny M. J., and Andrews, K. Z. (1997). "Soil Disturbance During Continuous Flight Auger Piling in Sand," *In Proceedings*, the Fourteenth International Conference on Soil Mechanics and Foundation Engineering, Volume 2, Hamburg, pp. 1085–1090.

Kim, M. H., and O'Neill, M. W. (1998). "Side Shear Induced in Drilled Shaft by Suction Change," *Journal of Geotechnical and Geoenvironmental Engineering*, ASCE, Vol. 124, No. 8, August, pp. 771-780.

Lacy, H. S., (1998). "Protecting Existing Structures Using Bored Piles," *In Proceedings*, Sixth Great Lakes Geotechnical and Geoenvironmental Conference on the Design and Construction of Drilled Deep Foundations, Indianapolis, IN.

Lenznicki, J. K., Esrig, M. I., and Gaibrois, R. G. (1992). "Loss of Ground During CFA Pile Installation in Inner Urban Areas," *Journal of Geotechnical Engineering*, ASCE, Vol. 118, No. 6, June, pp. 947–950.

Mandolini, A., Price, G., Viggiani, C., and Wardle, I. (1992). "Monitoring Load Sharing within a Large Pile Cap Foundation," *Géotechnique et Informatique*, Parigi, p. 113.

McRae, J. B. and Simmonds, T. (1991). "Long-Term Stability of Vibrating Wire Instruments: One Manufacturer's Perspective," *In Proceedings, The 3rd International Symposium on Field Measurements in Geomechanics*, Oslo, Norway, September, pp. 283-293.

Mcvay, M., Armaghani, B., and Casper, R. (1994). "Design and Construction of Auger-Cast Piles in Florida," *Transportation Research Record No. 1447*, TRB, Washington D. C, pp. 10-18.

Mitchell, J. S. (1973). "A Nonlinear Analysis of Bi-Axially Loaded Beam-Columns Using a Discrete Element Model," *Ph.D. Dissertation*, The University of Texas at Austin, August, 1973.

Neely, W. J. (1991), "Bearing Capacity of Auger-Cast Piles in Sand," *Journal of Geotechnical Engineering*, Vol. 117, No. 2, pp. 331-345.

Nesmith, W. M. (2002). "Design and Installation of Pressure-Grouted, Drilled Displacement Piles," *In Proceedings, Ninth International Conference on Piling and Deep Foundations*, DFI, Nice, France, pp. 561-568.

O'Neill, M. W. (1994). "Review of Augered Pile Practice Outside the United States," *Transportation Research Record No. 1447*, TRB, Washington D. C, pp. 3-9.

O'Neill, M. W. (1998). "Keynote Lecture: Axial Design and Lateral Design," *In Proceedings*, DFI Special Seminar: Augered Cast-In-Place Piles, Houston, Texas, pp. 1-54.

O'Neill, M.W. and Reese, L. C. (1972). "Behavior of Bored Piles in Beaumont Clay," *Journal of the Soil Mechanics and Foundations Division*, ASCE, Feb., pp. 195-213.

O'Neill, M.W. and Reese, L. C. (1999). "Drilled Shafts - Construction Procedures and Design Methods", *Publication No. FHWA-IF-99-025*, Department of Transportation, FHWA, Office of Implementation, McLean, VA.

O'Neill, M. W., Vipulanandan, C., Ata, A., and Tan, F. (1999). "Axial Performance of Continuous Flight Auger Piles for Bearing," *Final Report*, TxDOT Project No. 7-3940, University of Houston, Houston, Texas.

O'Neill, M. W., Ata, A. Vipulanandan, C., and Yin, S. (2002). "Axial Performance of Augered, Cast-in-Place (ACIP) Piles in Texas Coastal Soils, *ASCE Geotechnical Special Publication No. 116*, Vol. 2, Edited by O'Neill, M. W., and Townsend, T. C., ASCE, pp. 1290-1304.

Peck, R., and Hansen, W. E., and Thornburn, T. H. (1974). "*Foundation Engineering*," Second Edition, John Wiley and Sons, Inc., New York, NY.

Poulos, H. G. and Davis, E. H. (1980). "*Pile Foundation Analysis and Design*," John Wiley and Sons, Inc., New York, NY.

Randolph, M. F. and Wroth, C. P. (1978). "Analysis of Deformation of Vertically Loaded Piles," *Journal of Geotechnical Engineering*, ASCE, Vol. 104, pp. 1465-1488.

Rausche, F. Likins, G., and Hussein, M. (1994). "Formalized Procedure for Quality Assessment of Cast-In-Place Shafts Using Sonic Pulse Echo Methods," *Transportation Research Record No. 1447*, TRB, Washington D. C, pp. 30-38.

Reese, L. C. and O'Neill, M. W. (1988). "Drilled Shafts – Student Workbook", *Publication No.FHWA-IF-88-042*, Department of Transportation, FHWA, Office of Implementation, McLean, VA.

Rizkallah, V. (1988) "Comparisons of Predicted and Measured Bearing Capacity of Auger Piles," *In Proceedings, Deep Foundations on Bored and Auger Piles*, Balkema, Rotterdam, pp. 471-475.

Roberts, T. L. (1998). "Quality Control for Augered Cast-In-Place Piles in Texas and Louisiana," *In Proceedings*, DFI Special Seminar: Augered Cast-In-Place Piles, Houston, Texas, pp. 95-111.

Russo, G., and Viggiani, C. (1995). "Long Term Monitoring of a Pile Foundation," *In Proceedings*, 4th International Symposium on Field Measurements in Geomechanics, ISMES, p. 283.

Sayed, S. M. and Bakeer, R. M. (1992). "Efficiency Formula for Pile Groups," *Journal of Geotechnical Engineering*, ASCE, Vol. 101, No. 2, Paper No. 26553, pp. 278-299.

Texas Department of Transportation (1993). "TxDOT Specification Book".

Texas Highway Department (1972). "*Foundation Exploration and Design Manual*," Bridge Division, Second Edition, July.

Thorburn, S., Greenwood, D. A., and Fleming, W. G. K. (1993). "The Response of Sands to the Construction of Continuous Flight Auger Piles," *In Proceedings*, Deep Foundations on Bored and Auger Piles, Balkema, Rotterdam, pp. 429-443.

Tomlinson, M. J. (1957). "The Adhesion of Piles Driven in Clay Soils," *In Proceedings*, Fourth International Conference on Soil Mechanics and Foundation Engineering, Butterworths Scientific Publications, Ltd., London, England, Vol.2, pp. 66-71.

Van Impe, W. F. (1988). "Considerations on the Auger Pile Design," *In Proceedings, Deep Foundations on Bored and Auger Piles*, Balkema, Rotterdam, pp.193-218.

Van Impe, W. F., and De Clercq, Y. (1995). "A piled Raft Interaction Model," *Geotechnica*, Vol. 73, March, pp. 1-23.

Van Weele, A. F. (1988). "Cast-in-situ piles – Installation Methods, Soil Disturbance and Resulting Pile Behavior," *In Proceedings, Deep Foundation on Bored and Auger Piles*, Balkema, Rotterdam, pp. 219 - 226.

Vesic, A. S. (1977). "Pile Foundation Analyses and Design," *In Proceedings, IX ICSMFE*, Tokyo, Vol. 3, pp. 374 - 379.

Viggiani, C. (1993). "Further Experiences with Auger Piles in the Naples Area," *In Proceedings, Deep Foundations on Bored and Auger Piles*, Balkema, Rotterdam, pp. 445-455.

Wooley, J. A., and Reese, L. C. (1974). "Behavior of an Axially Loaded Drilled Shaft under Sustained Loading," *Research Report 176-2*, Project 3-5-72-176, Center for Highway Research, University of Texas, Austin, Texas.

Wright, S. J., and Reese, L. C. (1979). "Design of Large-Diameter Bored Piles," *Ground Engineering*, London, United Kingdom, Vol. 12, No. 8, pp. 47-51.

Zelada, G. A., and Stepenson, R. W. (2000). "Design Methods for Auger CIP Piles in Compression," *New Technological And Design Developments in Deep Foundations, Geotechnical Special Publication No. 100*, ASCE, August, Denver, CO.

APPENDIX A

Boring Logs at Krenek Road Bridge Site

Depth m (ft)	Log	N _{T-DOT} blows/ 0.30 m	N _{SPT} blows/ 0.30 m	s _u kPa (psi)	γ _t kN/m ³ (pcf)	Soil Classification
1.5 (5)	▼	14		69.0 (10.0)	20.1 (128.0)	CLAY, slightly sandy, stiff
3 (10)		19				
4.6 (15)		22				
6.1 (20)		22		96.6 (14.0)	20.1 (127.9)	CLAY, stiff -sand seam
7.6 (25)		20				
9.1 (30)		24				
10.7 (35)		23				
12.2 (40)		64				
13.7 (45)		27		124.2 (18.0)	20.9 (132.8)	CLAY, stiff, with sand fissures
15.2 (50)		33				
16.8 (55)	75					
18.3 (60)	61				SAND, clayey SAND, dense -very dense	
19.8 (65)	100/0.05 m	36				
21.3 (70)	100/0.17 m	51				
22.9 (75)	100/0.18 m	65				
24.4 (80)	39					
						SAND, dense -clay layer

Fig. A.1. Boring Log 2 (KR-2) at Krenek Road Site

Depth m (ft)	Log	N _{TxDOT} blows/ 0.30 m	N _{SPT} blows/ 0.30 m	s _u kPa (psi)	γ _t kN/m ³ (pcf)	Soil Classification
1.5 (5)	▼	10		86.2 (12.5)	19.9 (126.5)	CLAY, stiff
3 (10)		13				
4.6 (15)		14		70.3 (10.2)	18.0 (114.5)	CLAY, stiff
6.1 (20)		14				
7.6 (25)		19				
9.1 (30)		18		97.9 (14.2)	20.0 (127.2)	CLAY, stiff w/ sand seams
10.7 (35)		28				
12.2 (40)		53				SAND, slightly silty, dense

Fig. A.2. Boring Log 3 (KR-3) at Krenek Road Site

Depth m (ft)	Log	N _{TxDOT} blows/ 0.30 m	N _{SPT} blows/ 0.30 m	s _u kPa (psi)	γ _t kN/m ³ (pcf)	Soil Classification
1.5 (5)	▼	15		62.4 (9.1)	19.6 (125)	CLAY, stiff
3 (10)		16				
4.6 (15)		20			19.6 (125)	
6.1 (20)	▼	15		87.6 (12.7)	19.8 (126)	CLAY, stiff
7.6 (25)		24				
9.1 (30)		15				
10.7 (35)		33				
12.2 (40)		40				
						SAND, clayey

Fig. A.3. Boring Log 4 (KR-4) at Krenek Road Site

APPENDIX B

Stress-Strain Curves for Grout Samples

(Test and Production Piles)

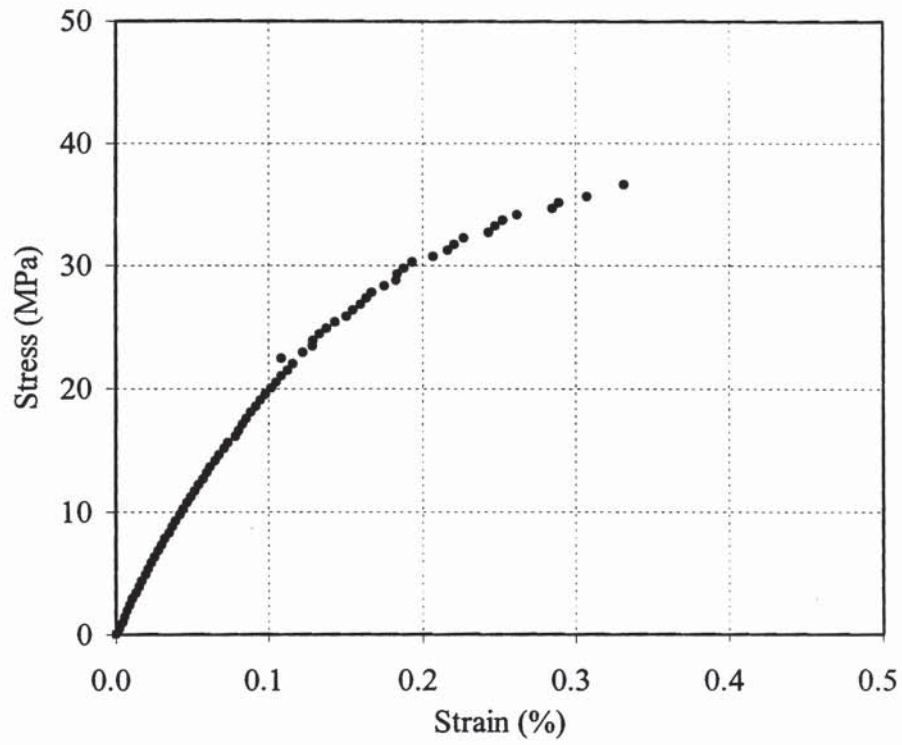


Fig. B.1. Stress-Strain Curve for Test Pile Sample 1 (TP-1)

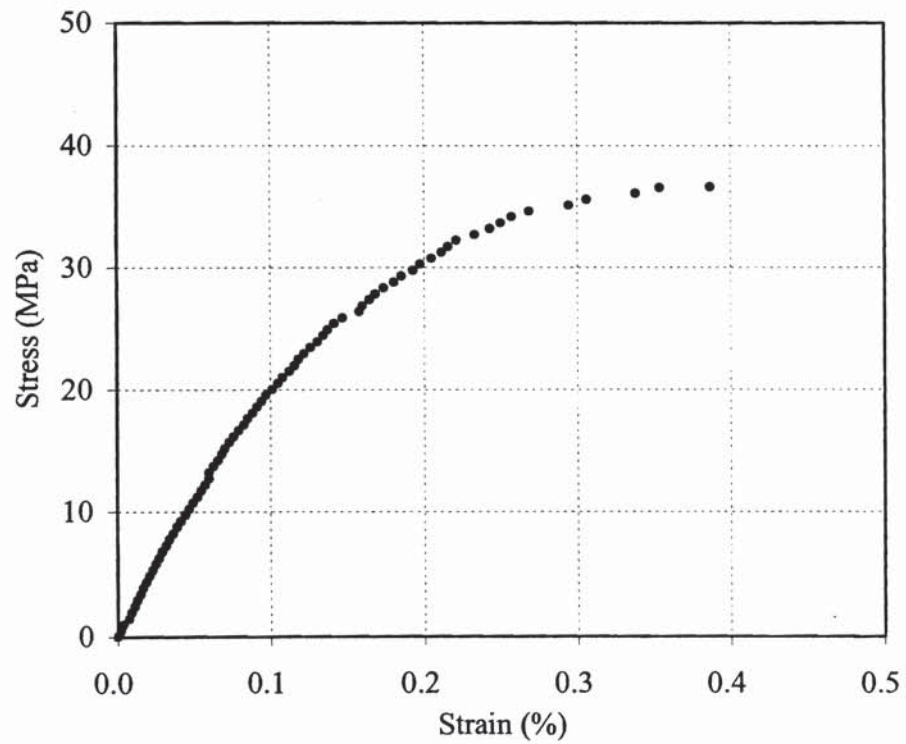


Fig. B.2. Stress-Strain Curve for Test Pile Sample 2 (TP-2)

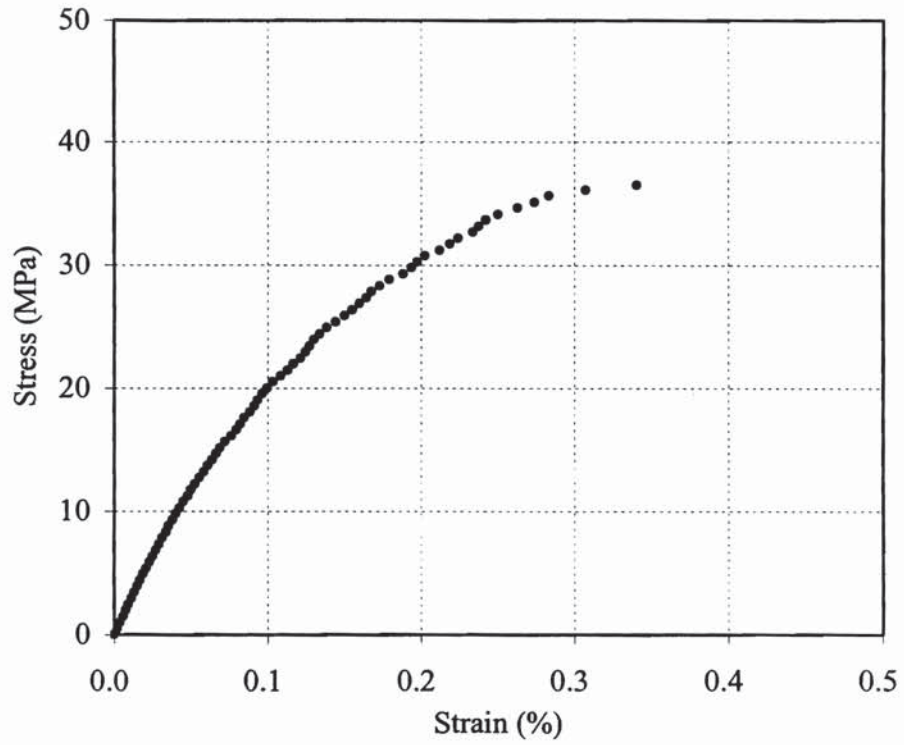


Fig. B.3. Stress-Strain Curve for Test Pile Sample 3 (TP-3)

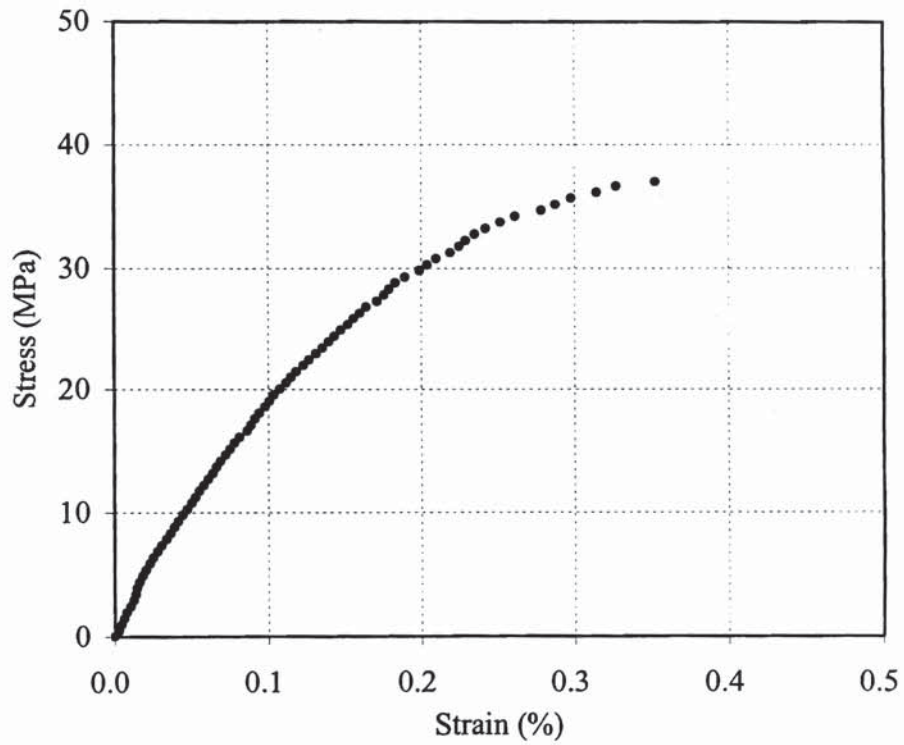


Fig. B.4. Stress-Strain Curve for Test Pile Sample 4 (TP-4)

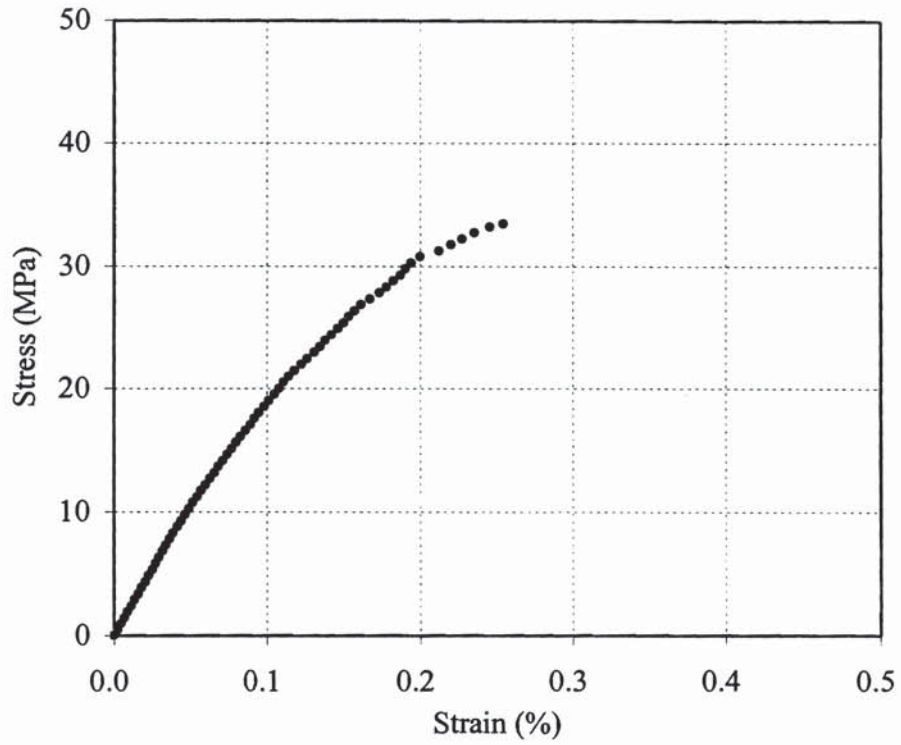


Fig. B.5. Stress-Strain Curve for Test Pile Sample 5 (TP-5)

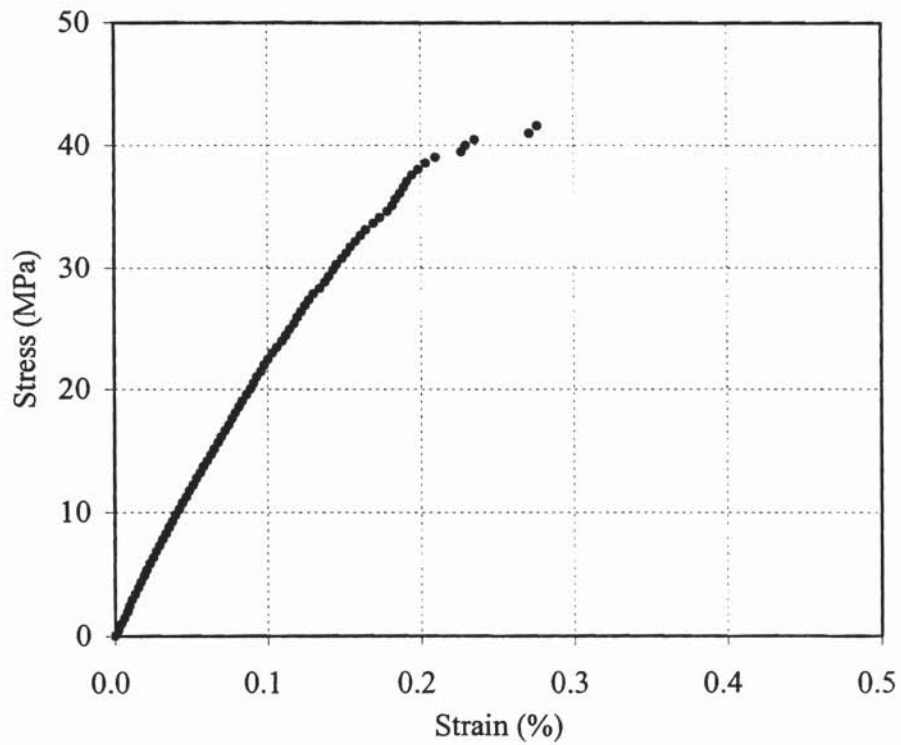


Fig. B.6. Stress-Strain Curve for Production Pile Sample 1 (B-23)

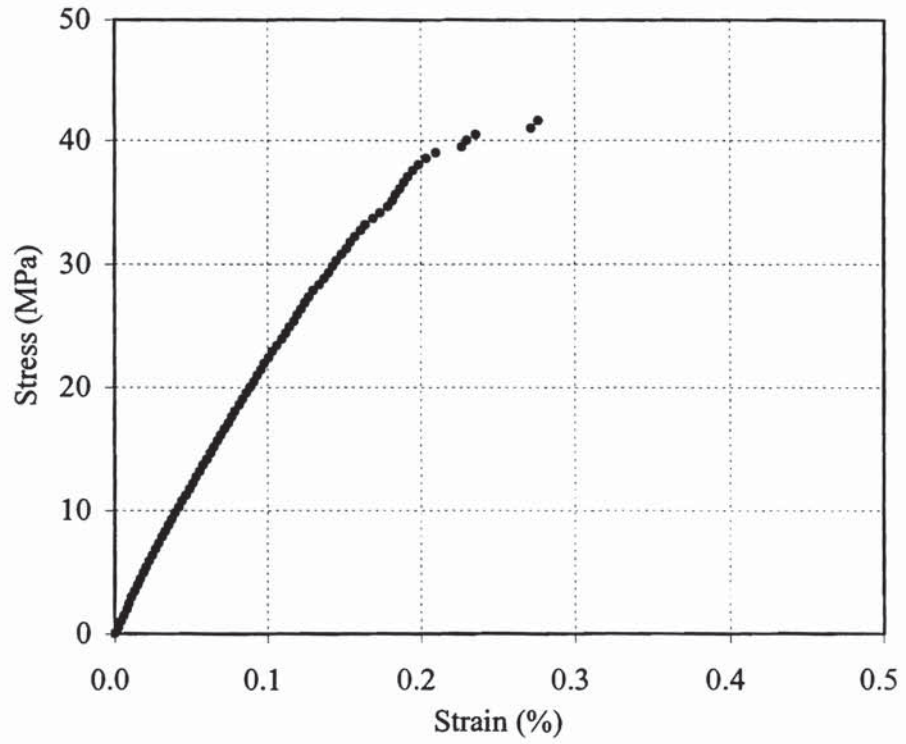


Fig. B.7. Stress-Strain Curve for Production Pile Sample 2 (B-24)

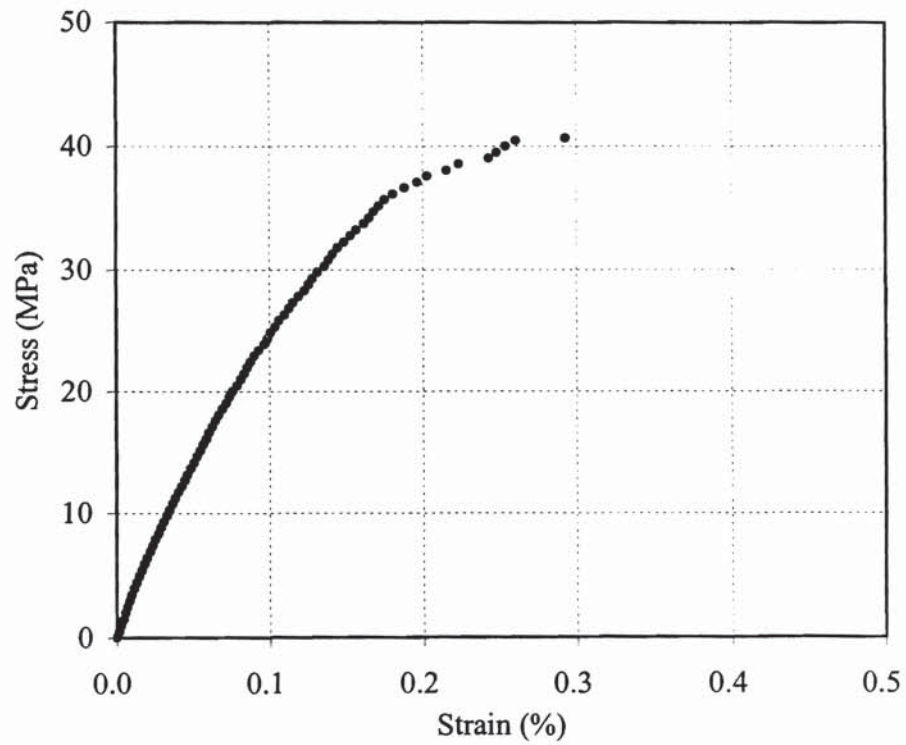


Fig. B.8. Stress-Strain Curve for Production Pile Sample 3 (B-25)

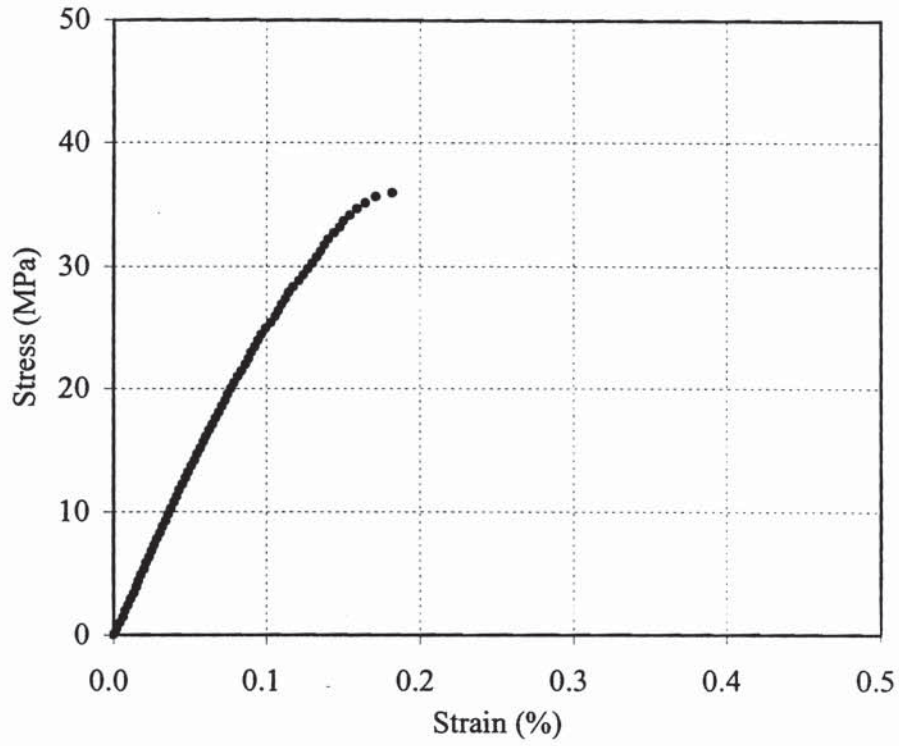


Fig. B.9. Stress-Strain Curve for Production Pile Sample 4 (B-26)

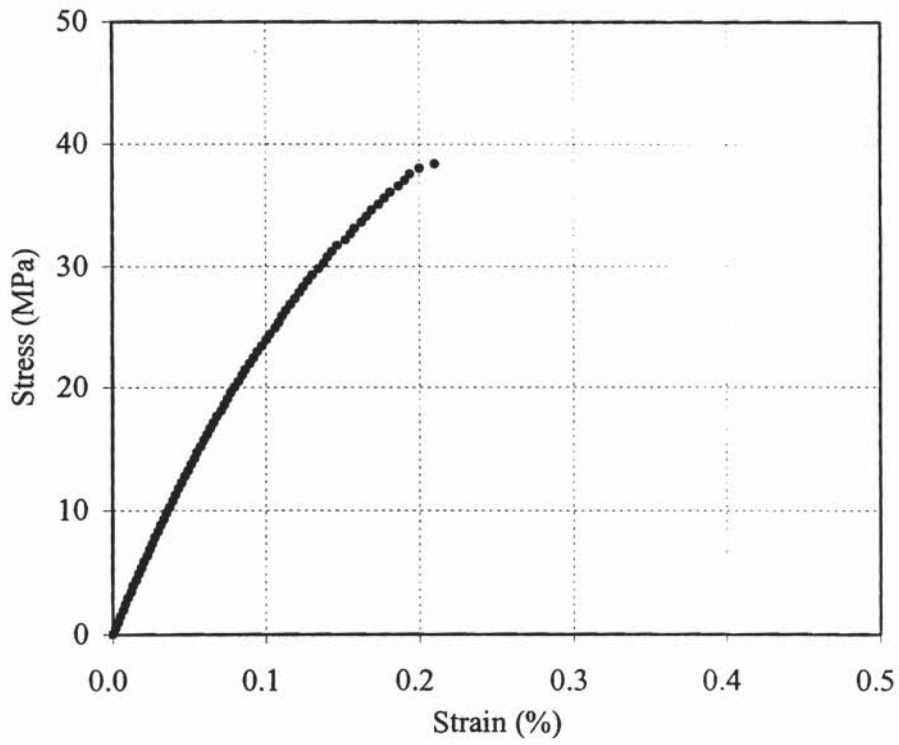


Fig. B.10. Stress-Strain Curve for Production Pile Sample 5 (B-31)

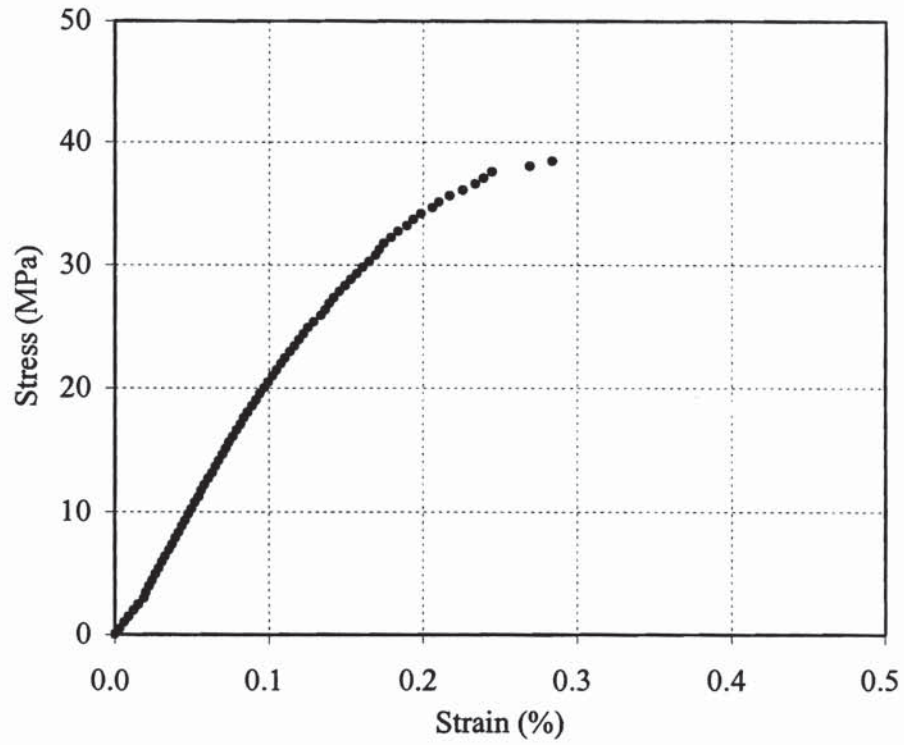


Fig. B.11. Stress-Strain Curve for Production Pile Sample 6 (B-32)

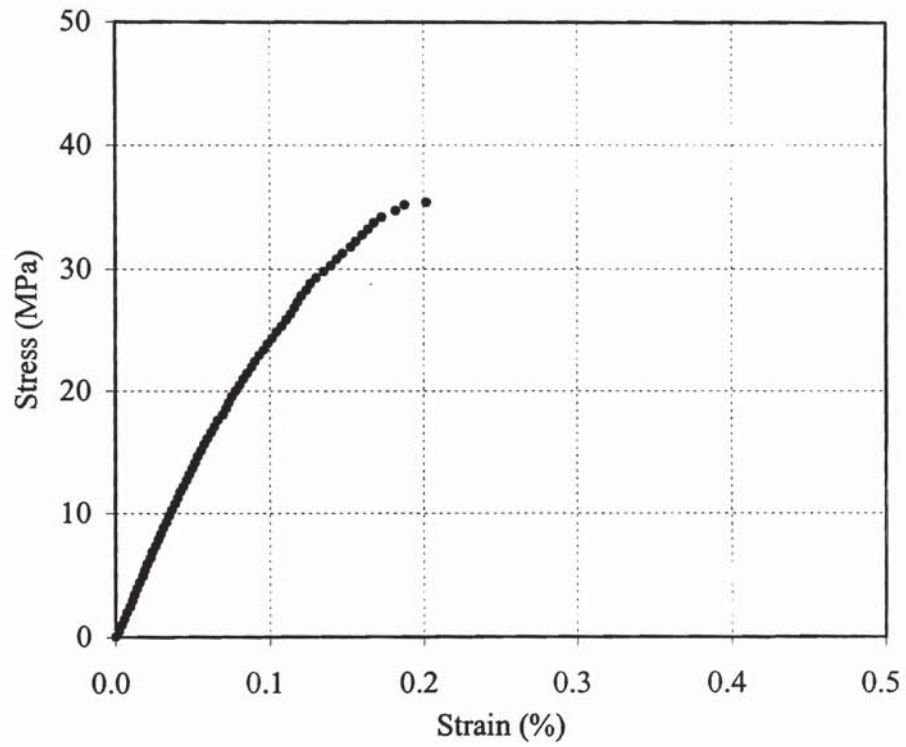


Fig. B.12. Stress-Strain Curve for Production Pile Sample 7 (B-34)

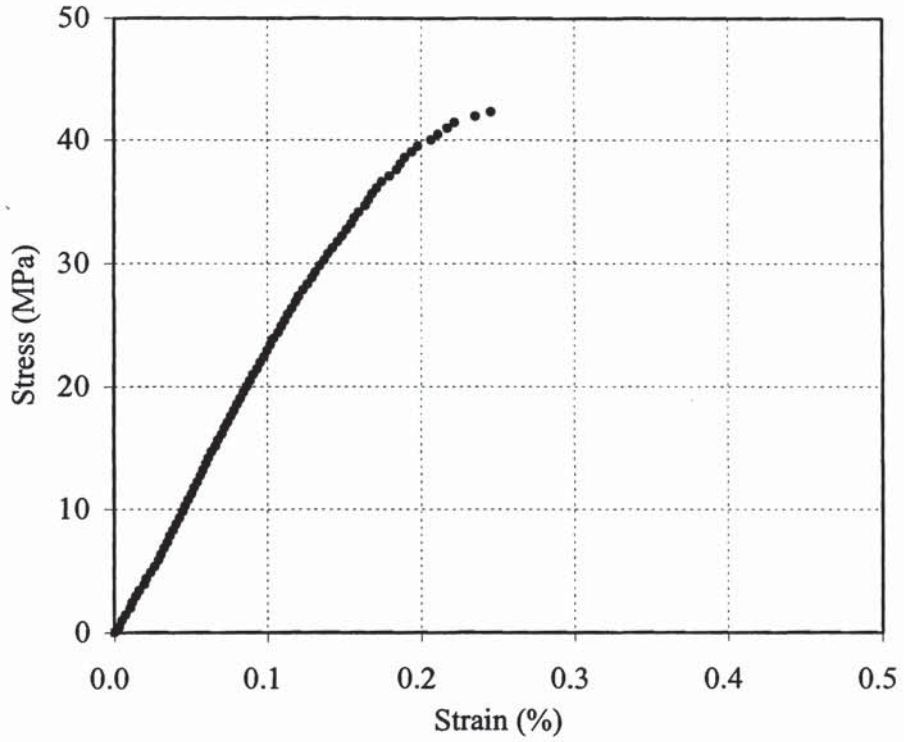


Fig. B.13. Stress-Strain Curve for Production Pile Sample 8 (A-15)

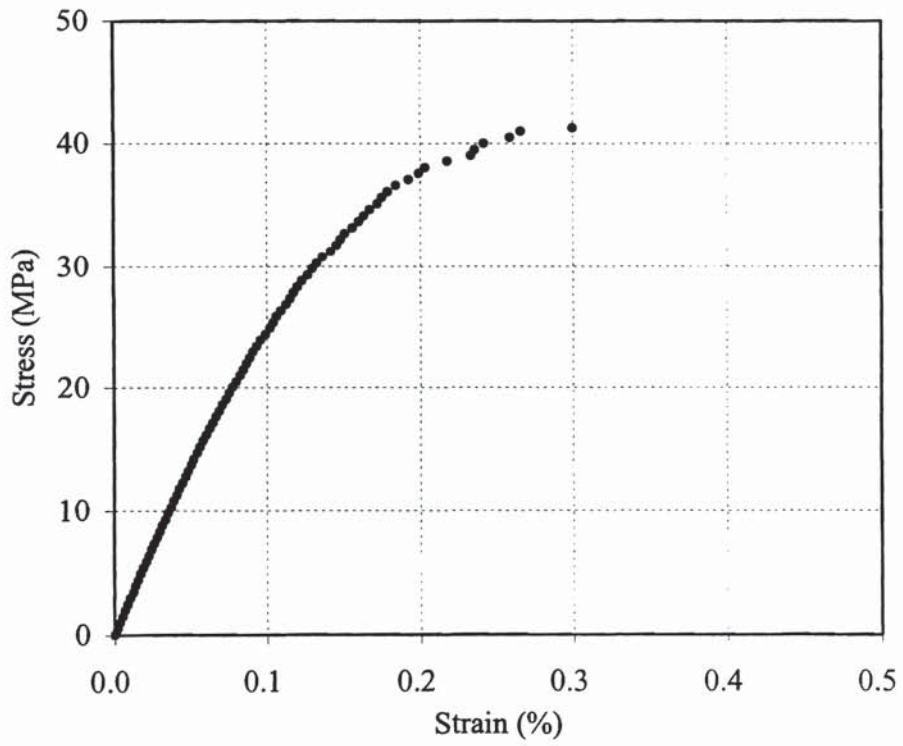


Fig. B.14. Stress-Strain Curve for Production Pile Sample 9 (A-16)

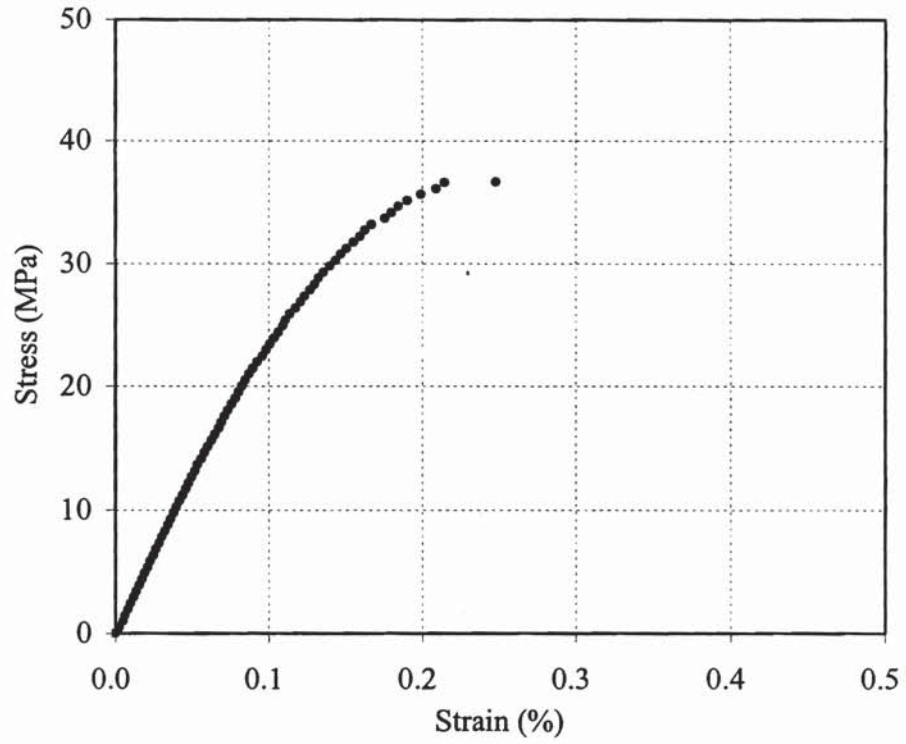


Fig. B.15. Stress-Strain Curve for Production Pile Sample 10 (A-17)

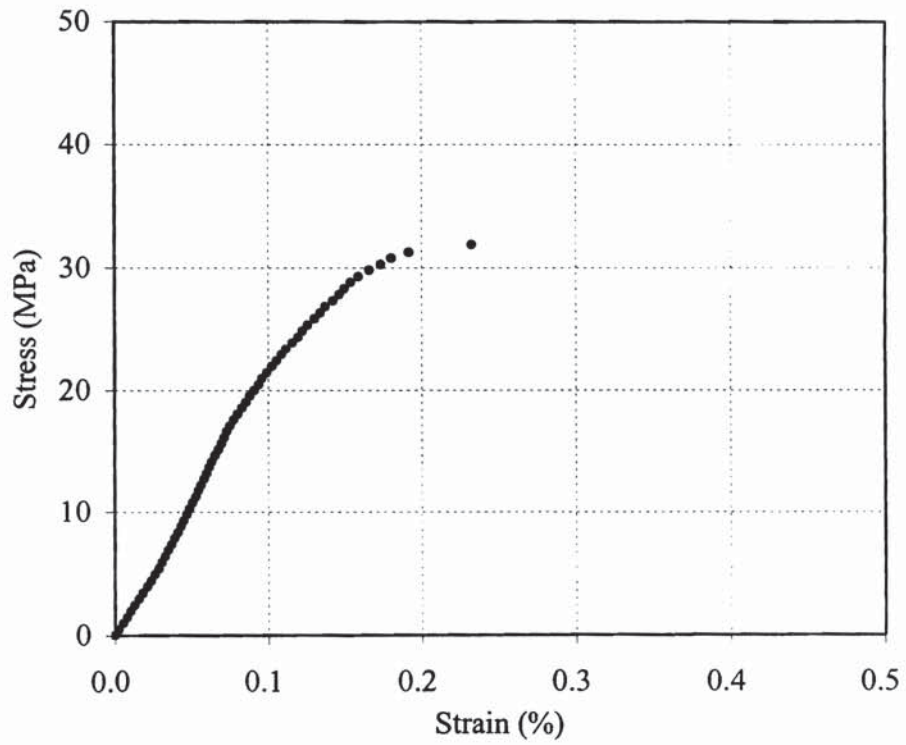


Fig. B.16. Stress-Strain Curve for Production Pile Sample 11 (A-18)

APPENDIX C

Grout Ratios for Test and 64 Production Piles

Table C.1. Grout Ratios for Test and Central Bent Piles under Footing A and B

Depth from surface		Grout Ratio								
ft	m	TEST	FA/P1	FA/P2	FA/P3	FA/P4	FB/P1	FB/P2	FB/P3	FB/P4
62	18.9	1.48	1.50	1.16	1.50	1.47	1.17	1.24	1.34	1.48
60	18.3	1.41	1.47	1.33	1.34	1.20	2.20	1.52	1.51	1.37
58	17.7	1.40	1.32	1.38	1.31	1.55	1.14	1.42	1.34	1.43
56	17.1	1.37	1.22	1.35	1.27	1.26	1.56	1.40	1.47	1.28
54	16.5	1.25	1.45	1.26	1.20	1.37	1.33	1.26	1.49	1.33
52	15.8	1.17	1.42	1.27	1.30	1.30	1.04	1.27	1.29	1.15
50	15.2	1.23	1.39	1.17	1.22	1.33	1.60	1.22	1.25	1.27
48	14.6	1.47	1.46	1.32	1.22	1.34	1.28	1.22	1.26	1.18
46	14.0	1.29	1.38	1.28	1.28	1.28	1.39	1.32	1.27	1.34
44	13.4	1.04	1.48	1.24	1.16	1.23	1.49	1.19	1.28	1.28
42	12.8	1.51	1.33	1.25	1.29	1.30	1.56	1.29	1.18	1.32
40	12.2	1.27	1.24	1.28	1.24	1.33	1.43	1.25	1.24	1.31
38	11.6	1.27	1.15	1.21	1.29	1.34	1.27	1.26	1.27	1.15
36	11.0	1.17	1.39	1.29	1.19	1.30	1.20	1.21	1.46	1.17
34	10.4	1.16	1.23	1.27	1.15	1.46	1.22	1.18	1.22	1.17
32	9.8	1.23	1.22	1.14	1.17	1.36	1.36	1.33	1.30	1.28
30	9.1	0.97	1.31	1.25	1.14	1.27	1.15	1.24	1.32	1.15
28	8.5	1.59	1.20	1.29	1.29	1.24	1.38	1.47	1.29	1.31
26	7.9	1.36	1.30	1.17	1.21	1.25	1.37	1.31	1.24	1.23
24	7.3	1.37	1.31	1.17	1.24	1.25	1.29	1.20	1.31	1.27
22	6.7	1.50	1.18	1.16	1.27	1.27	1.27	1.16	1.32	1.31
20	6.1	1.66	1.19	1.25	1.22	1.32	1.36	1.26	1.29	1.33
18	5.5	1.48	1.23	1.01	1.20	1.28	1.22	1.20	1.32	1.38
16	4.9	1.30	1.38	1.33	1.06	1.29	1.24	1.21	1.19	1.40
14	4.3	1.26	1.21	1.30	1.23	1.27	1.30	1.09	1.31	1.20
12	3.7	1.39	1.28	1.37	1.18	1.21	1.28	1.30	1.25	1.48
10	3.0	1.26	1.23	1.31	1.25	1.35	1.22	1.23	1.33	1.50
8	2.4	1.31	1.27	1.22	1.13	1.25	1.33	1.21	1.28	1.42
6	1.8	1.42	1.27	1.24	1.20	1.24	1.34	1.26	1.22	1.67
4	1.2	1.39	1.25	1.48	1.24	1.28	1.37	1.12	1.12	1.34
2	0.6	1.41	1.28	1.28	1.24	1.31	1.49	1.10	1.54	1.36
0	0.0	-	-	-	-	-	-	-	-	-
Average		1.34	1.31	1.26	1.23	1.31	1.35	1.26	1.31	1.32
St.Dev.		0.15	0.10	0.09	0.08	0.08	0.20	0.10	0.10	0.12
C.O.V.		0.11	0.08	0.07	0.06	0.06	0.15	0.08	0.07	0.09
Return Depth (ft)		18.0	14.7	15.1	14.6	10.8	17.4	10.7	12.1	5.2
Return Depth (m)		5.5	4.5	4.6	4.5	3.3	5.3	3.3	3.7	1.6

Table C.2. Grout Ratios for Central Bent Piles under Footing C and D

Depth from Surface		Grout Ratio							
ft	m	FC/P1	FC/P2	FC/P3	FC/P4	FD/P1	FD/P2	FD/P3	FD/P4
62	18.9	1.36	1.56	1.35	1.62	1.43	1.29	1.40	1.50
60	18.3	1.24	1.44	1.87	1.59	1.61	1.50	1.32	1.43
58	17.7	1.44	1.18	1.36	1.34	1.21	1.24	1.42	1.65
56	17.1	1.16	1.47	1.52	1.34	1.20	1.26	1.21	1.41
54	16.5	1.54	1.18	1.37	1.61	1.46	1.20	1.25	1.53
52	15.8	1.41	1.40	1.33	1.28	1.10	1.18	1.26	1.28
50	15.2	1.38	1.25	1.24	1.42	1.11	1.21	1.10	1.40
48	14.6	1.32	1.50	1.16	1.38	1.47	1.24	1.48	1.26
46	14.0	1.33	1.09	1.34	1.54	1.42	1.14	1.46	1.24
44	13.4	1.19	1.47	1.34	1.45	1.46	1.22	1.35	1.17
42	12.8	1.24	1.25	1.29	1.30	1.37	1.16	1.35	1.37
40	12.2	1.25	1.44	1.38	1.49	1.40	1.23	1.48	1.30
38	11.6	1.18	1.32	1.23	1.37	1.36	1.16	1.27	1.22
36	11.0	1.26	1.13	1.35	1.33	1.17	1.36	1.35	1.35
34	10.4	1.22	1.45	1.22	1.30	1.29	1.17	1.34	1.31
32	9.8	1.32	1.31	1.18	1.44	1.19	1.25	1.33	1.21
30	9.1	1.31	1.07	1.24	1.19	1.23	1.09	1.34	1.31
28	8.5	1.32	1.36	1.17	1.32	1.20	1.44	1.30	1.49
26	7.9	1.26	1.29	1.20	1.28	1.18	1.25	1.36	1.37
24	7.3	1.38	1.30	1.18	1.23	1.15	1.22	1.24	1.25
22	6.7	1.30	1.61	1.23	1.22	1.29	1.27	1.32	1.19
20	6.1	1.45	1.49	1.18	1.32	1.38	1.18	1.17	1.39
18	5.5	1.21	0.98	1.20	1.28	1.20	1.24	1.28	1.58
16	4.9	1.31	1.50	1.21	1.09	1.26	1.30	1.07	1.34
14	4.3	1.35	1.57	1.27	1.33	1.38	1.27	1.37	1.34
12	3.7	1.38	1.56	1.23	1.20	1.31	1.26	1.37	1.54
10	3.0	1.37	1.43	1.44	1.29	1.42	1.21	1.22	1.61
8	2.4	1.36	1.35	1.61	1.38	1.32	1.26	1.29	1.61
6	1.8	1.32	1.24	1.60	1.47	1.35	1.27	1.37	1.31
4	1.2	1.43	1.38	1.39	1.26	1.36	1.41	1.36	1.51
2	0.6	1.34	1.21	1.34	1.46	1.35	1.22	1.67	1.50
0	0.0	-	-	-	-	-	-	-	-
Average		1.32	1.35	1.32	1.36	1.31	1.25	1.33	1.39
St.Dev.		0.09	0.16	0.16	0.13	0.12	0.09	0.12	0.14
C.O.V.		0.07	0.12	0.12	0.09	0.09	0.07	0.09	0.10
Return Depth (ft)		19.3	14	5.8	13.4	17.4	11.1	19.9	22.9
Return Depth (m)		5.9	4.3	1.8	4.1	5.3	3.4	6.1	7.0

Table C.3. Grout Ratios for Central Bent Piles under Footing E and F

Depth from Surface		Grout Ratio							
ft	m	FE/P1	FE/P2	FE/P3	FE/P4	FF/P1	FF/P2	FF/P3	FF/P4
62	18.9	1.47	1.61	1.46	1.35	1.44	1.29	1.37	1.41
60	18.3	1.21	1.40	1.45	1.51	1.31	1.37	1.45	1.29
58	17.7	1.31	1.60	1.49	1.29	1.52	1.41	1.46	1.18
56	17.1	1.32	1.44	1.32	1.33	1.48	1.32	1.50	1.33
54	16.5	1.25	1.30	1.35	1.27	1.29	1.37	1.51	1.07
52	15.8	1.07	1.19	1.27	1.20	1.27	1.33	1.46	1.32
50	15.2	1.26	1.20	1.15	1.35	1.30	1.19	0.86	1.32
48	14.6	1.24	1.65	1.17	1.17	1.30	1.26	1.59	1.15
46	14.0	1.29	1.53	1.03	1.14	1.19	1.24	1.71	1.23
44	13.4	1.31	1.46	1.43	1.31	1.18	1.18	1.20	0.93
42	12.8	1.09	1.30	1.47	1.13	1.30	1.30	1.21	1.52
40	12.2	1.36	1.37	1.17	1.42	1.34	1.31	1.34	1.29
38	11.6	1.34	1.50	1.24	1.32	1.32	1.11	1.20	1.24
36	11.0	1.21	1.33	1.20	1.25	1.19	1.29	1.16	1.19
34	10.4	1.23	1.33	1.17	1.32	1.37	1.34	1.39	1.17
32	9.8	1.32	1.26	1.27	1.25	1.29	1.12	1.35	1.27
30	9.1	1.33	1.20	1.35	1.25	1.24	1.35	1.34	1.23
28	8.5	1.23	1.47	1.18	1.31	1.18	1.17	1.33	1.38
26	7.9	1.35	1.63	1.31	1.28	1.23	1.26	1.28	1.32
24	7.3	1.26	1.32	1.24	1.26	1.24	1.30	1.24	1.43
22	6.7	1.48	0.98	1.41	1.34	1.12	1.40	1.31	1.41
20	6.1	1.49	1.42	1.25	1.25	1.27	1.24	1.25	1.41
18	5.5	1.40	1.07	1.24	1.24	1.18	1.31	1.36	1.40
16	4.9	1.42	1.34	1.39	1.20	1.22	1.31	1.39	1.45
14	4.3	1.28	1.41	1.25	1.28	1.30	1.21	1.29	1.31
12	3.7	1.24	1.37	1.34	1.27	1.10	1.30	1.24	1.35
10	3.0	1.28	1.22	1.34	1.29	1.21	1.16	1.30	1.32
8	2.4	1.17	1.18	1.24	1.07	1.19	1.32	1.26	1.42
6	1.8	1.14	1.32	1.34	1.43	1.21	1.35	1.43	1.26
4	1.2	1.21	1.34	1.40	1.18	1.20	1.31	1.25	1.25
2	0.6	1.26	1.20	1.22	1.33	1.26	1.19	1.56	1.37
0	0.0	-	-	-	-	-	-	-	-
Average		1.28	1.35	1.29	1.28	1.27	1.28	1.34	1.30
St.Dev.		0.10	0.16	0.11	0.09	0.10	0.08	0.16	0.12
C.O.V.		0.08	0.12	0.09	0.07	0.08	0.06	0.12	0.09
Return Depth (ft)		13.4	9.1	11.8	17.4	17.5	9.6	17.5	12.9
Return Depth (m)		4.1	2.8	3.6	5.3	5.3	2.9	5.3	3.9

Table C.4. Grout Ratios for Central Bent Piles under Footing G and H

Depth from Surface		Grout Ratio							
ft	m	FG/P1	FG/P2	FG/P3	FG/P4	FH/P1	FH/P2	FH/P3	FH/P4
62	18.9	1.09	1.32	1.50	1.45	1.53	1.21	1.26	1.42
60	18.3	1.64	1.32	1.48	1.34	1.46	1.27	0.97	1.24
58	17.7	1.75	1.20	1.05	1.28	1.30	1.29	1.49	0.89
56	17.1	1.44	1.31	1.21	1.51	1.25	1.35	1.37	1.38
54	16.5	1.36	1.34	1.40	1.38	1.31	1.31	1.33	1.66
52	15.8	1.29	1.23	1.36	1.36	1.19	1.39	1.45	1.33
50	15.2	1.50	1.25	1.27	1.28	1.26	1.10	1.19	1.32
48	14.6	1.48	1.20	1.32	1.22	1.31	1.33	1.44	1.30
46	14.0	1.38	1.27	1.25	1.16	1.18	1.42	1.46	1.40
44	13.4	1.27	1.28	1.38	1.18	1.36	1.31	1.14	1.21
42	12.8	1.26	1.27	1.21	1.23	1.10	1.22	1.40	1.30
40	12.2	1.39	1.22	1.22	1.24	1.29	1.25	1.23	1.28
38	11.6	1.44	1.14	1.23	1.24	1.25	1.04	1.15	0.93
36	11.0	1.21	1.24	1.16	1.33	1.29	1.32	0.99	1.28
34	10.4	1.32	1.39	1.28	1.18	1.44	1.23	1.59	1.28
32	9.8	1.35	1.47	1.26	1.23	1.44	1.20	1.45	1.46
30	9.1	1.35	1.34	1.30	1.18	1.46	1.23	1.38	1.22
28	8.5	1.33	1.35	1.28	1.25	1.49	1.31	1.23	1.29
26	7.9	1.28	1.34	1.12	1.23	1.42	1.05	1.34	1.19
24	7.3	1.30	1.36	1.25	1.22	1.33	1.22	1.43	1.17
22	6.7	1.24	1.26	1.24	1.21	1.47	1.24	1.34	1.29
20	6.1	1.35	1.28	1.31	1.27	1.43	1.26	1.25	1.32
18	5.5	1.29	1.29	1.33	1.26	1.44	1.14	1.33	1.22
16	4.9	1.30	1.27	1.22	1.18	1.27	1.52	1.26	1.28
14	4.3	1.36	1.31	1.21	1.26	1.42	1.43	1.29	1.35
12	3.7	1.11	1.29	1.24	1.34	1.40	1.36	1.26	1.26
10	3.0	1.12	1.36	1.22	1.19	1.36	1.42	1.28	1.35
8	2.4	1.82	1.27	1.29	1.14	1.40	1.40	1.30	1.31
6	1.8	1.37	1.24	1.31	1.26	1.42	1.25	1.35	1.12
4	1.2	1.34	1.26	1.41	1.21	1.33	1.30	1.29	1.21
2	0.6	1.20	1.25	1.29	1.24	1.41	1.17	1.38	1.37
0	0.0	-	-	-	-	-	-	-	-
Average		1.35	1.29	1.28	1.26	1.36	1.28	1.31	1.28
St.Dev.		0.16	0.06	0.09	0.08	0.10	0.11	0.13	0.14
C.O.V.		0.12	0.05	0.07	0.07	0.07	0.09	0.10	0.11
Return Depth (ft)		5.9	17	19.3	14.7	16.5	15.4	9.5	9.7
Return Depth (m)		1.8	5.2	5.9	4.5	5.0	4.7	2.9	3.0

Table C.5. Grout Ratios for Abutment Piles (Group A, B, C, and D)

Depth from the bottom of the Abutment Cap		Grout Ratio							
ft	m	AA/PF	AA/PB	AB/PF	AB/PB	AC/PF	AC/PB	AD/PF	AD/PB
62	18.9	1.51	1.17	1.41	1.37	1.15	1.39	1.54	1.37
60	18.3	1.49	1.57	1.08	1.12	1.45	1.27	1.63	1.43
58	17.7	1.49	1.49	1.25	1.40	1.32	1.50	1.41	1.40
56	17.1	1.47	1.36	1.51	1.54	1.23	1.59	1.32	1.30
54	16.5	1.27	1.31	1.28	1.48	1.40	1.06	1.45	1.42
52	15.8	1.60	1.43	1.33	1.21	1.29	1.40	1.40	1.43
50	15.2	1.26	1.32	1.21	1.45	1.21	1.44	1.32	1.37
48	14.6	1.27	1.25	1.16	1.42	1.43	1.25	1.32	1.39
46	14.0	1.32	1.29	1.21	1.33	1.28	1.14	1.36	1.43
44	13.4	1.22	1.31	1.17	1.48	1.25	1.37	1.35	1.27
42	12.8	1.08	1.35	1.37	1.40	1.36	1.41	1.12	1.35
40	12.2	1.66	1.23	1.22	1.33	1.46	1.24	1.41	1.28
38	11.6	1.52	1.38	1.22	1.26	1.54	1.47	1.54	1.23
36	11.0	1.34	1.06	1.27	1.14	1.35	1.48	1.45	1.36
34	10.4	1.19	1.40	1.21	1.38	1.39	1.42	0.95	1.23
32	9.8	1.28	1.49	1.32	1.30	1.52	1.39	1.54	1.24
30	9.1	1.25	1.25	1.31	1.30	1.29	1.50	1.72	1.28
28	8.5	1.42	1.47	1.23	1.32	1.38	1.13	1.59	1.26
26	7.9	1.33	1.53	1.25	1.43	0.69	1.38	1.51	1.26
24	7.3	1.29	1.43	1.23	1.37	1.52	1.34	1.21	1.24
22	6.7	1.46	1.51	1.24	1.30	1.58	1.27	1.50	1.27
20	6.1	1.40	1.41	1.29	1.43	1.61	1.20	1.45	1.60
18	5.5	1.28	1.27	1.28	1.31	1.36	0.99	1.53	1.58
16	4.9	1.35	1.28	1.35	1.41	1.45	1.45	1.25	1.19
14	4.3	1.54	1.24	1.24	1.36	1.39	1.20	1.37	1.27
12	3.7	1.31	1.29	1.25	1.34	1.44	1.45	1.48	1.38
10	3.0	1.60	1.23	1.03	1.38	1.37	1.32	1.39	1.35
8	2.4	1.34	1.21	1.52	1.28	1.31	1.38	1.43	1.29
6	1.8	1.34	1.26	1.35	1.23	1.35	1.49	1.44	1.24
4	1.2	1.57	1.36	1.33	1.42	1.34	1.45	1.44	1.40
2	0.6	1.26	1.26	1.35	1.35	0.87	1.31	1.39	1.36
0	0.0	-	-	-	-	-	-	-	-
Average		1.38	1.34	1.27	1.35	1.34	1.34	1.41	1.34
St.Dev.		0.14	0.12	0.10	0.09	0.19	0.14	0.15	0.10
C.O.V.		0.10	0.09	0.08	0.07	0.14	0.10	0.11	0.07
Return Depth (ft)		19.6	16.1	15.4	23.1	15.7	22.7	20.7	18.9
Return Depth (m)		6.0	4.9	4.7	7.0	4.8	6.9	6.3	5.8

Table C.6. Grout Ratios for Abutment Piles (Group E, F, G, and H)

Depth from the bottom of the Abutment Cap		Grout Ratio							
ft	m	AE/PF	AE/PB	AF/PF	AF/PB	AG/PF	AG/PB	AH/PF	AH/PB
62	18.9	1.23	1.39	1.37	1.30	1.36	1.31	1.40	1.21
60	18.3	1.33	1.23	1.13	1.43	1.50	1.52	1.49	1.52
58	17.7	0.94	1.23	1.17	1.10	1.49	1.35	1.31	1.41
56	17.1	1.44	1.29	1.62	1.37	1.37	1.25	1.47	1.51
54	16.5	1.41	1.43	1.53	1.11	1.35	1.35	1.48	1.58
52	15.8	1.22	1.19	1.47	1.36	1.47	1.34	1.46	1.31
50	15.2	1.39	1.35	1.28	1.28	1.31	1.33	1.32	1.32
48	14.6	1.51	1.48	1.51	1.32	1.36	1.23	1.34	1.40
46	14.0	1.53	1.37	1.33	1.15	1.12	1.36	1.33	1.44
44	13.4	1.31	1.34	1.35	1.39	1.60	1.41	1.29	1.25
42	12.8	1.34	1.23	0.98	1.37	1.22	1.39	1.37	1.15
40	12.2	1.41	0.99	1.43	1.30	1.39	1.54	1.21	1.37
38	11.6	1.24	1.48	1.47	1.22	1.43	1.28	1.47	1.41
36	11.0	1.39	1.23	1.49	1.42	1.51	1.40	1.42	1.40
34	10.4	1.18	1.23	1.27	1.39	1.30	1.38	1.18	1.42
32	9.8	1.45	1.23	1.35	1.52	1.40	1.27	1.49	1.30
30	9.1	1.30	1.12	1.36	1.34	1.23	1.16	1.56	1.35
28	8.5	1.39	1.34	1.35	1.35	1.52	1.18	1.31	1.26
26	7.9	1.05	1.26	1.34	1.25	1.52	1.31	1.44	1.27
24	7.3	1.36	1.31	1.28	1.52	1.50	1.27	1.33	1.27
22	6.7	1.50	1.21	1.22	1.53	1.28	1.24	1.39	1.36
20	6.1	1.70	1.27	1.39	1.16	1.52	2.59	1.40	1.29
18	5.5	1.18	1.32	1.29	1.39	1.39	1.55	1.25	1.40
16	4.9	1.54	1.42	1.29	1.21	1.14	1.38	1.37	1.30
14	4.3	1.65	1.29	1.32	1.23	1.28	1.25	1.39	1.51
12	3.7	1.25	1.33	1.18	1.46	1.53	1.17	1.11	1.37
10	3.0	1.28	1.29	1.45	1.34	1.26	1.34	1.53	1.37
8	2.4	1.25	1.55	1.35	1.34	1.40	1.44	1.34	1.35
6	1.8	1.36	1.49	1.29	1.42	1.58	1.22	1.59	1.36
4	1.2	1.36	1.28	1.36	0.67	1.40	1.31	1.38	1.32
2	0.6	1.34	1.34	1.52	1.62	1.42	1.18	1.48	1.34
0	0.0	-	-	-	-	-	-	-	-
Average		1.35	1.31	1.35	1.32	1.39	1.36	1.38	1.36
St.Dev.		0.16	0.11	0.13	0.17	0.12	0.25	0.11	0.09
C.O.V.		0.12	0.09	0.10	0.13	0.09	0.18	0.08	0.07
Return Depth (ft)		18.8	17.2	17.9	20.1	18.6	20.4	16.5	14.6
Return Depth (m)		5.7	5.2	5.5	6.1	5.7	6.2	5.0	4.5

Table C.7. Grout Ratios for Abutment Piles (Group I, J, K and L)

Depth from the bottom of the Abutment Cap		Grout Ratio							
ft	m	AI/PF	AI/PB	AJ/PF	AJ/PB	AK/PF	AK/PB	AL/PF	AL/PB
62	18.9	1.40	1.36	1.32	1.23	1.24	1.28	1.19	1.39
60	18.3	1.47	1.59	1.42	1.28	1.54	1.35	1.46	1.30
58	17.7	1.36	1.29	1.14	1.38	1.45	1.33	1.41	1.36
56	17.1	1.50	1.21	1.18	1.34	0.95	1.14	1.52	1.05
54	16.5	1.52	1.45	1.46	1.38	1.49	1.32	1.16	1.38
52	15.8	1.47	1.34	1.19	1.26	1.40	1.34	1.43	1.33
50	15.2	1.16	1.33	0.98	1.15	1.32	1.22	1.54	1.19
48	14.6	1.29	1.27	1.29	1.25	1.22	1.18	1.31	1.26
46	14.0	1.49	1.28	1.22	1.19	1.20	1.18	1.40	1.28
44	13.4	1.45	1.01	1.49	1.21	1.23	1.23	1.35	1.20
42	12.8	1.20	1.49	1.16	1.04	1.11	1.24	1.29	1.24
40	12.2	1.39	1.53	1.16	1.29	1.46	1.16	1.37	1.27
38	11.6	1.40	1.46	1.32	1.24	1.24	1.18	1.40	1.18
36	11.0	1.38	1.47	1.35	1.35	1.27	1.43	1.25	1.28
34	10.4	1.08	1.31	1.29	1.21	1.13	1.42	1.43	1.19
32	9.8	1.30	1.36	1.22	1.51	1.39	1.33	1.36	1.17
30	9.1	1.49	1.24	1.34	1.26	1.31	1.23	1.25	1.25
28	8.5	1.38	1.35	1.38	1.21	1.19	1.29	1.33	1.18
26	7.9	1.28	1.10	1.14	1.45	1.56	1.31	1.32	1.33
24	7.3	1.31	1.34	1.16	1.36	1.46	1.22	1.30	1.19
22	6.7	1.22	1.38	1.30	1.30	1.20	1.40	1.24	1.25
20	6.1	1.12	1.42	1.33	1.22	1.58	1.30	1.35	1.25
18	5.5	1.13	1.23	1.30	1.35	1.29	1.26	1.25	1.12
16	4.9	1.31	1.25	1.38	1.27	1.35	1.37	1.31	1.41
14	4.3	1.35	1.25	1.40	1.29	1.28	1.42	1.38	1.37
12	3.7	1.27	1.22	1.37	1.21	1.50	1.43	1.30	1.36
10	3.0	1.38	1.15	1.27	1.45	1.40	1.07	1.33	1.22
8	2.4	1.20	1.34	1.38	1.13	1.52	1.41	1.40	1.28
6	1.8	1.15	1.34	1.39	1.20	1.37	1.35	1.13	1.14
4	1.2	1.46	1.20	1.29	1.18	1.42	1.35	1.49	1.20
2	0.6	1.35	1.34	1.42	1.22	1.28	1.34	1.43	1.24
0	0.0	-	-	-	-	-	-	-	-
Average		1.33	1.32	1.29	1.27	1.33	1.29	1.34	1.25
St.Dev.		0.13	0.12	0.11	0.10	0.15	0.09	0.10	0.09
C.O.V.		0.09	0.09	0.09	0.08	0.11	0.07	0.07	0.07
Return Depth (ft)		20.9	19.5	18.7	19.5	17.2	20.9	19.3	19.2
Return Depth (m)		6.4	5.9	5.7	5.9	5.2	6.4	5.9	5.9

Table C.8. Grout Ratios for Abutment Piles (Group M, N, O and P)

Depth from the bottom of the Abutment Cap		Grout Ratio							
ft	m	AM/PF	AM/PB	AN/PF	AN/PB	AO/PF	AO/PB	AP/PF	AP/PB
62	18.9	1.19	1.28	1.07	1.42	1.46	1.43	1.31	1.19
60	18.3	1.56	1.24	1.48	1.41	1.49	1.57	1.28	1.44
58	17.7	1.51	1.18	1.23	1.30	1.45	1.38	1.30	1.61
56	17.1	1.47	1.51	1.40	1.44	1.38	1.72	1.29	1.25
54	16.5	1.03	1.19	1.41	1.41	1.34	1.50	1.38	1.61
52	15.8	1.58	1.16	1.20	1.30	1.50	1.21	1.49	1.05
50	15.2	1.31	1.32	1.03	1.47	1.07	1.22	1.42	1.23
48	14.6	1.47	1.21	1.28	1.42	1.33	1.21	1.30	1.29
46	14.0	1.45	1.13	1.17	1.23	1.35	1.21	1.35	1.22
44	13.4	1.32	1.23	1.20	1.24	1.25	1.25	1.42	1.26
42	12.8	1.40	1.21	1.39	1.40	1.42	1.42	1.28	1.23
40	12.2	1.33	1.30	1.25	1.19	1.15	1.33	1.26	1.36
38	11.6	1.11	1.18	1.33	1.30	1.41	1.38	1.18	1.34
36	11.0	1.53	1.11	1.49	1.27	1.26	1.42	1.17	1.13
34	10.4	1.21	1.21	1.36	1.28	0.96	1.25	1.27	1.17
32	9.8	1.42	1.23	1.08	1.21	1.37	1.12	1.21	1.21
30	9.1	1.25	1.24	1.23	1.31	1.48	1.32	1.15	1.36
28	8.5	1.49	1.21	1.33	1.15	1.46	1.34	1.29	1.32
26	7.9	1.47	1.25	1.44	1.08	1.22	1.32	1.26	1.39
24	7.3	1.47	1.17	1.45	1.22	1.35	1.30	1.33	1.20
22	6.7	1.39	1.23	1.33	1.33	1.34	1.35	1.37	1.45
20	6.1	1.28	1.24	1.48	1.06	1.33	1.29	1.18	1.28
18	5.5	1.33	1.20	1.17	1.50	1.26	1.33	1.25	1.33
16	4.9	1.38	1.26	1.42	1.18	1.27	1.34	1.32	1.36
14	4.3	1.39	1.26	1.23	1.28	1.35	1.33	1.44	1.58
12	3.7	1.32	1.32	1.46	1.19	1.25	1.44	1.47	1.01
10	3.0	1.44	1.23	1.23	1.28	1.39	1.40	1.66	1.15
8	2.4	1.41	1.29	1.32	1.24	1.28	1.38	1.32	1.28
6	1.8	1.39	1.23	1.41	1.16	1.32	1.31	1.38	1.60
4	1.2	1.11	1.26	1.48	1.40	1.44	1.46	1.46	1.51
2	0.6	1.54	1.20	1.38	1.34	1.40	1.45	1.21	1.47
0	0.0	-	-	-	-	-	-	-	-
Average		1.37	1.23	1.31	1.29	1.33	1.35	1.32	1.32
St.Dev.		0.14	0.07	0.13	0.11	0.12	0.12	0.11	0.16
C.O.V.		0.10	0.06	0.10	0.09	0.09	0.09	0.08	0.12
Return Depth (ft)		15.4	13.3	16.9	19.0	12.6	19.8	9.4	17.0
Return Depth (m)		4.7	4.1	5.2	5.8	3.8	6.0	2.9	5.2

APPENDIX D

Examples of Load Calculations

1. Dead Load


Footing

Width ft	Length ft	Depth ft	Unit Weight pcf	Load		
				kN	ton	
8.5	8.5	4	150	192.8	21.7	per 4-pile group (Central Bent)

Column

Diameter ft	Length (Ave.) ft	Unit Weight pcf	Load		
			kN	ton	
3.5	16.9	150	108.5	12.2	per 4-pile group (Central Bent)

Bentcap

Width ft	Depth ft	Length ft	Unit Weight pcf	Load		
				kN	ton	
3.5	4.5	42.1	150	442.7	49.8	
3.5	1.0	8.5	150	19.9	2.2	
				422.9	47.5	(= 1 - 2) per 2 footings
				211.4	23.8	per 4-pile group (Central Bent)

Abutment Cap

Width ft	Length ft	Thickness ft	Unit Weight pcf	Load		
				kN	ton	
2	90.22	3.0	150	361.2	40.6	per 16-pile group (Abutment)
				45.1	5.1	per 2-pile group (Abutment)

Abutment Wall

Width ft	Length ft	Thickness ft	Unit Weight pcf	Load		
				kN	ton	
5.3	90.22	1.0	150	320.9	36.1	per 16-pile group (Abutment)
				40.1	4.5	per 2-pile group (Abutment)

Girder

# of beam	Length ft	Weight/ft kips/ft	Load		
			kN	ton	
10	90.0	0.821	821.7	92.4	per 4-pile group (Central Bent)
10	45.0	0.821	205.4	23.1	per 2-pile group (Abutment)

Deck

Width ft	Length ft	Thickness ft	Unit Weight pcf	Load		
				kN	ton	
81.1	90.0	0.71	150	862.2	96.9	per 4-pile group (Central Bent)
81.1	45.0	0.71	150	216.1	24.3	per 2-pile group (Abutment)

(8.5 in)

Extra (Rails and Concrete Traffic Barrier)

from TxDOT Structural Dept. Estimation	Load		
	kN	ton	
	84.8	9.5	per 4-pile group (Central Bent)
	20.1	2.3	per 2-pile group (Abutment)

Accumulated Dead Load

Group		Single		
MN	ton	MN	ton	
2.282	256.5	0.570	64.1	4-pile group (Central Bent)
0.527	59.2	0.263	29.6	2-pile group (Abutment)

(3) Summary of Truck Simulated Live Load

Group		Single	
MN	ton	MN	ton
0.284	31.9	0.071	8.0
0.110	12.4	0.055	6.2

4-pile group (Central Bent)
2-pile group (Abutment)

APPENDIX E

Abutment Settlement vs. Time

Fig. E. 1 shows the plot of abutment settlement vs. time. Six settlement pins were placed on the top of the abutment cap right after concrete was poured to measure south abutment settlements as shown in the figure. Least squares line shows the average abutment settlement.

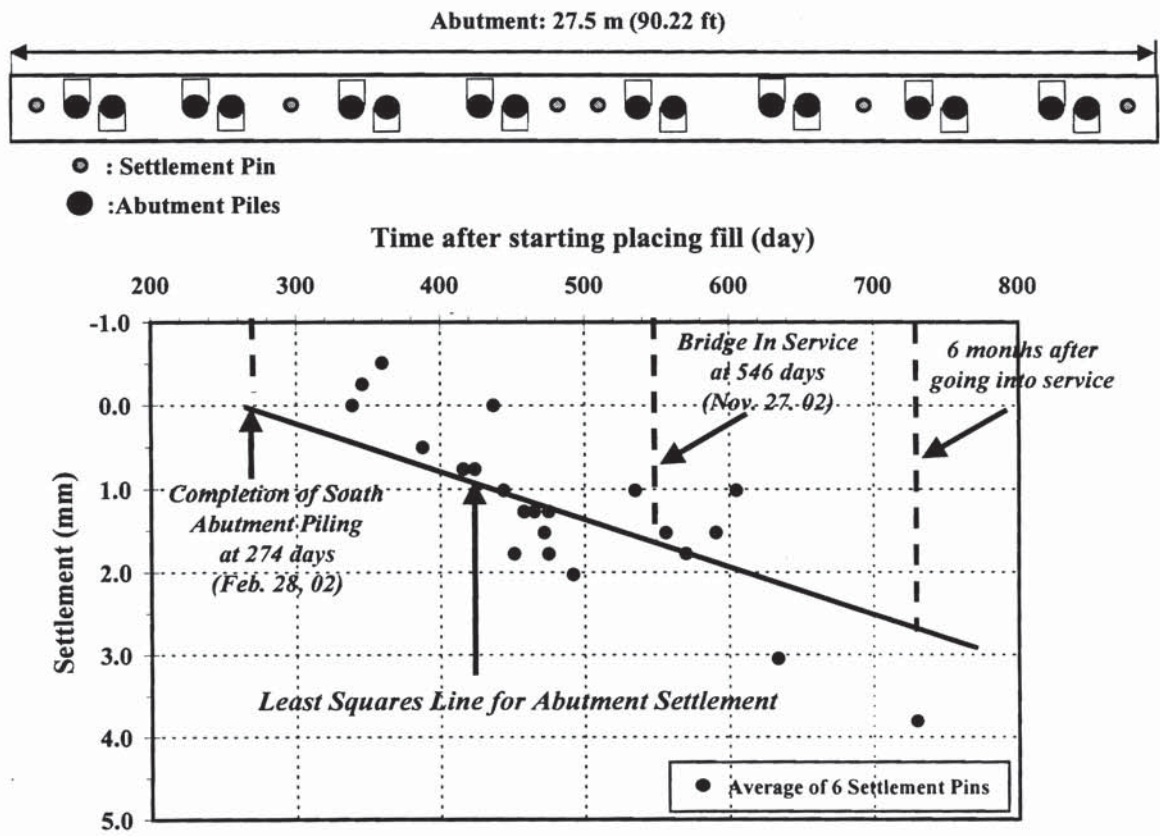


Fig. E.1. Abutment Settlement vs. Time

APPENDIX F

Fill Compaction Data

Compaction curve for south embankment (fill) was plotted as shown in Fig. F.1 with the in-field density data (Table F.1) provided by TxDOT East Harris County. The maximum dry unit weight was 17.0 kN/m^3 (108.3 lb/ft^3) at optimum moisture content of 8.5 %. Average unit weight of fill was 18.9 kN/m^3 (120.6 lb/ft^3).

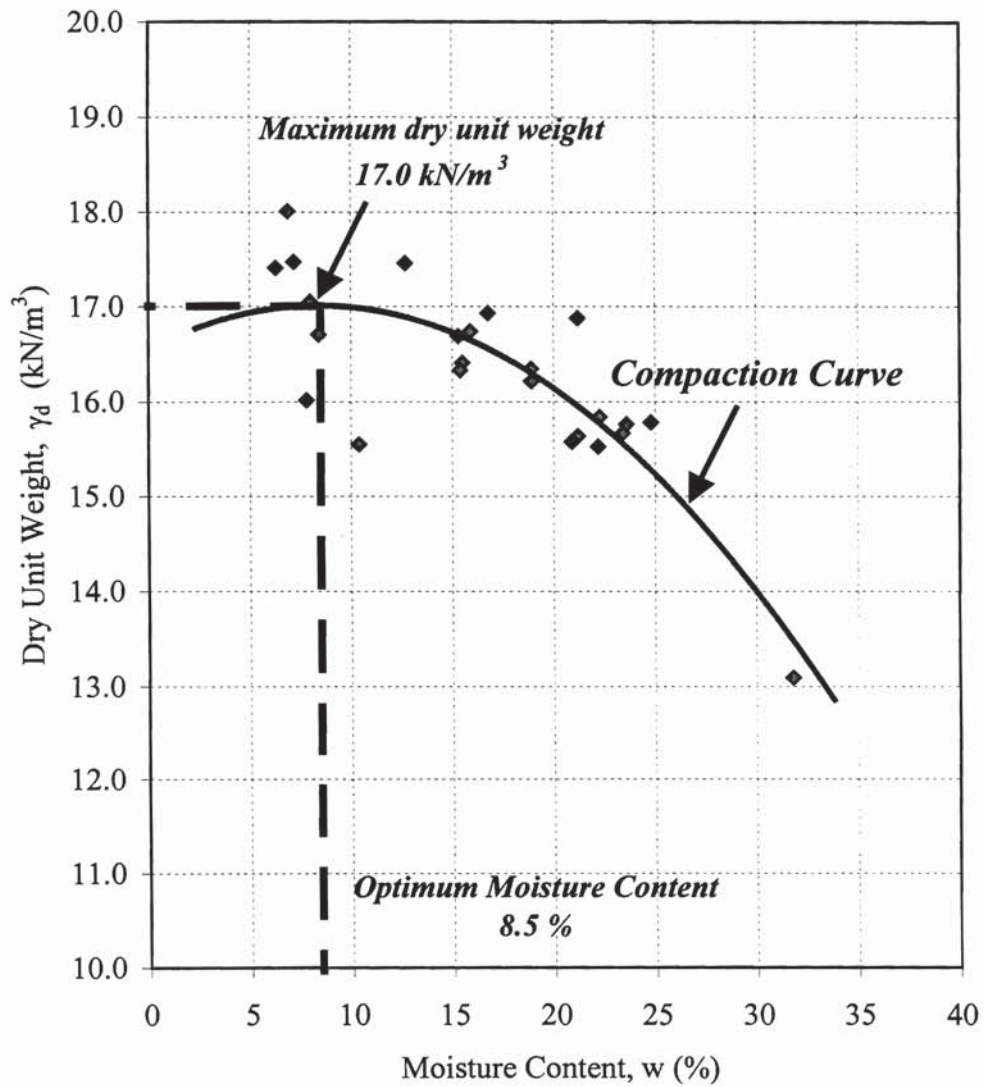


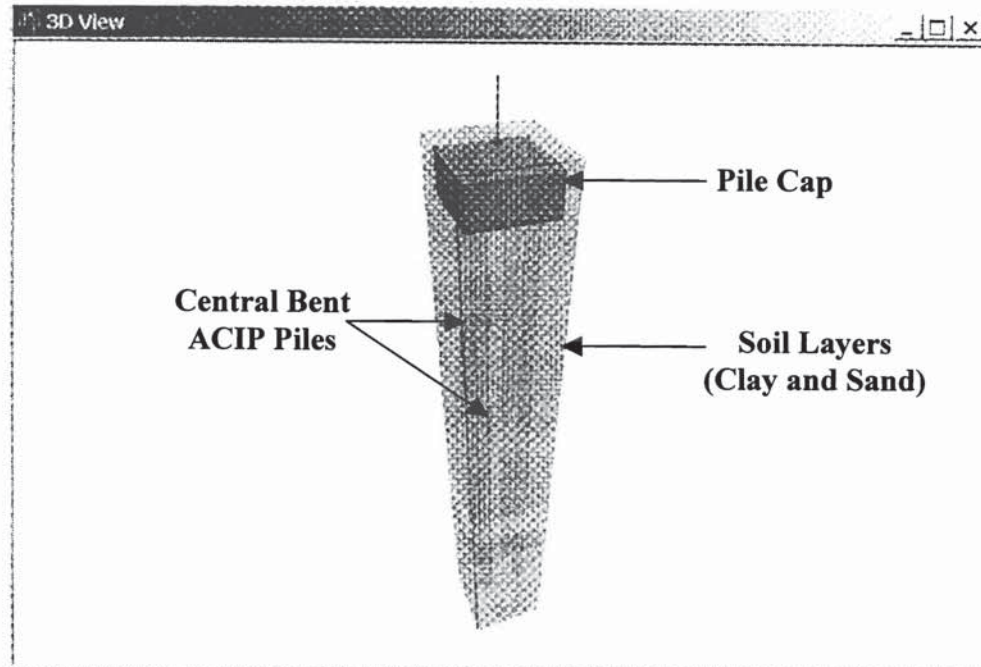
Fig. F.1. Fill Compaction Curve

Table F.1. Fill Compaction Data

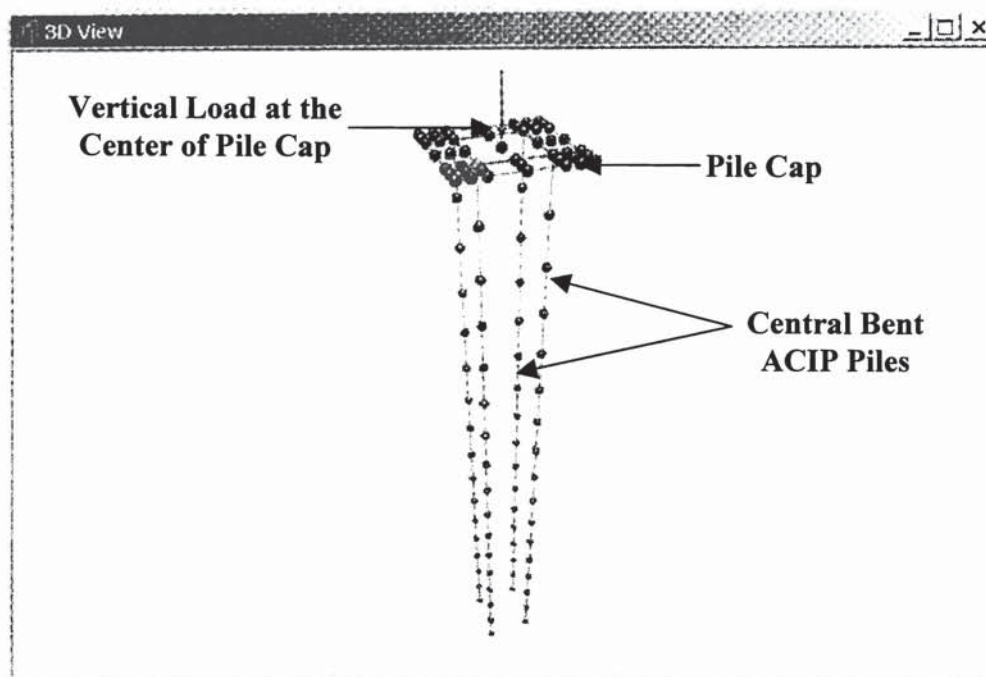
Compaction Data					
Test Location	w	γ_d		γ	
	%	pcf	kN/m ³	pcf	kN/m ³
0 to 3.7 m (12 ft)	12.7	111.2	17.5	125.3	19.7
	15.5	104.5	16.4	120.7	18.9
	31.8	83.4	13.1	109.9	17.3
	21.2	99.6	15.6	120.7	19.0
	23.4	99.8	15.7	123.2	19.3
	24.8	100.5	15.8	125.4	19.7
	23.6	100.4	15.8	124.1	19.5
	18.9	104.1	16.3	123.8	19.4
	15.9	106.6	16.7	123.5	19.4
	21.2	107.5	16.9	130.3	20.5
3.7 to 7.6 m (12 to 25 ft)	7.8	102.0	16.0	110.0	17.3
	7.2	111.3	17.5	119.3	18.7
	6.3	110.9	17.4	117.9	18.5
	8.0	108.6	17.1	117.3	18.4
	6.9	114.7	18.0	122.6	19.3
	8.4	106.4	16.7	115.3	18.1
	15.4	104.0	16.3	120.0	18.8
	15.3	106.3	16.7	122.6	19.2
	22.2	98.9	15.5	120.9	19.0
	20.9	99.2	15.6	119.9	18.8
Bottom 0.6 m (2 ft)	10.39	99.04	15.5	109.3	17.2
	16.79	107.84	16.9	125.9	19.8
	18.91	103.28	16.2	122.8	19.3
	22.27	100.88	15.8	123.3	19.4
Average			120.6	18.9	

APPENDIX G

3D View of FB-Pier Modeling Components for Pile Group Analysis



(a)



(b)

Fig. G.1. 3D View of FBPIer Modeling Components for Pile Group Analysis

